Universidade do Minho
Escola de Engenharia

Manuela Corrêa Alves da Silva

Stress-strain response of soft soils stabilised with alkali activated industrial by-products

janeiro de 2022

Stress-strain response of soft soils stabilised with alkali activated industrial by-products
Manuela Corrêa Alves da Silva
UMinho | 2021

Universidade do Minho
Escola de Engenharia

Manuela Corrêa Alves da Silva

Stress-strain response of soft soils stabilised with alkali activated industrial by-products

Tese de Doutoramento

Trabalho efetuado sob a orientação do
Professor Doutor Tiago F. S. Miranda
Professor Doutor Nuno Cristelo
Professor Doutor Mohamed Rouainia

janeiro de 2022

DIREITOS DE AUTOR E CONDIÇÕES DE UTILIZAÇÃO DO TRABALHO POR TERCEIROS

Acknowledgements

Looking back on my PhD progress, I realized that all the people that I met and all the circumstances that I experienced have come to help and shape me in this current state. I am very grateful for all I have been through, and this acknowledgement is a note to express my gratitude to them.

I would like to express my sincere gratitude to my supervisor, Professor Tiago Miranda, for his invaluable advice, continuous support, patience, and encouragement throughout my PhD. Its broad knowledge and experience strongly helped me during all the time of my academic research. Thank you for boosting the curiosity for research and having high expectations for this thesis. I am very grateful for involving me in various research projects, courses, and workshops.

I would also like to acknowledge my co-supervisors, Professor Mohamed Rouainia and Professor Nuno Cristelo, for all the time, assistance, and guidance, which were crucial for this work. Thanks to Professor Mohamed Rouainia for all your support during my journey at Newcastle University and for sharing with me your knowledge about constitutive models. Without this support, it would not have been possible to conduct some of the most fundamental research in the thesis.

My gratitude goes to Professor Nuno Araújo and technician Sr. Gonçalves for all of the support, advice, and training which they provided to make the laboratory testing programme of this research possible. I would also like to thank you all the technician from LEST laboratory at the University of Minho that somehow helped me in my tests.

I am also grateful to all my friends who have supported me along this way. A special thank you goes to Rita Neves, Isabel Sardo and Sara Barros for all their support and help. Thank you for being part of my life through these years, for the conversations and for the good times that we spent together.

And the last people, but the most important ones, to whom this PhD thesis is dedicated, are my family and fiancé. I am lucky to have them by my side. Thank you, David, for all your love and support, for believing and motivating me time and time again. Thank you, Mom, for guiding me through life and make me the person

I am today. Thanks for listening to me and being my best friend. Thank you to my brothers, Vinicius and Gustavo, who are my best advisors. Finally, I would like to thank my dogs, Nala, Simba, and Fox, for being literally by my side during the writing process, improving the quality of my days with love.

A very special gratitude goes to the Portuguese Science and Technology Foundation (FCT), under grant no. SFRH/BD/132692/2017 for proving the funding for this research. This research work was co-financed by the European Social Fund (FSE) through the Northern Regional Operational Program, and it was developed in the scope of the Doctoral Program in Civil Engineering at the University of Minho, in Portugal and at the University of Newcastle, in England.

STATEMENT OF INTEGRITY

I hereby declare having conducted this academic work with integrity. I confirm that I have not used plagiarism or any form of undue use of information or falsification of results along the process leading to its elaboration. I further declare that I have fully acknowledged the Code of Ethical Conduct of the University of Minho.

"Knowledge is the golden ladder over which we climb to heaven.
knowledge is the light which illuminates our path through this life and leads to a future
life of everlasting glory."
Mihajlo Pupin

"I never learned from a man who agreed with me." Robert A. Heinlein

.

Abstract

Alternative binders based on the alkaline activation technology have been strongly investigated over the last decades as a potential replacement for Portland Cement. However, little research has been devoted to the shear behaviour of soft soils stabilised with those type of binders and their numerical modelling using constitutive models. This PhD thesis aims to deepen the knowledge in this area through the characterisation of the short- and long-term shear behaviour of soft soils stabilised with alkali-activated binders and the numerical modelling of the stress-strain behaviour of these geomaterials using a advanced constitutive model.

In this context, triaxial tests were undertaken, after 28 and 90 curing days, in both a sandy lean clay and clay with high water content at reconstituted and stabilised states using alkali-activated blast furnace slags. The impact of the stress-history, represented by the overconsolidation ratio, and stress-state, represented by the initial mean effective stress, were investigated. Oedometer and isotropic consolidation tests were also undertaken. Scanning electron microscopy with energy dispersive spectroscopy, x-ray powder diffraction and leachate analyses were carried out to investigate the nature of the binding phases formed and the risk of contamination of soils. The results were used to calibrate an advanced kinematic hardening constitutive model proposed by Rouainia and Muir Wood, 2000 for natural clays. It was the first attempt of using this constitutive model in artificially cemented soils.

Additionally, the opportunity to be integrated within a research project related to the application of alkali-activated industrial wastes *in situ* allowed me to be deeply involved in constructing a full-scale prototype of a (sub)base layer stabilised with alkali-activated binders and conventional binders. Big challenges arose, including the definition of a construction methodology, equipment selection, on-site handling of distinct materials, quality control techniques, among others. The *in situ* performance of the stabilised geomaterials was assessed through falling weight deflectometer tests, plate load field tests and unconfined compressive strength tests after 36 and 90 days. For each layer, it was estimated the financial cost of the construction and the equivalent CO_2 emissions. The work showed the feasibility of the on-site application of alkali-activated binders in the stabilisation of soil layers in the context of transport infrastructures.

Keywords: Triaxial tests; Kinematic hardening model; SEM-EDS; XRD; Full-scale prototype

Resumo

Os ligantes alcalinos têm sido fortemente investigados nas últimas décadas como um potencial substituto do cimento Portland. Contudo, o comportamento ao corte de solos estabilizados com este tipo de ligantes é ainda uma área pouco explorada atualmente, juntamente com o uso de modelos constitutivos. A presente tese de doutoramento visa aprofundar o conhecimento existente nesta área, através da caracterização do comportamento ao corte de solos moles estabilizados com ligantes alcalinos a curto e longo prazo e a modelação numérica do comportamento tensão-extensão desses geomateriais utilizando um modelo constitutivo avançado.

Nesse contexto, foram realizados ensaios triaxiais, ensaios edométricos e de consolidação isotrópica, numa argila magra arenosa e numa argila com alto teor em água, ambos no estado reconstituído e estabilizado com escórias de alto-forno ativadas por álcalis, aos 28 e 90 dias de cura. O impacto do grau de sobreconsolidação, representado pela razão de sobreconsolidação, e do estado de tensão *in situ*, representado pela tensão média efetiva inicial, foram investigados no comportamento ao corte desses geomateriais. Foram realizadas análises de microscopia eletrônica de varrimento com espectroscopia de energia dispersiva e difração de raios-X e testes de lixiviados para investigar a natureza dos géis formados e o risco de contaminação dos solos. Os resultados foram utilizados na calibração de um modelo constitutivo de endurecimento cinemático proposto por Rouainia and Muir Wood, 2000 para argilas naturais que, até ao momento, não tinha sido utilizado em solos artificialmente cimentados.

Adicionalmente, a oportunidade de estar integrada num projeto de investigação relacionado com a construção à escala real de uma camada de (sub)base estabilizada com ligantes alcalinos e ligantes convencionais possibilitou-me enveredar por esta temática. Grandes desafios foram encontrados do longo deste projeto, entre os quais, a definição de uma metodologia de construção, a seleção de equipamentos, manuseio dos materiais *in situ*, definição dos ensaios de controle de qualidade, etc. O desempenho *in situ* dos geomateriais estabilizados foi avaliado através de ensaios de capacidade de carga com defletómetro de impacto, ensaios de carga em placa e de compressão uniaxial aos 36 e 90 dias. Para cada camada foram também estimados os custos financeiros de construção e as emissões de CO_2 equivalentes. Este projeto mostrou a viabilidade de utilização local dos ligantes alcalinos para a estabilização de camadas de solo no contexto das infraestruturas de transporte.

Palavras-Chave: Ensaios triaxiais; Modelo de endurecimento cinemático; SEM-EDS; XRD; Protótipo à escala real

Contents

List of Figures

List of Tables

Symbols

θ	Lode's angle
λ	Normal compression line
ν	Poisson ratio
f	Reference yield surface
ν	Specific volume
ψ	Stiffness interpolation exponent
$\boldsymbol{\varepsilon}$	Strain tensor
$\boldsymbol{\sigma}$	Stress tensor
κ	Swelling index
λ^*	Slope of normal compression line in ln p' (kPa) - ln (1+e) space
κ^*	Slope of swelling line in ln p' (kPa) - ln (1+e) space
$\delta\varepsilon_q$	Increment of triaxial shear strain
$\delta\varepsilon_v$	Increment of volumetric strain
$\boldsymbol{\sigma'}$	Current stress state
ϕ'_c	Critical friction angle
η_0	Anisotropy of initial structure
f_b	Bubble yield surface
ε_d	Damage strain
$\boldsymbol{\varepsilon^p}$	Plastic strain tensor
ε_q	Shear strain
ε_v	Volumetric strain
$\delta p'$	Increment of mean stress
δs	Increment of deviatoric stress
$\bar{\boldsymbol{n}}$	Normalized stress gradient on the bubble at the current stress-state
$\bar{\boldsymbol{\alpha}}$	Location of the centre of the bubble surface
$\tilde{\boldsymbol{\alpha}}$	Location of the centre of the reference surface
$\hat{\boldsymbol{\alpha}}$	Location of the centre of the structure surface

$\dot{\gamma}$	Plastic multiplier
$\overline{\boldsymbol{\sigma}}$	Stress referred to the centre of the bubble
$\widehat{\boldsymbol{\sigma}}$	Stress referred to the centre of the structure surface
$\boldsymbol{\varepsilon^e}$	Elastic strain tensor
$\boldsymbol{\sigma}_c$	Conjugate stress
ε_q^p	Plastic shear strain
ε_v^p	Plastic volumetric strain
$\dot{\widehat{\boldsymbol{\alpha}}}$	Movement of the centre of the structure surface
$\dot{\overline{\boldsymbol{\alpha}}}$	Translation rule of the bubble
$\{p_{\overline{\alpha}}, \boldsymbol{s}_{\overline{\alpha}}\}^T = \overline{\boldsymbol{\alpha}}$	Localization of the centre of the bubble surface
$\{p_c, 0\}^T = \widetilde{\boldsymbol{\alpha}}$	Localization of the centre of reference surface
$\{rp_c, (r-1)\boldsymbol{\eta}_0 p_c\}^T = \widehat{\boldsymbol{\alpha}}$	Localization of the centre of the structure surface
$\dot{\varepsilon}_q^p$	Equivalent plastic shear strain rate
$\dot{\varepsilon}_v^p$	Equivalent plastic volumetric strain rate
H_c	Associated plastic moduli at the conjugate stress points $\dot{\boldsymbol{\sigma}}_c$
M_θ	Slope of the critical state line expressed in function of the Lode angle θ
$b_{\max}$	Maximum distance between the bubble and structure surfaces
p_c	Hardening scalar variable that controls the size of the reference surface
r_0	Initial value of the ratio of the sizes of the structure surface and the reference surface
$\boldsymbol{\eta}_0$	Dimensionless deviatoric tensor (anisotropy of structure)
Δu	Excess pore water pressure
Δu_n	Normalised pore water pressure
A	Albite
A	Parameter that controls the relative proportions of distortional and volumetric destructuration
AAB	Alkali-activated binder
AABs	Alkali-activated binders
AAC	Alkaline activated cements
A_c	Cement content

Al	Aluminium
A_L	Lime content
Al_2O_3	Aluminium oxide
A_P	Super-absorbent polymer content
As	Arsenic
b	Normalized distance between the bubble and structure surface
B	Stiffness interpolation parameter
BaO	Barium oxide
BE	Bender elements
b_{max}	Maximum value of b
C&D	Construction and demolition aggregates
c'	Effective cohesion
Ca	Calcium
CaO	Calcium oxide
C–A–S–H	Calcium aluminosilicate hydrate gel
CBR	California Bearing Ratio
c_c	Virgin compression index
CD	Consolidated drained triaxial test
CDW	Construction and demolition waste
CO	Carbon Monoxide (air pollutant)
CO_2 (eq)	Equivalent carbon dioxide emissions
CO_2	Carbon dioxide
c_r	Recompression index
CS	Cleaning solution
C-S-H	Hydrated calcium silicate gel
CSL	Critical state line
c_u	Cohesion in undrained conditions
CU	Consolidated undrained triaxial test
Cu	Copper

DSM	Deep soil mixing
e	Void ratio
e_c	Critical void ratio
ECO_2	Embodied carbon dioxide emissions
E_d	Dynamic deformability modulus
EDS	Energy-dispersive X-ray spectroscopy analysis
EF_i	Emission factor (kgCO2/t)
E_{sec}	Secant deformability modulus
$E_{sec,n}$	Normalized secant deformability modulus
E_u	Undrained stiffness modulus
E_{v2}	Static deformability modulus obtained in the second load cycle of the plate load tests
F	Structure yield surface
FA	Fly ash
FASLG	Metallurgical slag
Fe_2O_3	Iron oxide
FWD	Falling Weight Deflectometer tests
G	Shear modulus
GGBS	Ground granulated blast furnace slag
G_{max} or G_0	Maximum or initial shear stiffness modulus
GWP	Global warming potential
H	Plastic modulus at the stress points $\dot{\boldsymbol{\sigma}}$
H_c	Plastic modulus at conjugate stress
IBP	Industrial by-product
ICL	Isotropic compression line
J_2	Second stress invariant
J_3	Third stress invariant
K	Bulk moduli
k	Parameter that controls the rate of loss of structure with damage strain
K	Potassium

K_2O	Potassium oxide
LL	Liquid limit
LOI	Loss on Ignition
LVDT	Linear Variable Differential Transformer
M	Critical state stress ratio or slope of the critical state line
M	Muscovite
M_θ	Dimensionless scaling function for deviatoric variation of M
MgO	Magnesium oxide
Mi	Microcline
MCC	Modified Cam Clay model
Na	Sodium
Na_2O	Sodium oxide
Na_2SiO_3	Sodium silicate
$NaAlO_2$	Sodium aluminate
NaCl	Sodium chloride
NaOH	Sodium hydroxide
N-A-S-H	Sodium aluminosilicate hydrate gel
Ni	Nickel
NO_x	Nitrogen oxides (air pollutant)
O	Oligoclase
OCR	Overconsolidation ratio
OCRs	Overconsolidation ratios
OPC	Ordinary Portland cement
p'	Mean effective stress
p'_o	Initial mean effective stress
p'_y	Yield stress
Pb	Lead
p_c	Stress variable controlling the size of the surfaces
p_{c0}	Initial centre of reference surface

PFA	Pulverised fly ash
PI	Plasticity index
PL	Plastic limit
PL	Plate Load field tests
PM	Particulates (air pollutant)
POFA	Palm oil fuel ash
q	Deviatoric stress
Q	Quartz
q_n	Normalised deviatoric stress
r	Parameter describing the ratio of sizes of structured and reference surfaces
R	Ratio of size of bubble and reference surface
r_0	Initial degree of structure
RSM	Response Surface Methodology
SCC	Structured Cam Clay model
SEM	Scanning Electron Microscopy analysis
Si	Silicon
SiO_2	Silicon dioxide
SO_2	Sulfur Dioxide (air pollutant)
Ev_2	Static deformability modulus obtained in the second load cycle of the plate load tests
T	Term in the definition of hardening modulus
TiO_2	Titanium dioxide
tr	Trace operator
$\mathrm{tr}[\cdot]$	Trace operator of $[\cdot]$.
UCS	Unconfined or uniaxial compressive strength
WG	Waste glass
XRD	X-ray diffraction analysis
XRF	X-ray fluorescence analyses

Zn	Zinc
ZrO_2	Zirconium dioxide
Δu	Pore pressure variation
ε_a	Axial strain
ζ	Curve that represents the envelope of peak strength situated above *M*
ρ_d	Dry density
$\rho_{d,max}$	Maximum dry density
σ'_v	Vertical effective stress
ϕ'	Effetive friction angle
ϕ_u	Friction angle in undrained conditions
ω	Water content
ω_0	Water content *in situ* at the start
ω_{lime}	Water content *in situ* after lime treatment
ω_{opt}	Optimum water content
ω_{stab}	Water content required for stabilisation
F	Structure surface
m	Ratio of extension and compression strengths
p	Mean pressure
$\boldsymbol{I}$	Second-rank identity sensor

1. INTRODUCTION

Chapter 1 presents the background of the research. The aim and objectives, research scope, methodology and outlines of the thesis are referred to.

1.1 Research background and motivation

Concrete is the most consumed man-made material on the planet (Rodgers, 2018).The huge consumption of this material is associated with its excellent performance and versatility, linked with the local availability of the raw materials. The key constituent of concrete is cement, which has a massive carbon footprint, contributing to ≈ 8 % of the world's carbon dioxide (CO_2) emissions (Andrew, 2018).

The production of Portland cement involves the extraction, crush, and ground of raw materials, mainly limestone and clay. Then these materials are mixed with others, such as iron ore or fly ash (FA). When limestone is heated, a chemical process called calcination is initiated, where CO_2 is burned off the limestone. Most of the emissions from the cement industry derive from the calcination process. Some chemical reactions occur up to form the final product at very high temperatures, the clinker. The clinker is cooled, ground, and mixed with gypsum and limestone to form cement. Therefore, cement production is a process that requires high consumption of energy and natural resources resulting in high straining of deposits of these materials and environmental impact.

Another aspect of strong importance is the waste generated from the construction and demolition of concrete structures that have increased with urbanisation. Growth of demand for concrete is expected with the population increase, especially in developing countries, which will result in higher CO_2 emissions and raw material consumption (Adesina, 2020). To overcome these issues and, thus, avoiding to reach a global temperature increase of 1.5°C and above, the concrete industry has put different strategies in place in recent years linked with the evolution of cement technology, which is expected to result in net-zero emissions in 2050 (IPCC, 2018). One of the recent advances in the concrete industry was the partial replacement of the conventional clinker (i.e., limestone) with wastes, such as slag, FA, filter sand etc., which helps not only to reduce the emissions but also to manage the wastes effectively.

Another alternative pathway that is gaining huge attention due to its potential are the alkali-activated binders (AABs). They are relatively recent, and numerous research is ongoing to understand the short- and long-term behaviours of the materials made or improved using this type of binder. These AABs are synthesised in an

alkaline medium, where alkaline activators are used to activate aluminosilicate-based precursors. The precursors are mostly waste materials, such as FA, slags, etc.

Some advantages are associated with the use of these binders instead of Portland cement. The reduction of volume excavation for the extraction of raw materials is one of them, together with the reduction of CO_2 emissions and air pollutants, including SO_2, NO_x, CO, and PM that are released into the atmosphere. Since the AABs incorporate wastes in their composition, their production paves an avenue to reuse the available local wastes, which minimizes the required landfill areas and the subsequent environmental impact resulting from their deposition. However, some limitations related to the properties of the activators used, fresh properties and varying composition of the precursors still limit the application of AABs in practice (Adesina, 2020; Provis, 2018).

Concerning the use of AABs for soil stabilisation, over the last decade, an increasing number of papers have reported their effectiveness on the enhancement of the geomechanical properties using distinct precursors, among which FA (Corrêa-Silva et al., 2019; Cristelo et al., 2015b, 2013), blast furnace slags (Fasihnikoutalab et al., 2020; Sargent et al., 2013), a mixture of FA and blast furnace slags (Singhi et al., 2016; Yi et al., 2015) and metakaolin (Zhang et al., 2015, 2013). Whilst there is extensive literature covering laboratory research concerning the performance of soft soils stabilised with AABs focusing on mechanical tests in a general way, chemical and environmental analysis, there is still scarce research related to the mechanical behaviour of stabilised geomaterials with AABs using triaxial tests. Understanding the shear behaviour of problematic soils before and after adding binder is of utmost importance for strength and deformation analysis at short- and long-term conditions and the development of geotechnical engineering projects. In this context, the short- and long-term experimental shear behaviour of soft soils stabilised with AABs using triaxial tests is one of the points investigated and was assumed as the first main question addressed by this thesis.

Apart from that but still linked to the shear behaviour of soft soils stabilised with AABs, another gap of knowledge was detected, more precisely concerning the use of existent constitutive models to predict the experimental behaviour of these geomaterials using triaxial test results. The majority of published papers on numerical modelling currently are based on the behaviour of soils stabilised with conventional binders, such as Portland cement. The use of constitutive laws is crucial in practical applications since they allow to

reproduce computationally, as far as possible, the experimental stress-strain response of a system under different and complex stress paths. In this context, the key question was raised regarding the possibility of use or propose modifications to an existent constitutive model to predict the experimental shear behaviour of soils stabilised with AABs. This was identified as the second main question to be addressed in a field practically unexplored up to now. In line with what was previously mentioned, it is intended that this PhD thesis can be seen as a step forward in the AABs field, helping to fill the lack of knowledge on the shear behaviour of geomaterials stabilised with this type of binder where both, the experimental behaviour of stabilised soil-AABs mixtures and the numerical modelling of these results through the use of an advanced constitutive model, are addressed.

1.2 Research aim and objectives

The mentioned lack of knowledge on the shear behaviour and numerical modelling of soils stabilised with AABs led to the definition of the research aim. In this context, this PhD thesis aims to address the two main topics, as referred to next:

- Characterisation of the short- and long-term experimental mechanical behaviour of soils stabilised with AABs using triaxial tests, more precisely the stress-strain response, stiffness degradation with strain, pore pressure and volumetric strain variations and stress-path and, the analysis of similar behaviour with soils stabilised with conventional binders, such as Portland cement. This aim requires some preliminary knowledge on the monotonic consolidated drained and undrained triaxial tests for soils, more precisely about bender elements (BE), local instrumentation, test methodologies for the saturation, consolidation and shear phases, and interpretation of results. The knowledge on the shear behaviour of reconstituted and stabilised soft soils with Portland cement is crucial for this aim. This will be the base for further developments with AABs.
- Selection, calibration and/or modification of an existent advanced constitutive model able to describe the experimental stress-strain behaviour of the selected soft soils with accuracy, before and after adding the AABs, at short- and long-term. In this context, the knowledge of the experimental shear behaviour of the soils stabilised with AABs referred to in the first aim is crucial, together with the knowledge of the constitutive models and the respective limitations in a general way. A deeper

knowledge of the selected constitutive model is also required in terms of how it works and the respective limitations, and the determination of the model parameters.

Additionally, the opportunity to be integrated within a research project related to the application of alkali-activated industrial wastes *in situ* allowed me to be deeply involved in constructing a full-scale prototype of a (sub)base layer stabilised with alkali-activated binders and conventional binders. This research project is in line and complement, in a certain way, the experimental and numerical work developed within the scope of the present PhD thesis. In this context, the most effective AAB formulations, previously developed and tested at the lab within the scope of the research project, were selected together with two formulations composed of traditional binders for comparative purposes. Big challenges arose during the process, including the definition of a construction methodology, equipment selection, on-site handling of distinct materials, definition of the quality control techniques, among others. For each layer, it was estimated the financial cost of the construction and the equivalent CO2 emissions. The work showed the feasibility of the on-site application of alkali-activated binders in the stabilisation of soil layers in the context of transport infrastructures.

1.3 Research methodology

To characterise the overall shear behaviour of soft soils stabilised with AABs at short (28 days) and long (90 days) terms, two different types of fine-grained soils were selected: a sandy lean clay and a clay with high plasticity. Also, an AAB composition with a known performance was selected to enhance the mechanical behaviour of both soils. To know the effectiveness of the AAB was crucial since the aim of this PhD thesis was not the development of AAB formulations in particular, but the characterisation of the mechanical behaviour of soft soils stabilised with AABs through triaxial tests, and the later use of these results to calibrate constitutive models. The selected binder is composed of two parts of ground granulated blast furnace slag (GGBS) and one part of sodium hydroxide (NaOH). The blast furnace slags are a residue obtained from the iron industry constituted by calcium aluminosilicate frameworks.

First, the chemical composition of the raw materials (i.e., GGBS and soils) and stabilised soils was determined at 28 and 90 curing days through scanning electron microscopy with energy dispersive spectroscopy (SEM-EDS) and X-ray diffraction (XRD) analyses to evaluate the type of gels formed.

1. INTRODUCTION

To characterise the mechanical behaviour of the non-stabilised and stabilised soils, monotonic consolidated drained and undrained triaxial tests were performed with BE and hall effect transducers to measure local strains. These tests were undertaken at 28 and/or 90 curing days for a wide range of initial mean effective stress (p'_0) and overconsolidation ratios (OCR). These tests allowed to:

- Evaluate the impact of the AAB on the overall behaviour (i.e., stress-strain response, stiffness degradation with strain, pore pressure and volumetric strains variations and stress-path) for both non-stabilised and stabilised soils.
- Quantify the improvement achieved in terms of shear strength parameters and stiffness adding the same AAB composition in two types of fine-grained soils. Although the same binder composition was added in both soils (two parts of GGBS and one part of NaOH), the binder dosage, that is, the amount of binder, was changed according to the water content of the soils.
- Analyse the impact of the stress-history (represented by the OCR) and stress-state (represented by p'_0) on the reconstituted and stabilised soil specimens built with the two selected soils.

To complement the triaxial test campaign, oedometer tests were performed in both soils, before and after stabilisation at both curing ages, with the objective to determine the preconsolidation stress and both the virgin compression (c_c) and the recompression (c_r) indexes. Also, isotropic consolidation tests were undertaken to determine the slopes of the normal compression (λ) and swelling (k) lines and the yield stress (p'_y).

To assess the risk of soil contamination resulting from the use of AAB to stabilise the soils, leachate tests were performed at 28 and 90 curing days.

The triaxial test results were used as a database for the selection and calibration of an existent constitutive model to reproduce the stress-strain behaviour observed at the laboratory for both non-stabilised and stabilised soils. The ability of the advanced constitutive model to reproduce the experimental behaviour was analysed considering the following aspects:

- The impact of the AAB and curing time.

- The impact of the stress-history (represented by OCR) and stress-state (represented by p'_0) on the shear behaviour.

To stabilise a full scale (sub)base layer with alkali-activated industrial wastes, the following methodology was adopted:

- Characterise the geomechanical behaviour of the soil *in situ*. Particle size distribution, Atterberg limits, compaction, Uniaxial Compressive Strength (UCS) and California Bearing Ratio (CBR) tests were undertaken. The applied AABs were selected based on previously performed laboratory tests. The chemical composition of the precursor and activator materials were determined through X-ray fluorescence (XRF) analyses. For comparative purposes, two formulations with conventional binders were selected to stabilise other sections of the layer.
- Define a construction methodology according to the composition of the AABs. Some aspects were considered, such as the use of conventional equipment and the conditions *in situ*, that is, the water content and the water content required for the compaction of the mixtures.
- Quantify the mechanical gains for each stabilised soil mixture, by means of Falling Weight Deflectometer (FWD) tests, Plate Load (PL) field tests, and UCS tests performed at 36 and 90 days.
- Estimate the financial cost of the construction for each stabilised soil layer considering the current prices in Portugal for the materials and the corresponding transportation cost at the time the full-scale prototype was built.
- Estimate the equivalent CO_2 emissions (CO_2e) resulting from the manufacture of the raw materials and their transportation to the site using a EFFC DFI Carbon Calculator Tool (v2.0) developed by the European Federation of Foundation Contractors (EFFC) and Deep Foundations Institute (DFI).

1.4 Thesis outline

The thesis outline is shown in Figure 1. As previously discussed, the aim was to characterise the experimental shear behaviour of soils stabilised with AABs and use the data from these tests to select and calibrate an advanced constitutive model to predict their stress-strain responses. This thesis is divided into four parts. **Part I** presents the research background and the motivation that leads to the origin of this thesis. Also, the relevant literature on AABs and triaxial behaviour of soils stabilised with AABs are included. The constitutive

model chosen to reproduce the experimental behaviour is explained here. In **Part II**, the laboratory test results performed in both soils, before and after stabilisation at both curing ages, is presented, and analysed, including monotonic consolidated drained and undrained triaxial tests, chemical and leachate tests. The ability of the constitutive model to reproduce the experimental stress-strain behaviour is also presented here. **Part III** is dedicated to the work developed within the scope of a research project, where a full-scale sub(base) layer was built using alkali-activated industrial wastes. **Part IV** presents the main findings from **PART II** and **III**, contributions from this thesis and suggestions for future work. The content of each Chapter is summarised as follows:

- Chapter 2 presents a literature review on soil stabilisation with AABs, including the alkaline activation concept, the use of two specific precursors, the blast furnace slags and low calcium FA in soil stabilisation and the factors affecting the alkali activation reactions. The second part presents the current understanding about the mechanical behaviour of soils stabilised with Portland cement and AABs through triaxial tests, more precisely the overall experimental and predicted responses using constitutive laws, and the constitutive model calibrated in the context of this research.
- Chapter 3 synthesises the geomechanical behaviour of a sandy lean clay stabilised with the alkali-activated blast furnace slags, which included the triaxial test results, SEM-EDS and XRD and leachate analysis at 28 and 90 curing days. Here, the laboratory campaign performed on reconstituted and stabilised soil specimens is presented and analysed. This Chapter is based in the article "Corrêa-Silva, M., Miranda, T., Rouainia, M., Araújo, N., Glendinning, S., & Cristelo, N. (2020). Geomechanical behaviour of a soft soil stabilised with alkali-activated blast-furnace slags. Journal of Cleaner Production, 122017. https://doi.org/10.1016/j.jclepro.2020.12201".
- Chapter 4 is dedicated to the prediction of the stress-strain response of the sandy lean clay stabilised with alkali-activated blast furnace slags at 28 and 90 curing days. The constitutive model used is presented and discussed here together with the accuracy of the predictions made by the model. This Chapter is based in the article "Corrêa-Silva, M., Rouainia, M., Miranda, T., Cristelo, N., 2021. Predicting the mechanical behaviour of a sandy clay stabilised with an alkali-activated binder. Eng. Geol. 292, 106260. https://doi.org/10.1016/j.enggeo.2021.106260".

- Chapter 5 analyses the behaviour of a stabilised clay with the alkali-activated blast furnace slags. Both experimental and predicted behaviours at 28 days are shown, together with SEM-EDS and XRD analyses and leachate tests carried out at 28 and 90 days. Consolidated undrained triaxial tests were undertaken on reconstituted and stabilised soil specimens at high water content. The challenge was to analyse the efficacy of the AAB to stabilise a clay at high water content. The same constitutive model employed in Chapter 4 was used, and the ability to predict a distinct stress-strain response was assessed. This Chapter is based in the article under submission process.

- Chapter 6 focus on the information on the construction methodology adopted to stabilise a full-scale (sub)base layer using alkali-activated industrial wastes and the performance *in situ* of these binders. Results of FWD, plate load and UCS tests are presented, together with the financial cost and environmental impact through CO_2e for each tested binder. This Chapter is based in the article "Miranda, T., Leitão, D., Oliveira, J., Corrêa-Silva, M., Araújo, N., Coelho, J., ... Cristelo, N. (2020). Application of alkali-activated industrial wastes for the stabilisation of a full-scale (sub)base layer. Journal of Cleaner Production, 242, 118427. https://doi.org/10.1016/j.jclepro.2019.118427".

- Chapter 7 summarises the main findings from **PART II** and PART **III** concerning the laboratory, numerical and research *in situ* about the use of AABs for soil stabilisation. Furthermore, research perspectives for future studies are proposed.

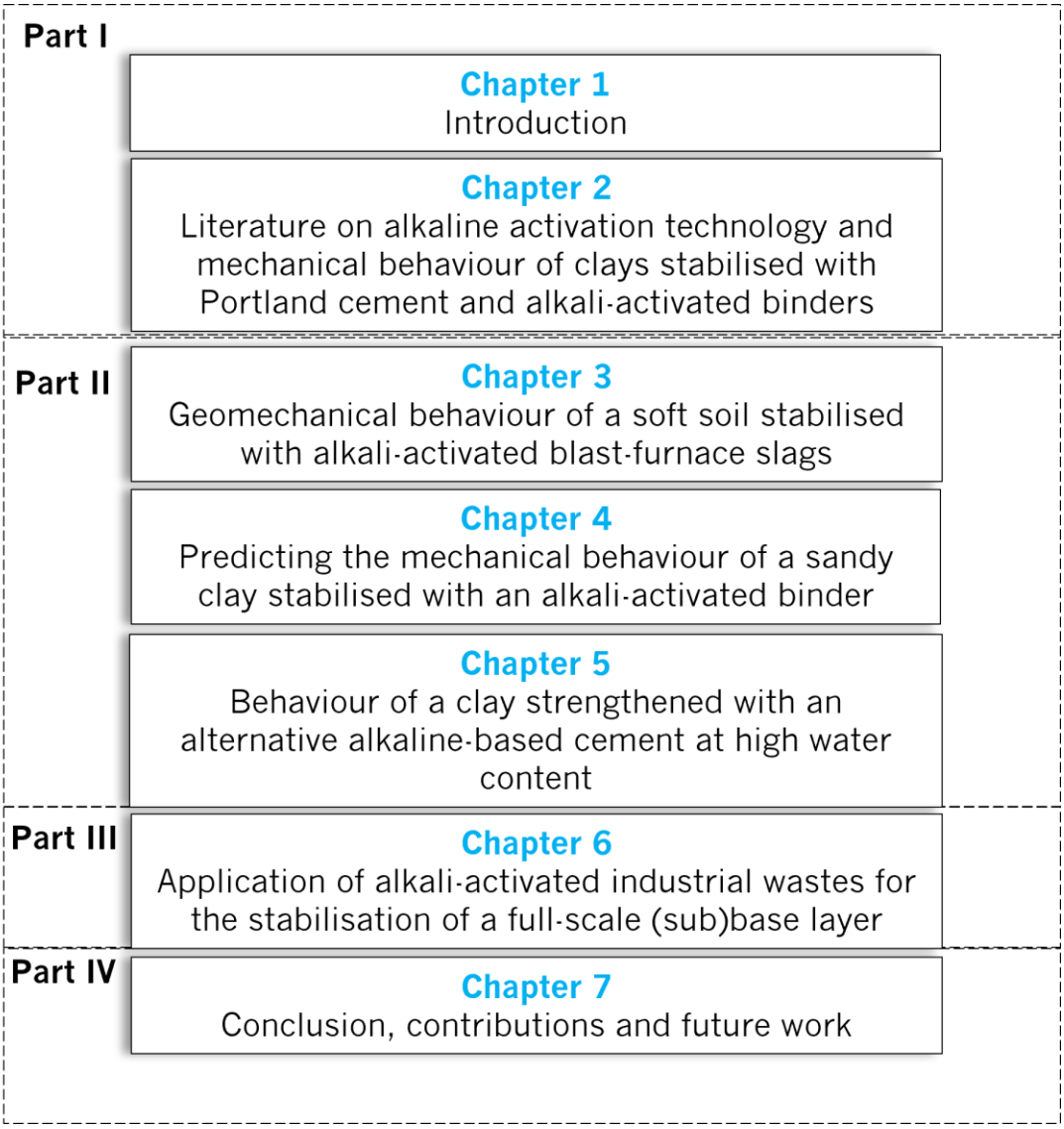

Figure 1. Thesis outline

2. LITERATURE ON ALKALINE ACTIVATION TECHNOLOGY AND MECHANICAL BEHAVIOUR OF CLAYS STABILISED WITH PORTLAND CEMENT AND ALKALI-ACTIVATED BINDERS

This Chapter focus on the published literature on alkali activation technology applied in soil stabilisation and the current understanding of the mechanical behaviour of clays stabilised with Portland cement and alkali-activated binders through triaxial tests. The experimental behaviour of the stabilised clays under different ranges of stress-history (represented by OCR) and stress-state (represented by p'_0) was addressed, as well as the numerical modelling of artificially cemented clays. Finally, a detailed description of the kinematic hardening model selected to be applied in Chapter 4 and Chapter 5 is made.

2.1 Soil stabilisation with alkali-activated binders

2.1.1 Alkaline activation technology

AABs are gaining increasing recognition and research interest in recent years due to their potential to mitigate global energy demand, waste generation and greenhouse gas emissions when used instead of Portland cement-based materials. The continued use of Portland cement is becoming less economically and environmentally sustainable. Nowadays, the construction sector is being confronted with numerous issues related with sustainability, including:

- The necessity to mitigate emissions of CO_2 and other pollutant substances that are released into the atmosphere at both national and international levels.
- The increasing demand for cement and concrete in developing and middle-income nations.
- The requirements for the materials performance that are increasing due to a more ambitious architectural, structural and/or engineering design.
- The increasing of the durability (service life) requirements considering that on a full lifecycle basis, both sustainability and durability must be analysed in parallel.
- The necessity to reuse industrial by-products or wastes instead than landfilling, which mitigates the required landfill areas and the risk of soil contaminations.

To overcome these issues, efforts have been undertaken to partially incorporate industrial by-products or wastes within the Portland cement composition, such as GGBS and FA. The total replacement of the Portland cement by the popular low carbon AABs is another option that has been intensively investigated over the last years.

The AABs are produced through the reaction of two main components that strongly influence their properties: the alkaline activator - the most common are NaOH and/or sodium silicate (Na_2SiO_3) (Samarakoon et al., 2019) - and aluminosilicate-based precursor material generally derived from industrial by-products (Figure 2). Since most materials in AABs are by-products or industrial waste, a small or no environmental footprint is normally attributed to these materials. However, as referred to in Chapter 1, the use or valorisation of

wastes has some limitations related to the limited volume generated from any single process compared to the throughput of a commercial-scale cement production facility and the high variability of these raw materials.

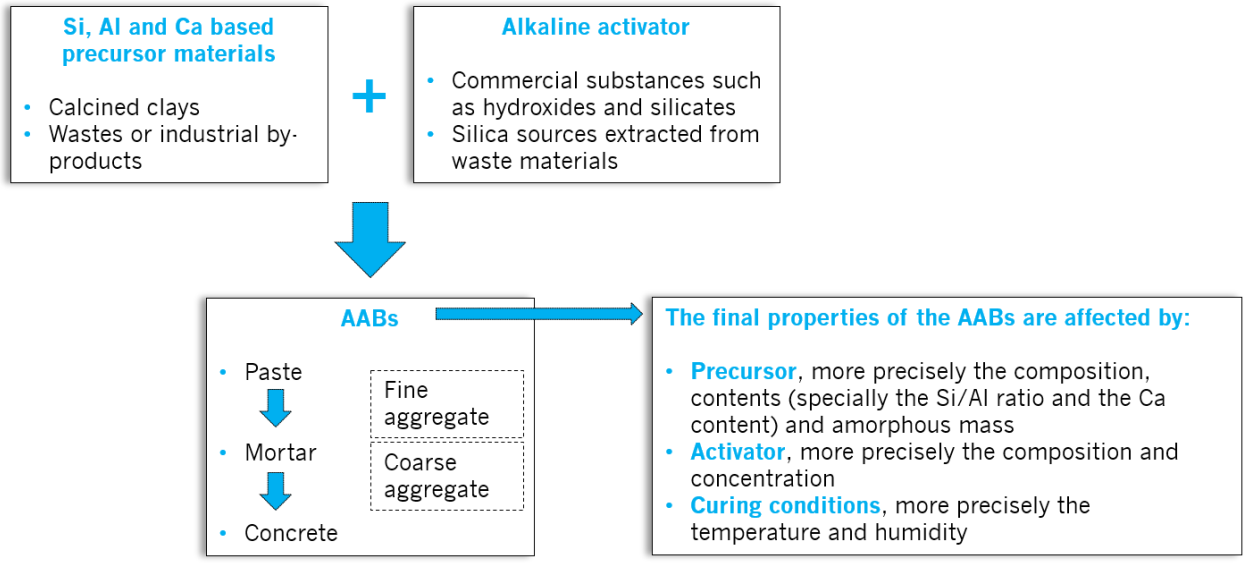

Figure 2. Synthesis of the AABs and factors that can affect their final properties

Based on the chemical composition, these binders can be divided in two major categories (Provis, 2014): low-calcium (geopolymer) and higher-calcium AABs. The concept 'geopolymer' was introduced by Davidovits in the 1970s (Davidovits, 2008), and describes the mechanism where low-calcium aluminosilicate precursors such as FA and calcined clays are activated in a high pH environment and forms a three-dimensional amorphous aluminosilicate gel free of calcium. However, the alkali-activation technology antedates this concept by more than 60 years, with a patent awarded to Kuhl in 1908 (Kuhl, 1908). Within the group of calcined clays, the kaolin is used due to their high amount of Si and Al. Another naturally occurring calcined clay extensively used is the metakaolin, that is obtained by heating the kaolin at temperatures of 750°C.

When calcium-based precursors such as alkali-activated blast furnace slags at moderate alkaline pH are used, a higher-calcium AABs is formed, known as calcium aluminosilicate hydrate (C–A–S–H) gel (Richardson et al., 1994), broadly comparable to the gel structure which results from Portland cement hydration but with low Ca content. Sodium aluminosilicate hydrate (N-A-S-H) type of gels are very common

to coexist as a minor secondary product in addition to C–A–S–H within much of the compositional range of alkali-activated blast furnace slags (Myers et al., 2013), and in increasing prevalence in blends with FA (Ismail et al., 2014) or metakaolin (Bernal et al., 2011).

The chemical reactions to synthesise the AABs involve the dissolution of Al, Si and Ca-based components within precursor materials when in contact with the activator, rearrangement, condensation and resolidification processes (Provis, 2014). The use of activators with different compositions and concentrations influences the performance of the polymerization reactions, which is reflected in the final properties of the AABs.

The combined use of alkali silicates and hydroxides allows a better dissolution of the precursor components and higher reaction rates (Samarakoon et al., 2019). According to Yang et al., 2008, the NaOH promotes the dissolution process of the raw materials, while the Na_2SiO_3 promotes the reorganization of the structure. Davidovits, 2013 reported that the use *in situ* of highly concentrated alkali hydroxide solutions (between 8M and 16M) may cause chemical burns when dealing with mass quantities, which may undermine construction safety regulations. However, the financial cost of these commercial alkaline activators and the environmental impact resulted from their productions are still considerable and, to overcome these issues, recent research has been devoted, with promising results, to the development of AABs mostly based on industrial wastes. Fernández-Jiménez et al., 2017 analysed the potential application of a solution used to wash moulds from the aluminium casting industry as an alkali activator for the inclusion in the production of alkaline cement, concluding that, in fact, this solution has a high potential to be used as an activator material. Silica sources extracted from waste materials, such as rice husk and waste glass, can be also used as supplementary silicates for the alkaline activator, together with alkaline hydroxides (Tchakouté et al., 2016a, 2016b). These silica sources need to be grinded and crushed into smaller sizes first to extract the silica. Tho-In et al., 2018 observed that these waste silica sources have a similar effect to commercial sodium silicate in the binder phase.

The final properties of the AABs are also influenced by the composition, content, and amorphous mass of the precursor materials (especially the Si/Al ratio and the Ca content) and by the curing conditions, more precisely the temperature and the humidity.

Rivera et al., 2019 synthesised simple (FA) and binary (FA and metallurgical slag (FASLG)) alkaline cements using the Response Surface Methodology (RSM), which is a tool used to plan the AAB formulations, by controlling the variables SiO_2/Al_2O_3 and Na_2O/SiO_2 molar ratios. The Variance Analysis revealed that, for the first 7 days of curing, the Na_2O/SiO_2 is statistically non-significant and the SiO_2/Al_2O_3 is the main responsible for this short-term strength development, for both types of mixtures. After 28 days, both variables for the FA mixture, as well as their interaction, showed to be statistically significant, while for the FASLG mixture, the SiO_2/Al_2O_3 and the $(SiO_2/Al_2O_3)*(Na_2O/SiO_2)$ interaction was not statistically significant. The authors justified this by the absence of a third variable - CaO/SiO_2, which plays an important role in the alkaline activation of high-calcium gel precursors.

Xiao et al., 2020 investigated the use of waste glass (WG) powder obtained by crushing soda-lime glass bottles and class C FA at ratios of 100:0, 75:25, 50:50, 25:75, 0:100 to synthesise geopolymer cement. Both raw materials were activated by NaOH solutions with concentrations of 0 M, 2.5 M, 5 M, 7.5 M, 10 M and cured at ambient temperature. The results indicated that the WG mostly acted as an inert filler at early ages due to the slow reaction rate. The strength increased considerably after 14 days, which was explained by the reaction between WG and FA. The microstructure and mineralogy suggested the coexistence of N-A-S-H and C-A-S-H gels within the geopolymer matrix. The results of leaching tests indicated the potential environmental impact caused by the leaching of excessive alkali. The sustainability analysis including the embodied energy and carbon footprint confirmed the environmental friendliness of the geopolymer.

Gharzouni et al., 2018 evaluated the influence of aluminium and calcium availability from two different aluminosilicate sources (Callvo-Oxfordian argillite and dredged sediment), on the formation, the structure, and the working properties of the resulting alkali-activated materials. These sources were previously dried, crushed, ground, and then calcined at 750 °C for 4 hours. The results showed that the sediment specimen presents higher reactive aluminium and lower reactive calcium compared to the argillite specimen. The calcium interacts with free silicon and aluminium and alkali cation in excess (sodium or potassium), leading to the formation of several networks (Si-O-Al and Si-O-Ca bonds). The low availability of aluminium in addition to the high availability of calcium favours the precipitation of secondary reaction products in detriment of the geopolymer network. The voids are filled by these products, which reduce the porosity and pore sizes but also lead to higher heterogeneity that decreases the mechanical performance of the final material. However,

the higher availability of aluminium and the lower availability of calcium in presence of high alkaline conditions favour the polycondensation reaction.

Cristelo et al., 2018 investigated the efficiency of using construction and demolition waste (CDW) with a high quantity of fines as aggregate materials. These aggregates were mixed with FA at different weight rates of 100/0, 90/10, 80/20, 70/30, 60/40, and then activated with NaOH and Na_2SiO_3. The authors concluded that the presence of FA enhances the compressive strength and elasticity module, with UCS higher than 8 MPa after 28 days at ambient temperature and relative humidity. This is higher than the necessary strength for geotechnical applications, such as road and railway foundations or infrastructure embankments, which are considered as effective applications for CDW aggregates.

Kaze et al., 2021 investigated the geopolymer performances synthesised from two calcined iron-rich laterite soils. These materials were used as precursors, and the geopolymers were cured at 20, 60 and 80°C. The results showed that the dissolution of the calcined laterites in 8 M NaOH increased the dissolution of Al, Si and Fe elements with increasing temperature from 20 to 80°C. Higher dissolutions resulted in an increase in the compressive strength of the binders at 7 and 28 days. The curing conditions of the geopolymer in the dry state resulted in higher compressive strength at all ages compared to those cured in the wet and wet-dry state. The authors suggested that both AABs can be used for various construction applications, especially in the precast industry.

2.1.2 Precursor and activator materials

In the scope of this research work, two industrial by-products or wastes were used to synthesise the AABs, the GGBS and Class F FA. These precursor materials were activated using commercial products, namely NaOH or NaOH and Na_2SiO_3, and a waste referred to as 'cleaning solution' (CS). Therefore, this Chapter will focus on the physical and chemical properties of these particular precursor and activator materials. The Chapter 2.1.3 will focus on geotechnical applications using the referred materials.

2. LITERATURE REVIEW

The GGBS is a by-product from the blast furnaces used to make iron. It is obtained by quenching molten iron slag in water or steam, to produce a glassy and granular product that is dried and then ground into a fine powder. The detailed process to obtain this product is following described (Siddique and Khan, 2011):

- First, a controlled mixture of iron-ore, coke and limestone are introduced within the blast furnaces at a temperature of about 1500°C. After melting, two products are obtained, molten iron and molten slag.
- The molten slag is mainly constituted by silicates and alumina from the raw-material iron-ore and by some oxides from the limestone. This product is also lighter and floats on the top of the molten iron.
- To granulating process of molten slag implies its cooling in large volumes of water. This rapid cooling optimizes the cementitious properties averting the formation of larger crystals. The resulting granular material contains ≈ 95 % amorphous calcium-aluminosilicates.
- This product is finally dried and ground in a rotating ball mill to a very fine powder that is called GGBS.

The blast furnace slags are off-white in colour and are mainly constituted by calcium oxide (CaO), silicon dioxide (SiO_2), aluminium oxide (Al_2O_3), and magnesium oxide (MgO), along with some other minor oxides in small quantities. Figure 3 shows a flow chart of the ironmaking processes and how the blast furnace slag is obtained. This product presents both cementitious and pozzolanic properties, which means that when in contact with water or water and calcium hydroxide, at ordinary temperatures, the GGBS will react chemically to form compounds possessing cement properties (Siddique and Cachim, 2018).

Nowadays, the GGBS is a supplementary cementitious material that has allowed the reduction of cement proportion in concrete, making it concrete more sustainable. It is economically available in large quantities, and it is suitable for use in ready-mix concrete, in the production of large quantities of site batched concrete and in precast product manufacturing (Samad and Shah, 2017).

Table 1 presents the environmental impact resulting from the production of one tonne of GGBS compared with Portland cement, according to Higgins, 2006. The raw product for GGBS production is molten slag,

which is a by-product of the ironmaking process. As a by-product, only the energy used for processing and grinding the GGBS was considered.

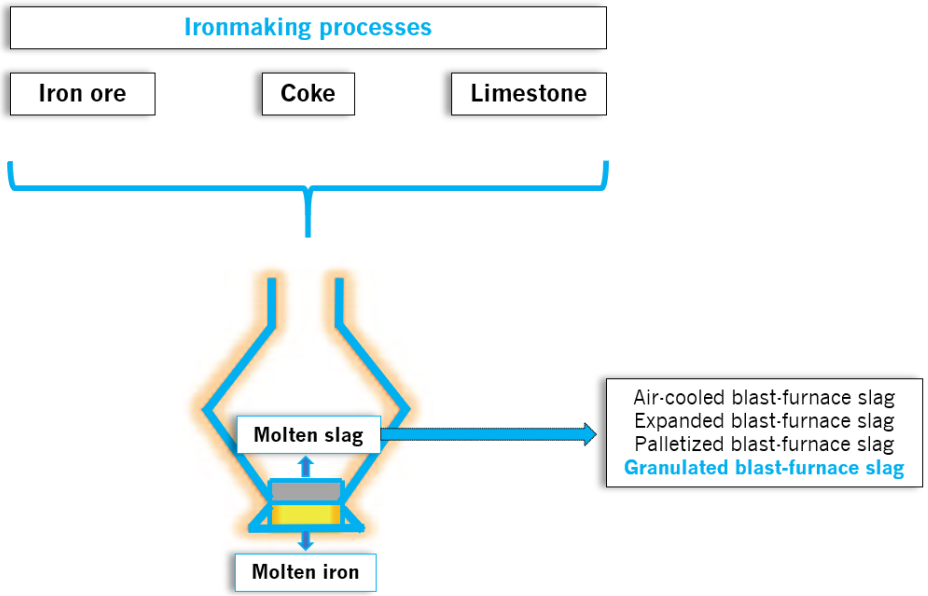

Figure 3.Flowchart of ironmaking process (adapted from Schoenberger, 2001)

Table 1. Environmental impact from GGBS and Portland cement production (Higgins, 2006)

Source	Measured as	Impact	
		Manufacture of 1 tonne of GGBS	Manufacture of 1 tonne of PC
Climate change	CO_2 equivalent (tonne)	0.05	0.95
Energy use	Primary energy (megajoule, MJ)	1300	5000
Mineral extraction	Weight quarried (tonne)	0	1.5
Waste disposal	Weight to tip	1 tonne saved	0.02 tonne

Nowadays, coal is the main source of energy throughout the world and, in 2015, supplied 29 % of the energy worldwide. Even with the increase in the use of renewables, the share of coal is expected to be 24 % by 2035. Up to 2035, the global energy consumption will increase by 30 % and, therefore, the volume of coal consumed per year will also increase from 3840 million tons oil equivalent (mtoe) in 2015 to 4032 mtoe in 2035. China is now the world's largest coal consumer, with 50 % of the global demand or 1920 mtoe, which is expected to remain until 2035, accounting for 47 % of global demand. India's coal consumption is expected to more than double between 2015 and 2035 (from 407 to 833 mtoe) to feed its power sector. The United

States' demand is expected to fall by half in 2035, from 396 mtoe in 2015 to 198 (British Petroleum, 2018). Bhatt et al., 2019 reported that only 1/4th of the total production of FA is reused, being that China and India have less than 50 % of utilisation rate. Denmark, Italy, and Netherlands have a 100 % FA utilization rate.

The FA is a by-product that results from the combustion of pulverised coal in electric power generating plants that has been recognized as problematic solid waste all over the world. During the combustion process, mineral impurities in the coal (clay, feldspar, quartz, and shale) fuse in suspension and float out of the combustion chamber with the exhaust gases. As the fused material rises, it cools and solidifies into spherical glassy particles referred to as FA. This by-product is separated from the exhaust gases using electrostatic precipitators or bag filters. The FA properties change considerably with the coal composition and plant operating conditions (boiler configuration, burning condition and temperature of the boiler, the particle size of the coal, and the gas cleaning equipment) (Mukherjee et al., 2008). More than 70 % of waste coal ash is categorised as FA, fine particulates captured by control equipment, ranging in size from 0.5 μm to 300 μm (Yao et al., 2015).

The FA precursor is a heterogeneous material, mainly constituted by SiO_2 (both amorphous and crystalline), Al_2O_3, and CaO. It is predominantly spherical in shape and mostly amorphous in nature. Through pozzolanic and/or hydraulic activity, the fly ashes contribute to the properties of hardened concrete. This industrial by-product is currently used as material for cement replacement in concrete or for many other building applications such as in road base, clean fill, filler in asphalt and mineral filler (Ghassemi et al., 2004).

The American Society for Testing Materials standard ASTM C 618, 2012 classifies the FA into two chemical types based on their industrial applications, Class F and Class C. Fly ashes with more than 70 % wt. % SiO_2+Al_2O_3+Fe_2O_3 are classified as Class F, while those with a SiO_2+Al_2O_3+Fe_2O_3 content between 50 % and 70 wt. % are classified as Class C. Also, Class C FA typically have a higher calcium content (CaO ≥ 15 %) than Class F (CaO < 5 %) (Ramme and Tharaniyil, 2004).

Class F FA presents pozzolanic properties, which means that the silica compounds react with calcium hydroxide at room temperature forming compounds with cementitious properties. In this case, the addition of an activator, such as quicklime or hydrated lime mixed with water, is needed to form cement since CaO

levels in Class F are low. On the other hand, Class C FA, with higher levels of CaO, presents self-cementing properties when in contact with water, hardening and getting stronger over time (Bhatt et al., 2019).

According to Higgins, 2006, the replacement of Portland cement by GGBS or FA into the concrete leads to a substantial reduction of greenhouse gas, primary energy use and mineral extraction. These values are reported in Table 2.

Table 2. Environmental impact for 1 tonne of concrete (Higgins, 2006)

Impact	100 % Portland cement	50 % GGBS	30 % FA
Greenhouse gas (CO_2) (kg)	142	85.4	118
Primary energy use (MJ)	1070	760	925
Mineral extraction (kg)	1048	965	1007

One important factor of measuring the sustainability of building materials is the *Embodied Energy*, which is, for any product system over the duration of its life, the energy consumed for raw material extraction, transportation, manufacture, assembly, installation, disassembly and deconstruction (Cement and Concrete Institute, 2011). Therefore, a material with low embodied energy is more sustainable. The embodied energy is measured in Embodied CO_2 (ECO_2), and it is normally expressed as CO_2 per mass (kg CO_2/tonne) or CO_2 per unit volume (kg CO_2/m^3). Table 3 summarises the ECO_2 determined for Portland cement, GGBS and FA for the year 2010 (United Kingdom Quality Ash Association, 2010).

Table 3. Embodied CO_2 of Portland cement, GGBS and FA (United Kingdom Quality Ash Association, 2010)

Materials	Embodied CO_2 (kg/tonne)
Portland cement Type I (CEMI)	913
GGBS	67
FA	4

Sodium hydroxide is a versatile product often referred to as caustic soda. This product is often commercialised in powder, flakes, and beads, all with the same chemical composition. The only difference is the shape and particle size. The required concentration of NaOH can be obtained by dissolving an adequate amount of this product in water. A large amount of heat is released during the NaOH dissolution. Some safety procedures should be considered during the NaOH handling:

- Avoid contact with eyes, skin, and clothing. Do not inhale, and wear protective eyewear, gloves, and clothing. Only use this substance in well-ventilated areas.
- Since the NaOH dissolution results in an exothermic reaction, the NaOH must be added to water and water must not be added to the NaOH. The water should not be cold or hot but should be warm, around 30°C - 40°C (Shi et al., 2003).

The NaOH is one of the most versatile chemicals, and it is produced through the electrolysis of sodium chloride with mercury, diaphragms, or membrane cells (Hong et al., 2014). It is both a resource-intensive and energy-intensive process since the electrolysis of sodium chloride implies significant electrical energy consumption, including the energy consumed during the brine extraction, essential to produce sodium chloride (Lima et al., 2010) The NaOH industry also has a significant contribution to carbon emissions, since numerous toxic compounds are also released into the atmosphere, including heavy metals and organochlorine compounds (Hong et al., 2014).

The Na_2SiO_3 or water glass is a compound obtained through fusion of silica and sodium carbonate together, under temperatures of 1300°C, and dissolution in water to produce an aqueous form. Over this process, large amounts of CO_2 are released into the atmosphere, and high energy consumptions are required to cause the fusion (Brykov and Korneev, 2008; Cristelo et al., 2015; Torres-Carrasco and Puertas, 2015). The characteristics of the commercial liquid Na_2SiO_3 are dependent on its composition that can be prepared by the mass ratio of SiO_2 to Na_2O from 1.60 to 3.85 (Amer et al., 2021). The toxicity of Na_2SiO_3 is dependent on the silica to alkali ratio and on the pH. Since it is an alkaline product, the Na_2SiO_3 should be handle with care. The same safety procedures for NaOH should be considered for the Na_2SiO_3 handling.

The financial cost associated with the production of the commercial reagents, such as NaOH and Na_2SiO_3, can add up significantly to the overall financial cost of the AABs. The use of commercial activators has hindered the environmental and financial performance of AABs. In an attempt to overcome this issue, scientific research has been undertaken, more recently, devoted to the use of wastes or industrial by-products as alkaline activators.

One of the industrial by-products that has been recently investigated is a strong sodium alkaline solution used to clean the aluminium extrusion dies called 'cleaning solution' (CS). This solution, after some cycles, becomes less reactive and is discarded, which represents a financial cost of 80 Eur/ton to the Portuguese industry for proper landfilling, considering that approximately 1000 tons of CS are produced per year (Cristelo et al., 2019). When discarded, the CS contains both NaOH and sodium aluminate ($NaAlO_2$) due to the dissolution of a superficial thin layer of aluminium. Currently, the published papers using this waste are devoted to the development of the AAB formulations with no particular practical application.

2.1.3 The use of blast furnace slags and low calcium fly ash in soil stabilisation

Nowadays, there is already significant research concerning the performance of AABs. Published papers about the type of gels formed based on the materials used, strength and stiffness gains are becoming more common in the literature. However, the large variability of precursors and activators and the heterogeneous composition of each waste make the chemical and mechanical characterisation of these binders a hard task. To overcome these issues, more studies are required in this field. In the context of geotechnics, the use of AABs to improve undesirable geotechnical properties of problematic soils is still relatively incipient. The mechanical performance of soils stabilised with AABs still needs to be more investigated, mainly when it implies complex analyses such as shear behaviour, *in-situ* performance, and numerical modelling. In this Chapter, relevant publications on the use of GGBS, FA, NaOH and Na_2SiO_3 for soil stabilisation will be presented.

Cristelo et al., 2013 investigated the rheological properties of alkaline activated FA used in *jet grouting* applications. The authors analysed six different grout compositions, defined based on Na_2O (alkali)/ash and activator/ash ratios. The activator was composed of Na_2SiO_3 and two different NaOH concentrations: 10.0 and 12.5 molal. Results showed a correlation between the fluidity of the grouts and UCS, with an increase of the former resulting in a decrease in the latter, which is a concern in *jet grouting* applications. The authors observed that this type of material seems to be less porous than cement-based grouts and presents higher drying shrinkage results than usual for concrete, which is in accordance with other authors.

Cristelo et al., 2015 carried out a study where the mechanical performance of a large spectrum of activator-ash-soil formulations used to build jet mixing columns was assessed, together with the financial costs and CO_2 (eq) emissions. The results showed a significant increase in strength, still well above the average values expected when improving the stress-strain behaviour of a poor soil. In terms of financial costs, the cement-based solution revealed to be more advantageous than the ash-based solution, with an average cost of 90 % of the cost of the ash-based solutions. On the other hand, the environmental analysis demonstrated that ash solutions are more efficient, presenting emissions of CO_2 33 % lower in relation to the emissions related to cement mixtures. The authors affirmed that the use of an industrial waste capable of activating FA replacing the activator could reduce the financial costs of the AABs and further increase the differential of the environmental performance between these two solutions.

Sargent et al., 2013 investigated the use of alkali-activated wastes on the enhancement of the mechanical properties and durability of an artificial soil produced by mixing fine silica sand with kaolin. Alkali-activated and non-activated pulverized FA, GGBS and red gypsum (RG) were added to the soil at 10 % by dry weight, both individually and together. The activator was composed of NaOH and Na_2SiO_3 at a ratio of 1:2. Of the mixtures tested, the alkali-activated blast furnace slag mixtures exhibited the highest strengths. The authors concluded that the AABs have the potential to be used as a replacement for Portland cement and lime in soil stabilisation.

Sargent et al., 2016 investigated the use of activated blast furnace slags at dosages of 2.5 % - 10 %, cement and lime for the stabilisation of an alluvial soil. The aim was to identify the most effective binder and corresponding dosage. The highest strength, stiffness, and durability were observed for the soil mixtures stabilised with 7.5 % and 10 % of NaOH-GGBS, both complying with the criteria required by EuroSoilSlab (2002). Also, the use of NaOH-GGBS binder showed to be potentially more sustainable than traditional binders. From the financial point of view, the GGBS-NaOH binder had a higher financial cost than cement.

Sharma and Sivapullaiah, 2016 evaluated the potential of using a binder constituted by FA and GGBS at a mixing ratio of 7:3 to reduce the swell potential and increase the UCS of an artificially expansive soil. The authors concluded that the addition of a binder or lime to the soil decreased the liquid limit and plasticity index and increased the shrinkage limit. The addition of a binder caused the flocculation of clay particles and

increased the number of coarser particles, which contributed to the reduction of the Atterberg limits. Compaction tests revealed a reduction of the optimum water content and an increase of maximum dry density with the increase of the binder content. The addition of 1 % of lime significantly increased the strength of the mixture. SEM and XRD analyses showed the formation of the C-S-H type gel.

Shubbar et al., 2018 developed a low carbon binder produced by blending Portland cement, GGBS and high calcium FA. The newly developed binder was constituted by 35 wt. % Portland cement, 35 wt. % GGBS and 30 wt. % of high calcium FA, with compressive strength and surface electrical of 30.8 MPa and 103.5 kΩ.cm after 56 days of curing. Also, the statistical analysis showed that the influence of the parameters examined on the development of the compressive strength of the mortars could be modelled with a coefficient of determination R^2 of 0.893 and that the importance of these parameters followed the order: curing time > high calcium FA% > Portland cement% > GGBS%.

Sukprasert et al., 2021 evaluated the influence of the following factors, FA: GGBS replacement ratio, NaOH concentration, and curing temperature, on the mechanical and microstructural properties of a silty sand. The authors found that the UCS values of FA based geopolymers with silty sand/GGBS blends increased with increasing NaOH concentration when cured at 25°C, 50°C and 80°C. An elevated curing temperature accelerated the geopolymerization reaction, leading to a higher UCS. The decrease in FA:GGBS ratio reduced the specific area of particles to be welded by FA geopolymerization products and reduced the geopolymer gel.

Phummiphan et al., 2018 developed a low-carbon pavement base material using GGBS as a replacement material and Class C FA as precursor for the geopolymerization process. The authors analysed the influence of GGBS content, Na_2SiO_3/ NaOH ratio, and curing time. The outcomes revealed that GGBS can be used as a replacement material with FA geopolymer to stabilise the marginal lateritic soil for the development of a low carbon stabilised pavement base. The amount of 10 % is the recommended one at high Na_2SiO_3/ NaOH ratios (> 80:20).

Xu and Yi, 2019 investigated the use of ladle furnace basic slag, which is a by-product from the steel refining process to alkali activate the GGBS for stabilising soft clay and immobilizing heavy metals. The authors

observed that the use of ladle furnace basic slag/GGBS at ratios of 2:8 - 5:5 led to a similar or even higher UCS results than when Portland cement is used after 56 days.

Lang et al., 2020 investigated the feasibility of using lime and carbide slag to activate GGBS as a potential substitute to Portland cement for stabilising dredged sludge. After 28, 60, and 90 days, the UCS using 20 % lime-GGBS to stabilise the dredged sludge was 1.38, 1.14 and 1.06 times higher than 15 % of Portland cement. Using 20 % carbide slag-GGBS, these values were 1.45, 1.12 and 1.02 times higher.

Mujtaba et al., 2018 assessed the engineering properties of two expansive soils stabilised with GGBS in proportions between 0 % and 55 %. In both soils, the laboratory tests showed that the maximum dry unit weight increased up to 10 % by adding 50 % GGBS. There was an increase in the CBR results after mixing 50 % GGBS from 3.2 % to 11.5 % for DG Khan soil and from 2.4 % to 10.7 % for Sialkot soil. The addition of 30 % GGBS to DG Khan soil reduced its swell potential from 8 % to 2 %. For Sialkot soil, the addition of 20 % of GGBS reduced its swell potential from 5 % to 2 %.

In most alkaline binders rich in Si and Al with low content of Ca, the development of the mechanical properties may not be fast enough in situations that require high strength and stiffness at younger ages (e.g., Class F FA). To overcome this issue, Rios et al., 2018 investigated solutions to increase reaction kinetics of alkali-activated FA binders for soil stabilisation of a silty sand pavement sub-base. Binders composed of FA, lime, sodium chloride (NaCl) and alkaline solutions (with NaOH and Na_2SiO_3) were mixed with soil and then subjected to UCS tests, triaxial tests and ultrasonic tests to evaluate the strength evolution with time. The results showed that the alkaline-activated mixtures based on soil, lime and FA were the most efficient in terms of UCS and stiffness. The addition of NaCl was particularly effective in increasing the rate of resistance development in the non-activated soil-lime and soil-lime-FA mixtures. Regarding the alkali-activated mixtures with FA, the addition of NaCl did not have a significant impact on the increase in strength and even impaired short-term behaviour. The alkali-activated soil-lime-FA mixtures exhibited a triaxial behaviour of a cemented soil, with peak values of cohesion and friction angles higher than 500 kPa and 50° and residual values higher than 27 kPa for cohesion and 49° for the friction angle.

Chowdary et al., 2021 assessed the strength and durability characteristics of geopolymer stabilised soft soils for deep mixing applications. The influence of binder content (10, 20, and 30 %), activator/binder ratio (0.5, 0.75, and 1.0), and initial soil moisture content was investigated. The results of UCS tests, flexure strength and durability against wetting drying cycles showed that a binder dosage higher than 10 % and an activator/binder ratio greater than 0.5 are necessary to meet the requirements of deep mixing applications. The increasing of the initial soil moisture content led to a reduced strength under unconfined compression and flexure, and thus increased binder dosage is required to meet the deep mixing requirements.

Lang et al., 2021 evaluated the effect of water content on the strength development and microstructure of a stabilised dredged sludge using GGBS activated with only NaOH and/or Na_2SiO_3. The authors observed that the optimum single activator content tended to increase with the increase of water content. The use of both activators showed to be more effective than a single one, with higher UCS results of stabilised dredged sludge. XRD and SEM analyses suggested that calcium silicate hydrate and calcium aluminate hydrate were the major hydration products. The results suggested the use of 20 % NaOH/Na_2SiO_3-GGBS binder with an optimum of 2/3, 2/3 and 1/4 as the replacement of equivalent Portland cement for the stabilisation of dredged sludge at a water content of 60, 70 and 80 %, respectively.

Wattez et al., 2021 investigated the interactions between alkali-activated blast furnace slags and organic matter for soil stabilisation/solidification, and they found that only NaOH activated slag is a suitable AAB for subbase layer development.

2.2 Current understanding on the mechanical behaviour of remoulded and stabilised clays with Portland cement and alkali-activated binders

2.2.1 Critical state in clays

According to ASTM D 2487, 2011, clay is a fine-grained soil, with 50 % or more soil particles passing a No. 200 (75-μm) US standard sieve and plasticity index ≥ 4, and the plot of plasticity index versus liquid limit falling on or above the “A” line. It is a potentially problematic soil, typically characterised by its undesirable geotechnical properties, such as high-water content, low strength, and susceptibility to large settlements.

Clay minerals are small particles that belong to the group of hydrous layer aluminosilicates (Civan, 2007). There are three main groups of clay minerals: kaolinite, which is a non-swelling clay, illite and smectite, also known as montmorillonite (Grim, 1942). Montmorillonite minerals present a high degree of swelling.

The nature and diversity of the geomechanical process involved in soil formation, including the stress to which the soil has been subjected, the formation environment, and the elapsed time in the geotechnical time scale, are responsible for the wide variability in the *in-situ* state of soils (Horpibulsuk et al., 2004). The time effect has a huge impact on the clay structure. The soil is left to age and creep, and the natural bonds develop at particle contacts. These natural bonds are the key component that controls the behaviour of the natural clay.

Some complex physicochemical processes happen in soil-water systems due to the soil mineralogy, amount of clay, organic substances, etc. (Chibowski, 2011). Two physicochemical processes, flocculation and dispersion, are common in clay soils and affect their properties. These physicochemical processes are affected by the electrochemical environment during the time of sedimentation, including pH, acidity, temperature, type of ions present, ionic strength and adsorption of the ions, etc. During flocculation, the clay particles dispersed in a solution come into contact and adhere to each other, leading to the formation of soil aggregates, including cemented clay clusters, flakes, or larger clusters. In the flocculated fabric, the clay particles can be associated with edge-to-face or edge-to-edge contacts, as shown in Figure 4. Dispersion is the process where the individual particles are liberated from each other and form a dispersion.

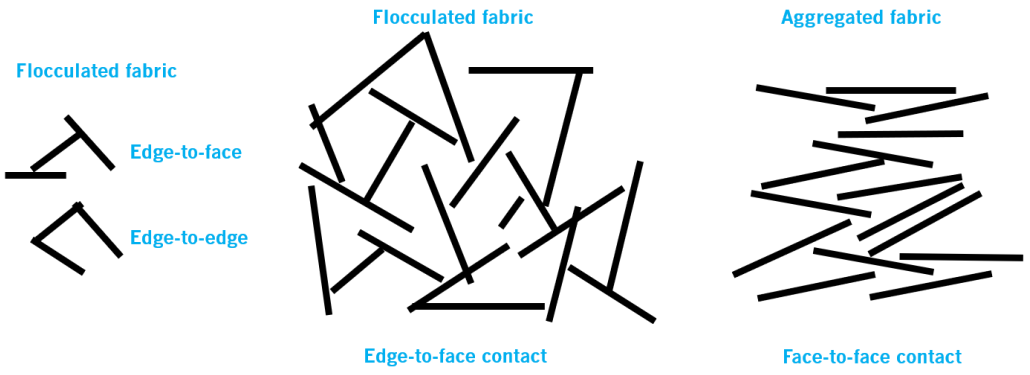

Figure 4. Clay fabric (adapted from Mitchell, 1993)

The fundamental behaviour of clays has been described qualitatively in terms of their fabric and structure since Casagrande, 1932 and Lambe, 1958, among others, presented their concepts on the internal make-up of this soil. According to Altschaeffl and Thevanayagam, 1991, the fabric refers to the geometrical arrangement of individual particles in a soil, including the geometrical distribution of pore spaces. The structure describes the combined effect of fabric, composition, and interparticle forces between the particles (Altschaeffl and Thevanayagam, 1991). The structure is, therefore, related to the gradation (e.g., inter-particle forces) and arrangement of soil particles, porosity, and pore size distribution, bonding agents and the specific interactions developed between particles through associated electrical forces. The soil fabric considers only the geometric/spatial arrangement of the constituent minerals particles, including void space.

Understanding the shear behaviour of potentially problematic soils, such as clays, is of utmost importance for strength and deformation analysis at short- and long-term conditions and the development of geotechnical engineering projects.

The critical state framework was proposed by Roscoe et al., 1958 and cited by Hattab, 2011. This theory was based on observations from triaxial compression tests on saturated clays, which revealed behavioural patterns that indicated the relationship between shear strain and deformation. The critical state of a soil was defined as an ultimate state toward which all triaxial path tend. At this stage, plastic shearing could continue indefinitely without any changes in the void ratio (e) and effective stresses in (e, p', q) space. Its projection in effective mean effective stress (p') - deviatoric stress (q) space is a straight line passing through the origin with the slope equal to the critical state line (M), and the projection in e - log p' space is the critical state line (CSL), which is parallel to the isotropic compression line (ICL), also known as the normal compression line. Roscoe et al., 1958 also introduced the notion of the critical void ratio (e_c), which represents the final e of the soil at ultimate strength. Many researchers develop constitutive models based on the critical state theory, such as the elastoplastic Cam clay-like models (Roscoe and Schofield, 1963; Roscoe et al., 1963; Schofield and Wroth, 1968), or more sophisticated models, like Dafalias and Herrmann, 1982 for bounding surface formulation of soil plasticity (Hattab, 2011).

The mechanical behaviour of clays is characterised to be nonlinear, plastic and time-dependent (viscous). The structures of clays found *in situ* vary greatly, depending on their formation processes and their

mechanical, electrochemical, and biological histories, and the mechanical behaviour of these soils may be highly dependent on their structure. In critical state mechanics, the state of the soil is characterised by three parameters, namely p', q and e. When a saturated clay is subjected to external pressure, the pressure is initially supported by the water in the pores, which leads to the generation of pore water pressure. If drainage is permitted in the system, the excess water begins to flow out of the soil matrix. As the water dissipates, the pressure is gradually transferred to the soil skeleton, and there is the rearrangement of the soil particles. The stress-history of the clays is defined based on the soil consolidation history. The behaviour of clays is conventionally identified as normally consolidated and overconsolidated clays, depending on the present and past history (Nagaraj et al., 1997). A normally consolidated clay is the one that is currently experiencing the maximum overburden effective stress in its history. An overconsolidated clay has already experienced a higher overburden stress in the past. The overconsolidation ratio (OCR) is defined as the ratio between the maximum overburden effective stress that the clay has experienced and the current overburden effective stresses. Briefly, the clay overconsolidation causes an increase in strength and reductions in permeability and settlement.

Under axisymmetric compression conditions, the isotropic part (p') of the stress tensor is defined by $p' = (\sigma'_1+2\sigma'_3)/3$ and the deviatoric part by $q = \sigma'_1 - \sigma'_3$, wherein σ'_1 is the major principal effective stress and σ'_3 is the minor principal effective stress (Figure 5). Two different behaviours can occur in clays:

- A contractile behaviour for normally (OCR = 1) or lightly overconsolidated (OCR ≈ 1) state, with a decrease of the void ratio (e) in drained condition (Figure 5 (a)) and decrease of the p' in undrained condition (Figure 5 (b)). There is a gradual evolution of both e and q, with respect to axial strain (ε), toward an ultimate state.
- A dilatancy behaviour when the OCR increases, with a contractile behaviour (decrease of e) in the first stages of the loading, followed by a dilatancy characterised by an increase of e in drained conditions (Figure 5 (a)) and an increase of p' in undrained conditions (Figure 5 (b)). At this stage, stress state and e converge to the critical state line (CSL) in $p' - q$ space and e - log p' as shown in Figure 5 (a) and (b).

The $M = q/p'$ parameter, that is, the slope of the line representing the critical states, can be associated with the Mohr-Coulomb criterion, which defines the failure envelop through the critical friction angle (ϕ'_c), according to the expression, $M = (6\sin \phi'_c)/(3 - \sin \phi'_c)$, for compression tests.

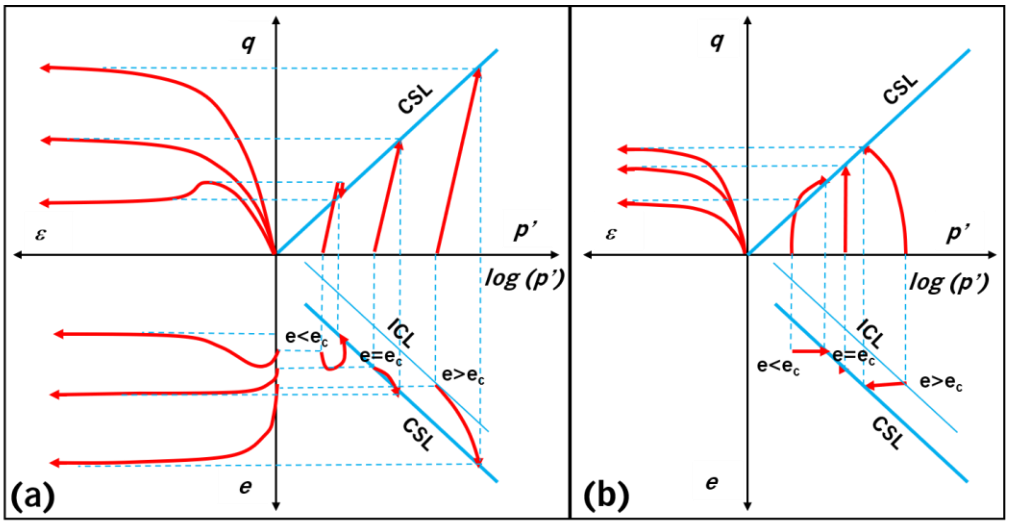

Figure 5. Schematic representation of the mechanical behaviour of clays: drained (a) and undrained (b) behaviour (adapted from Yin et al., 2013)

2.2.2 Stress-strain response, stiffness degradation and stress-path of remoulded clays

The shear behaviour of clay soils has been widely investigated by many researchers (Atkinson et al., 1990; Balasubramaniam, 1975, 1973, Roscoe et al., 1963, 1958), and is dependent of several factors, including the soil composition, structure, *in situ* stress-state, stress-history, degree of saturation, drainage conditions, loading conditions, including the effective stress-path and types of loading. The soil composition is related to the particle size distribution, size and shape of grains, content in organic matter, the mineralogy of the clay fraction, and soil chemistry.

According to Jardine (Jardine, 1992, 1991, 1985) cited by Correia, 2004, the reference shear behaviour of soils can be described from a model with multiple surfaces that delimit different zones, each one with a characteristic behaviour. When the soil (point O, Figure 6) is shear loaded, the soil behaviour can be described as follows:

- Zone I corresponds to the region where a shearing action from O up to the surface Y1 results in a linear elastic behaviour, that is, until it reaches the deformation ε_{y1} (corresponding to the OA region of the degradation curve of secant deformability modulus with strains (E(ε)). This value of strain is generally $\varepsilon \leq 10^{-6}$ (0.0001 %).
- In Zone II, which corresponds to the continuation of the shearing action until reaching the Y2 surface, the stress-strain behaviour is elastic, nonlinear, and hysteretic, that is, in loading-unloading cycles, the soil presents a complete recovery, without permanent deformations (corresponding to deformations between ε_{y1} and ε_{y2} and AB region). There is a decrease of the secant modulus with the increase of deformation. The energy dissipated in these hysteretic cycles is thought to be the result of yielding or crushing at the local level in the contacts between the particles and the viscosity of the soil constituent elements.
- In Zone III, which corresponds to the continuation of the shearing action for deformations higher than ε_{y2}, there is a continuation of the E_{sec} decrease (BC region) and an increase of the irreversible deformations (plastic). These plastic deformations are higher as the action approaches the surface Y3. The ε_{y3} value corresponds to the value of strain at peak resistance. For deformation levels higher than ε_{y3} (beyond the Y3 surface), irreversible or plastic deformations become dominant.

The initial or maximum stiffness modulus is an important soil parameter related to the predictions of the ground movements and field data interpretations. Atkinson and Sallfors, 1991 classified the strain levels into three categories:

- Very small strain level for shear strains (ε_q) ≤ 0.0001 %. At this level, the stiffness modulus is constant in the elastic range.
- Small strain level for 0.0001 % ≤ ε_q ≤ 0.1 %. Within this range, the stiffness modulus varies non-linearly with the strain.
- Large strain level for ε_q ≥ 0.1 %. The soil is close to failure and the soil stiffness is relatively small.

Parry, 1960 performed a series of drained and undrained compression triaxial tests on remoulded saturated clay specimens. The clay specimens were normally consolidated or overconsolidated before testing. The results of drained and undrained compression tests where the radial effective or total stress was kept

constant while the axial effective or total stress increased allowed the author to draw the following conclusions:

- Stress-strain and volume-change characteristics of saturated remoulded clays are strongly affected by the overconsolidation ratio and the drainage conditions.
- On normally consolidated specimens, the drained compression tests showed a substantial volume decrease during strain. The undrained compression tests showed an initial rapid pore-pressure increase, reduced to a negligible rate of change at failure. Although the tests were stopped shortly after failure, the trend of the results indicated that, under both drained and undrained conditions, no drop in strength would have occurred under continued strain.
- On heavily overconsolidated specimens, the drained compression tests showed an initial volume decrease followed by a continued volume increase at failure. The undrained tests showed an initial pore-pressure increase followed by a pore pressure decrease with a negligible rate of change at failure.
- The lightly overconsolidated specimens presented an intermediate behaviour between normally consolidated and overconsolidated specimens.

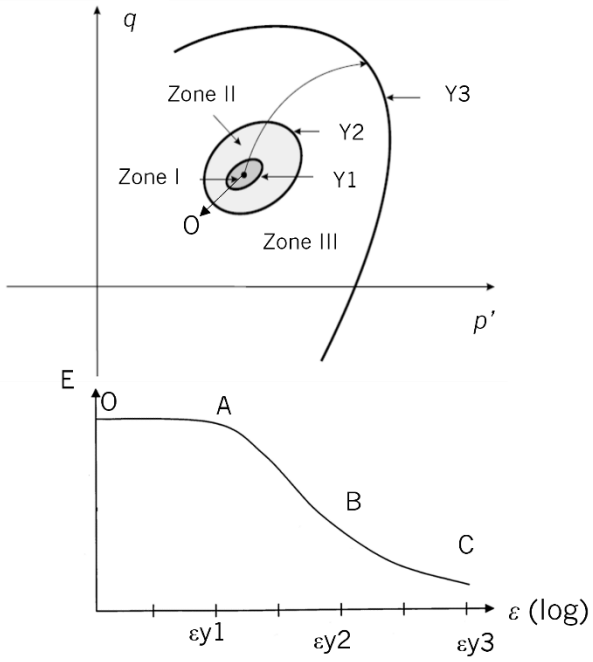

Figure 6. Reference behaviour of the soils (adapted from Jardine, 1992)

Hattab and Hicher, 2004 investigated the influence of the OCRs on the dilatant behaviour of a remoulded clay. All specimens were isotopically loaded up to the maximum consolidation pressure of 1000 kPa and then unloaded to the final desired consolidation pressure. The ratio between the maximum and final consolidation pressure gives the overconsolidation ratio applied to the specimens, which varied between 1 and 50. Figure 7 and Figure 8 illustrate the findings of the authors in terms of stress-strain behaviour, volumetric strain (ε_v (%)) and stress-path in relation to the OCR. The authors observed that the normally consolidated specimens are characterised by straight critical state (*M*) line as defined in the Cam clay model (Roscoe et al., 1958), while the overconsolidated specimens with OCR > 2 by a curve called ζ that represents the envelope of peak strength situated above *M*. Also, they verified that the respective position of *M* and ζ indicates that the peak friction angle is an increasing function of OCR. The *M* and ζ are intrinsic characteristics of the clay and in the plane (p' - q) delimit the size of the domain accessible by different stress-paths. Inside these boundaries, the stress plane can be divided into regions corresponding to a contractant, dilatant or no-volume change along the deviatoric stress paths. It was observed a contractile behaviour for OCR values between 1 and 2.5 and a dilatant behaviour for all the specimens with OCR > 2.5. During loading, the overconsolidated specimens dilate after having reached a given value of the deviatoric stress, while the normally consolidated or the slightly overconsolidated specimens showed a contractile behaviour since the beginning of the loading. Dilatant behaviour for OCR > 2.5 or a contractile behaviour for OCR < 2.5 started after an initial no-volume change phase.

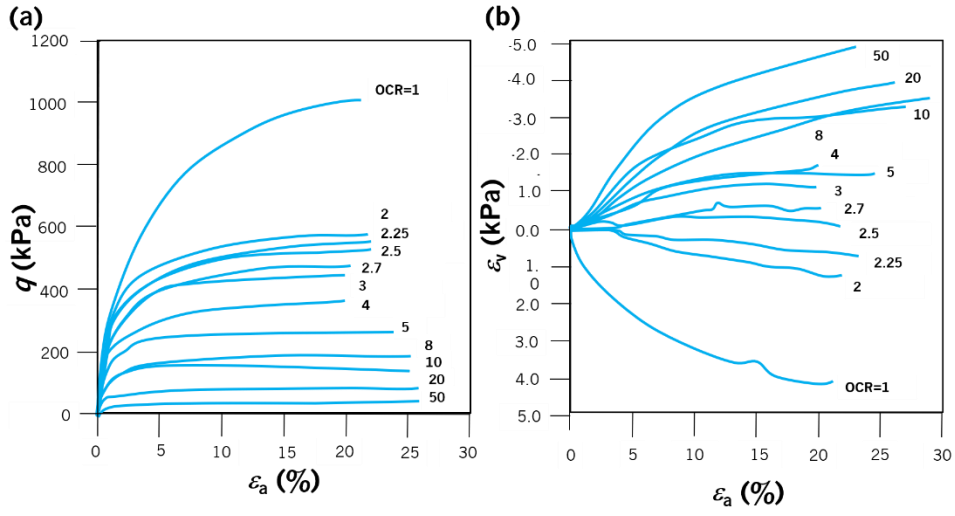

Figure 7. Stress-strain (a) and volumetric strain (b) responses (adapted from Hattab and Hicher, 2004)

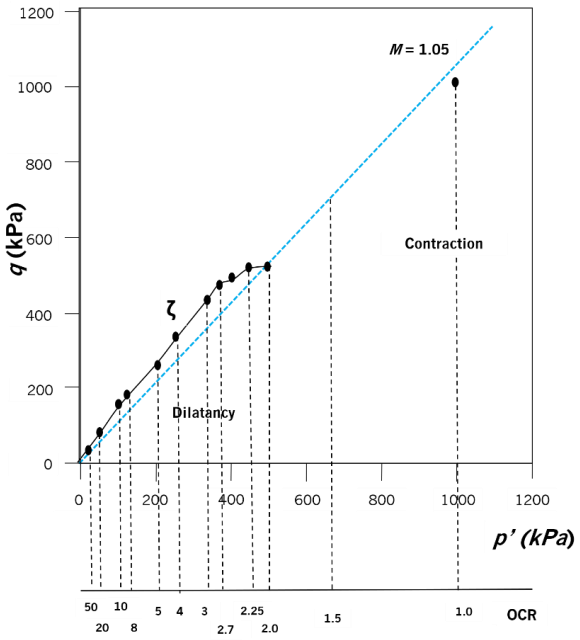

Figure 8. Stress-path responses (adapted from Hattab and Hicher, 2004)

In order to understand the deformation characteristics of the overconsolidated clays, a series of one-way cyclic tests and triaxial compression tests under undrained conditions with different OCRs was carried out by Gu et al., 2016 on reconstituted clay specimens. The remoulded specimens were initially loaded up to the maximum desired confining stress and then unloaded up to a final pressure of 100 kPa. All specimens started the shearing phase with the same p'_0=100 kPa, which allowed to directly analyse the impact of OCR on the results presented in Figure 9 and Figure 10. The OCR was varied between 1 and 8.

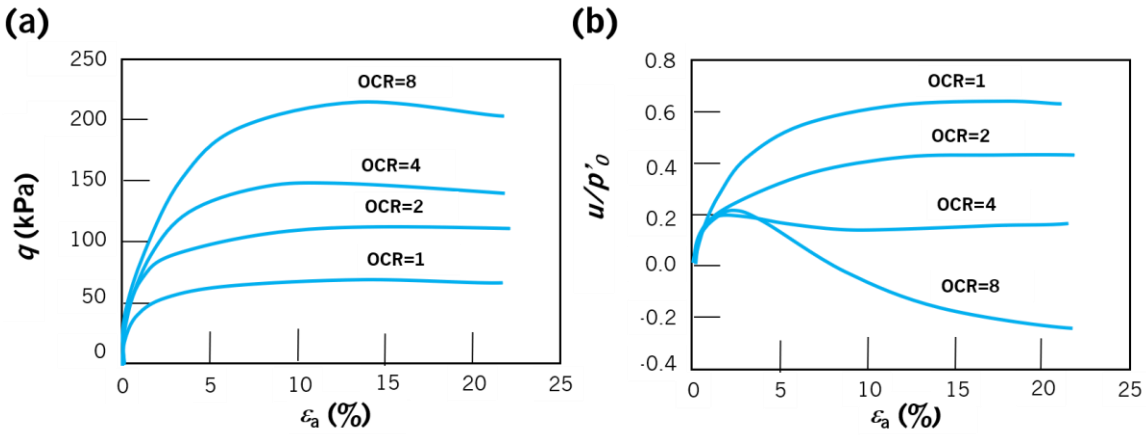

Figure 9. Stress-strain (a) and pore pressure (b) responses (adapted from Gu et al., 2016)

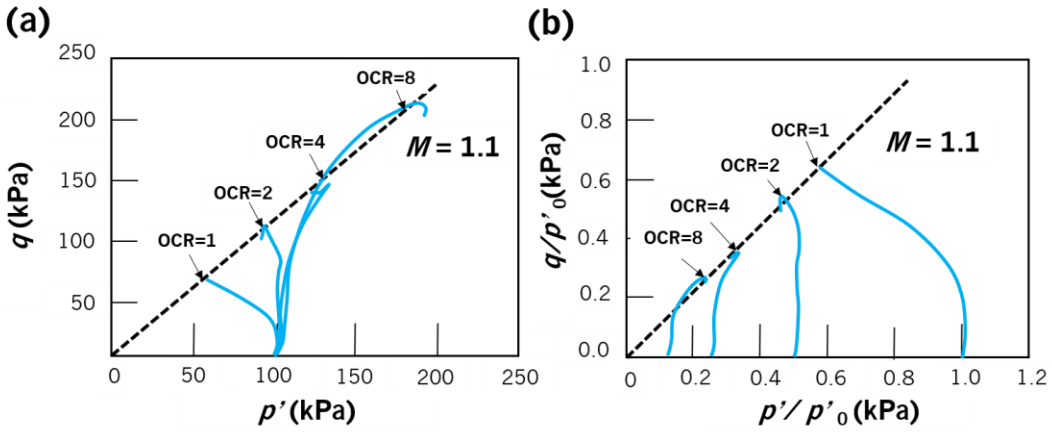

Figure 10. Stress-paths: before (a) and after (b) normalisation (adapted from Gu et al., 2016)

From the monotonic undrained triaxial compression tests, which are the main topic addressed here, Gu et al., 2016 observed that the shapes of all the stress-strain curves (Figure 9 (a)) are similar to each other. However, the peak shear strengths are very different. There was an increase in peak shear strengths with the increase of OCR. The OCR also affected the pore pressure variation, with the appearance of negative excess pore water pressure under higher OCRs. Curves with OCR of 1 and 2 presented a contractile behaviour from the beginning of loading until the end of the tests. This impact is also remarkable in Figure 10, where the effective stress-paths with different OCRs also showed distinct behaviours. A typical normally consolidated stress-path was observed for the tests with OCR=1, with the stress-path turning left. A lightly overconsolidated stress-path was observed for OCR=2 and overconsolidated stress-paths for OCR=4 and OCR=8, turning right before the end of the tests. All stress-paths fell on a straight failure envelope with a slope M=1.1.

The use of piezoelectric transducers, more precisely bender elements (BE), and local instrumentation installed on the surface of the specimens allowed Borja, 1991 and Hashiguchi, 1980 to record the changes in stiffness during the loading process within the range of small strains of the reconstituted clay specimens. The results are presented in Figure 11. The authors reported that the stiffness of the clays varied with the OCRs and the p_0 applied during consolidation.

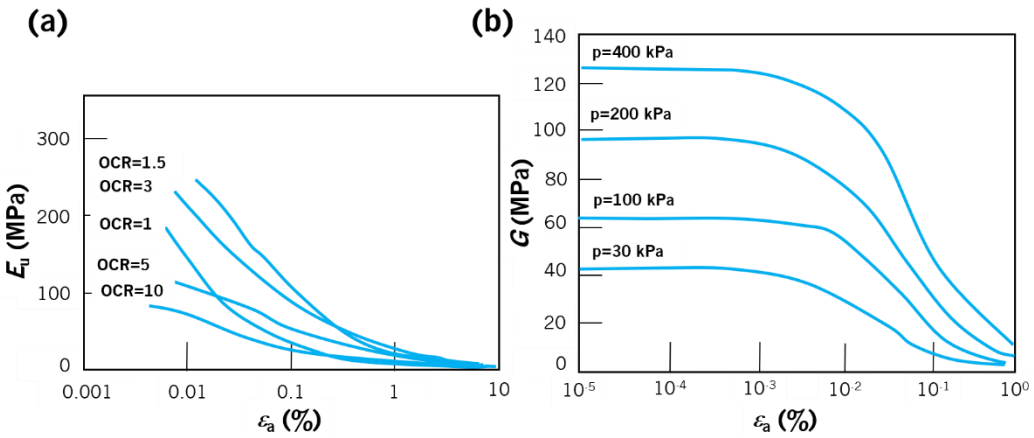

Figure 11. Dependence of clay stiffness on stress and strain level: undrained stiffness modulus (E_u) of Pentre clay (adapted from Hashiguchi, 1980) (a) and shear modulus (G) of a kaolin clay (adapted from Borja, 1991) (b)

2.2.3 Stress-strain response, stiffness degradation and stress-path of stabilised clays

In some geotechnical projects involving clays, stabilisation is needed to improve their geomechanical performance. One of the most frequent stabilisation techniques is the addition of small amounts of cementitious materials to clays. Reduced compressibility, higher bearing capacity and strength are some of the geotechnical properties that are improved with this approach. Their shear behaviour is also strongly changed after the addition of binders.

Whilst there is extensive laboratory research on the performance of soils stabilised with Portland cement and AABs focusing on mechanical tests in a general way, chemical and environmental analyses, research related to the shear behaviour of soils stabilised with AABs is still scarce. At the moment, the majority of the published studies about shear behaviour in stabilised clays were undertaken using Portland cement (e.g. Ho et al., 2021; Horpibulsuk et al., 2010; Kasama et al., 2006; Porbaha et al., 2000; Xiao et al., 2014), and constitutive laws have been developed based on the experimental behaviour of these stabilised materials. Considering that the characterisation of the shear behaviour of clayey soils stabilised with AABs through triaxial tests under different OCRs and p'_0 is one of the aims of this PhD thesis, this Chapter addresses, with more detail, mostly the shear behaviour of this type of soil stabilised with Portland cement and AABs under these conditions. These studies will be the basis for further developments with AABs presented in Chapter 4, 5 and 6.

Horpibulsuk et al., 2004 investigated the undrained shear behaviour of a cemented clay at effective confining pressures lower and higher than the mean effective yield stress. Results from isotropic consolidation tests showed that the mean effective yield stress values are 60, 220, 380, and 1800 kPa for the cemented specimens at cement contents of 6, 9, 12 and 18 %, respectively. The following conclusions were obtained from the triaxial test results at effective confining pressures lower than the mean effective yield stress (see Figure 12 and Figure 13):

- In terms of the stress-shear strain (ε_q (%)) response, the peak deviator stress was not influenced by the effective confining pressure. The peak strengths of the cemented specimens are higher than those observed for the uncemented specimens at the same effective confining pressures. Nevertheless, these peaks of cement specimens are practically equal even as the effective confining pressure increases. This was explained by the cementation, which was responsible for the insignificant changes of the fabric (reorientation of the soil) during the consolidation process.
- The pore pressure development is dependent upon the level of the confining pressure. There was an increase in the peak excess pore pressure with the increasing effective confining pressure. After the peaks, the excess pore pressure begins decreasing and stabilise at the residual state. At low effective confining pressure and higher cement content, there was the break of the specimens in small pieces, which resulted in the development of negative excess pore pressures and the tendency of dilatation depending on the drainage conditions.
- The undrained stress paths are located on the left side of the drained stress paths up to the peak values. After peaks, the paths move to the right side of the drained stress paths and level out.

For the effective confining pressures higher than the mean effective yield stresses, the following conclusions were obtained (see Figure 14 and Figure 15):

- There was an increase of the peak and residual shear strengths and peak excess pore pressure with the increase in the effective confining pressure. The change in fabric (reorientation of particles) during the consolidation phase brings the clay particles closer, enhancing the peak and residual shear strains. The shear resistance of the cemented clay is still higher than the one observed for the uncemented specimens, which implies that the contribution of the cementation bond to the shear

resistance is still available. Therefore, both cementation and fabric affect the triaxial response at this condition.

- The excess pore pressure development is positive, so the stress paths move to the left side (in Figure 15, for instance, the tests carried out with confining pressures equal to 600 kPa, 1000 kPa, 2000 kPa and 4000 kPa at cement content of 12 %).

The authors observed a single failure envelope at effective confining pressures lower and higher than the mean effective yield stress as shown in Figure 15. Higher values of friction angles were observed for cemented clays at cement contents between 6 % to 18 % when compared to the original clay. The cohesion was induced by the cementation, which increased with the increase in the quantity of cement.

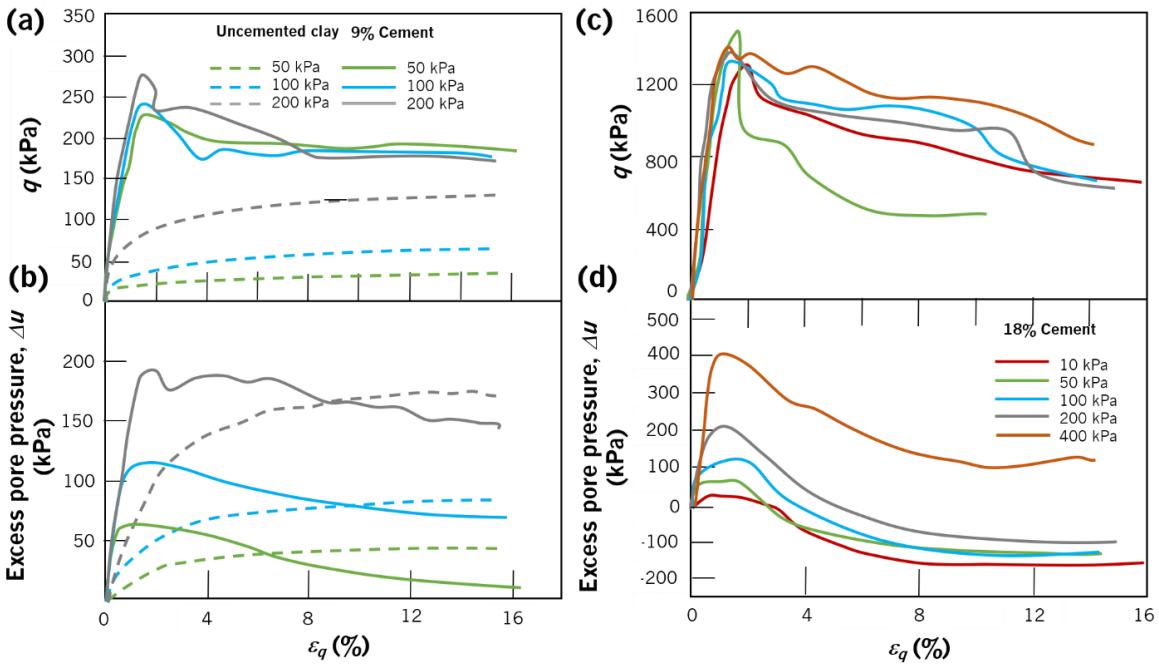

Figure 12. Stress-strain response in (a) and (c) and pore pressure variation in (b) and (d) of cemented specimens at cement contents of 9 % and 18 % for effective confining pressures lower than the yield stress (adapted from Horpibulsuk et al., 2004)

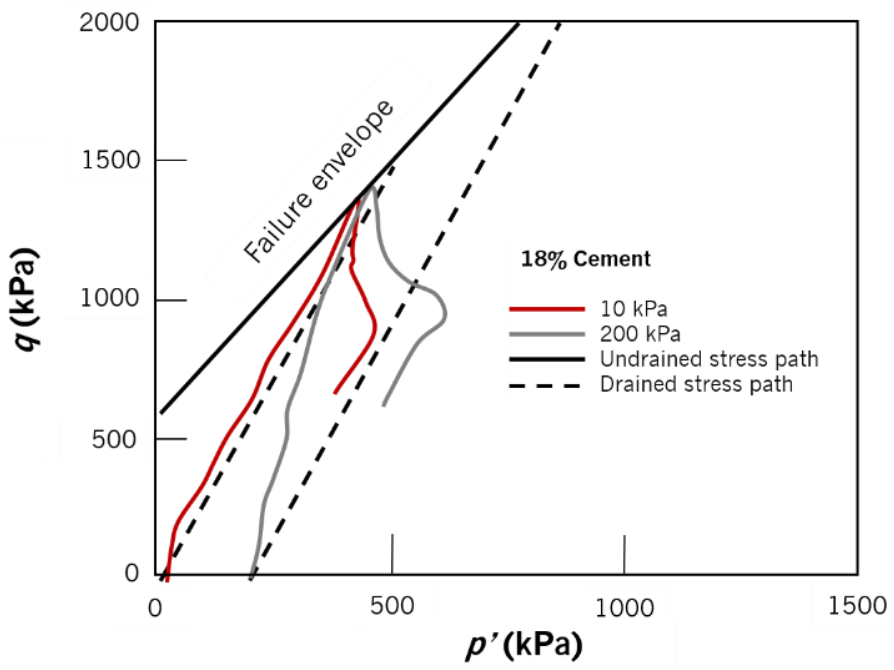

Figure 13. Stress-path of cemented specimens at cement content of 18 % for effective confining pressures lower than the yield stress (adapted from Horpibulsuk et al., 2004)

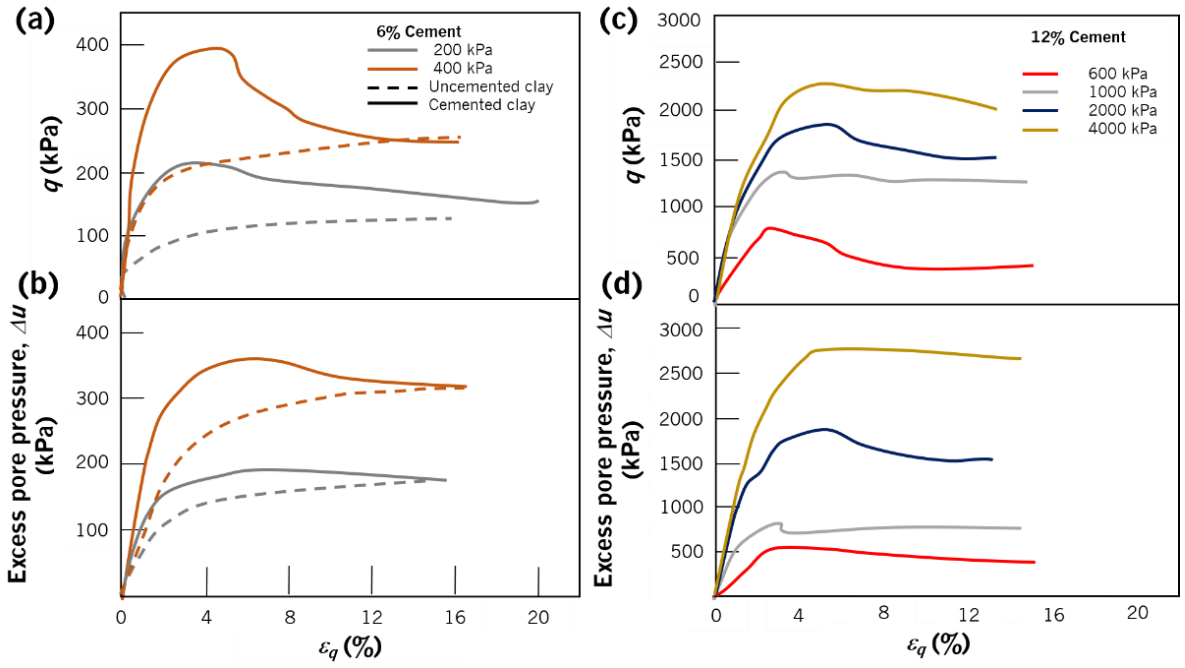

Figure 14. Stress-strain response in (a) and (c) and pore pressure variation in (b) and (d) of cemented specimens at cement contents of 6 % and 12 % for effective confining pressures higher than the yield stress (adapted from Horpibulsuk et al., 2004)

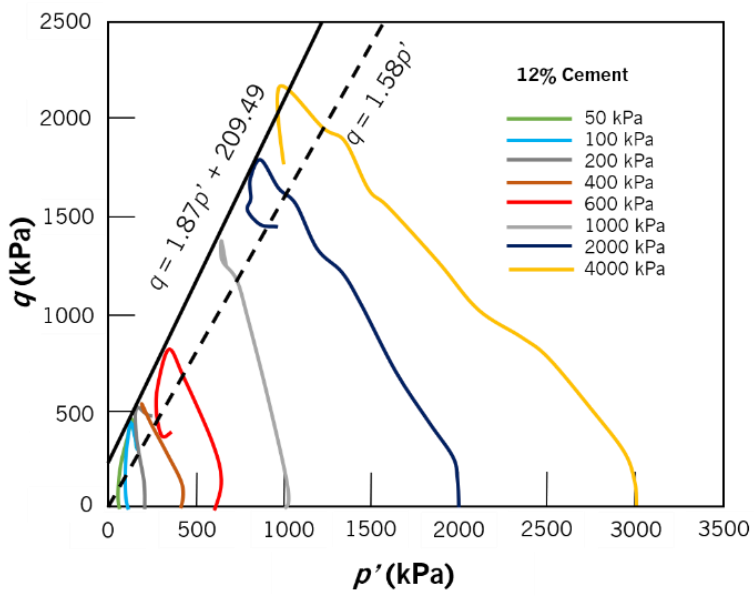

Figure 15. Stress-path of cemented specimens at cement content of 12 % for effective confining pressures higher than the yield stress (adapted from Horpibulsuk et al., 2004)

A similar behaviour was reported on the study carried out by Bian et al., 2017, where the undrained shear behaviour of a clay stabilised with combined contents of super-absorbent polymer (A_P) (0 %, 1 %, 5 % and 10 %), 3% cement (A_C) and lime (A_L) (7 % or 12 %) at high water content was investigated. The authors observed that, in fact, the compressibility and undrained shear strength of the stabilised material at preyield state are independent of the confining pressure. However, when the confining pressure is higher than the yield stress (i.e., postyield state), the increase of the confining pressure led to a drastic increase in compressibility of the cemented clay. Therefore, the undrained shear strength at postyield state depends on the confining stress. Also, there was an increase of the peak strength with the increase of A_P, A_L and curing time. For the applied stress level, the authors also observed a linear failure envelope for the cemented clay. Some of the relevant results obtained are presented in Figure 16, Figure 17, and Figure 18.

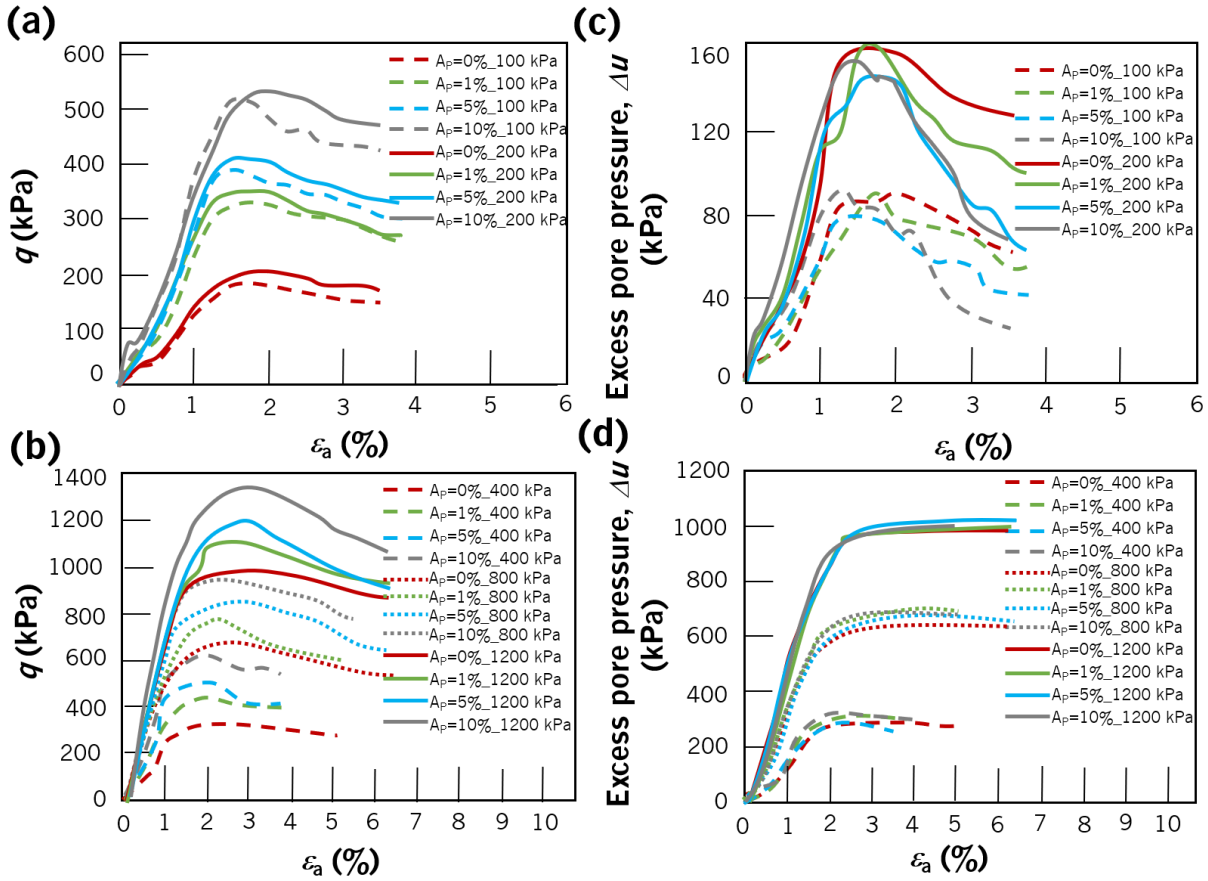

Figure 16. Effect of A_P content on the stress-strain behaviour of the cemented clay at preyield (a) and postyield (b) states. Effect of A_P content on pore pressure evolution of the cemented clay at preyield (c) and postyield (d) states (A_L= 12 %, curing days = 28) (adapted from Bian et al., 2017)

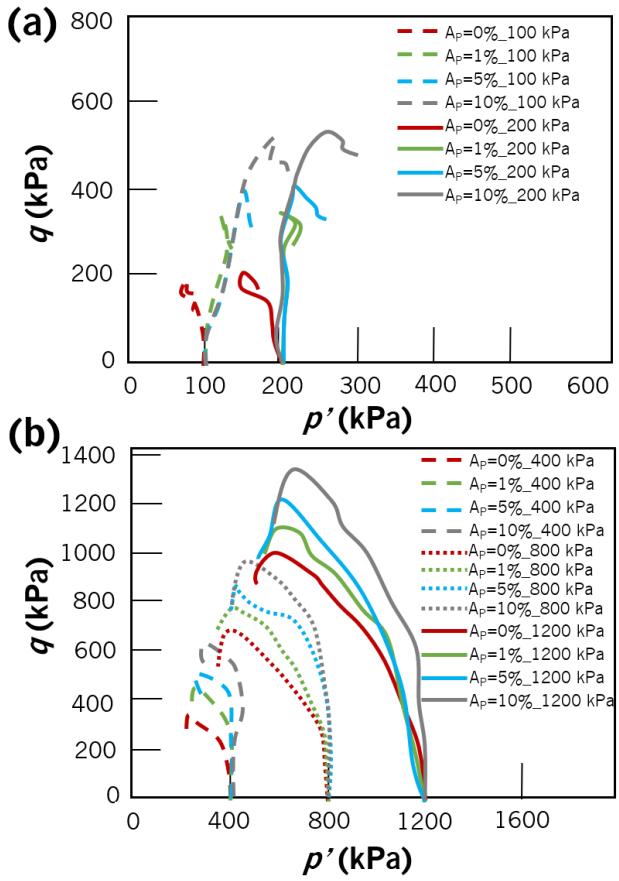

Figure 17. Effect of A_P content on the stress-path of the cemented clay at preyield (a) and postyield (b) states (A_L= 12 %, curing days = 28) (adapted from Bian et al., 2017)

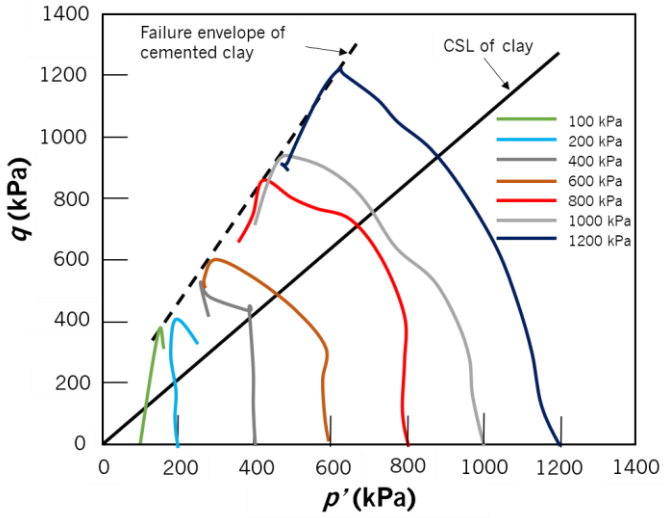

Figure 18. Stress-path and failure envelope of the cemented clay for (AL = 12 %, AC = 3 %, Ap=5 % and curing days = 28) (adapted from Bian et al., 2017)

Quiroga et al., 2017 investigated the experimental stress-strain behaviour of a remoulded laboratory-created clay and of a natural clay, both stabilised with 10 % and 20 % of cement, through isotropically consolidated undrained compression, extension, and cyclic loading. The results were then used to calibrate a constitutive model. During consolidation, OCRs were applied on the stabilised specimens, which varied between 1 and 9. Oedometer tests revealed that the preconsolidation stress for the laboratory-created clay and natural clay varied from 25 kPa and 130 kPa before stabilisation to 225 kPa and 1500 kPa after adding cement, respectively. The monotonic triaxial compression results are presented in Figure 19 and Figure 20. The excess pore water pressure (Δu) and q results were divided by the p'_0 to obtain normalised pore water pressure (Δu_n) and normalised deviatoric stress (q_n), where the effect of OCR can be directly analysed. The results showed that both clays exhibited a typical shear behaviour of a soft clay. The increase of the OCR led to an increase of the normalised strength, normalised stiffness, and an increased tendency for dilation during shear. For the applied stress level, the stabilised clays presented a behaviour reminiscent of those of overconsolidated clays, with dilation and peak-residual strength behaviours.

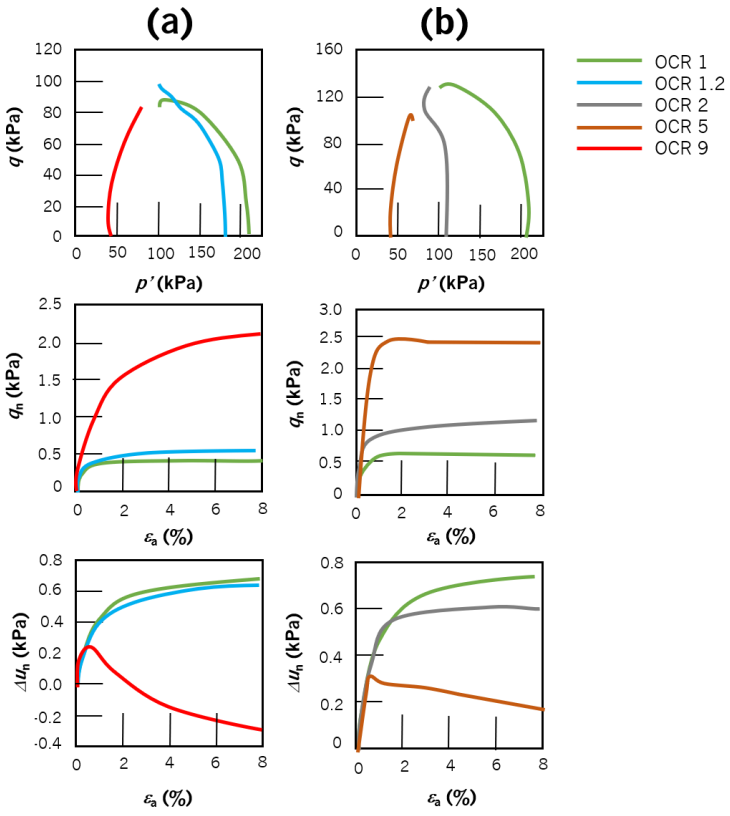

Figure 19. Triaxial test results of the laboratory-created clay (a) and natural clay (b) (adapted from Quiroga et al., 2017)

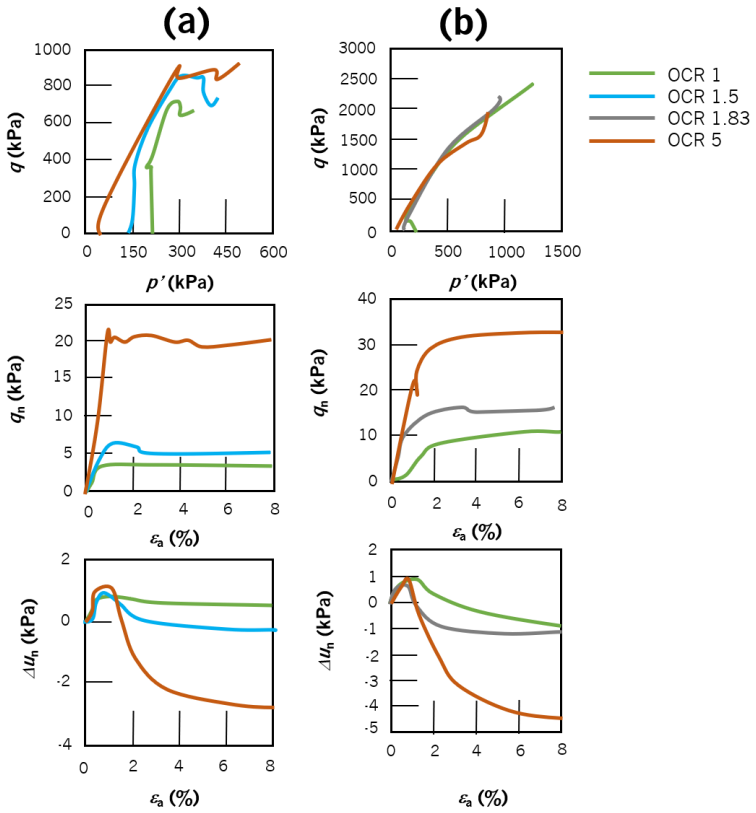

Figure 20. Triaxial test results of the stabilised laboratory-created clay (a) and stabilised natural clay (b) (adapted from Quiroga et al., 2017)

Yao et al., 2018 investigated the shear stiffness degradation of a stabilised clay with Portland cement. The maximum shear modulus was measured using BE, while the variation of the shear modulus with strain with a Drnevich long-tor resonant column. The local strain was measured by submersible miniature LVDTs, mounted onto the middle segment of the triaxial specimens, and the specimens were tested under different p'_0 and OCRs. The results of unconfined compression tests and isotropic compression tests allowed to draw the following conclusions:

- There was a high degree of consistency between the results of the BE, resonant column, and local strain test, with the resonant column results approaching the BE results as the strain level decreased and merging with the local strain measurement results as strain level increased.
- The effect of p'_0 becomes significant when it is higher than the yield stress.

- The results indicate that OCR has a significant effect on the modulus degradation behaviour but is not as significant as the effect of p'_0. Also, the higher the OCR, the greater is the contribution of overconsolidation to the modulus degradation curve.

Yao et al., 2020 proposed a conceptual framework for describing the small-strain shear modulus of a marine clay stabilised with Portland cement, considering the mix ratio, the effective stress, and the effect of OCR. Among other things, the authors concluded that the modulus of the overconsolidated specimens can be characterised by a sum of two components, one associated with effects of cementation and stress-history in the form of maximum mean effective stress, and the other associated with the effects of the current mean effective stress, OCR, and destructuration history. The results also showed that the effects of OCR and destructuration history are generally much less significant than that of effective stress.

Ahnberg, 2007 investigated the shear behaviour of two clays stabilised with cement, lime, slag, and FA in different combinations. The author observed that the strength of the stabilised soils varied considerably from 50 kPa - 1500 kPa depending on the type of clay, the type and quantity of binder, the curing stress and testing conditions. Stabilised soil specimens subjected to stress during cure resulted in an increase in strength and yield stress. The stabilised soils behaved in general in an overconsolidated and a normally consolidated manner, when the p'_0 applied in the triaxial tests was lower and higher than the yield stress, respectively. No significant difference was observed on the friction angle. The effective cohesion and friction angle varied from 5 to 175 kPa and from 30° to 36° in the Linkoping clay, respectively, and from 15 to 230 kPa and 28° to 38° in the Loftabro clay.

Rios et al., 2016a investigated the geomechanical behaviour of a silty sand stabilised with different contents of Class F FA (15 %, 20 %, and 25 %) and water or activated with Na_2SiO_3/NaOH ratio of 0.5 through UCS and triaxial compression tests at 28 curing days and SEM analysis. Results from triaxial tests showed very stiff stress-strain curves with an initial volume reduction followed by significant dilation. All tested specimens showed strain localization during shearing. For the alkali-activated mixtures, the peak strength envelope provided very high angles of shearing resistance (49° for the mixture with 25 % FA and 65° for the mixture with 15 % of FA), together with cohesion intercepts of 250 kPa and 290 kPa, respectively. Comparison between the data from the alkali-activated mixtures and results from soil-cement specimens allowed the

authors to conclude that the curing rates were different, with cement showing a significant strength development at an earlier age and stabilisation at 28 days, while the alkali-activated mixtures a slower, more progressive, and long-lasting strength increase, with significant improvements between 28 and 90 curing days.

Rios et al., 2018 carried out an experimental programme to assess strength evolution with time of silty sand mixtures stabilised with different binders based on Class F FA, lime, NaCl and alkali solutions. The aim of this study was to improve the reaction kinetics of the binders based on alkali-activated low calcium FA for soil stabilisation in road platforms. The experimental tests included UCS tests, consolidated undrained triaxial tests and seismic wave velocity measurements. Regarding the shear behaviour, the stabilised soil mixtures presented a very distinct stress-strain behaviour from the original soil, with a peak stress at very low strain levels, followed by a very abrupt strain softening due to bond degradation. The authors referred that the stiffness of the stabilised soil mixtures did not seem to be affected by the effective confining pressure for the applied pressure range, that is, the increase of the consolidation stress did not produce an increase in stiffness, but it did not damage the cemented structure either. It was also observed that the NaCl significantly improved the lime and lime-ash mixtures but provided only a slight improvement in the activated ash mixtures.

Rios et al., 2019 assessed the mechanical and durability performance of a silty sand stabilised with Class F FA activated with Na_2SiO_3 and NaOH or just Class F FA with water through UCS and indirect tensile tests, seismic wave measurements, CBR tests, expansion tests, wet and drying tests and triaxial compression tests. The results showed that the use of alkaline activators to activate the FA led to a very stiff stress-strain curve, conversely to the soil and soil - FA mixtures, associated with a brittle failure followed by strain-softening, as it is typical of stabilised materials with conventional binders. Peak strength parameters were found to be very high for the silty sand stabilised with FA, Na_2SiO_3 and NaOH, with an effective cohesion and friction angle of 231.6 kPa and 63.5°.

Sargent et al., 2020b investigated the small to large strain mechanical behaviour of an alluvium stabilised with alkali-activated blast furnace slags. The activator used was NaOH, and BE transducers were installed on the top and bottom of the undisturbed, reconstituted, and stabilised soil specimens. The triaxial test results

showed that the addition of alkali-activated blast furnace slags to the alluvium successful increased the shear strength up to four times when compared with the reconstituted alluvium specimens after 28 curing days. The undrained response was characterised by work hardening up to peak conditions, followed by strain softening. Under drained conditions, the stress-strain response was characterised by non-linear elastic work hardening behaviour up to the peak, followed by strain softening. The initial stiffness of the stabilised alluvium was also improved, which only started to degrade at shear strain levels of 1 %. The initial stiffness of the undisturbed alluvium started to degrade at lower levels of shear strains, around 0.001 %.

2.3 Constitutive models for remoulded and structured clays

2.3.1 Elastoplastic constitutive models

Soil, when subjected to external actions, deforms, changing its initial volume and shape. The magnitude of the deformations will depend, essentially, on the deformability parameters of the material, the magnitude of the imposed loading and also the range of strains induced by the structure to the soil. Therefore, to understand the behaviour of geotechnical engineering structures, it is fundamental to know the initial stress state and the induced stresses by external loads due to loading and/or unloading at the surface or at different depths. The distribution of these point-to-point stress states within the soil follows a set of differential equations called equilibrium equations, compatibility, and the constitutive laws of the material, which resolution is usually quite complicated. The constitutive laws concern the relations between stress and deformations.

Constitutive models are mathematical equations that intend to numerically explain the experimental behaviour of the materials. They are often used in the computational modelling of geotechnical problems to reproduce, analyse, and predict the stress-strain behaviour of geomaterials under external actions. The development of new constitutive models or the selection of existent models potentially capable to predict, with reasonable accuracy, the experimental behaviour of geomaterials requires a thorough knowledge of both the performance of the material under study, as well as the constitutive models and respective capabilities and limitations.

Chapter 2.3.1 aims to briefly describe the basic concepts associated with the various constitutive soil models that were developed based on the critical state theory. These concepts were the theoretical background for the development of the kinematic hardening model detailed in Chapter 2.3.3. Chapter 2.3.2 addresses studies concerning the use of constitutive models in clays stabilised with conventional binders (Portland cement or lime), which will be the base for further developments with AABs.

The critical state framework was proposed by Roscoe et al., 1958 and is related to the stress-state at which all clays would achieve under continuous plastic shearing without any changes in volume and effective stresses. Roscoe and his colleagues postulated that the evolution of a soil submitted to stress-strain paths is characterised by a surface in $p' - q - \nu$ space that contains all possible stress states of the soil (Figure 21).

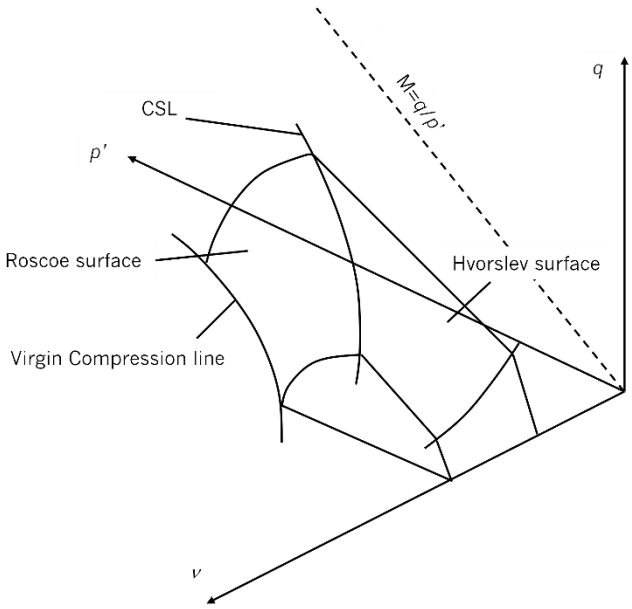

Figure 21. Roscoe – Hvorslev surface

The Roscoe – Hvorslev surface (see Figure 21) is defined as the surface made of the last part of the set of trajectories ending to a critical point and coming from all states of normally consolidated soils (loose materials) and from all states of overconsolidated soils (dense materials), respectively. In this space, the critical state is the intersection between these two surfaces. It was assumed a purely elastic behaviour when the stress-state is located inside the bounding surface and only recoverable deformations are predicted.

When the stress-state is on the bounding surface, the behaviour became elastoplastic, with a portion of strains being plastic and, thus, irrecoverable. When the critical state is achieved, the stress-state for the soil forms a line known as CSL in $p' - q - \nu$ space.

For the formulation of an elastoplastic constitutive model, four fundamental elements need to be specified, namely the elastic part, yield surface, flow rule and hardening rule as described below (Wood, 1990):

- Elastic part, which describes the purely elastic behaviour and also the elastic strains that occur due to the elastic-plastic behaviour when the stress-state is in contact with the yield surface.
- Yield surface. In conventional plasticity, a yield surface (F) provides a criterion that needs to be satisfied for plastic strains to occur. The equation of the yield surface is dependent on the current stress ($\boldsymbol{\sigma}'$) state and the hardening parameters ($\boldsymbol{k}$), $F(\boldsymbol{\sigma}', \boldsymbol{k}) = 0$. The size of the yield surface changes according to the variation of these two parameters.

When the stress-state is inside the yield surface ($F(\boldsymbol{\sigma}', \boldsymbol{k}) < 0$), purely elastic behaviour is assumed to occur. When the stress change engages a current yield surface, a combination of elastic and plastic responses occurs ($F(\boldsymbol{\sigma}', \boldsymbol{k}) = 0$). Further deformation of the material causes the stress-state to remain on the yield surface, even though the shape and size of the surface may change as the plastic deformation evolves. This is because stress states that lie outside the yield surface are non-permissible.

To determine the plastic part of the strain when the stress change engages a current yield surface, a flow rule and a hardening rule are required.

- Flow rule, which controls the mode of how the plastic deformations occur when the soil is yielding, i.e., the direction of the outward normal defines the direction of the plastic strain increment. The direction of the outward normal to the plastic potential surface defines the ratio (or relative magnitudes) of the various components of plastic deformations. A plastic potential is needed to specify the relative magnitudes of plastic distortion (or change in shape or shear strain) and of plastic change of size (or volumetric strain). In an associated flow rule, the yield surfaces and plastic potential surfaces are identical for a specific material. In this case, the plastic strain increment vector

is in the direction of the outward normal to the yield surface. The nature of the plastic deformations, or flow, is associated with the yield surface of the material. When the plastic potential function differs from the yield function, the flow rule is non-associated.

- The hardening rule is the last element used to describe the plastic response. Defines what are the absolute magnitudes of the plastic deformations and in which way the absolute magnitude of the plastic deformations is linked with the changing size of the yield surface.

The original Cam Clay model proposed by Roscoe and Schofield, 1963 and the Modified Cam Clay (MCC) model proposed by Roscoe and Burland, 1968 for reconstituted soils are two models based on the classical theory of elastoplasticity, with physical meaning parameters that can be obtained from triaxial and oedometer tests. However, the classical theory of plasticity does not allow any plastic deformations inside the yield surface to occur, which did not allow to correctly predict the real behaviour of the soils. Various techniques have been used in order to incorporate the real behaviour of the soils, such as hysteretic behaviour, the natural structure including the natural cementation and overconsolidation, etc., into numerical models.

The essence of the bounding surface plasticity theory proposed by Dafalias and Herrmann, 1982 is the hypothesis that plastic deformations can occur for stress states either within or on the bounding surface. Therefore, unlike classical yield surface elastoplasticity, the plastic states are not restricted only to those lying on a surface. Furthermore, the magnitude of the plastic deformations and stiffness of the soil is dependent on the distance of the current effective stress state to a reciprocate point on the bounding surface. As a result, there is a gradual decrease of stiffness as the yield surface is approached. This type of models has origin in conventional critical state model principles, wherein the plastic potential and hardening law are associated with the bounding surface that acts as a conventional yield surface.

The kinematic hardening concept was proposed to correctly model some fundamental features of the soil behaviour, including under cyclic loading. In the cyclic loading and during soil unloading, the behaviour is assumed to be totally elastic and, consequently, characteristics such as the energy dispersion that leads to a hysteretic behaviour and the accumulation of excess pore pressure were not correctly addressed. In the kinematic hardening model, there is the introduction of a small yield surface called the bubble that defines the extent of the real elastic region of the soil and moves inside the conventional yield surface according to

a kinematic hardening rule. When the stress-state is inside the bubble, purely elastic behaviour is predicted. Once the yield surface is engaged, there is a transition to an elastoplastic state and the predicted behaviour is governed by the plastic potential and hardening laws attributed to the bubble. Continued loading lead to the contact between the bubble surface and the external bounding surface. In that case, the external surface assumes the role of a conventional yield point and the behaviour is directed by the laws describing the outer surface.

When cement is added to a soil (cemented structured soil), a new soil-cement structure is formed with a completely distinct behaviour to the naturally structured soil or reconstituted soil, with increased strength and stiffness. Constitutive models for artificially cemented clays should have the ability to describe some important features in compression and shearing, including the strain-softening behaviour, which can be seen when the stress state is on the yield surface due to the crushing of soil-cementation structure.

Horpibulsuk et al., 2010, based on experimental data on the behaviour of cemented clays published by other authors, described their behaviour as explained next (see Figure 22):

- Based on the behaviour of the same clay in the reconstituted state, naturally structure state and cemented state, it seems that cemented and naturally structured clay exhibit similar behaviour under compression. Due to the effect of the cementation structure, the cemented clays can sustain a higher void ratio than the same clay at the natural state within the same stress state. During yielding, the breakdown of the cementation occurs, and the additional void ratio sustained by the cementation structure decreases. Therefore, the artificially cemented clays generally present a higher virgin compression index (λ) in (e – log p') space and a higher rate of breakage of cementation bonds compared to natural structured clays.
- In cemented clays, the increase of the cement content leads to the increase of both compressive and tensile strengths. So, the size of the initial yield surface of the cemented clay increases with cementation bond strength. Due to the cementation effect, the cemented clay mainly exhibits elastic behaviour when the stress-state is inside the state boundary surface, unlike the reconstituted and naturally structured clays.

- The resistance to elastic deformations and the yield stress increase with cementation bond strength, which is shown by the lower swelling index (κ) compared to naturally structured or reconstituted clays.
- In terms of shear behaviour, the cemented clay presents a final shear stress generally higher than the natural clay.
- The variation in mechanical properties of cemented clay seems to be basically isotropic.

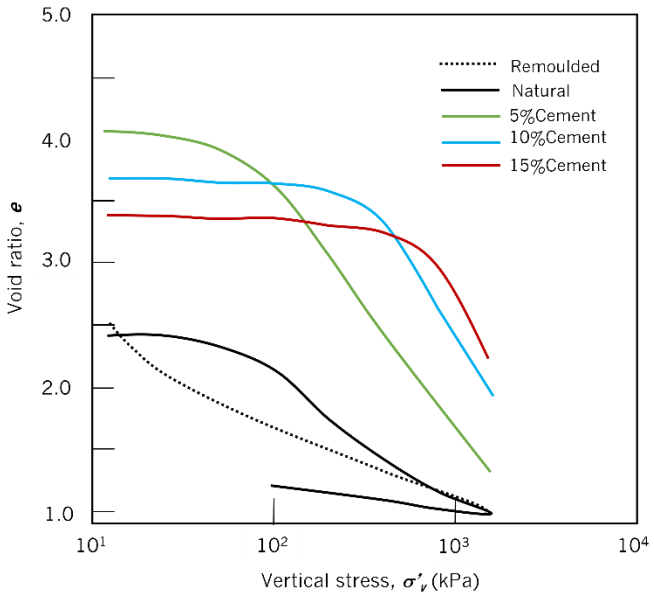

Figure 22. One-dimensional compression behaviour of a Bangkok clay stabilised with different cement content (Horpibulsuk et al., 2010)

Therefore, the constitutive models for cemented clays should have the capacity to describe the previously mentioned characteristics in both compression and shearing. Due to the lack of capacity of classical constitutive models, such as the MCC model, to successfully describe the behaviour of cemented clays, it became essential the development of constitutive models including the features of the soil-cement structure.

The elastoplastic constitutive models for structured (cemented structured or naturally structured) clays can be classified according to two categories, as cited by Yapage and Liyanapathirana, 2019:

- Critical state models based on the classical theory of plasticity. Included in this category are the models proposed by Kasama et al., 2000 and Lee et al., 2004 for cemented structured clays and the models proposed by Vatsala et al., 2001 and Horpibulsuk et al., 2010 for cemented and naturally structured clays.
- Combination of bounding surface plasticity and multi-surface kinematic bubble models. These models consider the effect of soil structure incorporating the stiffness nonlinearity in the elastic domain, the stress-history dependency of the material and the reduction of the size of the yield surface due to bond degradation introducing a damage-type mechanism. These models are able to describe the complex soil behaviour under cyclic loading and involve many model parameters, some of them difficult to determine from laboratory tests and do not have clear physical meaning. Rouainia and Muir Wood, 2000 proposed a kinematic hardening constitutive model for natural clays based on the critical state concept that is further detailed in Chapter 2.2.5.

2.3.2 Modelling the stress-strain behaviour of stabilised clays with Portland cement

Although there is extensive literature demonstrating that AABs are capable of producing engineering performances comparable to Portland cement or lime, the shear behaviour of soils stabilised with this type of alternative binder is still little known, as mentioned in Chapter 2.2.3, and research, where constitutive models are used to predict their experimental behaviour, are practically non-existent nowadays. Therefore, this Chapter will address studies concerning the use of constitutive models in clays stabilised with conventional binders (Portland cement or lime), which will be the base for further developments with AABs.

The elastoplastic MCC model, developed within the critical state framework, was formulated to predict the behaviour of reconstituted clays, where the soil structure is destroyed. This model describes important features related to the clay behaviour, strength, compression and dilatancy, and also the critical state at which soil elements can experience unlimited distortion without any changes in stress or volume. However, as seen from *in situ* tests, the behaviour of the clays can be significantly dependent on their structure. In this context, the Structured Cam Clay (SCC) model was proposed by Liu and Carter, 2002 to model the main characteristics of the behaviour of natural clays.

Horpibulsuk et al., 2010 proposed modifications to the original theoretical framework of the SCC model to describe the behaviour of clays with induced cementation caused by the addition of cement. Two modifications were proposed to the SCC model considering the special characteristics of the behaviour of cemented clays:

- Modification of the p' parameter to include the influence of cementation on strength and plastic deformations of cemented clays.
- Addition of a new destructuring function to represent the removal of the cementation structure that especially occurs in the formation of the final failure state for artificially and strongly cemented clays.

The revised model was then used to predict the behaviour of four cemented clays with various degrees of cementation and confining pressures. The authors concluded that the main features of the cemented clay behaviour can be reasonably well predicted by the modified SCC model.

Suebsuk et al., 2010 also presented some modifications to the original SCC model in order to be applied in destructured, naturally structured and artificially structured clays from the addition of cement. The influence of structure and destructuring on the mechanical behaviour was considered by the change or addition of the following parameters:

- Modification of the p' parameter, which is the sum of the current p' and the additional p' due to structure (structure strength). The presence of structure increases the modified p' and yield surface, enhancing the cohesion, peak strength and stiffness.
- Addition of a parameter to consider the destruction of the soil-cementation structure, which begins when the stress state is on the virgin yield surface. There is an abrupt destructuring after the failure (peak strength) state. The cemented structure is completely destroyed at the critical state when the yield surface becomes identical to the destructured surface.
- Introduction of a plastic potential to consider the influence of the structure on the plastic strain direction for both hardening and softening behaviours.

The simulations were carried out using the modified SCC model for different clays with both natural and artificial structures under different confining pressures, drainage conditions and cement contents. The comparison of these simulations with experimental data demonstrated that, in general, the model reasonably describes the behaviour of the various types of soil structures.

Suebsuk et al., 2011 formulated a model based on the framework of SSC designated as the Modified SCC model with Bounding Surface Theory to simulate the stress-strain behaviour of both naturally and artificially structured clay at overconsolidated state. The results show that the model can represent, quite satisfactorily, the mechanical response of structured clays under drained and undrained conditions.

The confining stress has a significant influence on the behaviour of artificially structured clays. Laboratory tests indicate that the effect of cementation gradually decreases with the increase of confining stress, mainly at high confining stresses, due to degradation of the cementation bonds. Several constitutive models were developed to simulate the behaviour of cemented clays. However, the decreasing effect of cementation, particularly at high confinement stresses, is not captured by these models. In this sense, Nguyen et al., 2014 developed a constitutive model based on the MCC model, wherein the model failure envelope was proposed in a way to merge with the CSL of the reconstituted clay-cement mixture, showing the diminishing effect of cementation due to degradation of cementation bonds for increased confining stresses. The results of the triaxial tests performed on Aberdeen clay (mixed with 5 % cement), Singapore clay (with 10 % cement) and Ariake clay (with 6 % cement) showed that the proposed model has a satisfactory performance, with a good approximation with the results obtained in the laboratory tests.

Quiroga et al., 2017 carried out an extensive campaign of laboratory tests to investigate the experimental stress-strain behaviour of a remoulded laboratory-created clay and a natural clay, both stabilised with 10 % and 20 % of cement contents, through isotropically consolidated undrained compression, extension, and cyclic loading. These results were used to calibrate a bounding surface elastoplastic constitutive model. The laboratory results and the predictions made by the model demonstrated that the model was able to make reasonable predictions of the stress–strain behaviour for natural and laboratory-created clays under monotonic loading. Under cyclic loading, the predictions for these materials were not satisfactory. This model also showed limitations on the prediction of the stress-strain behaviour of the stabilised clays.

Laboratory tests showed that cementation degradation due to p' and deviatoric strain influences the peak shear strength of artificially cemented clays. Basically, during the isotropic compression, the increase of p' beyond the initial yield stress led to a diminished effect of cementation that is caused by the degradation of cementation bonds, and there is a reduction of the void ratio of the artificially cemented clays until it approaches the ICL of the reconstituted soil. Additionally, the cementation bonds are progressively destroyed when the artificially cemented clay is subjected to shear deformation because major cracks formed within the samples. Following the softening process in the post-peak state, the cementation bonds are removed even further as the specimen approaches the CSL of the reconstituted soil-cement mixture. Once the artificially cemented clay travels on the CSL, the cementation bonds are completely destroyed, which results in only ultimate strength remaining. Based on these laboratory findings, Nguyen et al., 2017 developed a constitutive model, integrated into the critical state framework and Cam Clay model families, to predict the behaviour of artificially cemented clays during cementation degradation under different loading conditions. The proposed model includes the following characteristics:

- Nonlinear failure envelope that progressively merges with the CSL of the reconstituted soil-cement mixture as the p' increases.
- Modified p' in order to consider the effect of cementation and its degradation due to the p' and deviatoric strain.
- Formulated plastic potential function together with the elastoplastic stress-strain relationship. When there is no effect of cementation, the proposed model is reduced to a MCC model.

The results of undrained and drained triaxial tests under different p' in two non-cemented and artificially cemented clays with different cement contents demonstrated that the overall behaviour of the artificially cemented clays was very well predicted by the model.

2.3.3 A kinematic hardening model proposed by Muir Wood and Rouainia

The kinematic hardening constitutive model proposed by Rouainia and Muir Wood, 2000 for natural clays was the selected model in the scope of this work. This model was used to predict the stress-strain behaviour of two clayey soils, a sandy lean clay (in Chapter 4) and a clay with high plasticity (in Chapter 5) (ASTM D

2487, 2011), both artificially stabilised with AABs. The behaviour of both soils on the reconstituted state was also predicted using the mentioned model.

A description of the kinematic hardening constitutive model proposed by Rouainia and Muir Wood, 2000 is presented next largely based on the information published in this paper, where the model is described. This model was selected due to its flexibility in modelling different soil behaviours. The model, formulated within the framework of kinematic hardening with elements of bounding surface plasticity, is an extension of the Cam-clay model and was formulated in order to include the effects of damage to the structure caused by irrecoverable plastic strains due to sampling, laboratory testing or geotechnical loading. The model describes the essential phenomena of pre-failure behaviour of natural clays, including the stiffness variation with strain, volumetric change accompanying distortion and peak strength at small strains. Also, this model has the ability to model the initial anisotropy of the structure surface. The model is implemented in a finite element code and has been extensively applied in a wide range of geotechnical problems under monotonic and cyclic behaviour on natural, remoulded, and overconsolidated clays (Charlton and Rouainia, 2021; Elia et al., 2016; Elia and Rouainia, 2016; N. González et al., 2011; González et al., 2012; N. A. González et al., 2011; Panayides et al., 2012; Panayides and Rouainia, 2011; Rouainia et al., 2020).

Rouainia and Muir Wood, 2000 proposed a constitutive model based on the MCC model already able to describe the behaviour of the reconstituted clays. This model was inspired by the bubble model developed by Al-Tabbaa and Wood, 1989, where a kinematically hardening bubble was incorporated into the MCC model in order to predict the hysteretic response of soils, linked with the bounding surface plasticity concepts Dafalias, 1986. The kinematic hardening models permit the retention of some information concerning the recent stress history of the material. The proposed model was also extended in order to capture characteristics related to the initial structure and its progressive loss.

The model has three elliptic surfaces in the stress space: the kinematically hardening bubble which is the yield surface, f_b, the structure yield surface, F, and the reference yield surface, f, (Figure 23). The bubble surface splits the regions of elastic and plastic response and can move around with the current stress according to a kinematic hardening rule within an outer bonding surface. The current stress-state is always inside or on the bubble surface. Any stress path tending to move beyond the boundary of the bubble cause

a translational motion until it eventually is in contact with the structure surface. The structure surface acts as a bounding surface, limiting the admissible stress states, and contains the current magnitude and anisotropy of the structure. Therefore, its size and position reflect the effects of the soil structure. The destructuration takes place during plastic loading when the structure surface approaches the reference surface. The reference surface is used to model the intrinsic behaviour of the reconstituted or completely remoulded soil. When both structure and reference surface coincide, it is assumed that the soil structure is fully remoulded, with the structure completely destroyed. The model can be used to predict the behaviour of both structured and remoulded clays. The elastoplastic strain rate $\boldsymbol{\dot{\varepsilon}}$ contains two parts, elastic $\boldsymbol{\dot{\varepsilon}^e}$ and plastic $\boldsymbol{\dot{\varepsilon}^p}$ strain and is expressed according to Equation. 1.

$$\boldsymbol{\dot{\varepsilon}} = \boldsymbol{\dot{\varepsilon}^e} + \boldsymbol{\dot{\varepsilon}^p} \,. \qquad \text{Equation. 1}$$

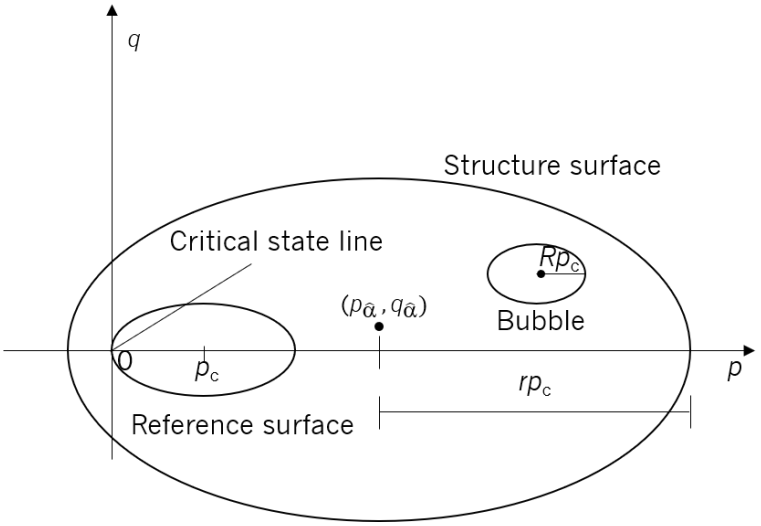

Figure 23. Schematic representation of the model surfaces (adapted from Rouainia and Muir Wood, 2000)

Elastic behaviour

When the stress-state is located inside the elastic domain, the predicted response by the model is isotropic. The response associated with the elastic part is expressed by the bulk (K) and shear (G) moduli as shown in Equation. 2, and both elastic properties are dependent of the pressure p'.

$$K = \frac{p}{k^*} \text{ and } G = \frac{3(1-2\nu)}{2(1+\nu)}K \qquad \text{Equation. 2}$$

Where k^* is the slope of the swelling line in ln p' (kPa) - ln (1+e) space. A constant value for Poisson ratio (ν) is also assumed.

The elastic response is given by Equation. 3. This response can be written using K and G to separate effects of changing size and changing shape according to Equation. 4.

$$\dot{\boldsymbol{\sigma}} = \boldsymbol{D}^{\boldsymbol{e}} : \dot{\boldsymbol{\varepsilon}}^{\boldsymbol{e}} \qquad \text{Equation. 3}$$

Where $\boldsymbol{D}^{\boldsymbol{e}}$ is the matrix form of the tensor of elastic moduli expressed as general function of K and G.

$$\begin{bmatrix} \delta\varepsilon_v \\ \delta\varepsilon_q \end{bmatrix} = \begin{bmatrix} 1/K & 0 \\ 0 & 1/3G \end{bmatrix} \begin{bmatrix} \delta p' \\ \delta s \end{bmatrix} \qquad \text{Equation. 4}$$

Where $\delta\varepsilon_v$ is the increment of volumetric strain, $\delta\varepsilon_q$ is the increment of triaxial shear strain, $\delta p'$ is the increment of mean stress and δs is the increment of deviatoric stress. An increment of $\delta p'$ produces no distortion $\delta\varepsilon_q$, and an increment of δs produces no change in volume.

Equations of the surfaces

The bubble surface, structure surface and reference surface have the same elliptical shape.

The reference surface is used to model the intrinsic behaviour of the reconstituted soil and can be written as,

$$f := \frac{3}{2M_\theta^2}(\boldsymbol{s}) : (\boldsymbol{s}) + (p - p_c)^2 - (p_c)^2 = 0 \qquad \text{Equation. 5}$$

Where p_c is the hardening scalar variable, which controls the size of the reference surface, p is the mean pressure and $\boldsymbol{s}$ the deviatoric stress. The p and $\boldsymbol{s}$ can be determined according to Equation. 6,

$$p := \frac{1}{3}\mathrm{tr}[\boldsymbol{\sigma}] \text{ and } \boldsymbol{s} := \boldsymbol{\sigma} - p\boldsymbol{I} \qquad \text{Equation. 6}$$

Where $\boldsymbol{I}$ is the second-rank identity sensor and $\mathrm{tr}[\cdot]$ is the trace operator of $[\cdot]$. The slope of the critical state line was expressed in function of the Lode angle θ, M_θ, and controls the shape of the reference, structure and bubble surfaces. It is defined by,

$$M_\theta = \frac{2mM}{(1+m)-(1-m)\sin 3\theta} \qquad \text{Equation. 7}$$

Where m is the ratio between the radii of the sections through the surface for axisymmetric extension and compression in the deviatoric plane and should be between 1 and 0.7. Lodes's angle θ is related to the second ($J_2 = \frac{1}{2}\boldsymbol{s} : \boldsymbol{s}$) and third ($J_3 = \frac{1}{3}s_{ij}s_{jk}s_{ki}$) deviatoric invariants, and M is the critical state stress ratio. Lodes's angle θ is related to J_2 and J_3,

$$\frac{-\pi}{6} \leq \theta = \frac{1}{3}\sin^{-1}\left[\frac{-3\sqrt{(3)}J_3}{2{J_2}^{3/2}}\right] \leq \frac{\pi}{6} \qquad \text{Equation. 8}$$

The bubble surface, which surrounds the elastic region, moves around within the external surface governed by a kinematic hardening rule. The bubble surface is defined as,

$$f_b := \frac{3}{2M_\theta^2}(\boldsymbol{s}-\boldsymbol{s}_{\bar{\alpha}}) : (\boldsymbol{s}-\boldsymbol{s}_{\bar{\alpha}}) + (p-p_{\bar{\alpha}})^2 - (Rp_c)^2 = 0 \qquad \text{Equation. 9}$$

Where $\{p_{\bar{\alpha}}, \boldsymbol{s}_{\bar{\alpha}}\}^T = \bar{\boldsymbol{\alpha}}$ denotes the localization of the centre of the bubble surface, the movement of which is controlled by its kinematic hardening rule. The constant parameter R corresponds to the ratio of the sizes of the elastic bubble and the reference yield surfaces.

The structure surface, which assumes the role of bounding surface, controls the development of destructuration through its interaction with the bubble. It is the feature of destructuration that enables the model to capture the characteristics of significant strain-softening. The structure surface is defined as,

$$F := \frac{3}{2M_\theta^2}[\boldsymbol{s} - (r-1)\boldsymbol{\eta}_0 p_c] : [\boldsymbol{s} - (r-1)\boldsymbol{\eta}_0 p_c] + (p - rp_c)^2 - (rp_c)^2 = 0 \quad \text{Equation. 10}$$

Where $\boldsymbol{\eta}_0$is the dimensionless deviatoric tensor controlling the structure and r, which controls the size of the structure surface, is the ratio of the sizes of the structure surface and the reference surface. As showed in Equation. 10, both the size and the location of the structured surface are affected by the process of destructuration through the variable parameter r. The position of the centre of the structure surface $\{rp_c\,, (r-1)\boldsymbol{\eta}_0 p_c\}^T = \widehat{\boldsymbol{\alpha}}$ with respect to the centre of reference surface $\{p_c\,, 0\}^T = \widetilde{\boldsymbol{\alpha}}$ provides the model with an anisotropic initial structure. The centre of the structure surface can be located off the mean effective stress axis, allowing the model to accommodate the soil anisotropy that is common in natural structured clays. The location of the structure surface is governed by the parameter $\boldsymbol{\eta}_0$.

Destructuration process

The degree of structure, r, controls the ratio of the sizes of the structure surface and the reference surface. It was modelled to be a monotonically decreasing function of the plastic strain, which allows the model to predict the progressive degradation of the material. The effects of cementation over a geological timescale can be incorporated through a controlled increase of r. The destructuration law is written as,

$$r = 1 + (r_0 - 1)\exp\left[\frac{-k\varepsilon_d}{(\lambda^* - \kappa^*)}\right] \quad \text{Equation. 11}$$

The incremental form of the destructuration law is written as,

$$\dot{r} = -\frac{k}{(\lambda^* - \kappa^*)}(r-1)\dot{\varepsilon}_d \quad \text{Equation. 12}$$

Where r_0 is the initial value of r, k is a parameter that expresses the rate of destructuration with strain, λ^* is the slope of normal compression line and $\kappa^*$is the slope of the swelling line. Since the destructuration process occurs in both compression and shearing stages, the rate of the destructuration strain, $\dot{\varepsilon}_d$,

incorporates these two components, the plastic volumetric and deviatoric strains. The destructuration strain, $\dot{\varepsilon}_d$, is assumed to have the following form,

$$\dot{\varepsilon}_d = \left[(1-A)\left(\dot{\varepsilon}_v^p\right)^2 + A\left(\dot{\varepsilon}_q^p\right)^2\right]^{\frac{1}{2}} \qquad \text{Equation. 13}$$

Where A is a non-dimensional scaling parameter, $\dot{\varepsilon}_q^p = \left[\frac{2}{3}(\dot{\varepsilon}^p : \dot{\varepsilon}^p)\right]^{\frac{1}{2}}$ is the equivalent plastic shear strain rate and $\dot{\varepsilon}_v^p = \frac{1}{3}tr[\dot{\varepsilon}^p]$ is the plastic volumetric strain rate. In Equation. 13, when A = 1, the destructuration is totally distortional, while for A = 0 the destructuration is totally volumetric. The use of r_0=1 and $\boldsymbol{\eta}_0$=0 into the model, it reduces to the bubble model of Al-Tabbaa & Wood, 1989. If, in addition R=1, then the model reduces to Cam Clay.

Hardening functions

The bubble yield surface provides a criterion for determining if there is the development of plastic strains caused by an increment of stress. The magnitude of these strains is determined using a flow rule and a hardening rule.

Like the Cam Clay model, it is assumed that the direction of the plastic strain increment is normal to the bubble surface at the current state (see Figure 24). The hardening functions follow the same logic of the hardening functions proposed by Al-Tabbaa & Wood, 1989, with the addition of elements that capture the effects of changing structure. The following assumptions were made:

- First, there is the assumption of isotropic hardening, which implies that there is a variation in size of all three surfaces whenever any plastic strain occurs.
- Second, if a stress increment requires the transition of the bubble relative to the structure surface, this translation is described according to a kinematic hardening rule.
- Third, the hardening model equation is described in order to provide the model with Cam-Clay type behaviour for the special case when the bubble yield surface is touching the structure surface at the current stress state. The predicted behaviour is identical to Cam Clay when the parameter that

governs the size of the structure surface, r, is equal to 1, and the reference and structure surfaces coincide as in the model of Al-Tabbaa & Wood, 1989.

- Four, the stiffness is dependent on some geometric measure of the distance between the bubble and the structure surfaces. If plastic strains occur when the bubble surface is not in touch with the structure surface at the current stress-state, the plastic stiffness was made to be higher and was defined in a way so that its magnitude gradually degrades as the two surfaces approach under monotonic loading.

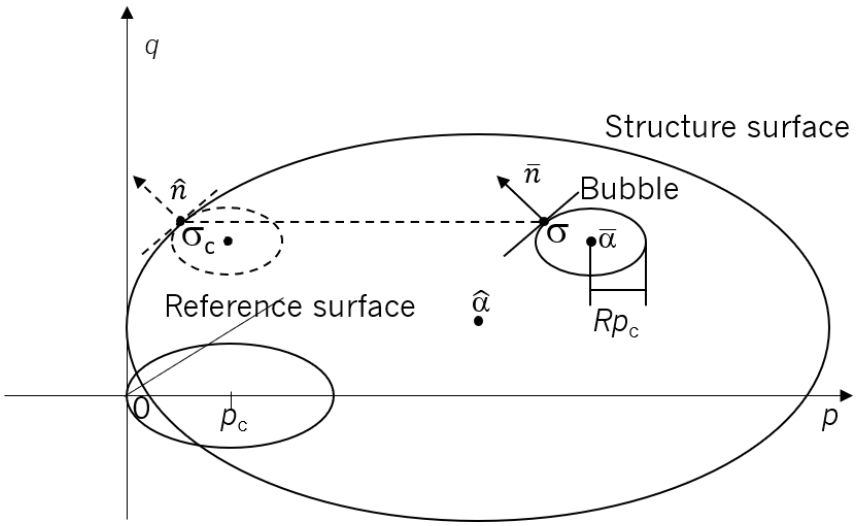

Figure 24. Schematic representation with the conjugated stress point and the outward normals of the bubble and structure surface (adapted from Rouainia and Muir Wood, 2000)

The assumption of isotropic hardening means that a volumetric hardening rule is adopted, where the change in size of the reference surface, p_c, is governed only by plastic volumetric strain rate, $\dot{\varepsilon}_v^p$, given by,

$$\frac{\dot{p}_c}{p_c} = \frac{\dot{\varepsilon}_v^p}{\lambda^* - \kappa^*} \qquad \text{Equation. 14}$$

It was assumed an associated flow rule, which means that the plastic potential was expressed by the same equation as the bubble yield surface. Thus, the movement of the bubble is engaged ($f_b = 0$), marked the onset of plastic deformation, with the progress of the plastic strains given by,

$$\dot{\varepsilon}^p = \dot{\gamma}\bar{\boldsymbol{n}} \qquad \text{Equation. 15}$$

Where $\dot{\gamma}$ is the plastic multiplier and f_b must satisfy the Kuhn-Tucker conditions $\dot{\gamma} \geq 0$, $\dot{\gamma} f_b = 0$ and $f_b \leq 0$. The $\bar{\boldsymbol{n}}$ represents the normalized stress gradient on the bubble at the current stress-state. For the stress point on the yield surface,

$$\dot{\gamma} = \frac{1}{H}(\bar{\boldsymbol{n}} : \dot{\boldsymbol{\sigma}}) \qquad \text{Equation. 16}$$

For the conjugate stress point on the structure surface (see Figure 24),

$$\dot{\gamma} = \frac{1}{H_c}(\bar{\boldsymbol{n}} : \dot{\boldsymbol{\sigma}}_c) \qquad \text{Equation. 17}$$

The stress associated with the centres of the bubble and the structure surfaces is given respectively by,

$$\bar{\boldsymbol{\sigma}} = \sigma - \bar{\alpha} \qquad \text{Equation. 18}$$

$$\hat{\sigma} = \sigma - \hat{\alpha} \qquad \text{Equation. 19}$$

The scalar plastic moduli H and H_c are associated with the stress points $\dot{\boldsymbol{\sigma}}$ and $\dot{\boldsymbol{\sigma}}_c$, respectively. For any stress point, $\dot{\boldsymbol{\sigma}}$, on the bubble ($f_b = 0$), there is a conjugate point $\dot{\boldsymbol{\sigma}}_c$ on the structure surface $F = 0$ having the same direction of the outward normal, as shown in Figure 24. This is a specific characteristic common to bounding surface plasticity models (e.g. (Dafalias, 1986)).

The kinematic hardening model proposed by Rouainia & Muir Wood, 2000 incorporates some elements of the bounding surface plasticity theory (Dafalias, 1986) for the formulation of the hardening modulus where the bubble and structure surfaces are not in touch. The expression associates the magnitude of H to the hardening modulus at the conjugate point H_c through an expression that incorporates the degree of the approach of the bubble to the structure surface. Thus, one can obtain,

$$\frac{\widehat{\boldsymbol{\sigma}_c} - \widehat{\alpha}}{r} = \frac{\boldsymbol{\sigma} - \overline{\alpha}}{R}$$ Equation. 20

The translation rule of the bubble, $\dot{\overline{\boldsymbol{\alpha}}}$, was formulated in order to ensure a smooth transition between the bubble and the structure surface, avoiding the intersection of these two surfaces. This was achieved by requiring the centre of the bubble to translate relatively to the centre of the structure surface in a direction parallel to the line that join the current stress and the conjugate point (line associated with b in Figure 25). The expression for the centre of the bubble was defined considering this movement.

The combination of the consistency on the bubble given by,

$$\overline{\boldsymbol{n}} : \left[\dot{\overline{\boldsymbol{\sigma}}} - \frac{\dot{p_c}}{p_c}\overline{\boldsymbol{\sigma}}\right] = 0$$ Equation. 21

with this geometry requirements for non-intersection leads to the translation rule of the centre of the bubble, $\dot{\overline{\boldsymbol{\alpha}}}$,

$$\dot{\overline{\boldsymbol{\alpha}}} = \dot{\widehat{\boldsymbol{\alpha}}} + (\overline{\boldsymbol{\alpha}} - \widehat{\boldsymbol{\alpha}})\left(\frac{\dot{r}}{r} + \frac{\dot{p_c}}{p_c}\right) + \frac{\overline{\boldsymbol{n}} : \left\{\dot{\widehat{\boldsymbol{\sigma}}} - \widehat{\boldsymbol{\sigma}}\left[\left(\dot{r}/r\right) + \left(\dot{p_c}/p_c\right)\right] + \overline{\boldsymbol{\sigma}}\left(\dot{r}/r\right)\right\}}{\overline{\boldsymbol{n}} : (\boldsymbol{\sigma}_c - \boldsymbol{\sigma})}(\boldsymbol{\sigma}_c - \boldsymbol{\sigma})$$ Equation. 22

This translation of the centre of the bubble rule requires three variable terms necessary to specify. The first term, $\dot{\widehat{\boldsymbol{\alpha}}}$, describes the movement of the centre of the structure surface. The second term, $(\overline{\boldsymbol{\alpha}} - \widehat{\boldsymbol{\alpha}})\left(\frac{\dot{r}}{r} + \frac{\dot{p_c}}{p_c}\right)$, defines the scaling of the space inside the structure surface that follows any change in the value of r and p_c. The third term, $\frac{\overline{\boldsymbol{n}} : \left\{\dot{\widehat{\boldsymbol{\sigma}}} - \widehat{\boldsymbol{\sigma}}\left[\left(\dot{r}/r\right) + \left(\dot{p_c}/p_c\right)\right] + \overline{\boldsymbol{\sigma}}\left(\dot{r}/r\right)\right\}}{\overline{\boldsymbol{n}} : (\boldsymbol{\sigma}_c - \boldsymbol{\sigma})}(\boldsymbol{\sigma}_c - \boldsymbol{\sigma})$, describes the translation of the elastic bubble along the line joining the current and the conjugate stress points (Figure 25).

The plastic modulus H is assumed to be dependent on the Euclidean distance between the current stress and conjugate stress when the structure and bubble surfaces are not in touch. The magnitude of H is reduced to the plastic modulus H_c at the conjugate point when the bubble and the structure surface are in touch at the current stress.

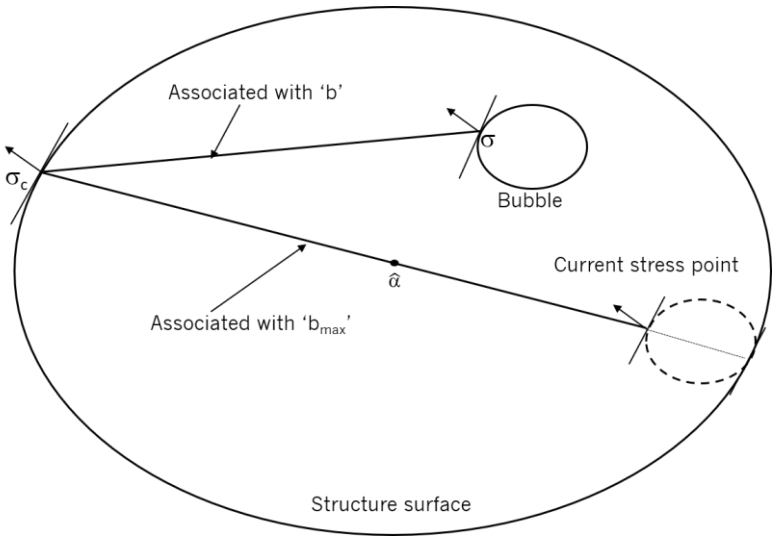

Figure 25. Schematic representation demonstration the movement rule of the bubble surface along the line linking the current and the conjugate stress points (adapted from Rouainia and Muir Wood, 2000)

Plastic modulus at conjugate stress

During loading, when the bubble is forced to translate towards the structure surface, the two surfaces will be in touch, and the response of the model is controlled by the structure surface ($F = 0$). The consistency condition on the structure surface is give, by,

$$\hat{\boldsymbol{n}} : \left[\dot{\hat{\boldsymbol{\sigma}}} - \hat{\boldsymbol{\sigma}}\left(\frac{\dot{r}}{r} + \frac{\dot{p_c}}{p_c}\right)\right] = 0 \qquad \text{Equation. 23}$$

The join of the Equations 11, 12, 14, 16 and 17 together with the expression of the plastic volumetric strain rate $\dot{\varepsilon}_v^p = \frac{1}{3} tr[\dot{\varepsilon}^p]$ presented in Equation. 13 led to the following expression for the plastic modulus, H_c,

$$H_c = \frac{rp_c\left\{T\left[(p-p_{\bar{\alpha}})+\left(\frac{3}{2M_\theta^2}\right)(\boldsymbol{s}-\boldsymbol{s}_{\bar{\alpha}}):\boldsymbol{\eta}_0+Rp_c\right]-(p-p_{\bar{\alpha}})\left(\frac{3}{2M_\theta^2}\right)(\boldsymbol{s}-\boldsymbol{s}_{\bar{\alpha}}):\left(\frac{\boldsymbol{\eta}_0}{r}\right)\right\}}{(\lambda^*-\kappa^*)\left[(p-p_{\bar{\alpha}})^2+\left(\frac{3}{2M_\theta^2}\right)(\boldsymbol{s}-\boldsymbol{s}_{\bar{\alpha}}):(\boldsymbol{s}-\boldsymbol{s}_{\bar{\alpha}})\right]} \quad \text{Equation. 24}$$

Where the quantity T is given by,

$$T=(p-p_{\bar{\alpha}})-k\left(\frac{r-1}{r}\right)\times\left[(1-A)(p-p_{\bar{\alpha}})^2+\frac{3A}{2M_\theta^4}(\boldsymbol{s}-\boldsymbol{s}_{\bar{\alpha}}):(\boldsymbol{s}-\boldsymbol{s}_{\bar{\alpha}})\right]^{1/2} \quad \text{Equation. 25}$$

The proposed formulation of the hardening modulus able the kinematic hardening model proposed by Rouainia & Muir Wood, 2000 to reduce to the kinematic hardening bubble extension of Cam Clay for reconstituted soils as formulated by Al-Tabbaa & Wood, 1989 when the parameters r_0 and $\boldsymbol{\eta}_0$ is equal to 1 and 0, respectively. For natural soils, the initial measure of structure, r_0, and thus, r, might be higher than 1, which implies that in Equation. 25, both plastic compression and plastic distortion contribute to the destructuration of the soil according to the value of A ($0 < A < 1$).

Plastic modulus at current stress

In line with the conditions for smooth change of stiffness as the bubble approaches the structure surface and the non-intersection rule, the distance between these two surfaces, b, is given by,

$$b=\bar{\boldsymbol{n}}:(\boldsymbol{\sigma}_c-\boldsymbol{\sigma}) \quad \text{Equation. 26}$$

For the case wherein the bubble and structure surfaces are in touch, the conjugate and current stress points are the same and, therefore, the value of b in Equation. 26 is equal to 0. The maximum distance, $b_{\max}$, is obtained when the bubble is in contact with the external surface at a stress point which is diametrically opposite to the conjugate point, $\boldsymbol{\sigma}_c$ (see Figure 25). In that case, the current stress state is situated on the bubble diametrically opposite to this point of tangency. The value of $b_{\max}$ is given by,

$$b_{\max} = 2\left(\frac{r}{R} - 1\right)\bar{\boldsymbol{n}} : \bar{\boldsymbol{\sigma}} \qquad \text{Equation. 27}$$

The Equation. 27 defines the hardening modulus for the cases when the stress point is located on the structure surface ($b = 0$) or when the bubble and structure surfaces are not in touch. The hardening modulus at the current stress point in general is given by,

$$H = H_c + \frac{1}{\|\bar{\boldsymbol{n}}\|^2}\frac{B{p_c}^3}{(\lambda^* - \kappa^*)R}\left(\frac{b}{b_{\max}}\right)^{\psi} \qquad \text{Equation. 28}$$

Where ψ and B are material parameters that control the rate of decay of stiffness with strain and the magnitude of the contribution of the interpolation term, respectively. This definition for the plastic modulus H allows for plastic deformation to occur for stress states inside the structure surface, in function of the distance b.

The model parameters required for the numerical simulations using the kinematic hardening model are summarized in Table 4.

Table 4. Parameters required in the kinematic hardening model proposed by Rouainia and Muir Wood, 2000

	Symbol	
	m	Ratio of extension and compression strengths
	p_{c0}	Initial centre of reference surface
Elastic/Elastic-plastic parameters introduced by the modified Cam Clay type of models	k^*	Slope of swelling line in ln p' (kPa) - ln (1+e) space
	λ^*	Slope of normal compression line in ln p' (kPa) - ln (1+e) space
	M	Critical state stress ratio
	ν	Poisson ratio
Parameters introduced by the bubble model	R	Ratio of size of bubble and reference surface
	B	Stiffness interpolation parameter
	Ψ	Stiffness interpolation exponent
Parameters introduced by the structure surface	A	Destructuration strain parameter
	k	Destructuration parameter
	η_0	Anisotropy of initial structure
	r_0	Initial degree of structure

2.4 Concluding remarks

Based on the present state of the art with respect to the mechanical behaviour of clays stabilised with Portland cement and AABs, some of the most relevant conclusions that can be drawn are:

- There is a growing interest in the development of AABs over the last decades, especially for geotechnical applications. Most research has focused on the development of AABs based on precursor materials from industrial by-products or wastes and commercial alkaline activators, with a significant financial cost. The most used activators are NaOH and Na_2SiO_3. There is extensive literature on the use of activated FA and blast furnace slags for soil stabilisation. Recent studies have been devoted to the development of AABs totally produced from wastes.
- Although there is extensive literature covering laboratory investigations into the performance of soft soils stabilised with Portland cement and AABs that focus on mechanical tests in general, chemical, and environmental analysis, there is still scarce research about the mechanical behaviour of soft soils stabilised with AABs using triaxial tests. The review shows a lack of information on the development or use of existing constitutive laws to predict the stress-strain behaviour, stiffness degradation and stress-path of soft soils stabilised with AABs.
- Most of the literature studies were focused on the characterisation of mechanical behaviour of clays, before and after adding Portland cement, using triaxial tests, and on modelling the stress-strain behaviour of artificially cemented clays.

Therefore, a deep understanding of the main features of the shear behaviour of soft soils stabilised with AABs is crucial for the development or selection of existent constitutive models able to predict, with accuracy, the experimental behaviour. Further work is needed in order to understand the main similarities between the shear behaviour of soft soils stabilised with AABs and conventional binders, namely with Portland cement.

3. GEOMECHANICAL BEHAVIOUR OF A SOFT SOIL STABILISED WITH ALKALI-ACTIVATED BLAST-FURNACE SLAGS

The use of industrial by-products in the context of soil stabilisation has recently been explored as a mean to substitute the massive use of ordinary Portland cement (OPC), whose production has severe environmental impacts. Therefore, the purpose of the present investigation was to assess the geomechanical behaviour of a soft soil stabilised with a sustainable alkaline binder incorporating ground granulated blast furnace slags (GGBS), a residue from the iron industry, activated with NaOH at short (28 days) – and long (90 days) term. The mechanical characterisation included the performance of oedometer and triaxial testing, where the impact of both, initial mean effective stress (p'_0) and overconsolidation ratio (OCR) effects, was analysed on the stress-strain and volumetric strain curves, stiffness degradation and, triaxial failure surfaces of the specimens. Also, SEM-EDS, XRD and leachate analyses were also carried out at both curing ages. The mechanical results showed a significant increase of the shear strength and stiffness, and a stress-strain behaviour typical of artificially cemented soils with OPC. The detection of Si, Ca and Al suggests the formation of C-A-S-H, which explain the more pronounced development of strength and stiffness up to 28 days. No risk of soil contamination was detected due to the addition of activated GGBS to the soil.

Keywords: soil stabilisation; alkaline activation; oedometer test; triaxial test; SEM-EDS and XRD; leachate analysis

---

This Chapter is based in the article:

Corrêa-Silva, M., Miranda, T., Rouainia, M., Araújo, N., Glendinning, S., Cristelo, N., 2020. Geomechanical behaviour of a soft soil stabilised with alkali-activated blast-furnace slags. J. Clean. Prod. 122017. https://doi.org/10.1016/j.jclepro.2020.122017

3. GEOMECHANICAL BEHAVIOUR OF A SOFT SOIL STABILISED WITH ALKALI-ACTIVATED BLAST-FURNACE SLAGS

3.1 Introduction

Chemical soil stabilisation is a common treatment applied to overcome the low geomechanical properties of soils, in which cementitious materials, such as Ordinary Portland Cement (OPC) or lime, are added to the *in situ* soil to achieve the desired engineering requirements of strength, deformability, and durability. However, OPC production (the key component of the second most-consumed main made material on the planet, the concrete) involves the extraction and consumption of large amounts of raw materials and energy, and has a massive carbon footprint, contributing with up to 7 % of the world's CO_2 emissions (Li et al., 2019b; Maddalena et al., 2018). Part of the emissions is related to the high kiln temperature (i.e., 1450 °C) and limestone decomposition in raw materials during the production process (Gartner, 2004). Also, solid waste management has been a huge problem due to the increasing amounts of solid waste materials disposed into the environment (Onyelowe, 2019).

The use of industrial by-products (e.g. fly ash (FA), cement kiln dust, steel slag, waste water sludge ash, calcium carbide residue, glass waste, limestone waste ash, etc.) in the construction sector has increased in order to achieve more sustainable waste management practices (James and Pandian, 2015). More precisely, their incorporation for soil stabilization purposes have recently gained widespread acceptance, with more and more industrial wastes being investigated because of their potential for modifying positively soil properties with engineering interest.

In this context, alkali-activated binders are a new potential type of sustainable binders that have been shown an enormous potential to become an alternative to OPC. These binders, which result from a combination of residues and/or wastes with chemical activators, are still at a relatively early stage of development and, hence, need further research work to become technically and economically viable as construction materials (Miranda et al., 2020). However, even at an early stage, economic and environmental benefits are associated with the use of such binders, mainly related to the reduction in carbon footprint and conservation of the natural resources necessary to the production of OPC. Utilization of such recycled raw materials in soil stabilisation can also help optimize waste management strategies, reducing the common option of landfilling and its associated environmental problems.

3. GEOMECHANICAL BEHAVIOUR OF A SOFT SOIL STABILISED WITH ALKALI-ACTIVATED BLAST-FURNACE SLAGS

Alkali-activated binders requires two main components, the solid precursor rich in SiO_2 and Al_2O_3 (highly pozzolanic properties) and the activator based on an alkali metal (usually Na or K). Due to the high pH provided by the activator, there is a destruction of the Si-O-Si, Al-O-Al and Al-O-Si covalent bonds present in the precursor. The Si and Al are released and, at the same time, the Na^+, K^+ or Ca^{2+} species act as charge-balancing interlayer cations, compensating the excessive negative charges resulting from the modification of the Al^{3+} (Myers et al., 2013). Hydration products accumulate and precipitate, forming sodium aluminosilicate hydrate (N-A-S-H) gel (Fernández-Jiménez et al., 2017). If calcium (Ca) is present in the mixture, a nanocrystalline product is formed, known as calcium (alumino) silicate hydrate, or simply C-A-S-H (Myers et al., 2015a).

Alkali-activated binders are fast emerging as an alternative material choice due to its effectiveness on the improvement of soil geotechnical properties. Teing et al., 2019 investigated the effect of alkaline activation reactions on residual soil by using different amounts of FA (40 %, 50 %, 60 % and 70 % by soil weight) and KOH (10M). The authors concluded the unconfined compressive strength (UCS) progressively increases with the increasing of FA and curing time. Al-Rkaby, 2019 evaluated the unconfined compression and shear strength of a sand and sand-ground granulated blast-furnace slag (GGBS) based material activated with Na_2SiO_3 and NaOH. The results revealed that the alkaline binder acted as a cementing agent, increasing the UCS, cohesion and friction angle of the stabilised soil. A similar trend was observed by Corrêa-Silva et al., 2019 on a clayey soil stabilized with class F FA (low Ca content)-Na_2SiO_3-NaOH, who found that the friction angles increased by 73.6 % (total stress) and 50 % (effective stress) in the critical state and there was an increase of 2 times of the peak cohesion (total stress). Moreover, the results of UCS, pulse velocity tests, California Bearing Ratio, and triaxial tests in stabilized soil mixtures with cement, lime, and FA-Na_2SiO_3-NaOH revealed that the use of the FA-Na_2SiO_3-NaOH binder provided a similar or even better (at longer curing time periods) mechanical performance when compared with cement or lime. The effect of the clay content on soil stabilisation with alkaline activation was investigated by Abdeldjouad et al., 2019. A solution of KOH (10M) was used to activate soils with and without palm oil fuel ash. The results of UCS and microstructural analyses showed that clay minerals play an important role in soil stabilisation with alkaline activation. Finally, Miranda et al., 2020 evaluated the viability of using different alkaline activated cements to stabilise a sub(base) layer tested in a full-scale trial. Results of quality control tests, environmental impact and financial analyses carried

out in five segments (soil-cement, soil-lime, soil-FA-NaOH, soil-FA-Na_2SiO_3-NaOH and soil-FA-solid activator that is residue originally used to clean aluminium extrusion dies) showed, among other relevant conclusions, that the alkaline activated cements have *in situ* performance (strength and stiffness) similar to the ones observed with cement, with still some margin of optimization due to their almost embryonic stage of development.

Until now, published works have focused mainly on the chemical and mechanical characterisation of alkaline stabilised soils in general, and also on environmental impact assessment. Investigation devoted to the exclusive characterisation of the stress-strain behaviour of such materials, which is extremely important for a better prediction of the mechanical behaviour in the field and for the development and validation of numerical models, is still scarce and insufficient. The present paper aims to contribute to fill that specific knowledge gap, by presenting an extensive campaign of triaxial tests on soil stabilised with alkaline cements, and focusing on the stress-strain behaviour of a clayey soil stabilised with GGBS, an alumino-silicate based pozzolanic residue, very frequently used as an additive in Portland cement-based pastes, activated with a sodium hydroxide solution. The impact of the stress-state (represented by the initial mean effective stress (p'_0)) and stress-history (represented by the overconsolidation ratio (OCR)) on the stress-strain behaviour was investigated after 28 and 90 days under one-dimensional consolidation and triaxial compression. Both effects have an influence on the compressibility and permeability of the soils and play an important role in the behaviour of clayey soils. Also, scanning electron microscopy with energy dispersive spectroscopy (SEM-EDS), x-ray powder diffraction (XRD) and leachate analyses were carried out to investigate the nature of the binding phases formed and the risk of soil contamination.

One final remark regarding the use of NaOH as the main component of the activator. The CO_2eq of this reagent is considerable – 999 kg per ton of NaOH produced, according to the data base produced by the specialised and international ECOINVENT – and could easily deter one of the main objectives of this alternative solution: the higher sustainability and the smaller carbon footprint. However, based on previous work addressing the environmental performance of alkali activated binders applied in geotechnics (Cristelo et al., 2015), the use of sodium hydroxide is clearly a more sustainable option than Portland cement. This

was true in the mentioned research, which used a NaOH minimum concentration of 10 molal, and is even more in the present case, when a concentration of 1/3 (3.5 molal) was exclusively used.

3.2 Materials and methodology

3.2.1 Material characterisation

The collected soil is classified as a "CL - sandy lean clay", according to the unified soil classification (ASTM D 2487, 2011), and as a sandy clay of low plasticity according to the British Soil Classification System (BSI, 2015). Its treatment is justified, since it is a poor-quality soil for pavement subgrade, with more than 50 % of silts and clays (Figure 26). The soil is mainly composed by Al and Si which, combined, form 81 % of its total mass (Table 5). The X-ray powder diffraction spectra of the materials was recorded at room temperature, with a PANalytical X'Pert MPD diffractometer, using the λ = 0.154 nm Kα line of a Cu anode (Bragg–Brentano geometry) equipped with a X'Celerator detector. The spectra were obtained between 8° and 60° (2θ), using a step of 0.017° with 100 s/step. The diffractograms showed that the predominant mineralogical phases of the soil are quartz, muscovite, and albite (Figure 27). Table 6 summarises the geotechnical properties of the soil.

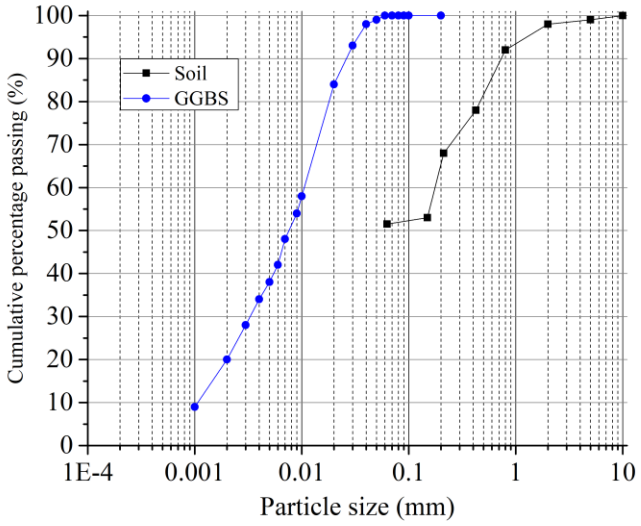

Figure 26. Soil and GGBS's particle size distribution

Table 5. Chemical composition (wt. %) of the soil and GGBS (obtained from an EDS analysis of 2 samples per material, each comprising 10 points)

Element (wt. %)	Al_2O_3	CaO	CuO	Fe_2O_3	K_2O	MgO	MnO	Na_2O	SO_3	SiO_2	TiO_2
Soil	24.39	-	0.13	2.04	2.02	1.60	-	0.98	-	68.38	0.46
GGBS	12.34	37.29	0.17	0.35	1.16	8.92	0.61	-	2.55	35.92	0.69

Table 6. Geotechnical properties of the soil

Property			Results		Units
Atterberg limits (a)		Liquid limit	LL	32.4	%
		Plastic limit	PL	10.5	%
		Plasticity index	PI	21.9	%
Compaction (b)		Optimum water content	ω_{opt}	12.4	%
		Maximum dry density	$\rho_{d,max}$	1.92	Mg/m³
Oedometer tests (c) (e)		Compression index	c_c	0.1391	
		Recompression index	c_r	0.0236	
		Preconsolidation stress		100	kPa
Consolidated undrained (CU) triaxial tests (d) (e)	Effective stress (at ε_a = 3 %)	Cohesion	c'	0	kPa
		Friction angle	ϕ'	30	°
		Slope of the critical state line	M	1.2	
	Total stress (at ε_a = 3 %)	Cohesion	c_u	71	kPa
		Friction angle	ϕ_u	7	°
	Secant deformability modulus (f)		E_{sec}	{18, 37, 67}	MPa
	Shear modulus (g)		G	{235,684, 1000}	MPa

(a) BS 1377 2 (1990); (b) BS 1377 4 (1990); (c) BS 1377 5 (1990); (d) BS 1377 8 (1990); (e) Non-stabilised soil specimens for the one-dimensional consolidation and triaxial tests were built using the slurry consolidation method (De Sheeran and RJ, 1971) with a water content (ω) and dry density (ρ_d) of 17.4 % and 1.81 Mg/m³, respectively; (f) E_{sec} at (ε_a) = 0.5 % and p'_0 = {150, 337, 600} kPa; (g) G at shear strain (ε_q) = 0.001 % and p'_0 = {150, 337, 600} kPa

Blast furnace slag supplied by Hanson Cements Ltd was chosen as precursor material, with a granulated grain size of 0-5 mm, density at 20°C of 2.4-3 Mg/m³ and pH of 10-12 (DEV-S4-eluate according to EN 12457-4) (Figure 26). As shown in the XRD analysis (Figure 27) and Table 5, the precursor is mainly composed by glass phases (amorphous material) and, its main elements are calcium aluminosilicate frameworks (Ca, Si and, Al ≅ 85.55 wt. %). The commercial activator chosen to ensure the high pH in the

mixtures was NaOH, originally in granular form and later dissolved in deionised water to a pre-determined concentration of 3.5 molal.

3.2.2 Specimen preparation

The stabilised soil specimens were built using the static compaction method described in ASTM D 1632 (2007) with water content (ω) = 17.4 % and dry unit weight (ρ_d) = 1.81 Mg/m^3, wherein the solid elements (92.5 % of soil, 5 % of GGBS, and 2.5 % of NaOH of the total dry soil weight) were firstly mixed and then added to distilled water. For triaxial tests, the mixture was placed in layers into PVC moulds with a height and diameter of 140 mm x 70 mm, respectively, and each layer was manually compacted. The stabilised soil specimens for the one-dimensional consolidation tests were made inside the oedometer ring (20 mm (height) x 50 mm (diameter)) following the static compaction method described above. In the end, the specimens were wrapped with cling film and kept in a humid chamber at a constant temperature and humidity of 20°C ± 1°C and 95 %, being only extruded from the moulds before starting the tests. Finally, for comparison purposes, the compaction conditions of the stabilised and non-stabilised soil specimens were held identical.

3.2.3 Laboratory testing

A suite of laboratory tests was conducted to assess the overview behaviour of the stabilised soil in the short (28 days) - long (90 days) term.

The mineralogy phases and chemical composition were determined by XRD and SEM-EDS analyses on unpolished stabilised soil specimens. The SEM analyses were performed on a FEI Quanta 400 scanning electron microscope, with 30 kV, in low vacuum mode (1.3 mbar), avoiding the deposition of a conductive layer. The device was coupled with an EDS analyser, from EDAX. Although the focus of the laboratory testing was to assess the geomechanical behaviour of the stabilised soil, the characterisation of the binding phases was fundamental to enhance the understanding of how the evolution of the shear strength parameters and stiffness over time progresses. For the analyses, small pieces extracted from the triaxial specimens after the test were collected, soaked in acetone and dried at 28 and 90 days for arresting the reactions according to the methodology described by Zhang and Scherer, 2011 to stop the cement hydration.

3. GEOMECHANICAL BEHAVIOUR OF A SOFT SOIL STABILISED WITH ALKALI-ACTIVATED BLAST-FURNACE SLAGS

The geomechanical behaviour of the stabilised soil was assessed by two tests, namely: one-dimensional consolidation and triaxial tests. Shear strength and stiffness were obtained via consolidated drained triaxial tests (BS 1377 8, 1990), where the impact of a large range of OCR and p'_0 (Table 7) was assessed on the stress-strain and stiffness degradation curves, volumetric strain curves and failure surface modes. The OCR was imposed during the consolidation phase, through loading and unloading of the specimens. Compressibility was assessed by oedometer testing (BS 1377 5, 1990), from which the preconsolidation stress and both the virgin compression (c_c) and the recompression (c_r) indexes were determined.

Table 7. Triaxial tests

ID	Consolidation		OCR
	Maximum (kPa)	Final (kPa)	
OCR1 (150)	150	150	1.0
OCR1 (337)	337	337	1.0
OCR1 (600)	600	600	1.0
OCR3.3 (150)	500	150	3.3
OCR6 (84)	500	84	6.0
OCR12.2 (41)	500	41	12.2

Finally, leachate analyses were carried out to evaluate the risk of contamination due to the addition of small amounts of GGBS and NaOH to the soil. Two stabilised soil specimens were tested, after 28 and 90 days curing, from which the eluates were extracted according to EN 12457-4, 2002. This European standard describes a one stage batch test, at a liquid to solid weight ratio of 10/l, performed on particles below 10 mm. It aims to guide the process of obtaining an extract of solid waste, and not to obtain an extract of the actual leachate produced from a solid waste in the field, nor to simulate site-specific leaching conditions. At the start of the test, the specimens were weighted, crushed with a cutting device and sieved through a 10 mm nominal screen size sieve. If no more than 5 % (mass) was retained, the fraction above 10 mm was reintroduced in the crushed sample. Otherwise, the oversized fraction was crushed for a second time, taking care to avoid excessive grinding. A sample of approximately 90 g was then collected, using a sample splitter, and placed in an individual glass bottle. The leachant (in this case, distilled water) was then added to the same bottle, corresponding to 90 g of crushed material to 0.9 l of water. The pH was measured immediately

after the water was added, using a standard pH-meter. The bottle was shaken for 24 h, at a rotation speed of 20 rpm, on a platform rotator, and the pH was measured again. After a resting period of 15 min, a leachate sample of 200 ml was collected using a graduated pipette. Approximately 50 ml were separated from the sample and added 5 ml of Nitric Acid, in order to lower the pH value and thus maintain the metals content in the leachate. The remaining 150 ml of eluate remains intact, and both samples were analysed to determine the concentration of the elements of interest. The eluate results were subsequently compared with the limiting values for inert waste defined by the Annex IV of the Portuguese Law Decree n. 183 (2009), which establishes in which kind of landfill a certain material can be disposed, according to the percentage content of several elements on the leachate (inert waste, non-hazardous waste and, hazardous waste) with the inert waste showing the stricter limits.

3.3 Results and discussion

3.3.1 XRD and SEM-EDS analyses

XRD analysis

Figure 27 shows the XRD results of the stabilised soil after 28 and 90 days curing. For comparative purposes, the non-stabilised soil specimens XRD results were also plotted in the same Figure. Both mineralogical compositions (stabilised and non-stabilised soil) are very similar, with albite (A), muscovite (M) and quartz (Q) as the main minerals.

When comparing the results of the non-stabilised and stabilised soil specimens after 28 curing days, no new mineral phases were detected. However, lower peak intensities and, inclusive the total disappearance of some peaks, namely muscovite and albite at 30 2θ, albite at 50 2θ and muscovite at 57 2θ, were noticed, which suggests that there was dissolution of some mineral phases and, possibly, the formation of cementitious gels (Cristelo et al., 2011). The high magnitude of the quartz peak detected after 28 days in the stabilised soil only confirms the highly crystalline nature of this mineralogical phase.

After 90 curing days, two new mineralogical phases were detected, the microcline (Mi) and oligoclase (O). Also, a general reduction and/or the disappearance of some peaks of M, Q, and A minerals was noticed. However, these peak intensities reductions from 28 to 90 days were less pronounced compared with the 28 days curing specimens. Although less pronounced, but still in line with what was observed previously, these aspects suggest that there was the formation or/and development of hydration products until at least 90 days.

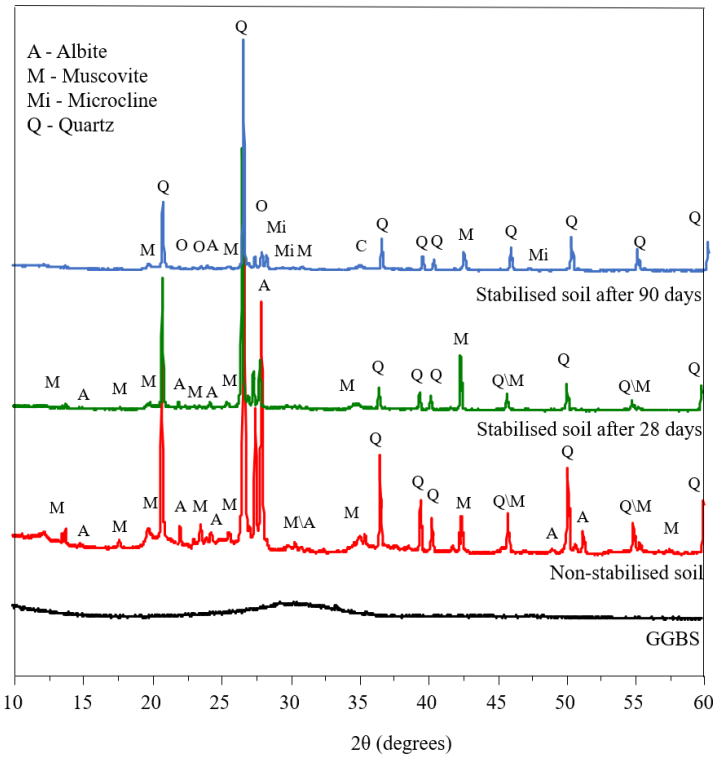

Figure 27. XRD analyses results

SEM-EDS analysis

Figure 28 displays SEM images of the original and stabilised soil after 28 and 90 days curing. A variety of face-to-face, edge-to-edge, and edge-to-face contacts can be seen between soil particles and hydration products. The gel distribution among the particles seems to be fairly homogeneous, especially after 90 days, which is coherent with the observations presented by Lloyd et al. (2009). The voids between the soil particles

have become mostly filled with gel, which altered the microstructure and produced a denser and less permeable material. Due to its irregular polyhedron forms, GGBS particles cannot be found easily through the SEM images. However, soil particles are easily spotted, surrounded, and bonded by the gel matrix.

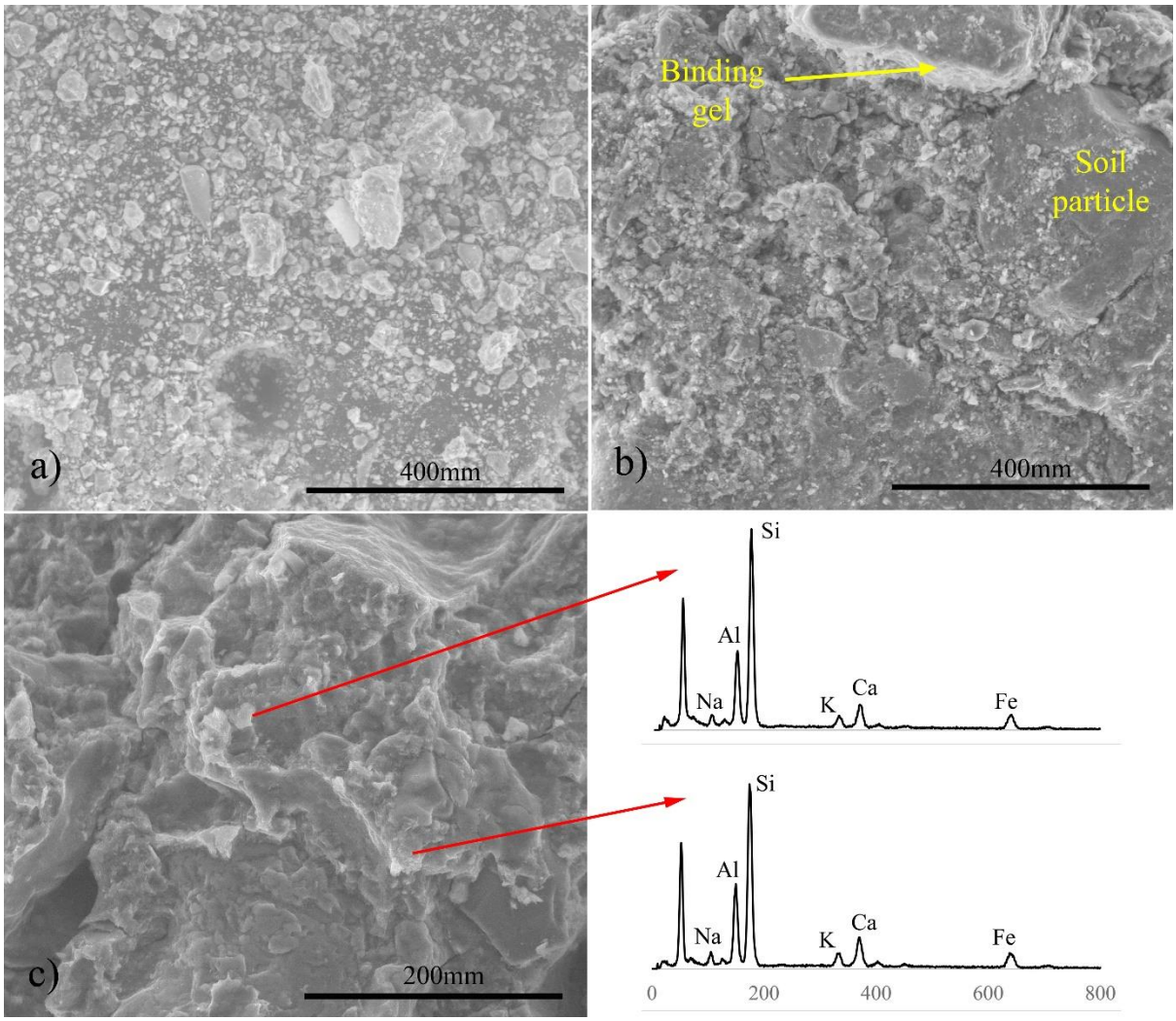

Figure 28. SEM images of the original (a) and stabilised soil after 28 (b) and 90 days (c)

A more detailed EDS study, comprising approximately 40 points on three different images, was conducted on the 90-day curing samples, to estimate the composition of the gel, as it controls the final properties of the binding matrix and, consequently, the mechanical behaviour (shear strength, stiffness, and compressibility)

of the stabilised soil. As an example of the general composition of the soil, two of the EDS spectra obtained are also included in Figure 28.

The EDS data showed that Si and Al were the elements with the highest concentrations in the gel phase, but sodium and calcium were also present, in average weight contents (from the total number of data points collected) of 5.2 % and 7.2 %, respectively. These values suggest the formation of a N,C-A-S-H type gel, with average weight ratios of Ca/Si = 0.138 and Al/Si = 0.311. This Ca/Si ratio is significantly lower than what is usually found in C-S-H systems, which is approximately 1.7 (Richardson, 1999). Such difference is explained by the incorporation of extra Al, as a consequence of the addition of secondary materials, like coal fly ash or, as is the case, blast furnace slag (Li et al., 2018). It is also a consequence of the high silicon content (Li et al., 2019a), resulting from the amorphous phase of the precursor (the quartz from the soil might also contribute, but to a lower degree). This change in the Ca/Si ratio does not greatly alter the foil-like morphology of the gel, compared with what would be obtained from a C-S-H (Li et al., 2019a; Myers et al., 2015b).

3.3.2 Mechanical tests

One-dimensional consolidation test

Compression curves for the soil in its non-stabilised and stabilised states after 28 and 90 curing days are displayed in Figure 29. Pre-consolidation pressures and compressibility indices are provided in Table 8. Compression indices are indicators of the compressibility of the soil/mixture, while the pre-consolidation stress represents the highest effective stress that the soil has ever experienced and defines the boundary between stiff and soft deformation response of the soil. The vertical yield stress was determined by the intersection of the virgin compression (post-yield) and compression (pre-yield) lines.

A stiffer response is observed in the stabilised soil specimens (see Figure 29). After 28 days, the specimen with 7.5 % GGBS-NaOH exhibited an improved consolidation behaviour when compared with that observed in its non-stabilised state, as proven by the reduction of the virgin compression (c_c) and recompression (c_r) indices of 77.7 % and 12.5 %, respectively (Table 8). Between 28 and 90 days, these reductions were 58 %

and 83 %. Moreover, as previously observed in stabilised soils with cement or lime, artificially cementation using the alkaline binder also increased the pre-consolidation stresses from σ'_v = 100 kPa (non-stabilised soil) to σ'_v = 200 kPa (stabilised soil at 28 days) and σ'_v = 1000 kPa (stabilised soil at 90 days) which is in accordance with other studies (Kasama et al., 2000; Quiroga et al., 2017). Although less noticeable than in the non-stabilised soil curves, in the stabilized mixtures, when the pre-consolidation stress (post-yield) is achieved, the stiffness slightly falls (slope of the ν - log σ'_v curves show a sudden change) and, for pressures below of this value, the one-dimensional response is stiff and essentially recoverable.

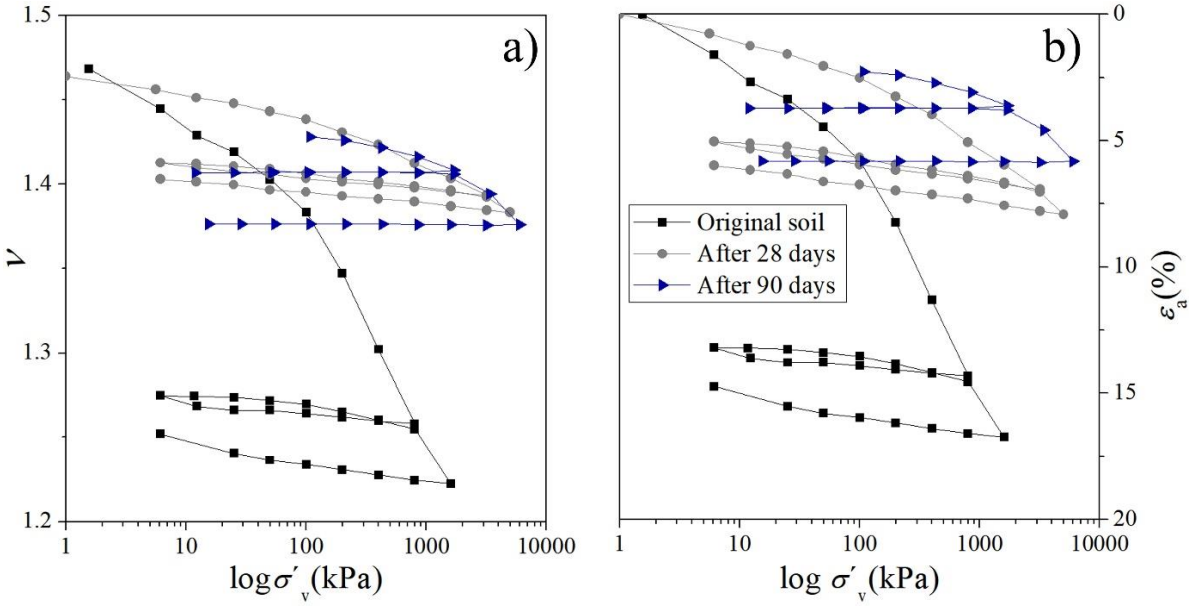

Figure 29. Compression curves: specific volume (ν) - vertical effective stress (σ'_v) (a); and axial strain (ε_a) - vertical effective stress (σ'_v) (b)

In summary, a significant improvement in compressibility and therefore stiffness was observed after 28 and 90 curing days in the stabilised 7.5 % GGBS-NaOH specimens. This behaviour, mainly caused by the development of cementitious bonds between the soil particles, was also responsible for the enhancing of the pre-consolidation stress over time.

Table 8. Compression indices

		Non-stabilised Soil	Stabilised soil	
			28 days	90 days
Compressibility indices	c_c	0.1391	0.0309	0.0165
	c_r	0.0236	0.0075	0.0017
Pre-consolidation stress	σ'_v	100	200	1000

Triaxial tests

To assess the influence of the overconsolidation ratio (OCR) effect on the shear strength and stiffness of the stabilised soil, results of deviatoric stress, q, pore pressure variation, Δu, and secant deformability modulus, E_{sec}, were normalized to q_n, Δu_n, and $E_{sec,n}$ by dividing all the data by the value of initial mean effective stress (p'_0).

Triaxial results reported from Figure 30 to Figure 33 demonstrate that regardless of the OCR or p'_0 applied during the tests, the stabilised soil with 7.5 % GGBS-NAOH exhibited an experimental behaviour (Figure 30 and Figure 31) under monotonic triaxial compression similar to the one observed in cement clay mixtures (Quiroga et al., 2017) cured in similar laboratory conditions, with peak/residual strength and dilatation, increased normalised strength/stiffness and tendency for dilatation during the shear phase. A resembling behaviour was also reported by other authors (Asghari et al., 2003; Ghadakpour et al., 2020; Xiao et al., 2014) in stabilised soft soils with cement. Regarding the stress-strain behaviour, the impact of confinement stress (represented by p'_0) is clearly visible on the curves. An increase of p'_0 (OCR = 1) led to an increase in both peak/residual shear strength (Figure 30 (a) and (b)). Normalized results showed an increased normalized peak/residual strength with the increasing of OCR (Figure 30 (c) and (d)). All specimens presented a strain-hardening behaviour before the peak deviatoric stress followed by strain-softening until the failure state was reached.

From 28 (Figure 30 (a)) to 90 (Figure 30 (b)) curing days, no significant differences are visible in terms of shear strength gains. For similar p'_0values, peak/residual deviatoric stresses at both curing ages were very similar, showing that the highest impact of the addition of the alkaline binder to the soil occurred up to 28

days. As reported by other authors, the early-strength development using GGBS is quicker than compared with aluminosilicates precursors with low calcium content (e.g. Class F FA) due to the considerable Ca amount present in its composition (Sargent et al., 2013).

Finally, the linear region of the stress-strain curves (Figure 30 (a) and (b)) demonstrate that the impact of p'_0 on the initial stiffness of the specimens tested with OCR = 1 is not clear since no significant increase of stiffness with the increasing of $p'_0$was observed. At 90 curing days, the slopes of the linear regions are higher compared to 28 days, i.e., there are measurable stiffness gains, and also are practically overlapped (Figure 30b), showing that also at this curing age stiffness is almost p'_0independent. Normalized results showed an increase of normalized strength with the increasing of OCR showing the impact of the stress history in the geomechanical behaviour of the stabilised soil.

Similar trends were observed in all volumetric strain curves, ε_v- ε_a, during the shear phase (Figure 31): a contractive behaviour ($\Delta\varepsilon_v > 0$) up to the peak deviatoric stress followed by a dilatant behaviour ($\Delta\varepsilon_v < 0$) until the end of the test; an increased tendency for dilation with decreasing of p'_0.

Mohr-Coulomb shear strength parameters were derived from the triaxial tests to determine the effective shear strength of the stabilised soil (Table 9). Residual parameters were determined at ε_a = 4.1 % (28 days) and ε_a = 5.3 % (90 days), when the respective shear stresses stabilised. For comparison purposes, the shear strength parameters of the original soil are also presented.

Table 9. Shear strength parameters

Material	Curing time (days)	Total stress		Effective stress			
		Residual		Peak		Residual	
		c (kPa)	ϕ (°)	c' (kPa)	ϕ' (°)	c' (kPa)	ϕ' (°)
Original soil	-	71	7	-	-	0	30
Stabilised soil	28 days	-	-	334	49	0	48
	90 days	-	-	503	42	0	44

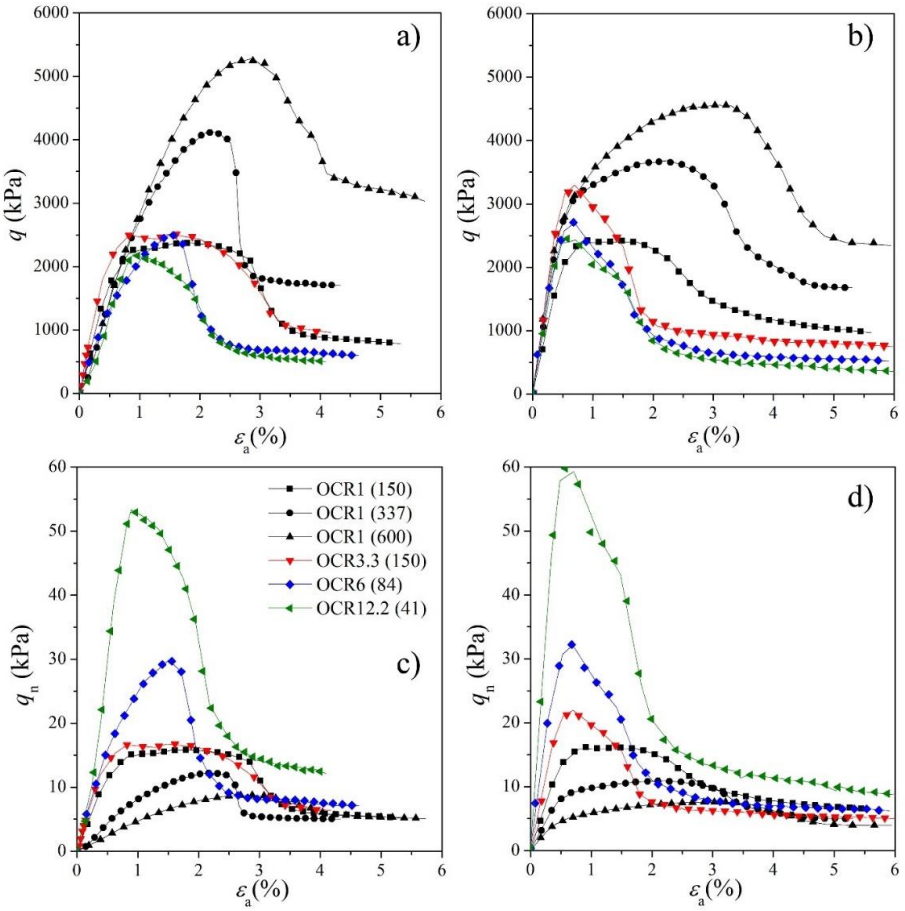

Figure 30. Deviatoric stress response: q - ε_a after 28 days (a) and 90 days (b); q_n - ε_a after 28 days (c) and 90 days (d)

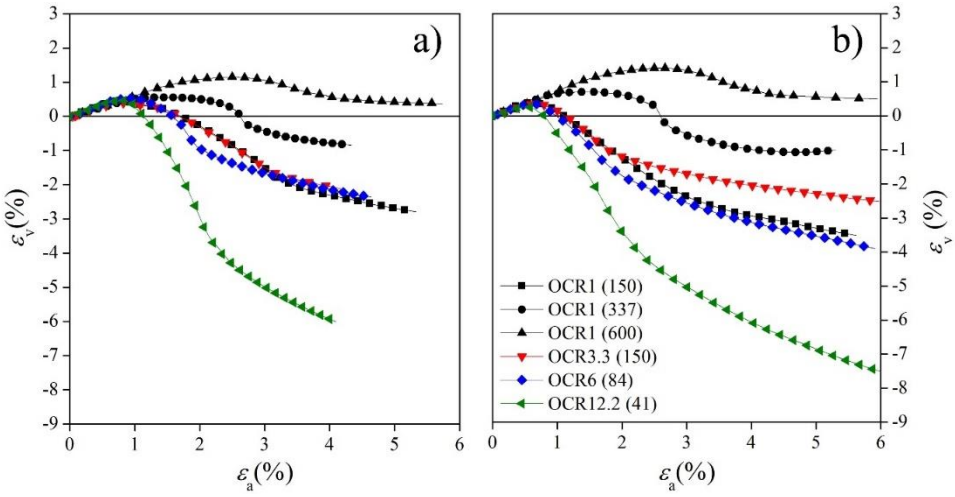

Figure 31. Volumetric strain curves: ε_v - ε_a after 28 days (a) and 90 days (b)

Although the effective shear strength parameters of the non-stabilised and stabilised soil were determined under different drainage conditions, the 28-day peak values (c' = 334 kPa and ϕ' = 48°) clearly represent a significant improvement of the shear strength due to the addition of the alkaline binder. Fundamentally, the GGBS-NaOH acted like glue, connecting the soil particles through the development of cementitious bonds. Between 28 and 90 days, the peak c' value increased from 334 kPa to 503 kPa (≅ 51 %), which shows that there was a continuous development of the gel beyond the initial period of 28 days. On the other hand, a slight decrease in both the peak (≈ 14 %, from 49° to 42°) and residual (≈ 8 %, from 48° to 44°) values of ϕ' was observed between 28 and 90 days, which may be explained by the development of additional volumes of AA gel, increasing cohesion but, at the same time, slightly mitigating the frictional component of the soil's strength. As expected, null values of residual c' were obtained for the non-stabilised and stabilised soil after 28 and 90 days since, at large strains, there is a complete breakdown of cementitious connections between the soil particles.

Though there were variations in both the peak and residual values of the cohesion (c') and friction angle (ϕ'), between 28 and 90 days, graphical representations of the strength envelopes (Figure 32) show an overlapping of the peak and residual states at both curing ages, which indicates that there were no significant modifications of the total shear strengths from 28 to 90 days. As previously mentioned, the addition of 7.5 % GGBS-NaOH to the soil was responsible for the increasing of ϕ from 30° to 48° after 28 days, which translated in an increase of the slope of the critical state line (M) from 1.3 to 1.97. After 90 days, the mentioned reduction of the residual ϕ', from 48° to 44°, implied a reduction of the critical state line slope to 1.80.

Stiffness degradation curves at both curing ages are shown in Figure 8. When compared the E_{sec} at ε_a = 0.5 % of the non-stabilised (Table 6) and stabilised soil (Figure 33), it is evident that there were large stiffness increments of the material after the addition of GGBS-NaOH. After 28 days, the results show stiffness increments 4 to 19 times higher than those of the non-stabilised soil. At 90 days, these values were 8 to 21 times higher. After 28 days (Figure 33 (a)), for 0.5 % < ε_a < 1 %, it was observed a decrease of the E_{sec} between 10 % and 44 %. After 90 days (Figure 33 (b)), there was a more pronounced decrease for the same strains range (between 20 % and 66 %). For ε_a > 3 %, all stabilised soil specimens presented practically negligible

stiffness values, which remained approximately constant until the end of the tests. Normalized results showed an increase of normalized stiffness with the increasing of OCR.

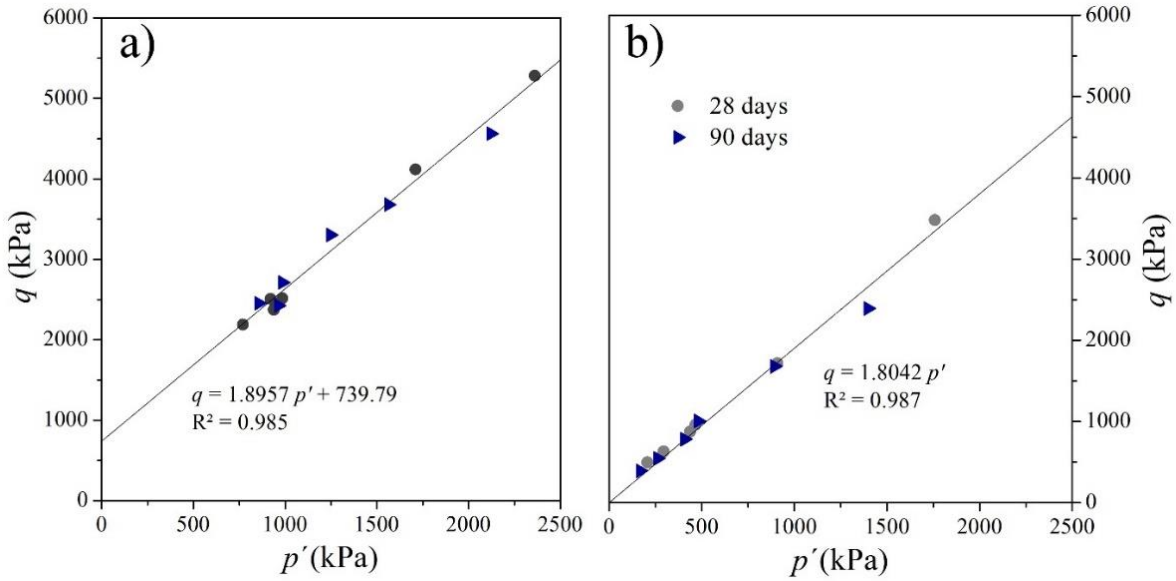

Figure 32. Overlap of strength envelopes after 28 and 90 days of curing: peak (a) and residual (b)

Based on the triaxial behaviour of the stabilised sandy clay soil with 7.5 % GGBS-NaOH, the following conclusions can be drawn:

- The stress-history (represented by OCR) had influence on the normalized shear strength/stiffness and normalised tendency for dilatation of the material.
- The impact of the stress-history (represented by p'_0) on the shear strength is also evident, observing an increase of both peak/residual deviatoric stresses on the tests with OCR=1 with the increase of p'_0. On the other hand, the impact of p'_0 on the stiffness results is not so clear.
- The highest shear strength/stiffness gains were observed up to 28 days. From 28 to 90 days, the total peak/residual shear strength remained practically constant. However, an enhancement of the stiffness over this curing period was observed.

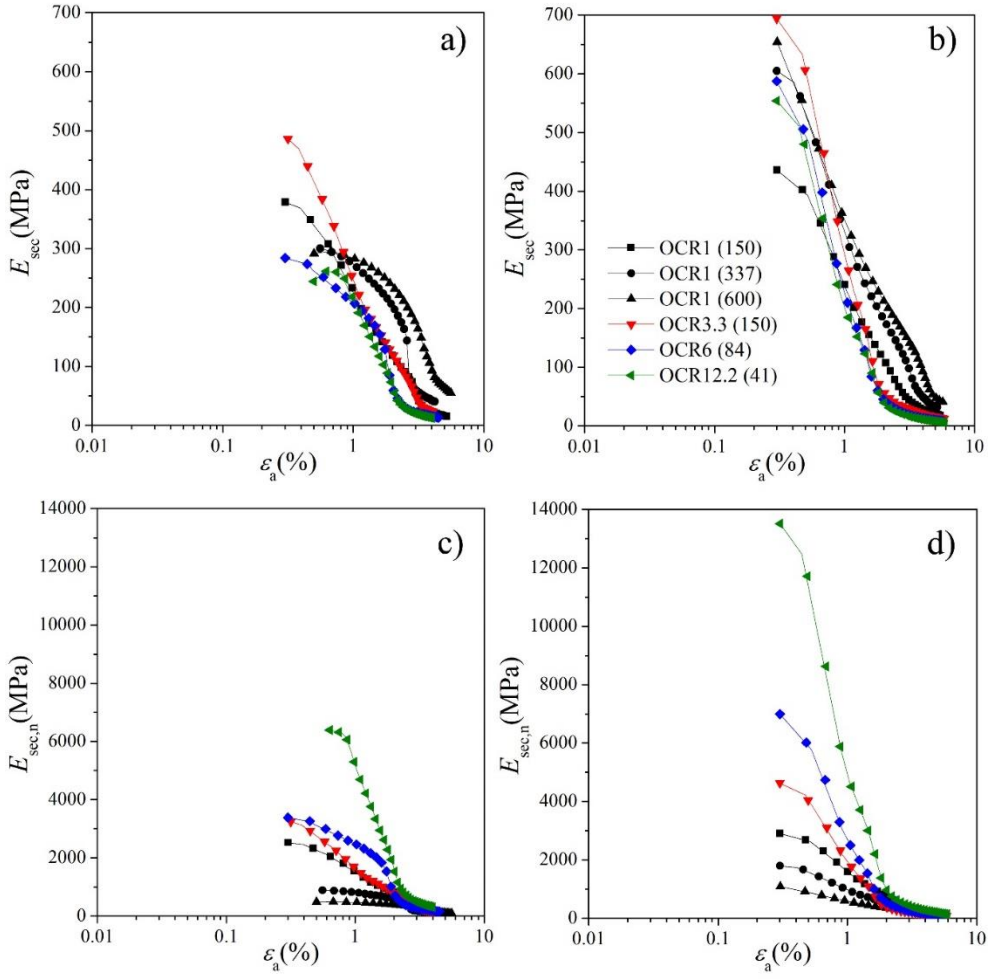

Figure 33. Secant deformability modulus: E_{sec}- ε_a after 28 days (a) and 90 days (b); $E_{sec,n}$- ε_a after 28 days (c) and 90 days (d)

Figure 34 illustrates the failure modes observed on the stabilised soil specimens after shearing phase. Most of them presented a well-defined failure surface, typical of stiff materials. The increase of OCR (consequently decreasing of p'_0) led to the formation of a larger number of vertical cracks (Figure 34 (d), (e) and (f)). On specimens with OCR = 1, the increase of p'_0 led to a shear failure, with a nearly 45° slope surface (Figure 34 (a), (b) and (c)).

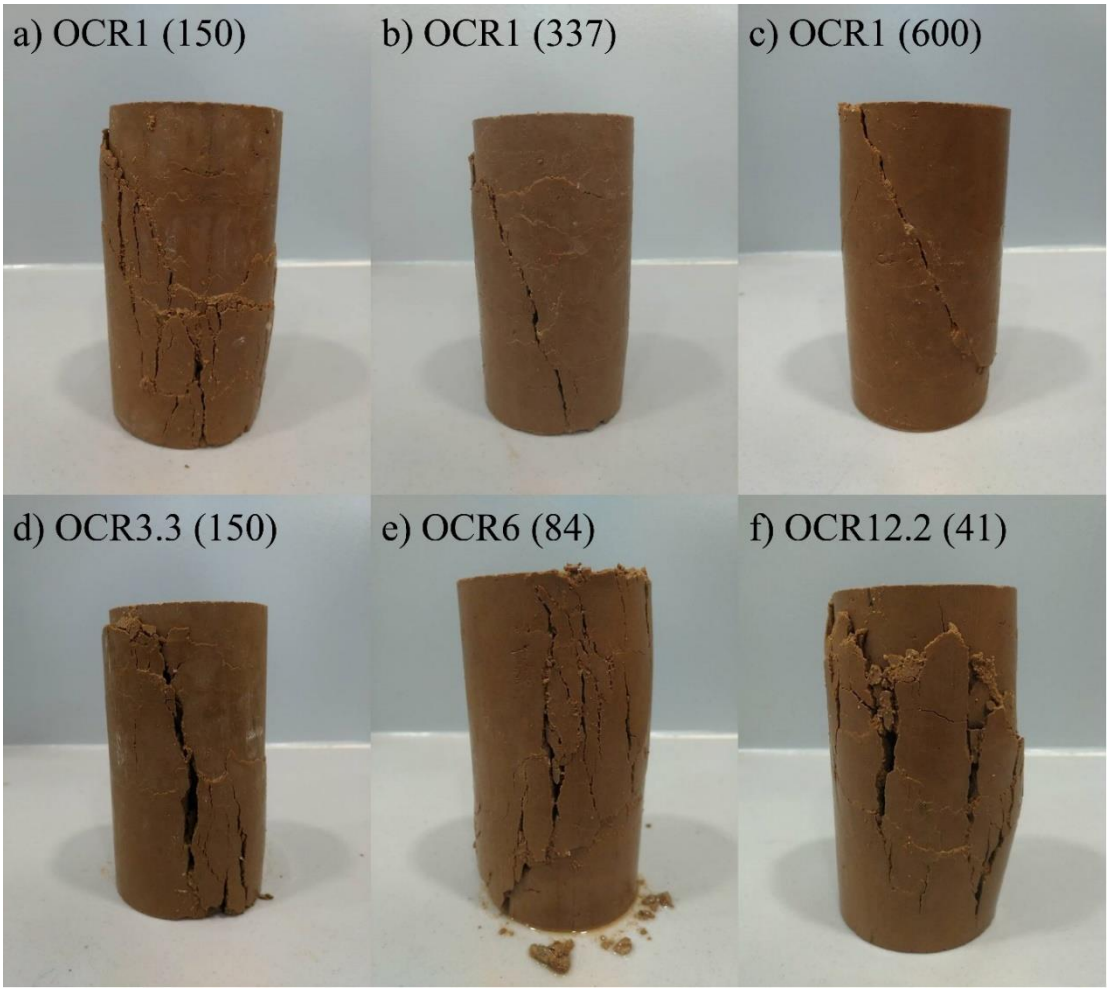

Figure 34. Typical failure modes on the stabilised soil

3.3.3 Leachate analysis

Leachate results are summarized in Table 10, along with the corresponding limit values for a material to be considered as "inert waste" as defined by Annex IV of the Portuguese Law-Decree no. 183/2009.

From the leachate results, the concentration of all analysed elements complies with the legal requirements so that the tested materials can be classified as "inert waste" at both ages. Therefore, the addition of 7.5 % of GGBS-NaOH to the soil, besides significantly increase its strength and stiffness, does not represent a risk for soil contamination according to the used Decree of law.

Table 10. Leachate results and corresponding limits imposed by the Law-Decree no. 183/2009

Element	Limits for 'inert waste' (mg/kg)	Leachate results of the stabilised soil (mg/kg)	
		28 days	90 days
As	0.5	0.0	0.2
Cr	0.5	0.1	0.0
Cu	2.0	0.0	0.0
Ni	0.4	0.1	0.0
Pb	0.5	0.0	0.0
Zn	4.0	0.1	0.1
Clorets	800	45.5	44.7
Fluoride	10	0.8	1.3
Sulphate	1000	25.5	0.0

3.4 Conclusions

The geomechanical behaviour of a soft soil stabilised with 7.5 % GGBS-NaOH was investigated at short (28 days) – long (90 days) term. The SEM-EDS and XRD analyses and the mechanical results allowed to reach the following conclusions:

- The main binding phase was C-A-S-H, similar to that formed in blended cement concrete.
- Oedometer test showed a significant reduction of the soil compressibility after the addition of GGBS-NaOH and an increase of the pre-consolidation stress up to 90 days. Under triaxial compression, the stabilised material exhibited a behaviour reminiscent of cement-clay mixtures, with peak/residual strength and dilatation, increased normalised strength/stiffness and normalised tendency for dilatation. The total peak/residual shear strength remained practically constant at both curing ages.
- According to the leachate results, the stabilised soil is considered an 'inert material' and, therefore, there is virtually no risk of soil contamination when using the developed binder.

4. PREDICTING THE MECHANICAL BEHAVIOUR OF A SANDY CLAY STABILISED WITH AN ALKALI-ACTIVATED BINDER

There is a growing interest in the mechanical behaviour of low performing soils strengthened with alkali-activated materials that have been promoted as low-carbon-footprint binders. This paper focuses on the mechanical behaviour of a sandy lean clay stabilised with alkali-activated blast furnace slags after short (28 days) and long (90 days) curing periods and on the numerical prediction of the observed stress-strain responses using a kinematic hardening constitutive model. The main compositions of the soil and blast furnace slags were determined by Energy-Dispersive X-ray Spectroscopy (EDS) analyses, while the mineralogical phases by X-ray powder diffraction (XRD). Scanning Electron Microscopy (SEM) analyses were carried out on blast furnace slags and soil, before and after stabilisation, at 28 and 90 curing days. Consolidated undrained and drained triaxial tests were conducted on both non-stabilised and stabilised geomaterials in a range of initial mean effective stresses from 41 to 600 kPa and overconsolidation ratios from 1 to 12.2. These test results were used to calibrate and analyse the ability of a kinematic hardening constitutive model to predict the stress-strain responses of both geomaterials. It was the first attempt of using this constitutive model in artificially cemented soils. Triaxial test results carried out on the stabilised sandy lean clay specimens at both curing periods showed a behaviour resembling those observed for cement-mixed clays. The model was able to successfully predict the smooth elastoplastic transition observed on the reconstituted sandy clay specimens and also the peak/residual shear strains and strain-softening behaviour after peak strengths observed after adding the alkali-activated binder to the soil at both curing ages.

Keywords: soil stabilisation; alkali-activated binder; SEM-EDS and XRD analysis; triaxial tests; kinematic hardening constitutive model

---

This Chapter is based in the article:

Corrêa-Silva, M., Rouainia, M., Miranda, T., Cristelo, N., 2021. Predicting the mechanical behaviour of a sandy clay stabilised with an alkali-activated binder. Eng. Geol. 292, 106260. https://doi.org/10.1016/j.enggeo.2021.106260

4. PREDICTING THE MECHANICAL BEHAVIOUR OF A SANDY CLAY STABILISED WITH AN ALKALI-ACTIVATED BINDER

4.1 Introduction

Unperforming foundation soils are characterized by their low shear strength and stiffness, which can be overcome by adding cementitious binders such as ordinary Portland Cement (OPC) or lime. However, there are growing environmental concerns over the significant carbon footprint associated with the use of OPC. The OPC production is responsible for at least 7% of the world's CO_2 emissions (Maddalena et al., 2018), and the average emissions for each cubic meter of concrete production are approximately 0.2 t, which amounts to 0.08 t CO_2 per ton of concrete (Gartner, 2004). These statistics are environmentally unsustainable if the construction industry wants to make an impactful contribution towards achieving the global aim of net zero carbon emissions within the next 30 years. This has led to high levels of research interest over recent years in the development of alternative low-carbon waste-based binders.

One class of low-carbon footprint binders that has a great potential for replacing OPC are the alkali-activated binders. These binders are commonly synthesised from sodium-based activators (e.g., sodium hydroxide (NaOH) and/or sodium silicate (Na_2SiO_3)) mixed with silica (SiO_2) and alumina (Al_2O_3) rich industrial residues or wastes, such as fly ash (FA) (Araújo et al., 2020; Cristelo et al., 2015; Rios et al., 2016b; Vitale et al., 2017), palm oil fuel ash (POFA) (Lokmane Abdeldjouad et al., 2019; Pourakbar et al., 2015), blast furnace slags (Bensaifi et al., 2019; Fasihnikoutalab et al., 2020; Thomas et al., 2018; Wang et al., 2020), glass powder, rice husk ash and silica fume (Canakci et al., 2019; Gao et al., 2020; Geraldo et al., 2017). The source of SiO_2 and Al_2O_3 should be subjected to thermal treatment before adding the alkaline activators to reduce the amount of crystallisation water and create an amorphous chemical structure with a very reactive response (Cristelo et al., 2012). At the initial stage, the high pH environment causes the dissolution of the SiO_2 and the Al_2O_3 available on the system. The Si and Al released causes an excess of negative charges that are compensated by the sodium. The reaction products precipitate and form the cementitious compounds responsible for the enhancement of the soil properties. When low calcium (Ca) precursors (e.g. type F FA) are used, a three-dimensional amorphous gel is formed, represented by the chemical structure N-A-S-H (Fernández-Jiménez et al., 2017). This gel requires aggressive synthesis conditions to be formed, such as a highly alkaline medium and elevated temperature (Abdullah et al., 2020). On the other hand, when aluminosilicate materials are mixed and activated with calcium-based components (e.g. slag), a (N,C)-A-S-H

type gel is usually formed. Contrary to N-A-S-H gel, the (N,C)-A-S-H is capable of developing under ambient temperature and low-alkali conditions, mostly due to the catalyser effect of the Ca (Abdullah et al., 2020).

Some benefits can be linked with the use of alkali-activated binders instead of OPC. The absence of limestone calcination is one of them since it is an energy-intensive process that produces calcium oxide and releases CO_2 into the atmosphere. Furthermore, the alkali-activated binders incorporate industrial residues or wastes into their composition, which allows a significant rate of reuse and valorisation of these materials, thereby promoting circular economy and reducing the need for landfill. In terms of financial cost, it is still rather early to develop an accurate cost estimation associated with this novel soil stabilisation solution due to the limited field-scale applications, which are far from being optimised or understood. Issues such as the injection and mixture with the soil, the need for compaction, the role of natural phreatic level on the properties and requirements of the binder, are factors that cast significant doubts over the material and working costs of the proposed stabilisation technique. Nevertheless, Cristelo et al., 2015 compared the cost of the techniques when applied to the production of jet mixing columns. The authors concluded that the cost of the least expensive alkali-activated cement solution was still 13% higher than the Portland cement-based solution, mostly due to the cost of the activator. Miranda et al., 2020 assessed the viability of using different alkali-activated cements to stabilise a (sub)base layer in a full-scale trial. Concerning the cost and environmental impact analyses, the authors concluded that an optimization of the alkaline binder formulations is required. This optimization should focus on the reduction of the used quantity of NaOH and/or Na_2SiO_3, or even by replacing them for a cheaper material or by other waste with no commercial cost, preferably in a solid form.

Recent research has reported the effectiveness of the alkali-activated binders in soil stabilisation, with benefits on swell suppression and enhancement of strength and stiffness both at laboratory and field-scale (Consoli et al., 2020; Cristelo et al., 2015; Miranda et al., 2020; Obuzor et al., 2012; Yu et al., 2020). However, although there is extensive literature focusing on mechanical tests in a general way, and chemical and environmental analysis, there is still scarce research related to the mechanical behaviour of these stabilised geomaterials through triaxial tests. Corrêa-Silva et al., 2019 undertaken triaxial tests on a lean clayey sand stabilised with low Ca FA and NaOH-Na_2SiO_3 after 28 days and reported an improvement of all shear strength parameters and stiffness, with an increase of the critical friction angle in 50% and 73% in effective and total

stress. Rios et al., 2019 noticed a significant evolution of strength and stiffness beyond 28 curing days in a silty sand stabilised with low Ca FA and NaOH-Na_2SiO_3 and very high peak strength parameters (ϕ' = 63.5° and c' = 231.6 kPa) with stress-strain behaviour typical of cemented soils. In another study, Abdullah et al., 2019 observed that the addition of increasing amounts of a slag/FA geopolymer (0%, 10%, and 20%) in different types of clays considerably increased the yield stress and modified the stress-strain behaviour from ductile into a brittle post-peak response. A strain-softening behaviour after the peak strength caused by the progressive breakdown of the artificial cemented bonds was observed by Rios et al., 2018 in soil mixtures with lime and alkali-activated FA, with peak strength at very low strain levels. Sargent et al., 2020b observed an undrained response characterized by work hardening up to peak conditions followed by strain-softening in an alluvium soil stabilized with activated blast furnace slags.

Apart from that, but still linked to the shear behaviour of soft soils stabilised with alkali-activated binders, another gap of knowledge was detected related to the use of existent constitutive models to predict the experimental behaviour of these geomaterials using triaxial test results. The majority of published papers on numerical modelling currently are based on the behaviour of soils stabilised with conventional binders, such as OPC. The ability to predict the mechanical behaviour of stabilised soil with alkali-activated binders is crucial for practical applications.

Many researchers have developed constitutive models incorporating the influence of breakage of structure on the overall behaviour of artificially cemented soils. The elastoplastic theory within the critical state framework with softening plasticity is a common feature for the majority of constitutive models found in the literature for structured soils (Yapage and Liyanapathirana, 2019). Horpibulsuk et al., 2010 extended the theoretical framework of the Structured Cam Clay model to consider the features of the behaviour of cemented clays, modifying the mean effective strength parameter and adding a new destructuring function. The authors concluded that, after modifications, the behaviour of cemented clays was reasonably well represented by the model. Nguyen et al., 2014 proposed a new model, based on the Modified Cam Clay, to capture the cementation effect that diminishes as the confining pressure increases in cemented clays, and noticed that the main features of the undrained stress path and stress-strain relationship, and cementation degradation for high confining pressures, were well predicted by the model. Quiroga et al., 2017 used a

bounding surface elastoplastic model to predict the monotonic and cyclic stress-strain behaviours and stress-paths of stabilised clays with OPC with different overconsolidation ratios (OCR) and found that, although the model was able to predict very well the monotonic behaviour of non-stabilised clays, the predictions made for cyclic behaviour and for stabilised clay were only of limited success. Nguyen et al., 2017 developed a constitutive model, integrated into the critical state framework and Cam Clay model families, to predict the behaviour of artificially cemented clays during cementation degradation under different loading conditions. The model includes the following characteristics: (i) nonlinear failure envelope that progressively merges with the critical state line of the reconstituted soil-cement mixture as the mean effective stress increases; (ii) modified mean effective stress, in order to consider the effect of cementation and its degradation due to the mean effective stress and deviatoric strain; (iii) formulated plastic potential function together with the elastoplastic stress-strain relationship. When there is no effect of cementation, the proposed model is reduced to the Modified Cam Clay model. The results demonstrated that the overall behaviour of non-cemented and artificially cemented clays was well predicted by the model.

This paper aims to contribute to the emerging knowledge on alkali-activated binders, exploring the ability of an existent kinematic hardening model to predict the stress-strain behaviour of a sandy lean clay stabilised with alkali-activated blast furnace slags. Monotonic triaxial tests were carried out on the reconstituted and stabilised sandy clay specimens applying a wide range of initial mean effective stresses (p'_0) and OCR at short (28 days) and long (90 days) term. The compositions of the soil and blast furnace slags were determined by EDS analyses and the mineralogical phases by XRD. SEM analyses were also carried out on the soil specimens, before and after stabilisation at 28 and 90 curing days, and blast furnace slags. The experimental triaxial curves were then used to calibrate the model for both non-stabilised and stabilised geomaterials. The impact of the alkali-activated binder addition, OCR and p'_0 was analysed on the overall experimental response and numerical predictions.

4.2 Kinematic hardening constitutive model

A brief description of the kinematic hardening constitutive model proposed by Rouainia and Muir Wood, 2000 is presented in this section, while the model equations are listed in the Appendix. The model, formulated within the framework of kinematic hardening with elements of bounding surface plasticity, is an extension of the Cam Clay model and successfully describes the essential phenomena of pre-failure behaviour of natural clays: stiffness variation with strain, volumetric change accompanying distortion and peak strength at small strains. This model was formulated to consider the temporary existence of structure and its progressive degradation with plastic strains. The model was implemented into finite element codes and has been extensively validated in the last decade against a range of geotechnical problems under static and cyclic loading on natural and remoulded clays (Charlton and Rouainia, 2021; Elia et al., 2016; Elia and Rouainia, 2016; González et al., 2012; Panayides et al., 2012; Rouainia et al., 2020).

The model has three elliptic surfaces: the bubble surface, f_b, the structure surface, F, and the reference surface, f (Figure 35). The bubble surface splits the regions of elastic and plastic responses and moves around with the current stress according to a kinematic hardening rule. The current stress state is always constrained to remain within or on the bubble. Any stress path tending to move beyond the boundary of the bubble cause a translation motion of this surface until it is eventually in contact with the structure surface. The structure surface acts as a bounding surface. It contains the current magnitude and anisotropy of structure and governs the development of destructuration through its interface with the bubble. Therefore, its size and position reflect the soil structure. During plastic loading, the destructuration process occurs when the structure surface approaches the reference surface. It is the feature of destructuration that enables the model to capture the strain-softening behaviour. When both the structure and reference surfaces are coincident, it is assumed that soil entirely lost its initial structure. The reference surface is used to model the intrinsic behaviour of the reconstituted or completely remoulded soil. This model was formulated in order to consider the initial anisotropy of the soils and can be used in both reconstituted and structured soils.

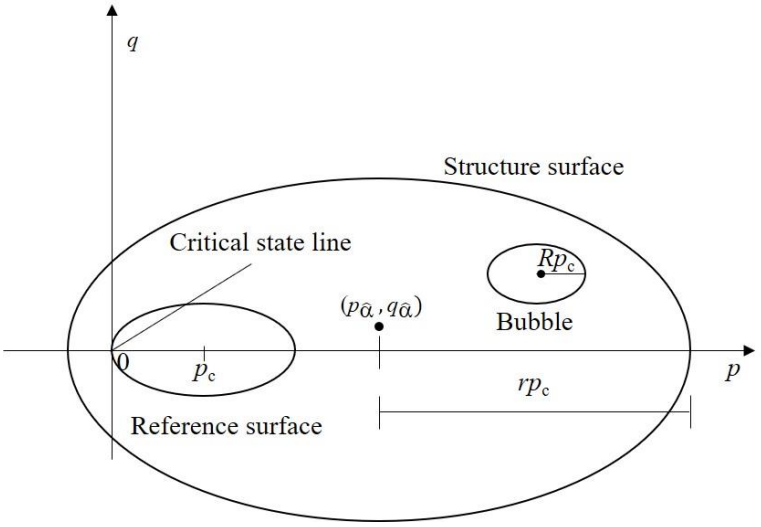

Figure 35. Schematic representation of the model surfaces of Rouainia & Muir Wood (2000) constitutive model

4.3 Laboratory testing

4.3.1 Materials and specimen preparation

The soil used in this experiment is a fine-grained material with ≈ 52% of silt and clay (Figure 36) classified as a CL - sandy lean clay (ASTM D 2487, 2011) and sandy clay soil with low plasticity (BSI, 2015). The soil has a liquid limit (LL) and plastic limit (PL) of 32% and 11% (BS 1377 2, 1990). The maximum dry density is 1.92 Mg/m^3 for an optimum water content of 12.4% (BS 1377 4, 1990). About 81% of the total mass is Si and Al (Table 11), and the X-ray powder diffraction (XRD) pattern shows quartz, muscovite, and albite as the main mineralogical phases (Figure 37), which is very common in this type of soil.

Table 11. Main chemical compositions (wt. %) of the soil and GGBS determined by Energy-Dispersive X-ray Spectroscopy (EDS)

Material	Al_2O_3	CaO	CuO	Fe_2O_3	K_2O	MgO	MnO	Na_2O	SO_3	SiO_2	TiO_2
Soil	24.39	-	0.13	2.04	2.02	1.60	-	0.98	-	68.38	0.46
GGBS	12.34	37.29	0.17	0.35	1.16	8.92	0.61	-	2.55	35.92	0.69

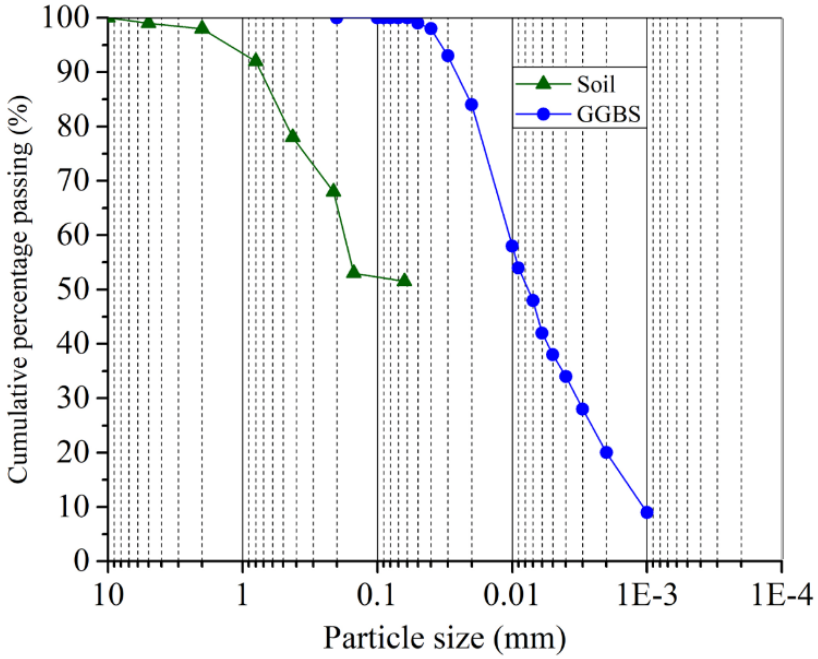

Figure 36. Particle-size distribution curves of the soil and GGBS

Blast furnace slag is a residue obtained from the iron industry, wherein iron ore, limestone, and coke are heated up to 1500°C. When these products melt, two products are produced – molten iron, and molten slag. The molten slag is mainly composed of silicates and alumina from the original iron, combined with some oxides from the limestone. The process of granulating the slag involves cooling the molten slag through high-pressure water jets, which prevents the formation of larger crystals. The granulated slag is dried and ground into a very fine powder (Siddique, 2008). The granulated blast furnace slag (GGBS) used in this study is mainly composed of calcium aluminosilicate frameworks (Ca, Si and, Al ≈ 86% wt. %) (Figure 36 and Table 11). It is an amorphous material (see Figure 37), with a light grey colour, a density at 20°C of 2.4 - 3.0 Mg/m^3, and a pH of 10-12 (DEV-S4-eluate according to EN 12457-4). The commercial activator used was granulated NaOH in a concentration of 3.5 molal.

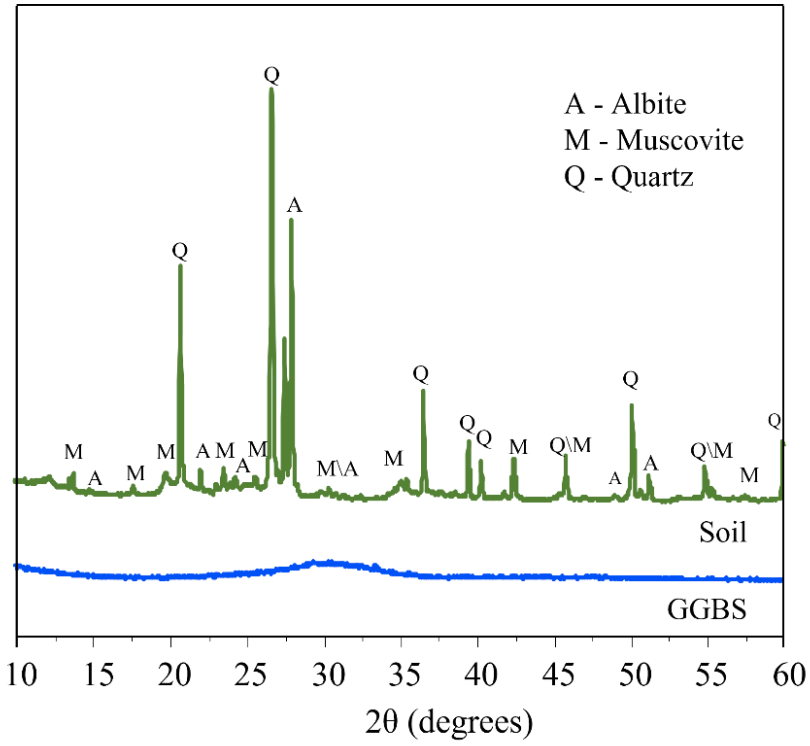

Figure 37. XRD analysis results of GGBS and soil

Non-stabilised soil specimens were built by mixing the dried soil with 26% of water (content between PL and LL) using an electric mixer for 5 minutes, according to the slurry consolidation method described by De Sheeran and RJ, 1971. The slurry was then transferred to a consolidation equipment (Figure 38), where axial loads were applied incrementally to the specimen through a pressure/volume controller. The soil was then extruded from the equipment when the axial stress reached 100 kPa, with a water content (ω) = 17.4% and dry unit weight (ρ_d) = 1.81 Mg/m^3, trimmed in specimens with 70x140 mm^2, and wrapped in cling film. The specimens were kept in a humid chamber at a constant temperature and humidity of 20°C ± 1°C and 95% until the test data.

Two advantages are associated with the use of the slurry consolidation method: 1) the specimens are practically saturated when placed into the triaxial chamber, thus reducing the time of the saturation stage; and 2) the stresses applied during the construction of all specimens are controlled. The control of the stress-history was crucial for the application of the OCR during the triaxial tests.

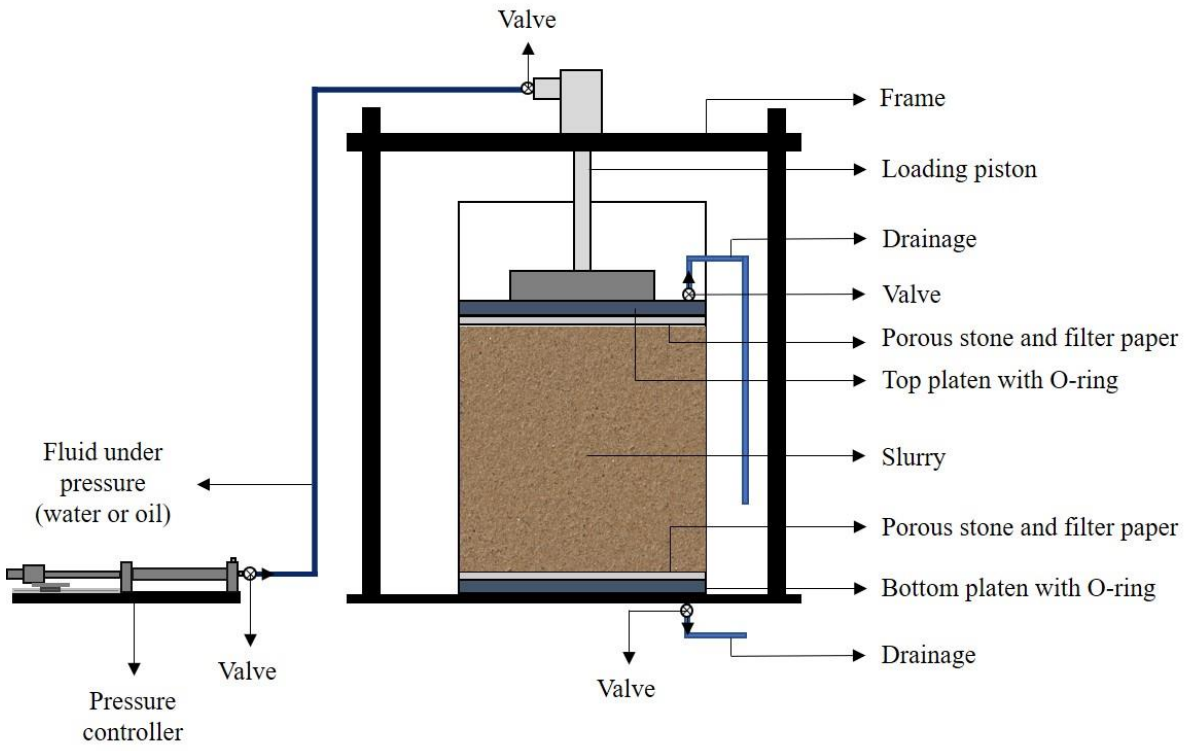

Figure 38. Slurry consolidation equipment

The fine-grained soil was stabilised with an alkali-activated binder composed of GGBS and NaOH (2 parts of GGBS – 1 part of NaOH) at 7.5% dosage, in a concentration of 3.5 molal. This binder was developed by Sargent et al., 2020a, 2020b, 2016. The short-term strength gains and the enhanced geomechanical properties of the stabilised material motivated its application in this study. The GGBS used has a significant amount of Ca. Aluminosilicate sources with a higher Ca content requires shorter curing periods to form the reaction products.

First, the solid materials (92.5% of soil, 5% of GGBS, and 2.5% of NaOH of the total dry soil weight) were mixed and then added to 17.4% of distilled water. The homogenised mixture was statically compacted in layers with ρ_d = 1.81 Mg/m^3 into a PVC mould according to the static compaction method (ASTM D 1632, 2007), wrapped in cling film and kept in a humid chamber at a constant temperature and humidity of 20°C ± 1°C and 95% as the non-stabilised specimens. The specimens were extracted from the mould and rectified

before the beginning of the tests. Considering that NaOH is highly caustic, the preparation of the stabilised soil specimens was carried out with gloves, masks, and glasses, avoiding direct contact with skin or eyes.

In Figure 39, the SEM images of the reconstituted soil and after adding GGBS-NaOH for 28 and 90 curing days are shown. There is no specific orientation of the particles before (Figure 39 (a)) and after (Figure 39 (c) and (d)) the stabilisation, which suggests that both materials can be considered isotropic.

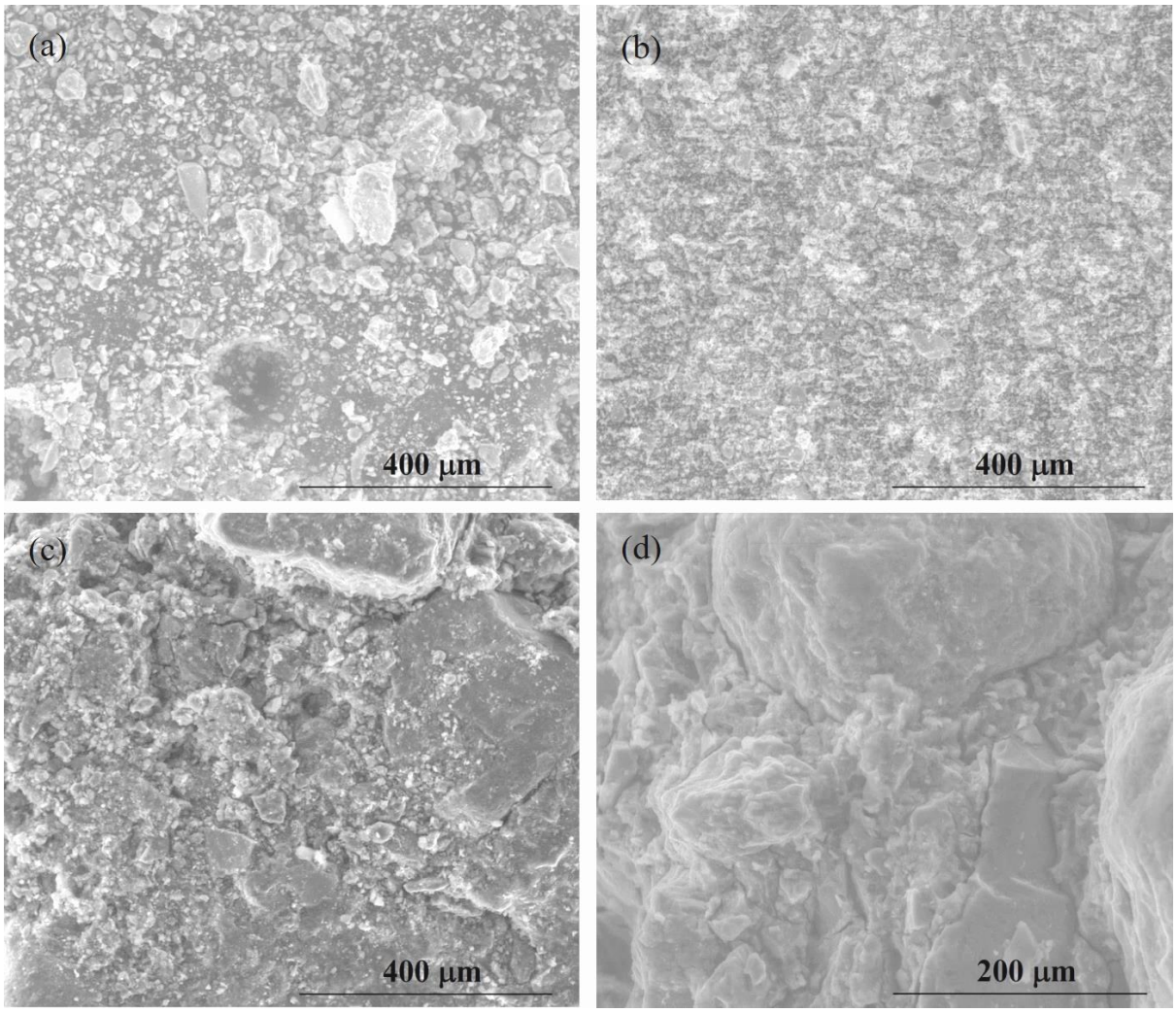

Figure 39. SEM images of the GGBS (b) and soil before (a) and after adding GGBS at 28 (c) and 90 (d) days

4.3.2 Testing program

To obtain a comprehensive understanding of the mechanical behaviour of reconstituted and stabilised soil, particularly the stress-strain response at different ages, consolidated undrained (CU) and drained (CD) triaxial tests were undertaken after 28 and 90 days according to BS 1377 8, 1990, with monotonic displacement control, at a rate of 5 μm/min and 2 μm/min, respectively. For the sake of simplicity, all non-stabilised soil specimens were sheared at a rate very close to the calculated ones, at 5 μm/min. This rate was slow enough to capture the small strains using the bender element (BE) piezometric transducers. The stabilised soil specimens were sheared at 2 μm/min, a rate lower than the determined one to ensure that both backpressure and pore pressure were very close to each other and that no excess of pore pressure would be created due to the shearing rate. During the isotropic consolidation, the OCR was imposed by loading the specimens to maximum pressure and then unloading them to the final pressure values indicated in Table 12.

The BE were installed on the reconstituted soil specimens to obtain the relationship between the initial shear stiffness (G_{max}) and the applied p'_0 and OCR and the stiffness degradation curves from small to large strains levels. The peak-to-peak methodology was used to estimate the travel time of the shear waves. Hall effect local strain transducers were also attached to the middle third of the specimens for higher accuracy in the deformation measurement.

The G_{max} and shear stiffness (G) curves from small to large shear strain (ε_q) levels are shown in Figure 40. For ε_q equal to 0.0001%, G_{max} ranged from 94 kPa to 400 MPa for 150 kPa $\leq p'_0 \leq$ 600 kPa. The most pronounced G degradation happened for strains levels between 0.1% $\leq \varepsilon_q \leq$ 1.2%. The specimens with higher G_{max} (ε_q = 0.0001%) underwent the most drastic reduction of the stiffness up to $\varepsilon_q \approx$ 1% (≈ 30%) (OCR 1 (337) and OCR 1 (600)). For the remaining tests, the G degradation was less noticeable. In the end, all specimens showed similar residual G values, varying between 51 MPa $\leq G \leq$ 194 MPa.

Table 12. Triaxial tests

Specimen type	Curing time	Drainage conditions	Specimen ID	Consolidation phase		Shearing phase	
				Loading (kPa)	Unloading (kPa)	p'_0	OCR
Non-stabilised	-	Undrained	OCR 1 (150)	150	150	150	1.0
			OCR 1 (337)	337	337	337	1.0
			OCR 1 (600)	600	600	600	1.0
			OCR 6 (84)	500	84	84	6.0
			OCR 12.2 (41)	500	41	41	12.2
Stabilised	28 and 90 days	Drained	OCR 1 (150)	150	150	150	1.0
			OCR 1 (337)	337	337	337	1.0
			OCR 1 (600)	600	600	600	1.0
			OCR 3.3 (150)	500	150	150	3.3
			OCR 6 (84)	500	84	84	6.0
			OCR 12.2 (41)	500	41	41	12.2

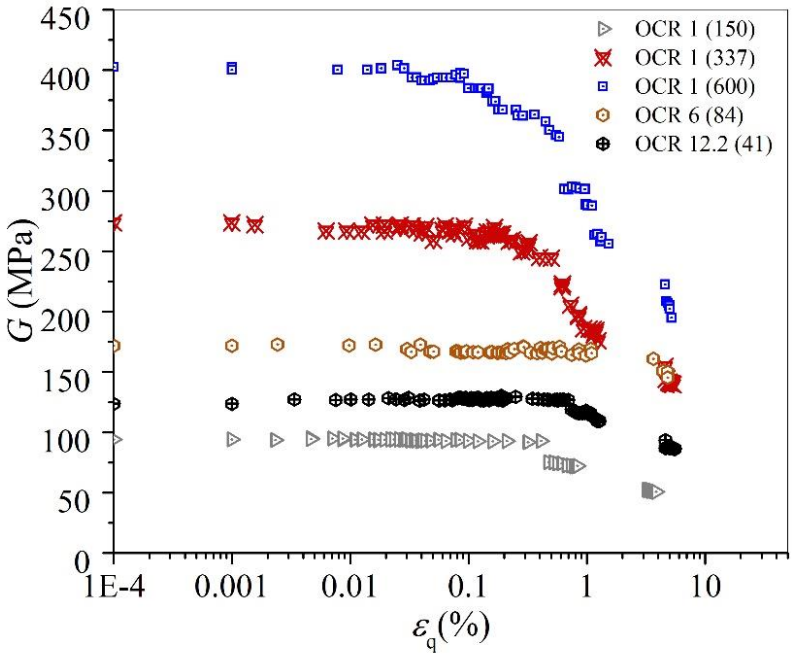

Figure 40. Shear stiffness G - ε_q (a) curves

4.4 Performance of the kinematic hardening model

For the simulation of the mechanical behaviour, the resulting set of model parameters M, ν, R, A, B, k, ψ, η_0, λ^*, k^*, p_{c0} and r_0 are listed in Table 13 and Table 14 (see notation in the appendix section). The parameters k^* and ν describe the elastic response. The elastic/elastic-plastic parameters ν, k^*, λ^*, M are common to the Modified Cam Clay model. The parameters R, B and ψ were introduced by the bubble surface, while the parameters A, k, η_0 and r_0 by the structure surface.

The calibration of almost all parameters was carried out manually, by means of a trial-and-error procedure (best-fitting between the experimental curves with the calibrated ones).

The following initial aspects, together with the drainage conditions (CD or CU), were considered in the model: the size of the surface (p_{c0}), the centre of the bubble yield surface ($\overline{\alpha}$) and the centre of the structure surface ($\widehat{\alpha}$) (or initial degree of soil structure (r_0)) and anisotropy (η_0)). For each material, the parameters M, ν, R, A, B, k, ψ, r_0 and η_0 were kept constant, while the remaining ones, λ^*, k^*, and p_{c0}, were fitted according to the stress-history (represented by OCR) and stress-state (represented by p'_0) applied during the tests, and also curing time (28 or 90 days). To highlight the effects of OCR and p'_0 on the stress-strain response, the predicted and experimental data of the deviatoric stress (q) were normalised to q_n by dividing all results by p'_0.

Table 13. Constant parameters

	Parameters								
Specimen type	M	ν	R	A	B	k	ψ	r_0	η_0
Reconstituted	1.2	0.22 (a)	0.05	0.5	2.0	3.0	0.2	1.1	0
Stabilised	1.97	0.20 (b)	0.05	1.0	2.0	3.5	5.5	12.0	0

(a) Value adopted by Rouainia and Muir Wood (Rouainia and Muir Wood, 2000) for a clayey soil; (b) Value determined by Rios et al., 2017 for an artificially cemented soil with alkaline binder

Table 14. Fitted parameters according to OCR, *p'0* and curing time

Specimen type	Curing time	Specimen ID	Depth (a)	Parameters		
				λ	*k*	p_{c0}
Non-stabilised		OCR 1 (150)	7.28	0.1	0.005	72
		OCR 1 (337)	16.37	0.1	0.005	158
		OCR 1 (600)	29.14	0.1	0.005	280
		OCR 6 (84)	4.08	0.1	0.005	165
		OCR 12.2 (41)	1.99	0.1	0.005	130
Stabilised	28 days	OCR 1 (150)	7.28	0.075	0.001	550
		OCR 1 (337)	16.37	0.05	0.0042	875
		OCR 1 (600)	29.14	0.09	0.005	1000
		OCR 3.3 (150)	7.29	0.075	0.001	600
		OCR 6 (84)	4.08	0.035	0.0025	700
		OCR 12.2 (41)	1.99	0.04	0.001	650
	90 days	OCR 1 (150)	7.28	0.075	0.0005	550
		OCR 1 (337)	16.37	0.07	0.0015	800
		OCR 1 (600)	29.14	0.08	0.003	800
		OCR 3.3 (150)	7.29	0.03	0.0005	800
		OCR 6 (84)	4.08	0.035	0.0008	725
		OCR 12.2 (41)	1.99	0.03	0.0007	725

(a) The depth was estimated considering a volumic weight of 20.59 kN/m³

Two parameters were directly drawn from the experimental data: the critical state stress ratio (*M*) and anisotropy of the initial structure (η_0). The *M* parameter corresponds to the slope of *q*/ *p*' at axial strain ε_a = 3% for the reconstituted sandy lean clay. After stabilisation, *M* was determined at ε_a = 4.1% (28 days) and at ε_a = 5.3% (90 days). In line with the SEM image shown in Figure 5, both materials were considered as isotropic materials (η_0=0) in the model.

A Poisson ratio (ν) equal to 0.22 and 0.20 was adopted for the reconstituted and stabilised sandy lean clay according to the values adopted by Rouainia and Muir Wood, 2000, for a clayey soil, and determined by Rios et al., 2017, for an artificially cemented soil with an alkaline binder. The destruction (*k*) and stiffness

interpolation exponent (ψ) parameters control the way in which plastic strains falls as the bubble approaches the structure surface. The increase of k from 3 (reconstituted soil) to 3.5 (stabilised soil) led to an increase in the rate at which structure is lost with a continuous strain (the destructuration occurred faster) but also to a reduction in both strength and stiffness. The stiffness interpolation exponent (ψ) was increased from 0.2 (reconstituted) to 5.5 (stabilised soil) resulted in a softer behaviour at both small and large strain regions. Although the values of some parameters, in particular, were not the expected ones, the combined effect of all fitted parameters conducted to the final calibrated curves presented in sections 4.1 and 4.2.

According to the literature, the OCR is equivalent to the maximum p'_0 value applied on the soil during the consolidation phase divided by the final p'_0 value. For the non-stabilised soil, the parameter p_{c0} in the model - which controls the initial size of the surfaces - was estimated based on the real OCR applied in the laboratory, and it was equal to half of the maximum value of p'_0. Consequently, and as expected, there was an increase of p_{c0} with the increase of p'_0 for tests with OCR = 1 and the increase of OCR led to a reduction of p_{c0} (Table 14). Besides OCR and p'_0, the artificial cementation provided by the alkaline binder strongly affected the experimental stress-strain behaviour of the stabilised sandy lean clay as illustrated in Figure 43, leading to a huge increase of the peak and post peak shear strengths. In this case, the p_{c0} parameter was fitted considering this additional strength provided by the alkali-activated binder. This parameter greatly increased at 28 curing days, which resulted in a considerable enlargement of all model surfaces (bubble, structure, and reference surfaces). The peak and post peak strengths remained almost constant from 28 to 90 curing days. Therefore, the p_{c0} parameter did not change significantly at both curing periods.

The binder also significantly modified the initial degree of soil structure (r_0), increasing it from 1.1 (reconstituted soil) to 12.0 (stabilised soil). This huge increase resulted in higher and sharper peak strengths in the stress-strain relationship. Since the shear strength remained almost unchanged from 28 to 90 days, the parameter r_0 was kept constant for both ages.

The peak strain position was manually fitted based on the experimental curves, modifying the elastic/plastic parameters that control the slopes of the normal compression (λ^*) and swelling (κ^*) lines. The linear regions of the stress-strain curves on the reconstituted soil are almost overlapped (Figure 41), and the maximum

stresses were achieved for similar strain levels. In this case, the λ^* and k^* were kept unchanged in all simulated curves regardless of the adopted p'_0 and OCR. After stabilisation, there was more variability in the peak positions and both parameters were fitted for each experimental curve and curing age. The experimental curves show a sharper slope of the linear region after adding the alkali-activated binder (Figure 43 (a)) to the soil at 28 days, which became even higher with the development of the bonds (Figure 43 (b)) at 90 days. Thus, the k^* parameters for the stabilised soil simulations at 28 days are lower than before the stabilisation (Table 14). At 90 days, this parameter assumed even lower values.

Finally, the increase of the destructuration strain parameter (A) from 0.5 (reconstituted soil) to 1 (stabilised soil after 28 and 90 days) slightly speeds the loss of structure, contributing to a sharper post-peak response. The increase of r_0 from 1.1 (reconstituted soil) to 12 (stabilised soil) allowed to obtain a higher and sharper peak better fitted to the experimental stress-strain relationship. The decreasing of the parameter r_0 decreases the initial soil structure, and a r_0 value closer to 1 (r_0=1.1, Table 3) allowed to predict the stress-strain behaviour of the soil at a reconstituted state.

4.4.1 Reconstituted sandy lean clay

The experimental (full lines) and the predicted (dotted lines) curves for the sandy lean clay are shown in Figure 41, Figure 42 and Figure 45. A typical stress-strain behaviour commonly observed in clays was observed for the tested soil (Quiroga et al., 2017), with no peaks in the q - ε_a curves (Figure 41 (a)). The maximum deviatoric stresses occurred at 0.2% $\leq \varepsilon_a \leq$ 1.5%. An increase of p'_0 (OCR = 1) led to an increase in both peak/post peak shear strength (Figure 41 (a)). Increased normalised strength were observed for OCR > 1 (Figure 41 (b)). Also, although there are no peaks in the q - ε_a curves for OCR = 6 and 12.2, the OCR impact becomes clearly perceptible when the stress-path responses are analysed in Figure 42. A contractile behaviour was observed for OCR = 1, with the stress-path moving to the left side together with significant positive pore pressure. A dilatant behaviour was noticed for OCR > 1, with the stress-path first approaches the peak value and subsequently moves to the right side toward the critical state. All the effective stress paths converged towards a single linear failure envelope as shown by the laboratory data in Figure 42. The

typical failure mode observed in all specimens (Figure 45 (a)) is characterised by a homogeneous deformation, with the absence of shear band formations.

The great similarity between experimental and predicted curves in Figure 41 demonstrates that the kinematic hardening model is able to predict, with accuracy, the stress-strain behaviour of the sandy lean clay for a wide range of applied p'_0 and OCR. The basic features of the stress-strain behaviour, such as the linear region, the smooth elastic-plastic transition, and the maximum deviatoric stresses, are well captured by the model.

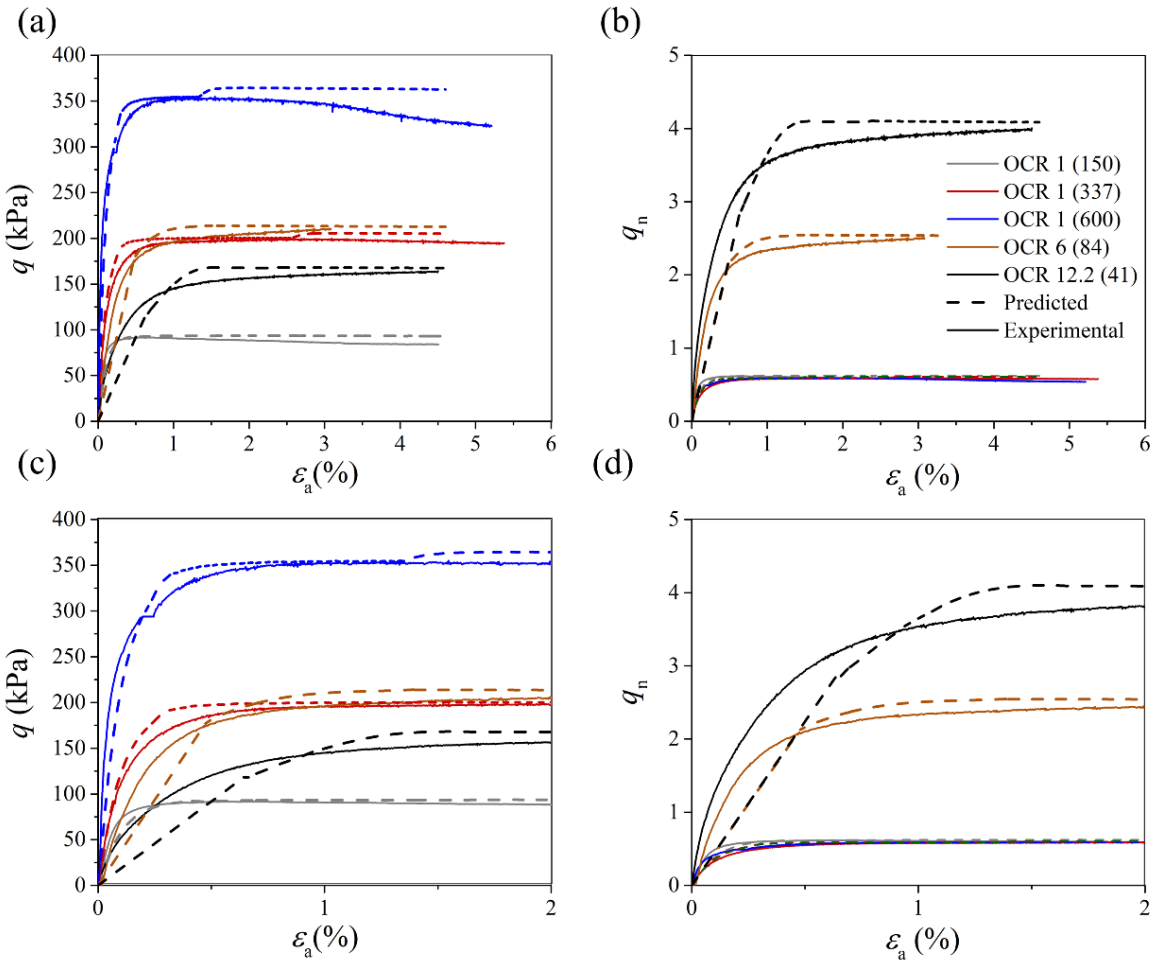

Figure 41. Stress-stress response obtained from triaxial tests: q - ε_a (a) and q_n - ε_a (b). Magnification of the initial stress-strain response between 0% and 2%: q - ε_a (c) and q_n - ε_a (d)

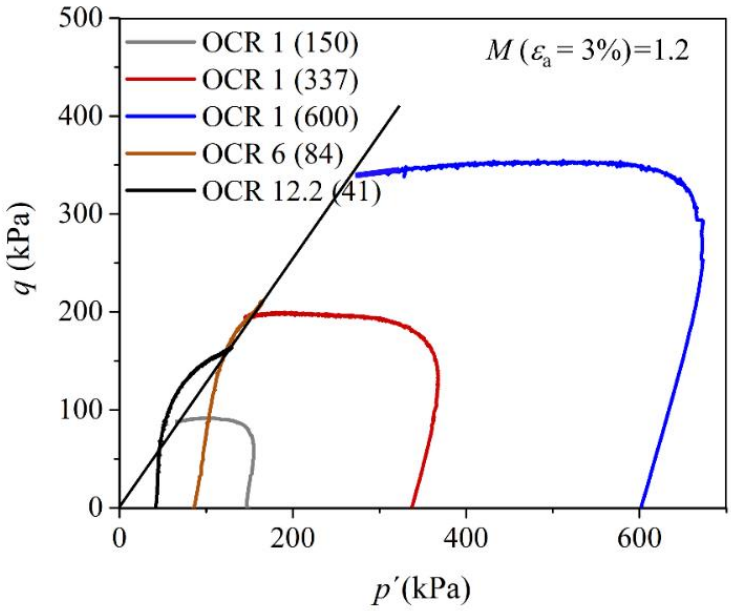

Figure 42. Effective stress-path obtained from triaxial tests

4.4.2 Stabilised sandy lean clay with GGBS-NaOH binder

Experimental (full lines) and predicted (dotted lines) curves for the stabilised sandy lean clay are presented in Figure 43 and Figure 44. A very distinct stress-strain behaviour was observed after stabilisation at 28 curing days, with pronounced peak strengths accompanied by a strain-softening behaviour upon failure due to the localised strains and development of shear planes. From 28 to 90 days, the overall shape of the stress-strain curves and the peak/post peak deviatoric strengths remained practically unchanged.

Regarding the impact of the GGBS-NaOH addition, there was a significant growth of the shear strength (Figure 43) up to 28 days compared to the original soil (Figure 41) at the same confining pressures, which is explained by the Ca content available in the system that affects the rate of gel formation. As previously mentioned, high-Ca reaction products require shorter curing periods to form than the low-Ca ones. From 28 to 90 days, the shear strength remained almost constant. After 28 days, the post peak strength was 3 to 10 times higher than those measured on the reconstituted sandy lean clay, while at 90 days was 3 to 12.

With the normalization of the experimental data, the OCR impact becomes perceptible. All curves with OCR=1 are close to each other, and there was an increase of the normalised strength (Figure 44) with the increase of OCR for both curing ages. The p'_0 applied on the stabilised sandy lean clay specimens also appears to influence its q - ε_a relation. For the tested specimens with OCR=1, there was an increase of both peak and post peak strengths with the increase of p'_0 (Figure 43 (a) and (b)) at 28 and 90 days. The peak strengths for both curing ages were recorded up to $\varepsilon_a \leq 1.5\%$ for $p'_0 \leq 150$ kPa and between $1.5\% \leq \varepsilon_a \leq 4\%$, for $p'_0 >$ 150 kPa (OCR 1 (337) and OCR 1 (600)). On the other hand, the impact of p'_0 on the linear region of the stress-strain curves for the specimens with OCR =1 is not clear at both curing ages. These linear regions seem to be practically overlapped in Figure 43 (a) and (b), and no significant increase of stiffness with the increase of p'_0 was observed.

In general, the stress-strain behaviour of the stabilised sandy lean clay at both curing ages was characterised by a strain-hardening response up to the peak strength followed by a strain-softening behaviour, increased peak/post peak shear strengths compared to the reconstituted soil and increased normalised strength/stiffness. A similar stress-strain behaviour was reported by other authors under triaxial compression in soils stabilised with OPC (Horpibulsuk et al., 2004; Quiroga et al., 2017) and with other alternative binders (Bian et al., 2017; Pu et al., 2019).

The general characteristics of the stress-strain behaviour of the stabilised sandy lean clay, i.e., the increased peak/post peak strengths and stiffness for all the range of applied OCR and p'_0, and also the reduction of the deviatoric stress after peak strength during softening (in some cases a drastic reduction), were well predicted by the model as demonstrated in Figure 43. For specimens with OCR 6 (84) and OCR 12 (41) (Figure 43), the model was able to represent the strain-softening part of the curves, but the strength drop of the predicted curves was less abrupt than the real ones at both curing ages. The strain-hardening and strain-softening behaviours observed for OCR 1(337) and OCR 1 (600) at 90 days and the positions of peak strains were not well captured by the model. For these curves, the model was able to represent well the linear regions and post peak strengths for $\varepsilon_a \geq 4\%$.

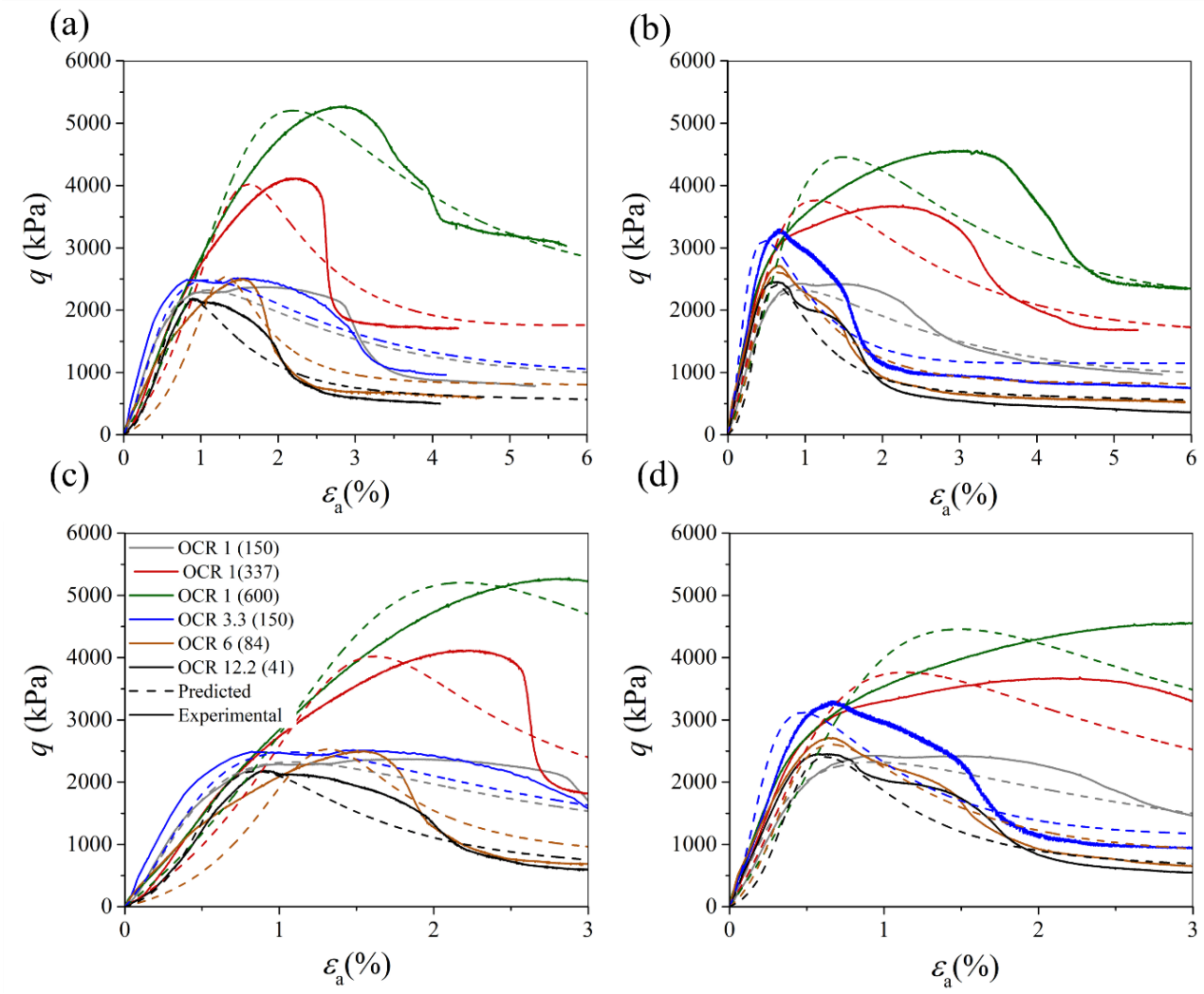

Figure 43. Stress-stress response obtained from triaxial tests: q - ε_a after 28 days (a) and 90 days (b). Magnification of the initial stress-strain response between 0% and 3%: q - ε_a after 28 days (c) and 90 days (d)

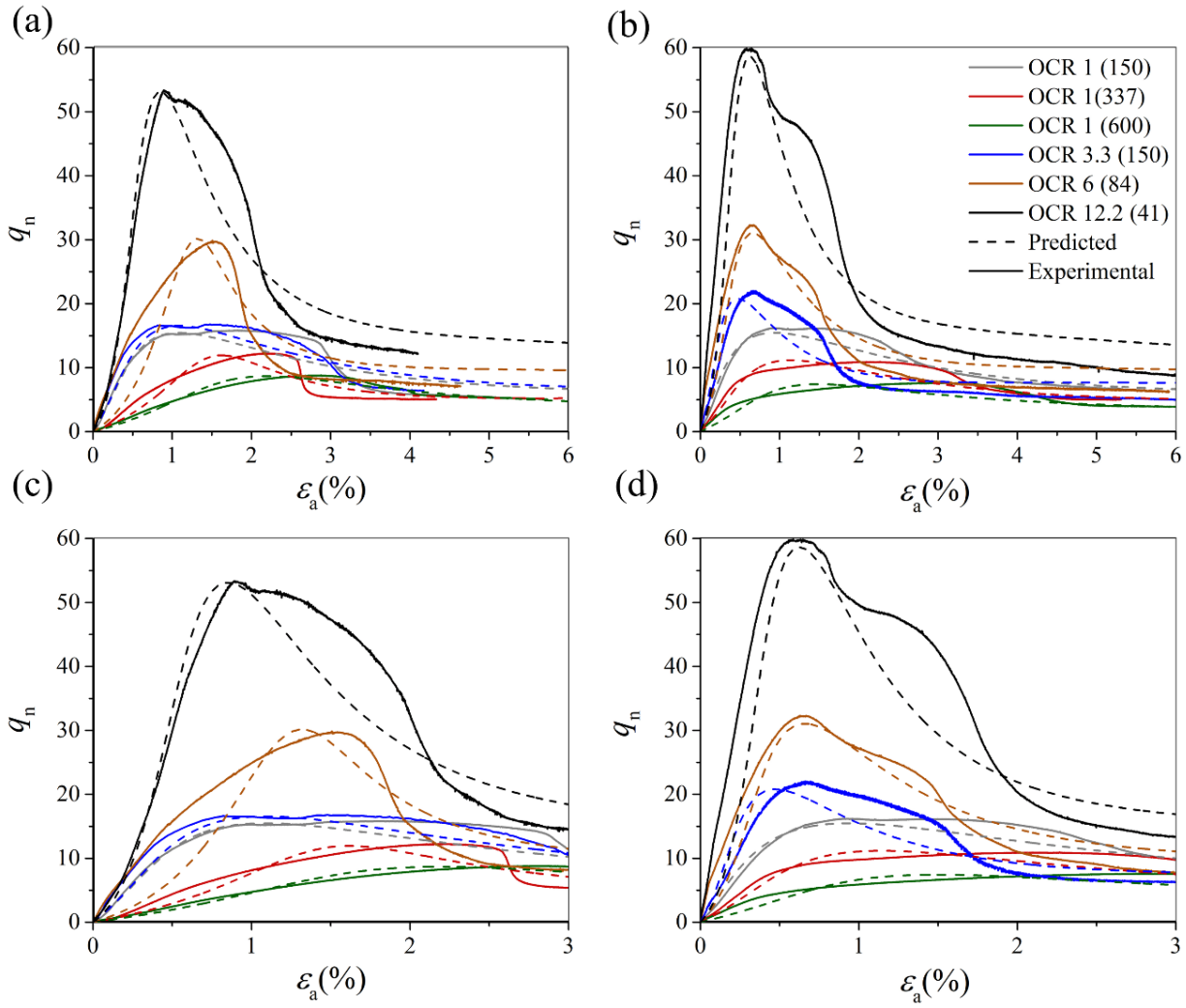

Figure 44. Normalised stress-strain response obtained from triaxial tests: q_n - ε_a after 28 days (a) and 90 days (b). Magnification of the initial stress-strain response between 0% and 3%: q - ε_a after 28 days (c) and 90 days (d)

The failure modes in Figure 45 showed that higher levels of applied p'_0 on the stabilised sandy lean clay specimens led to the formation of the typical shear failure cracks with an approximately 45° slope (Figure 45 (b)). On the specimens sheared under lower levels of p'_0, there was the formation of near-vertical cracks (Figure 45 (c)).

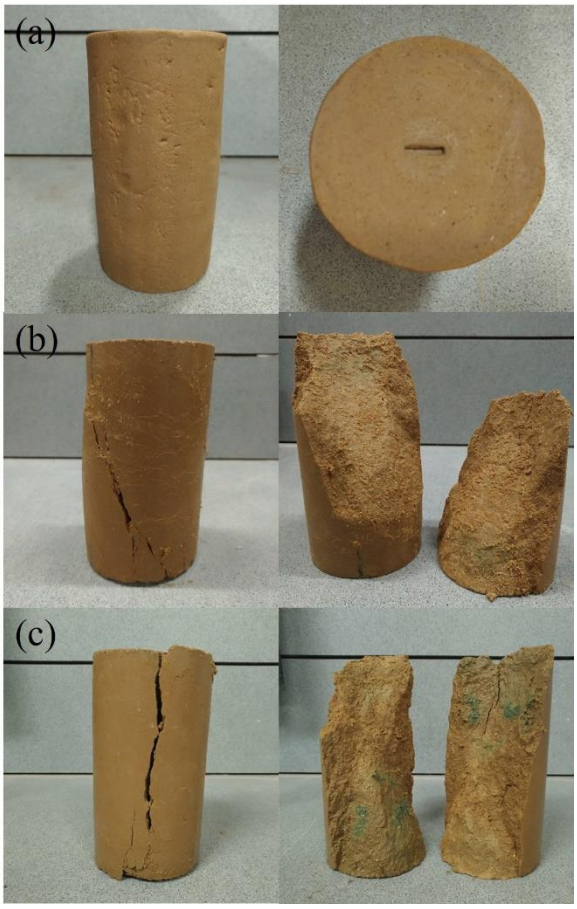

Figure 45. Typical failure modes of reconstituted (a) and stabilised soil specimens with OCR 1 (600) and OCR 6 (84) after 28 days at the end of the triaxial tests

4.5 Conclusions

The mechanical behaviour of a reconstituted and stabilised sandy lean clay with an alkali-activated blast furnace slags was investigated at short (28 days) and long (90 days) terms through triaxial tests for a wide range of OCR and p'_0. The experimental results were used to analyse the ability of a kinematic hardening model for natural clays to predict the stress-strain behaviour of both geomaterials. It was the first attempt of using this constitutive model in artificially cemented soils. The analysis of the results revealed the following insights:

- The stress-strain behaviour of the sandy clay was strongly affected by the addition of the GGBS-NaOH binder, exhibiting pronounced and increased peaks strengths mainly up to 28 days. The overall

stress-strain behaviour of the sandy lean clay stabilised with GGBS-NaOH is quite similar to soft soils stabilised with conventional binders, such as OPC.

- Both p'_0 and OCR influenced the experimental stress-strain behaviour of the reconstituted and stabilised sandy lean clay. Thus, both were considered on the prediction of the stress-strain responses through the p_{c0} parameter. The binder also strongly modified the stress-strain behaviour of the stabilised sandy lean clay, and its influence was incorporated into the model by increasing the initial size of the surfaces through the parameters p_{c0} and r_0.
- The constitutive model, originally developed to predict the behaviour of natural clays, was able to predict the main features of the stress-strain behaviour of the sandy lean clay stabilised with the alkali-activated binder for the range of p'_0 and OCR considered, which demonstrates the potential of the model to be applied to materials than the natural clays for which was initially formulated for. This also suggests that the behaviour of clayey soils stabilised with other alkaline binders can also be adequately predicted by the same constitutive model or by other existent constitutive laws for natural clays. The experimental results also point to the possibility of using constitutive models initially developed for artificially cemented soils with OPC in soils stabilised with alkali-activated binders.
- The present work is a first exploration of the numerical modelling of soils stabilised with environmentally friendly alkali-activated binders, which is an important step towards their application in the field.

5. BEHAVIOUR OF A CLAY STRENGTHENED WITH AN ALTERNATIVE ALKALINE-BASED CEMENT AT HIGH WATER CONTENT

This paper focuses on the mechanical behaviour of a clay at high water content stabilised with an alkali-activated binder under a wide range of initial mean effective stress (p'_0) (10 kPa $\leq p'_0 \leq$ 1200 kPa) and on the prediction of the experimental stress-strain responses observed using a kinematic hardening constitutive model for natural clays. The alkali-activated binder was synthesised from blast furnace slags and sodium hydroxide. Monotonic consolidated undrained triaxial tests were conducted on reconstituted and stabilised clay specimens cured for 28 days to evaluate the effects of cementation on the overall shear behaviour. Triaxial test results were used next on the calibration of the model parameters. Scanning electron microscopy with energy dispersive spectroscopy (SEM-EDS), X-ray diffraction (XRD), and leachate analyses were performed at 28 and 90 days to investigate the nature of the gel formed and the risk of soil contamination. The main product formed was calcium aluminosilicate hydrate (C-A-S-H) with a low CaO/SiO_2 ratio, and no risk of soil contamination was found. Triaxial test results revealed the binder potential when added to the clay at high water content, with enhanced shear strength and stiffness. Moreover, the compressibility and undrained shear strength in the pre-yield state showed to be independent of the initial mean effective stress (p'_0), unlike what was observed in the post-yield state where the shear strength seems to be affected by p'_0. The model provided reliable predictions that agreed with the experimental results and captured the main features of the artificially cemented clay for the range of p'_0 tested.

Keywords: alkali-activated binder, stabilised clay; constitutive model; triaxial tests; SEM-EDS; XRD; leachate analysis

---

This Chapter is based in the article under submission process.

5. BEHAVIOUR OF A CLAY STRENGTHENED WITH AN ALTERNATIVE ALKALINE-BASED CEMENT AT HIGH WATER CONTENT

5.1 Introduction

Soft clay-rich soils are frequently found in geotechnical engineering practice. These soils, known to be potentially problematic due to their undesirable geotechnical properties, such as high-water content, low strength, and susceptibility to large settlements, are significantly challenging. Many stabilisation methods based on the addition of cementing agents (e.g., Ordinary Portland cement (OPC), lime, slag, fly ash, etc.), such as deep mixing, shallow soil mixing, and jet grouting, are now routinely applied to increase the bearing capacity, reduce deformability as well as control the swelling of these poor soils. Although many cementing binders have been developed, the OPC is still the most extensively used binder due to its availability and effectiveness.

Cement production is one of the main factors affecting environmental pollution, in which huge amounts of CO_2 and air pollutants, including SO_2, NO_x, CO, and particulate matter (PM), are released into the atmosphere (Lei et al., 2011). Approximately 90% of the CO_2 emissions of industrial origin are related to the cement industry (Xi et al., 2016), which corresponds to around 8% of the global CO_2 emissions (Andrew, 2018). To address this issue, efforts have been made to develop low carbon footprint binders with similar performance to OPC in recent years.

Alkali-activated binders have gained huge research attention due to their potential. These binders are synthesised from amorphous Si-Al based wastes in an alkaline environment. When OPC, blast furnace slag, or cement kiln dust are used as the calcium-based precursor to blend with aluminosilicate precursors, the hydration products consist of a mixture of C-S-H (calcium silicate hydrate) and C-(N)-A-S-H (calcium-sodium aluminosilicate hydrate) type gels (Palomo et al., 2015; Zhang et al., 2017). Calcined clays (e.g., metakaolin), fly ash, or mine waste with high silica and alumina and low calcium contents lead to the formation of a three-dimensional, essentially amorphous, aluminosilicate gel (Davidovits, 2013).

Researchers have extensively reported the effectiveness of adding alkali-activated binders with distinct precursors for soil stabilisation, including fly ash (Corrêa-Silva et al., 2019; Cristelo et al., 2015, 2013; Miranda et al., 2020), blast furnace slag (Fasihnikoutalab et al., 2020; Sargent et al., 2013), a blend of fly

ash and blast furnace slag (Singhi et al., 2016; Yi et al., 2015) and metakaolin (Zhang et al., 2015, 2013). Regarding the shear behaviour of the stabilised materials, the authors have reported, in general, an increase in stiffness and of the peak and residual shear strength after stabilisation, regardless of the curing period. Furthermore, Abdullah et al., 2019 noticed that the confining stress has a considerable influence on the stress-strain behaviour and pore pressure development of a clay stabilised with a fly ash / granulated slag geopolymer. Corrêa-Silva et al., 2020 and Rios et al., 2017 observed a stress-strain behaviour typical of cemented-treated soils when studying the behaviour of sandy clay and silty sand stabilised with alkali-activated blast furnace slags and fly ash, respectively. Corrêa-Silva et al., 2020 also noticed that the confinement stress has a significant impact on the shear strength of the treated soils, where an increase in both peak and residual deviatoric stresses was observed with the increase of the initial mean effective stress. Increased normalised shear strength/stiffness and a tendency for dilation were also observed during the shear phase with increasing overconsolidation ratio (OCR). Sargent et al., 2020b reported higher values of maximum dilatation for an alluvial soil stabilised with alkali-activated blast furnace slags than those observed on reconstituted and undisturbed soil for the same confining stress. The authors associated this trend with the onset of softening behaviour caused by the breakdown of the cementitious bonding structure.

Understanding the shear behaviour of stabilised clays is of huge importance for strength and deformation analysis in engineering practice. Numerous constitutive models for cement-treated clays have been developed by extending the constitutive models representing the 'natural bond' for natural clays to the 'artificial cementation bond' structured for stabilised clays (Horpibulsuk et al., 2010; Yapage and Liyanapathirana, 2019). For the calibration of such models, triaxial response data is essential, and the data published in this subject is limited when alkali-activated binders are used to stabilise soft soils.

This paper aims to investigate the mechanical behaviour of a reconstituted and stabilised clay at high initial water content using alkali-activated blast furnace slags cured for 28 days through the performance of triaxial tests. Monotonic consolidated undrained (CU) triaxial tests based on a wide range of initial mean effective stress (p'_0) and isotropic compression tests were undertaken for both materials, using hall-effect transducers for a more accurate measurement of the deformations of the specimens. To complement the experimental campaign, scanning electron microscopy (SEM), energy dispersive spectroscopy (EDS) and X-ray diffraction

(XRD) tests were carried out to characterise the microstructure of the soil-binder matrixes; while the environmental performance was assessed by collecting a leaching solution after short (28 days) and long (90 days) curing periods in order to characterise the risk of soil contamination. The triaxial tests' data was then used to explore the capacity of a kinematic hardening constitutive model, as proposed by Rouainia and Muir Wood, 2000, to predict the stress-strain behaviour experimentally observed for both reconstituted and stabilised clay specimens. The model is implemented in a finite element code and has been extensively applied in a wide range of geotechnical problems under monotonic and cyclic behaviour on natural, remoulded, and overconsolidated clays (Charlton and Rouainia, 2021; Elia et al., 2016; Elia and Rouainia, 2016; N. González et al., 2011; González et al., 2012; N. A. González et al., 2011; Panayides et al., 2012; Panayides and Rouainia, 2011; Rouainia et al., 2020).

5.2 Kinematic hardening constitutive model

Rouainia and Muir Wood, 2000 proposed a kinematic hardening model for natural clays with loss of structure. The input model parameters required for the numerical simulations are summarized in Table 15.

The model, formulated within the framework of kinematic hardening with elements of bounding surface plasticity, is an extension of the Modified Cam Clay able to describe the behaviour of reconstituted clays, in which an extra yield surface or bubble was introduced inside an external bounding surface and moves around with the current stress state according to a kinematic hardening rule. This model was formulated in order to include the effects of damage to the structure caused by irrecoverable plastic strains due to sampling, laboratory testing or geotechnical loading.

The model has three elliptical surfaces, the bubble surface, the structure surface, and the reference surface (see Figure 46). The elastic strain region is bounded by the bubble surface, within which the initial stress state must lie. When the stress path moves beyond the bubble boundary, there is a translation motion of the bubble until the bubble and structure surface come into contact. The structure surface contains information about the magnitude and anisotropy of the structure. It assumes the role of the bounding surface and controls the development of destructuration when the structure surface approaches the reference surface during plastic loading. When both the structure and reference surfaces coincide, the soil completely loses the initial

structure and is referred to as reconstituted or fully remoulded soil. The model describes the essential phenomena of pre-failure behaviour of natural clays, including the stiffness variation with strain, volumetric change accompanying distortion and peak strength at small strains.

Table 15. Model parameters (Rouainia and Muir Wood, 2000)

	Symbol	
	m	Ratio of extension and compression strengths
	p_{co}	Initial centre of reference surface
Elastic/Elastic-plastic parameters introduced by the modified Cam Clay type of models	k^*	Slope of swelling line in ln p' (kPa) - ln (1+e) space
	λ^*	Slope of normal compression line in ln p' (kPa) - ln (1+e) space
	M	Critical state stress ratio
	ν	Poisson ratio
Parameters introduced by the bubble model	R	Ratio of size of bubble and reference surface
	B	Stiffness interpolation parameter
	Ψ	Stiffness interpolation exponent
Parameters introduced by the structure surface	A	Destructuration strain parameter
	k	Destructuration parameter
	η_0	Anisotropy of initial structure
	r_0	Initial degree of structure

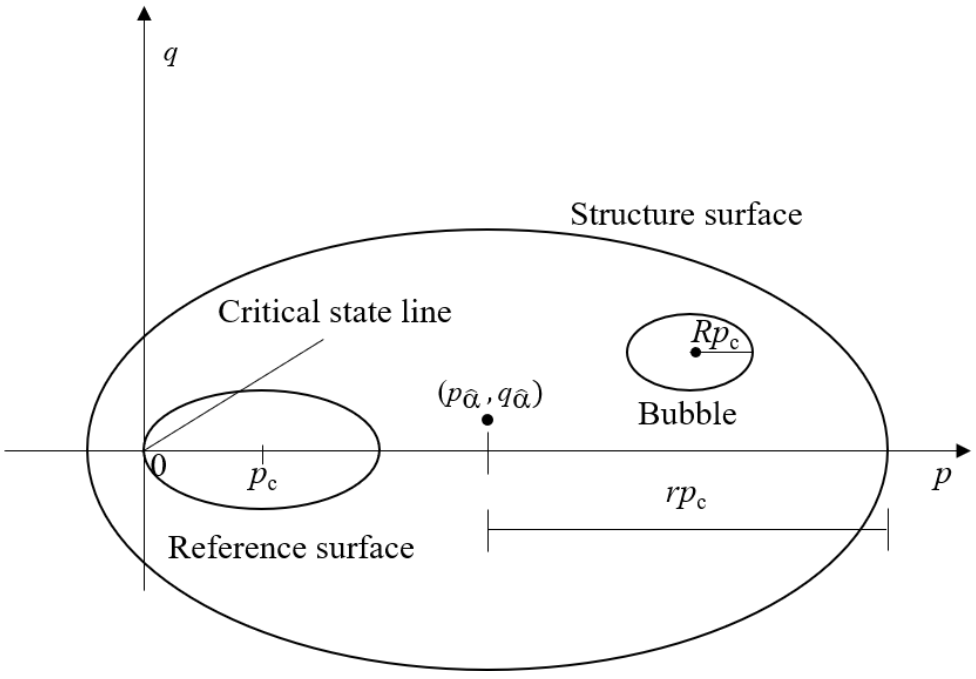

Figure 46. Rouainia and Muir Wood, 2000 model surfaces

5.3 Materials and laboratory testing

5.3.1 Materials

The clay was collected in the north of Portugal and is mainly composed of kaolinite (Figure 48). According to the unified soil classification (ASTM D 2487, 2011) and the AASHTO system used for highway construction purposes (AASHTO M 145-91, 2017), the soil is classified as CH - clay with high plasticity and fits into the group classification A-7-6 with a group index of 47. It is a poor-quality soil in terms of its geotechnical properties with a high plasticity index and, therefore, suited for stabilisation. The grading curve and the physical properties of the clay are shown in Figure 47 and Table 16. The chemical analysis of the clay showed high aluminium oxide (Al2O3) and silicon dioxide (SiO2) contents in a total mass of 96.73% (Table 17).

The binder used to stabilise the clay is composed of two parts of ground granulated blast furnace slags (GGBS) and one part of sodium hydroxide (NaOH), in dosages of 5%, 10%, 12.5%, and 15% (by the soil dry weight), and was developed by Sargent et al., 2020a, 2020b, 2016. The blast furnace slags were supplied by Hanson Cements Ltd in granulated form and are characterised by a density of 2.4 - 3 Mg/cm^3 at 20°C and pH of 10 - 12 (DEV-S4 - eluate according to EN 12457-4) (Figure 47). It is an amorphous precursor (Figure 48) with a light grey colour, mainly formed by oxides of calcium (CaO), aluminium (Al_2O_3), and silicon (SiO_2), in a total of ≅ 85.55 wt.% (Table 17). The granulated NaOH is a commercial alkali activator white in colour. The grains were dissolved in distilled water before adding to the clay and GGBS.

5. BEHAVIOUR OF A CLAY STRENGTHENED WITH AN ALTERNATIVE ALKALINE-BASED CEMENT AT HIGH WATER CONTENT

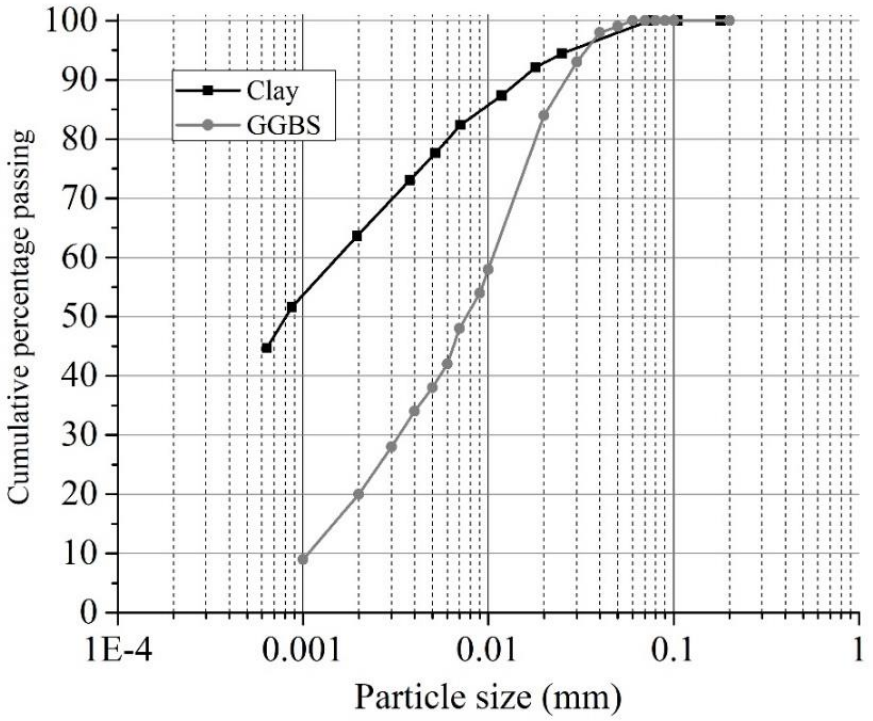

Figure 47. Particle size distributions of the clay and GGBS

Table 16. Physical properties of the clay

Property		Results		Units
Atterberg limits (a)	Liquid limit	LL	58	%
	Plastic limit	PL	15	%
	Plasticity index	PI	43	%
Specific gravity (b)	G	2.57		
Compaction (c)	Optimum water content	ω_{opt}	20.4	%
	Maximum dry density	$\rho_{d,max\ axax}$	1.44	Mg/m³
Oedometer test (d) (e)	Compression index	c_c	0.274	
	Recompression index	c_r	0.048	

(a) (BS 1377 2, 1990)
(b) (NP 83, 1965)
(c) (BS 1377 4, 1990)
(d) (BS 1377 5, 1990)
(e) Reconstituted soil specimen built based on the slurry consolidation method described by Liu et al.(Liu et al., 2017), with water content (ω) and dry density (ρ_d) of 44% and 1.16 Mg/m³

Table 17. Clay and GGBS compositions obtained from EDS analysis of two specimens for each material, each comprising 10 points

Element (wt. %)	Al_2O_3	CaO	CuO	Fe_2O_3	K_2O	MgO	MnO	Na_2O	SO_3	SiO_2	TiO_2
Clay	38.13	0.09	0.04	0.6	0.96	0.77	-	0.3	0.23	58.6	
GGBS	12.34	37.29	0.17	0.35	1.16	8.92	0.61	-	2.55	35.92	0.69

5.3.2 Specimen preparation and binder selection

Reconstituted soil specimens were built based on the slurry consolidation method described by Liu et al., 2017. Dried clay was mixed with the initial water content (ω) of 65% (5% higher than the liquid limit (see Table 16) using an electric machine. The clay slurry was placed inside the consolidation equipment and consolidated under incremental loading until a dry density (ρ_d) of 1.16 Mg/m^3 and water content of 44% was reached. The maximum applied stress was approximately 55 kPa. The specimen was then extruded, placed on a rotating pedestal, and trimmed with a height and diameter of approximately 140 mm x 70 mm. Finally, the specimen was wrapped and cured in a climatic chamber at a temperature and humidity of 20°C ± 1°C and 95%, respectively.

The stabilised clay specimens were prepared by initially mixing the dried clay with GGBS according to the amounts referred to in Table 18. The NaOH was separately dissolved in 44% of distilled water. The liquid phase was then added to the solid materials, and an additional manual mix was done in order to obtain a final homogeneous mixture. Next, the mixture was statically compacted based on ASTM D 1632 (ASTM D 1632, 2007) into PVC moulds with 140 mm height x 70 mm diameter, with ρ_d and ω of 1.16 Mg/m^3 and 44%, equal to the reconstituted clay specimens. The specimens were kept inside the moulds, wrapped with cling film, and cured under controlled conditions and were only extruded before starting the tests.

Table 18. Binder dosages

Binders			2 parts of GGBS - 1 part of NaOH	
	Soil (%)	Water (%)	GGBS (%)	NaOH (%)
5%GGBS-NaOH	95	44	3.33	1.67
10%GGBS-NaOH	90	44	6.67	3.33
12.5%GGBS-NaOH	87.5	44	8.33	4.17
15%GGBS-NaOH	85	44	10	5

A short campaign of unconfined compressive strength (UCS) tests was conducted, after curing for 28 days, to define a suitable binder dosage to enhance the clay strength up to engineering applications' requirements, which typically ranges between 300 kPa ≤ UCS ≤ 3000 kPa for most deep/shallow soil mixing scenarios (EuroSoilStab, 2002). The specimens were not saturated before testing and were tested under monotonic displacement control at a rate of 0.18 mm/min.

Table 19. UCS test results after 28 curing days

Binders	UCS_{max} (kPa)
Reconstituted clay	54
5%GGBS-NaOH	130
10%GGBS-NaOH	2780
12.5%GGBS-NaOH	4170
15%GGBS-NaOH	5570

The stabilised specimen strengths observed after 28 days of curing were higher than those observed on the reconstituted clay specimens, even for the lowest binder dosage. However, the degree of strength development changed significantly with the binder dosage. The minimum dosage of GGBS-NaOH required to accomplish the EuroSoilStab criterium was 10% and, thus, the binder used to stabilise the clay was composed of 10%GGBS-NaOH. For 10%GGBS-NaOH, the NaOH was dissolved in water in a concentration of 1.89 molal.

5.3.3 Laboratory testing

Monotonic CU triaxial tests were performed on reconstituted and stabilised clay specimens after 28 curing days to investigate the mechanical behaviour of both materials regarding peak deviatoric strength, pore pressure response, stress-path, and failure envelopes. Triaxial test results were used next on the calibration of the model parameters to predict the stress-strain responses. Isotropic compression tests were also carried out to evaluate compressibility and to determine the yield stresses. SEM-EDS, XRD, and leachate analyses were also carried out after 28 and 90 curing days to complement the mechanical tests.

SEM-EDS and XRD analyses

The SEM-EDS and XRD analyses were carried out on unpolished reconstituted and stabilised clay specimens after 28 and 90 curing days. Little pieces of stabilised clay specimens were soaked in acetone and dried according to the method described by Zhang and Scherer, 2011 to guarantee that the chemical reactions were stopped at the desired curing time.

The XRD analysis is a well-established method for mineralogical characterisation. Most soil minerals are crystalline structures, and when in interaction with X-rays, a specific diffraction pattern is produced. The XRD spectra of the materials were recorded with a PANalytical X'Pert MPD diffractometer, using the λ = 0.154 nm Kα line of a Cu anode (Bragg - Brentano geometry) equipped with a X'Celerator detector. The spectra were obtained at room temperature, between 8° and 60° (2θ), using a step of 0.017° with 100 s/step.

The SEM-EDS analysis was used to visualise the microstructure and morphology of the particles and to know the elemental composition of some specific areas. The SEM analyses were performed on a FEI Quanta 400 scanning electron microscope, with 30 kV, in low vacuum mode (1.3 mbar), avoiding the deposition of a conductive layer. The device was coupled with an EDS analyser, from EDAX.

Triaxial tests

Monotonic CU triaxial and isotropic compression tests were done on reconstituted and stabilised clay specimens after 28 days, according to BS 1377 8 (BS 1377 8, 1990), for 10 kPa $\leq p'_0 \leq$ 1200 kPa. Table 20 summarises the triaxial tests carried out. Under triaxial compression, all specimens were sheared at a loading rate of 5 μm/min. An external LVDT was installed on the top of the triaxial chamber to measure the external axial strains. The local strains were measured with hall-effect transducers (2 axials and 1 radial), installed at the mid-height of the specimens, to characterise the behaviour of the materials at small strain (ε_a) levels ($\varepsilon_a \geq 0.001\%$). The OCR was applied on the reconstituted clay specimens during the consolidation phase, increasing the effective stress to the maximum desired value (p'_{max}) and then reducing it to the final value (p'_{final}), which is equal to p'_0 applied during the shear phase. The OCR corresponds to the ratio of p'_{max} by p'_{final}.

Table 20. Triaxial tests

	Specimen ID	OCR	p'_{max} (kPa)	p'_{final} (kPa) = p'_0 (kPa)
Reconstituted clay	OCR 1 (150)	1	150	150
	OCR 1 (350)	1	350	350
	OCR 1 (700)	1	700	700
	OCR 2 (350)	2	700	350
	OCR 4.7 (150)	4.7	700	150
Stabilised clay	10	1	10	10
	40	1	40	40
	150	1	150	150
	270	1	270	270
	350	1	350	350
	700	1	700	700
	1200	1	1200	1200

Leachate tests

Leachate tests were done according to EN 12457-4, 2002 on reconstituted and stabilised clay specimens after 28 and 90 curing days to assess the risk of soil contamination. This standard specifies information on leaching of granular waste or sludges at a ratio liquid/solid of 10 l/kg, for particle sizes below 10 mm. A specimen of approximately 90 g was collected and placed into a bottle with 0.9 l of leachant (in this case, distilled water) for 24 h and shaken at a rotation speed of 20 rpm. The eluates were then collected according to the procedure described by the standard and analysed. The leachate results were compared with the limit values of inert waste defined by Annex IV of the Law Decree n. 183, 2009b. This law establishes in which kind of landfill the waste can be deposed, classifying it according to one of three categories, namely: landfill for inert waste, which has the stricter limit values, landfill for non-hazardous waste, and landfill for hazardous waste.

5.4 Results and discussion

5.4.1 XRD and SEM-EDS analyses

XRD analysis

In Figure 48, the XRD spectrum obtained for each material is shown. The major crystalline minerals found within the clay were kaolinite (k), quartz (Q), and muscovite (M). Nacrite (N) was also detected, which is a clay mineral and a form of kaolinite. Kaolinite is a very stable clay mineral composed of very strongly

connected silica and alumina plates. No peak was detected in the GGBS spectrum, meaning that the precursor is practically an amorphous material.

The clay spectrum composition after adding 10%GGBS-NaOH is very similar to the original clay spectrum, with no new mineral phase detected after 28 and 90 days. The main differences observed are regarding the peak intensities that are lower on the stabilised clay after 28 days. After 90 days, these intensities are even lower than 28 days, which suggests the dissolution of some mineral phases and, possibly, the formation of cementitious gel (Cristelo et al., 2011). More precisely, these reduced peaks are essentially muscovite, kaolinite and quartz and are located approximately at 12.5 2θ, 20 2θ, 25 2θ, between 35 2θ and 40 2θ, 45 2θ and 50 2θ.

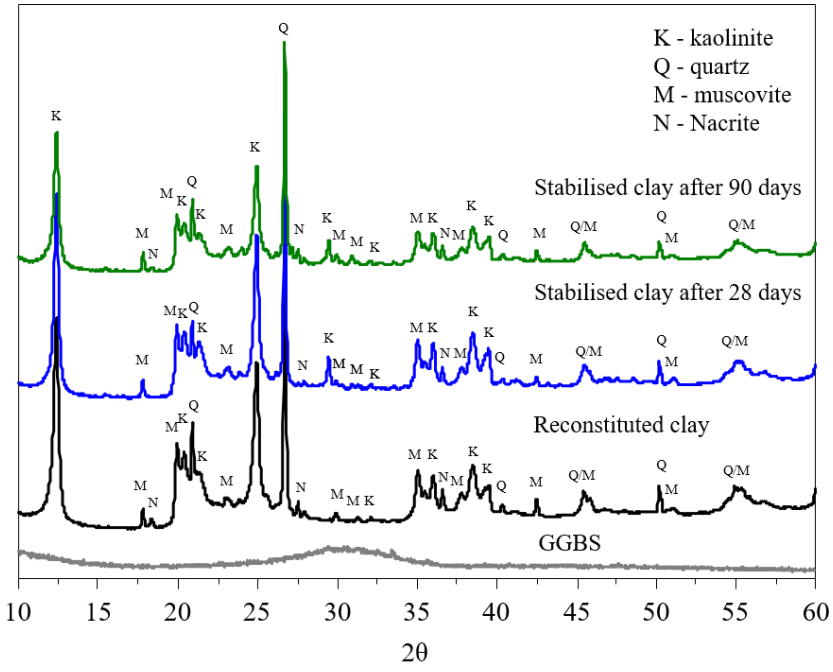

Figure 48. XRD spectrum results

SEM-EDS analysis

The SEM images were taken at a magnification of 300x, 100x, and 300x respectively, and are presented in Figure 49 (a), (b), and (c). Examples of EDS spectra recorded for each material are shown in Figure 49 (d).

It can be seen in Figure 49 (a) that the reconstituted clay has a discontinuous structure due to the absence of gel, where the voids are more visible. Unlike the gel, the clay particles (Figure 49 (a)) have a well-defined shape and boundaries and a smooth surface texture. After adding 10%GGBS-NaOH (Figure 49 (c)), the soil matrix seems to be denser and homogeneously covered by a layer of amorphous gel, with the soil particles surrounded and bonded by the cementitious gel. Physically, the pores or air spaces have decreased, and the gel seems to act as a binding substance, creating more connections and greater cohesion between the clay particles. Also, there is no specific orientation of the clay particles before (Figure 49 (a)) and after stabilisation (Figure 49 (b) and (c)), which means that both can be considered to have identical properties in all directions (isotropic materials). In Figure 49 (b), a larger area of stabilised clay can be seen characterised by a compacted matrix without loose or unbound particles. The cracks in darker areas were due to the process of specimen preparation.

The EDS spectrum of the reconstituted clay showed the presence of high aluminium oxide (Al_2O_3) and silicon dioxide (SiO_2) contents (wt.%≅ 96.73%) and trace amounts of Fe_2O_3, K_2O and Na_2O (Figure 49 (d) and Table 17).

A more detailed quantitative analysis was conducted on the stabilised clay at 28 days of curing, comprising 10 points on one SEM image, to estimate the gel composition. From the total EDS data, Si and Al were the elements with the highest concentration. Na and Ca were also detected in average contents of 4.63% and 3.22%, respectively. This suggests the formation of N, C-A-S-H type gel with a composition of $0.002 \leq CaO/SiO_2 \leq 0.234$ and $0.446 \leq Al_2O_3/SiO_2 \leq 0.725$. The average weight ratios were $CaO/SiO_2 = 0.05$ and $Al_2O_3/SiO_2 = 0.67$, wherein the CaO/SiO_2 ratio is significantly lower than usually found. For instance, Garcia-Lodeiro et al., 2011 reported ratios between $0.72 \leq CaO/SiO_2 \leq 1.94$ in C-A-S-H system. Such difference is explained by the incorporation of only a small amount of blast furnace slag into the system (90% clay, 6.67% of GGBS, and 3.33% of NaOH), and also by the use of a precursor with high SiO_2 content (≅ 35.92% - Table 17).

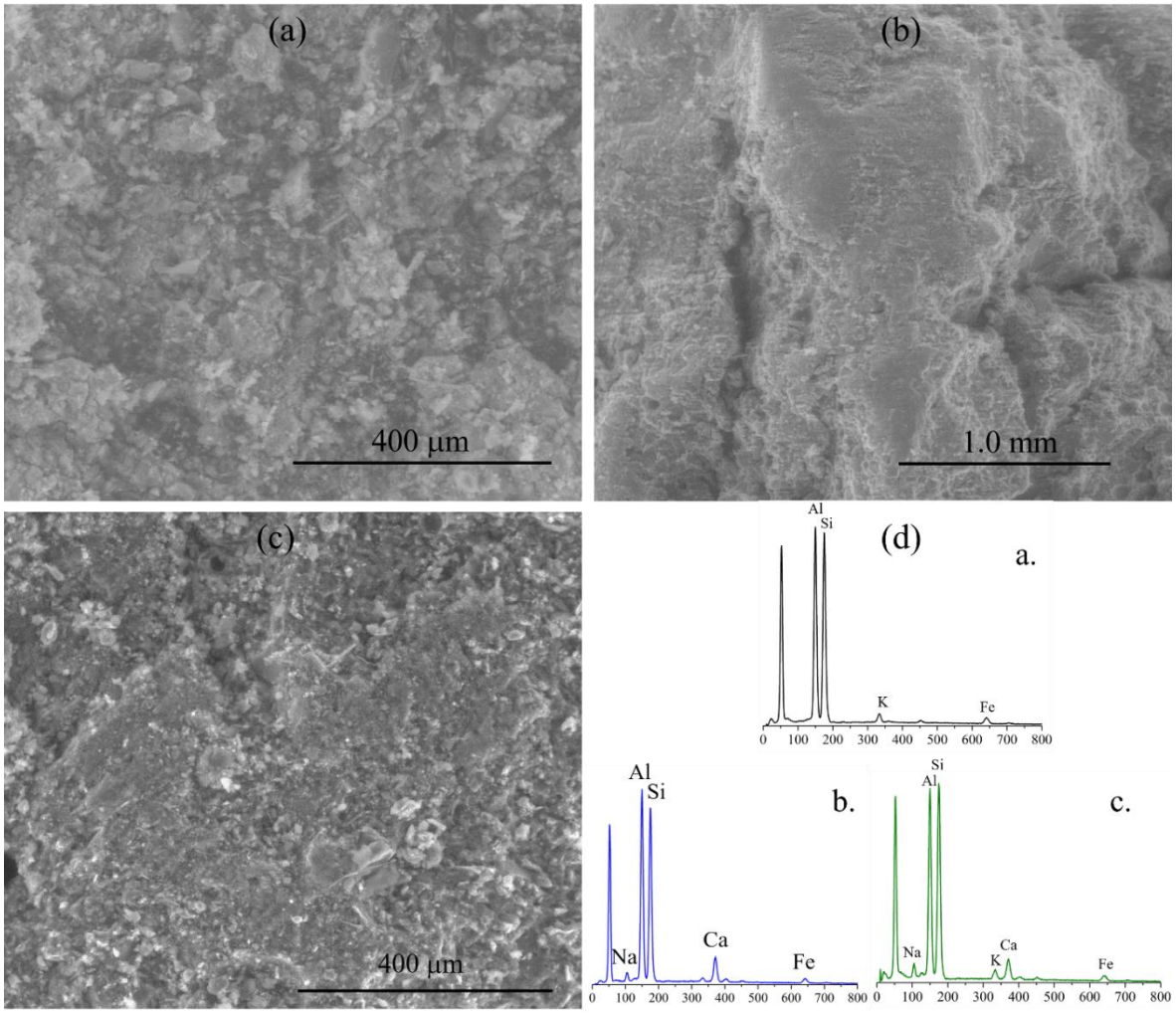

Figure 49. SEM images of the reconstituted (a) and stabilised clay after 28 (b) and 90 (c) days and the respective EDS data (d)

5.4.2 Shear behaviour

Isotropic compression response

Figure 50 shows the isotropic compression curves in a "1 + initial void ratio ($1+e_0$) - logarithmic mean stress (log p')" space. The slopes of the normal compression (λ) and swelling (k) lines and the yield stress (p'_y) determined according to the Casagrande method are summarised in Table 21.

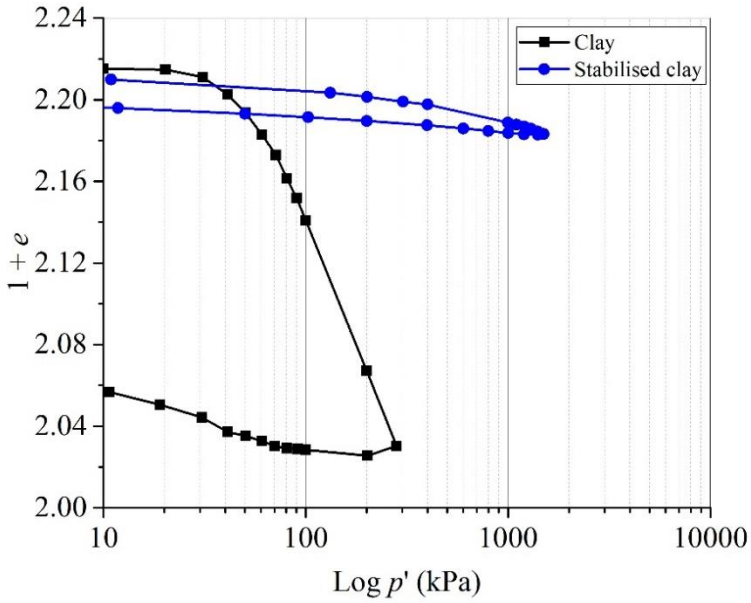

Figure 50. Isotropic compression response of the reconstituted and stabilised clay after 28 curing days

Table 21. Isotropic compression results for the reconstituted and stabilised clay after 28 days

	log p' - (1+e) space		ln p' - ln (1+e) space	
	λ	κ	λ^*	κ^*
Reconstituted clay	0.2421	0.0083	0.1093	0.0037
Stabilised clay after 28 days	0.0381	0.0074	0.0172	0.0034
Yield stress (p'_y) (kPa)	55		745	

A stiffer behaviour was observed on the stabilised clay, with slopes of λ and κ reduced 6.4 and 1.1 times compared with the reconstituted clay. For the reconstituted clay, the onset of irrecoverable or plastic strain is a well-defined p'_y point at 55 kPa. This yield stress is due to the stress-history applied during the specimen preparation. After adding 10%GGBS-NaOH, the p'_y increased significantly to 745 kPa. However, the p'_y point observed on the stabilised clay compression curve is not a well-defined point as the one observed in its reconstituted state. The use of higher axial stresses could result in a more well-defined linear virgin compression zone. It is believed that the variation in p'_y was caused by the development of strong cementation bonds within the matrix of the stabilised clay. The pre-yield state ($p'_0 < p'_y$) is characterised by small compressibility, with the soil structure restraining the deformation essentially recoverable. At the post-yield

state ($p'_0 < p'_y$), there was a gradual breakdown of the cement bonds as the mean effective stress (p') increases.

The formulation of the kinematic hardening model requires the parameter values of λ and κ in the ln p' (kPa) - ln (1+e) space. These values were determined according to Equation. 29 and are also summarised in Table 21.

$$\lambda^* = \frac{\lambda}{1+ e_0} \text{ and } k^* = \frac{k}{1+ e_0} \qquad \text{Equation. 29}$$

Consolidated undrained shear behaviour

In Figure 51, the experimental q (kPa) - ε_a (%), Δu (kPa) - ε_a (%) and q (kPa) - p' (kPa) curves obtained from triaxial tests for the reconstituted clay are shown through solid lines.

A behaviour typical of normally consolidated clays was observed for specimens consolidated with p'_0 higher than the isotropic yield stress ($p'_0 > p'_y$) (OCR 1 (150), OCR 1 (350), OCR 1 (700)), with the absence of peak deviatoric strengths (Figure 51 (a)) and increase of pore pressures up to the end of the tests (Figure 51 (b)). The increase in pore pressure led to the stress-path move to the left after yielding and before failure (Figure 51 (d)). On the test OCR 4.7 (150), the impact of the OCR is clear. Although it is not noticeable in the pore pressure development (Figure 51(b)), Figure 51 (d)) shows a typical stress-path of overconsolidated clays, with a slight decrease of the pore pressure before the specimen failure moving the stress-path to the right. The impact of p'_0 and OCR is clear in the stress-strain curves. There was an increase of the deviatoric strength for $\varepsilon_a \approx 2.5\%$ (Figure 51 (a)) with the increase of OCR and p'_0.

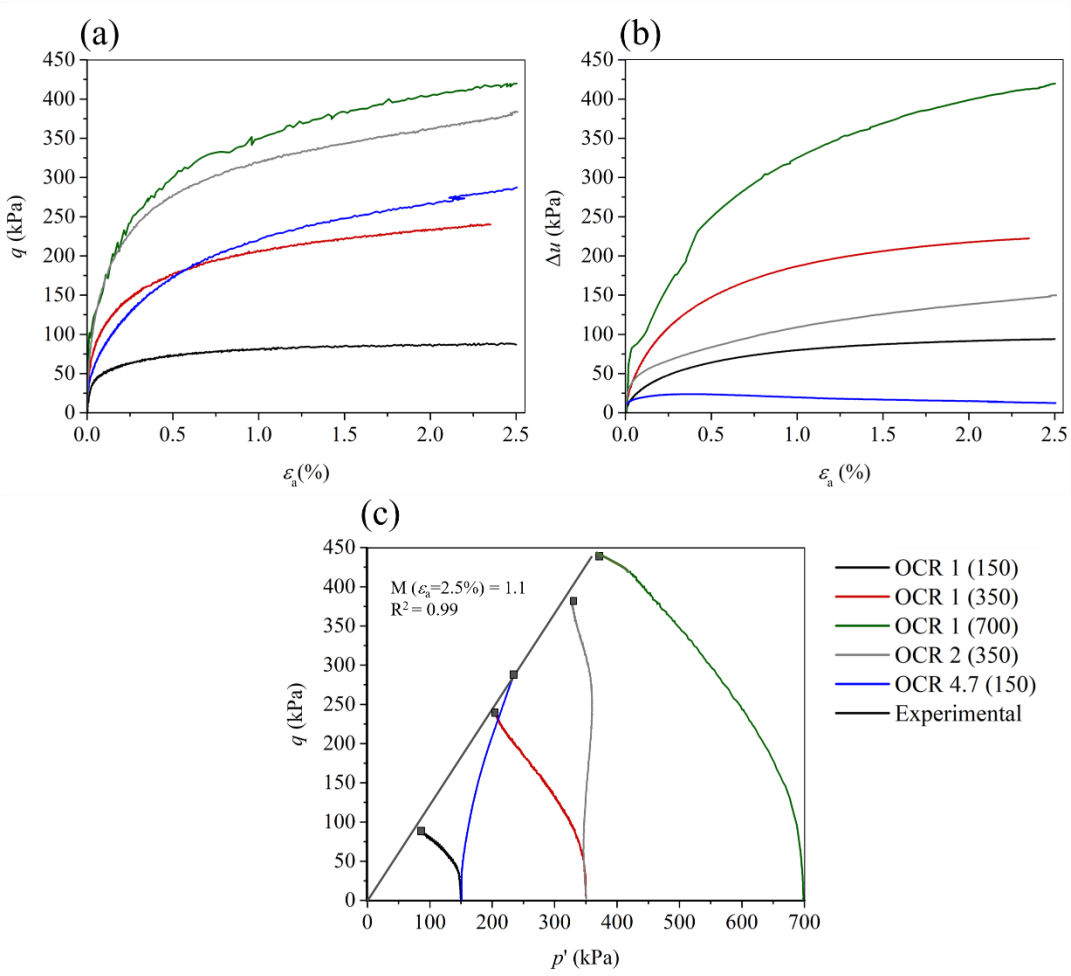

Figure 51. Triaxial test results for the reconstituted clay: (a) q (kPa) - ε_a (%), (b) Δu (kPa) - ε_a (%), (c) q (kPa) – p' (kPa)

The experimental q (kPa) - ε_a (%), Δu (kPa) - ε_a (%) and q (kPa) - p' (kPa) curves obtained from triaxial tests for the stabilised clay after 28 days is presented in Figure 52 by solid lines. The stress-strain behaviour of the clay changed significantly after the addition of 10%GGBS-NaOH (Figure 52 (a)). This behaviour is characterised by higher values of the peak/post peak deviatoric strength compared to its reconstituted state and by a stress-strain behaviour almost linear before peak followed by a softening up to the end of the tests. The reconstituted clay exhibited nonlinear stress-strain curves before the maximum stress and a strain hardening behaviour for higher p'_0 values (OCR 1 (350) and OCR 1 (700) - Figure 51 (a)). Deviatoric shear strengths (Figure 52 (a)) for $\varepsilon_a \approx 2.5\%$ up to 10, 3.5, and 3.3 times higher than those recorded for the

reconstituted clay (Figure 51 (a)) were observed after stabilisation for p'_0 = 150 kPa, 350 kPa, and 700 kPa, respectively. The peak deviatoric strengths were observed for $\varepsilon_a > 0.15\%$ and $\varepsilon_a < 1\%$.

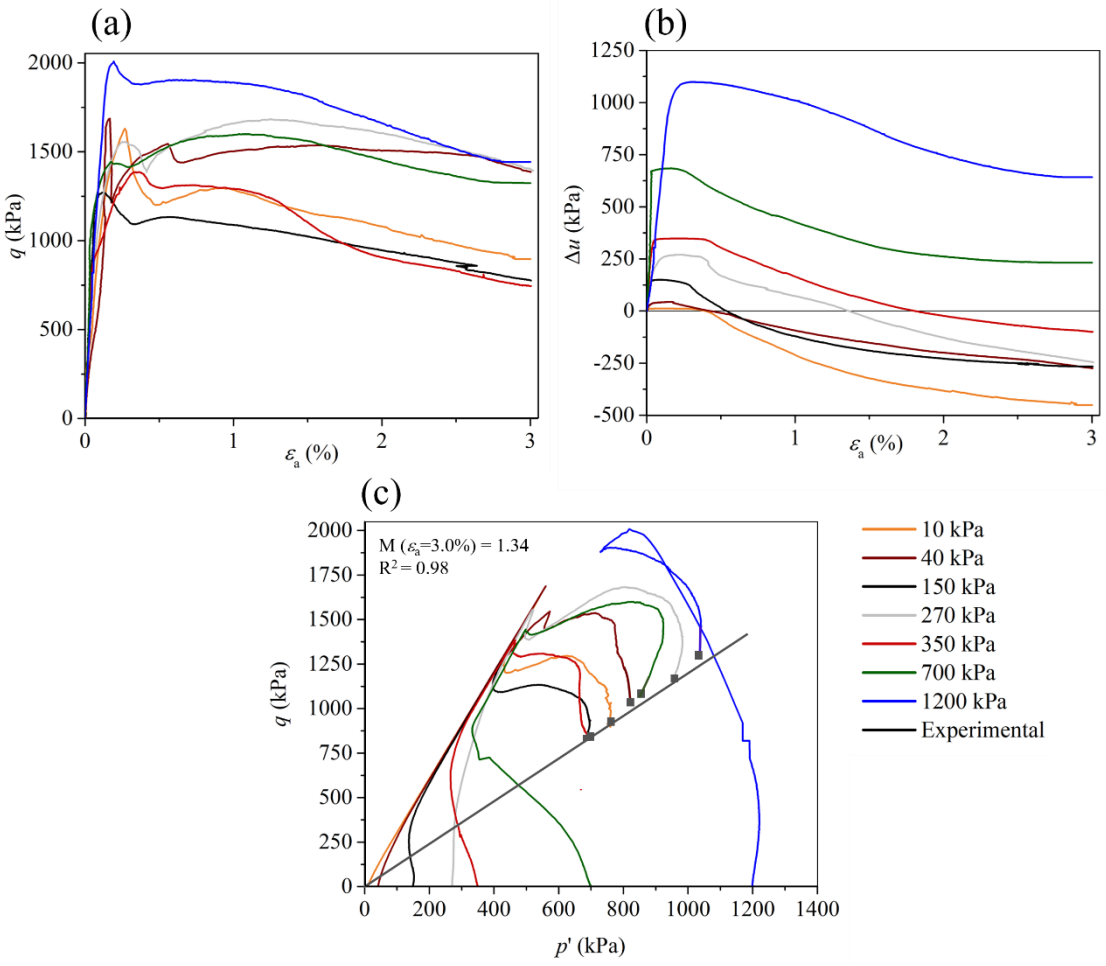

Figure 52. Triaxial test results for the stabilised clay after 28 days: (a) q (kPa) - ε_a (%), (b) Δu (kPa) - ε_a (%), (c) q (kPa) – p' (kPa)

At pre-yield state (for $p'_0 < p'_y$), a strain-softening behaviour was observed in Figure 52 (a), with the increasing of the deviatoric stress up to the peak value followed by a reduction to a lower value of q. Also, the stress-strain curves overlap, with similar values of peak deviatoric strength even for increasing p'_0. The authors believe that this behaviour was caused by the artificial cementation effect within the soil matrix when the state of stress is inside the state boundary surface. It is believed that similar to what happens with cement-treated clays for $p'_0 < p'_y$, the development of artificial cementation within the clay matrix led to an almost

insignificant change of the fabric during the consolidation phase (i.e., the reorientation of the clay particles), and therefore, the increase of p'_0 did not affect the peak deviatoric strength. At post-yield state (for $p'_0 > p'_y$), a strain-softening behaviour post peak strength was also observed for p'_0 = 1200 kPa (Figure 52 (a)). However, in this case, there was a more evident rise of the peak deviatoric strength, which denotes that at this condition, both the progressive breakdown of the cementation and the change in the fabric contributes to the enhancement of the peak strength.

An increase of the pore pressure up to the peak strength at low strain levels followed by a decrease until the end of the test was observed for $p'_0 < p'_y$ (Figure 52 (b)). In opposition to what was observed in the q (kPa) - ε_a (%) plot (Figure 52 (a)), the trend of u in Figure 52 (b) shows that p'_0 had a significant impact on pore pressure generation, with an increase of the peak of pore pressure with the increase of p'_0 at pre-yield and post-yield states. For specimens with $p'_0 \leq 350$ kPa, once u had peaked and started decreasing, it decreased to negative values. For p'_0 = 1200 kPa ($p'_0 > p'_y$) (Figure 52 (b)), there was also an increase of the pore pressure up to the peak and then a slight decrease until the end of the tests. More stable values of u were measured for $\varepsilon_a > 2.5\%$.

For $p'_0 < p'_y$, the stress paths are situated on the dry side of the critical state in Figure 52 (c), where at first there was an approach to the peak strength, and then the stress paths move to the right before ending the tests. For $p'_0 > p'_y$ (i.e., p'_0 = 1200 kPa), the stress-path is similar to that observed for normally consolidated or lightly overconsolidated clays, located on the wet side, moving to the left after the peak strength before ending the test.

A behaviour similar to the one presented in Figure 52, that is, two distinct shear responses at p'_0 lower (pre-yield state) and higher (post-yield state) than p'_y due to the artificial cementation, was also described by other authors in clays stabilised with distinct binders as cement, a super-absorbent polymer mixed with ordinary Portland cement and hydrated lime, or fly-ash (Bian et al., 2017; Efthymiou and Kavvadas, 2019; Horpibulsuk et al., 2004; Kamruzzaman et al., 2009).

Regarding the linear region of the stress-strain curves in Figure 52 (a), they are almost overlapped, suggesting that the p'_0 applied on the stabilised clay specimens does not seem to influence the initial stiffness. In other words, no significant increase of stiffness was observed when increasing p'_0.

The shear strength parameters and failure envelopes determined from the triaxial tests using the Mohr-Coulomb criterion are shown in Table 22. The shear strength parameters were calculated at ε_a = 2.5% and ε_a = 3% for the reconstituted and stabilised clay, respectively.

Table 22. Shear strength parameters

	Effective stress				Total stress			
	Peak		Post peak		Peak		Post peak	
	c' (kPa)	ϕ' (°)	c' (kPa)	ϕ' (°)	c (kPa)	ϕ (°)	c (kPa)	ϕ (°)
Reconstituted clay	-	-	0	26	-	-	0	13
Stabilised clay	429	28	0	34	606	10	375	12

The reconstituted clay was characterised by a null cohesion (c) at ε_a = 2.5%, in total and effective stresses, due to the break of inter-particle bonding within the matrix soil during the specimen preparation. At ε_a = 2.5%, a friction angle (ϕ) of 26° was obtained for the clay in effective stress while in total stress was 13°. In terms of effective peak strength, the stabilised clay failure was characterised by a c' = 429 kPa (induced by the artificial cementation) and ϕ' of 28°. In total stress, the peak strength parameters were c = 606 kPa and ϕ = 10°. At ε_a = 3%, the ϕ' was of 34° while the ϕ was 12°. These results suggest that the cementation not only added cohesion between clay particles but also made them coarser, increasing their effective friction angle. At ε_a = 3%, the c' was null due to the total breakdown of the cementation welding and distortion of the clay fabric during shear. In total stress, the stabilised clay presented and post peak c of 375 kPa and ϕ of 12° that is practically equal to the ϕ observed before adding 10%GGBS-NaOH.

The failure modes observed on the reconstituted and stabilised clay specimens were quite distinct. Reconstituted specimens exhibited a slight enlargement of the middle section, while the stabilised specimens showed the formation of localised shear bands with slopes near to 45°, which corresponds to positive

dilatancy associated with shear deformation (Figure 53). This is consistent with the decrease in pore pressure recorded from peak deviatoric stress in the Δu (kPa) - ε_a (%) curves (Figure 52 (b)).

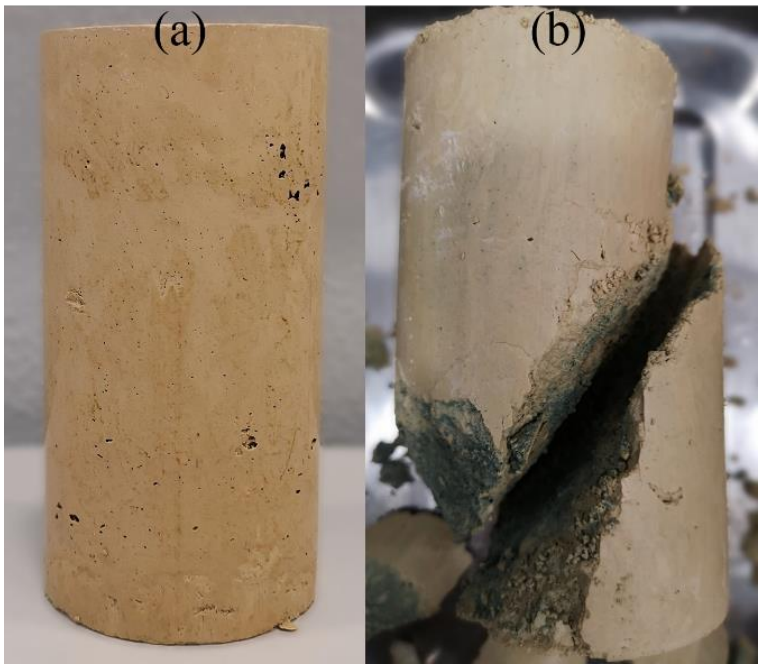

Figure 53. Stabilised clay specimen (a) before testing and (b) after failure for p'_0 = 350 kPa

5.4.3 Leachate analysis

Table 23 presents the results of the leachate analyses and the limit values for a material to be considered as 'inert waste', according to Annex IV of the Portuguese Law-Decree no. 183/2009. Based on Table 23, the concentrations of all elements are below the limit values, so the analysed materials can be classified as 'inert waste' at both curing ages. Therefore, the addition of 10%GGBS-NaOH to the clay besides greatly improving its mechanical behaviour, resulted in a material classified as inert waste and is unlikely to represent a risk for soil contamination according to thresholds provided by Law-Decree of Portugal.

Table 23. Leachate results and the limit values established by Law Decree no. 183/2009 for inert waste

Element	Limit values for 'inert waste'(mg/kg) Annex V Law no. 183/2009	Leachate results		
		Clay	Stabilised clay after 28 days	Stabilised clay after 90 days
As	0.5	0.0	0.3	0.3
Cr	0.5	0.01	0.0	0.0
Cu	2.0	0.0	0.0	0.0
Ni	0.4	0.0	0.0	0.1
Pb	0.5	0.0	0.0	0.0
Zn	4.0	0.0	0.0	0.0
Clorets	800	13.1	13.0	12.7
Sulphate	1000	9.3	104.8	49.8

5.5 Model calibration and predicted stress-strain curves

The kinematic hardening model has 12 input parameters (see Table 15). The fitted set of parameters for the reconstituted and stabilised clay cured for 28 curing days is shown in Table 24 and Table 25. The majority of the parameters was manually fitted, by means of a trial-and-error procedure (best-fitting between the experimental curves with the calibrated ones). The triaxial test results were crucial during this task since they helped with the estimation of these parameters. Details about the calibration process are given next.

Table 24. Fitted set of kinematic hardening model parameters for reconstituted clay proposed by (Rouainia and Muir Wood, 2000)

Model parameters	Reconstituted clay				
	OCR 1 (150)	OCR 1 (350)	OCR 1 (700)	OCR 2 (350)	OCR 4.7 (150)
p_{co}	84	186	362	350	352
κ^*	0.000148	0.00013	0.000192	0.000081	0.000108
λ^*	0.04	0.063	0.1	0.8	0.1
M	1.1	1.1	1.1	1.1	1.1
ν	0.45	0.45	0.45	0.45	0.45
R	0.3	0.23	0.19	0.1	0.14
B	8	8	8	8	8
Ψ	2.8	2.8	3.2	3.5	3.8
A	1	1	1	1	1
k	4.6	0.8	0.8	4.6	4.6
η_0	0	0	0	0	0
r_0	1.2	1.2	1.2	1.2	1.2

Table 25. Fitted set of kinematic hardening model parameters for stabilised clay after 28 curing days

Model Parameters	Stabilised clay after 28 days						
	p'_0 = 10 kPa	p'_0 = 40 kPa	p'_0 = 150 kPa	p'_0 = 270 kPa	p'_0 = 350 kPa	p'_0 = 700 kPa	p'_0 = 1200 kPa
p_{c0}	610	610	475	475	475	475	580
κ^*	0.00002	0.000035	0.000032	0.000023	0.00002	0.00001	0.00013
λ^*	0.02	0.035	0.03	0.025	0.05	0.03	0.025
M	1.3	1.3	1.3	1.3	1.3	1.3	1.3
ν	0.45	0.45	0.45	0.45	0.45	0.45	0.45
R	0.03	0.03	0.03	0.03	0.03	0.03	0.03
B	2	4	4	1.6	2.5	1.9	0.9
Ψ	1.8	1.8	1.8	5.5	5.5	5.5	5.1
A	0.1	0.1	0.1	0.1	0.5	0.3	0.3
k	3.1	1	2.8	1.3	3.5	1.15	1.15
η_0	0	0	0	0	0	0	0
r_0	2.05	2.05	2.05	5	5	5	5

The first step in the calibration process was the establishment of the initial conditions of the tests, that is, the size of the surfaces (p_{c0}), centre of the bubble yield surface ($\bar{\alpha}$) and the centre of the structure surface ($\hat{\alpha}$) or r_0 and η_0, besides the drainage conditions (drained or undrained).

Within the elastic domain, the response of the model is isotropic, and the elastic properties are expressed by the bulk and shear moduli, K and G, which depend on the pressure p'. Two parameters are required to describe the elastic behaviour, namely κ^* and ν. The ν was fixed equal to 0.45 for both reconstituted and stabilised clay that is a value close to 0.5 since the triaxial tests were conducted in undrained conditions.

The elastic parameter κ^* and the plastic/elastic-plastic parameter λ^* determined in log p' - (1+e) scale (Table 21) were first converted in the ln p' - ln (1+e) scale using Equation. 1. Both κ^* and λ^*, which control the stiffness in the elastic region and the peak position on the stress-strain curves, were introduced into the model and then manually calibrated for each material and p'_0 applied in the tests. Lower values of κ^* were fitted for the stabilised clay cured for 28 days compared to its reconstituted state, which is in line with the isotropic compression results presented in Figure 50.

The parameter M, which controls the geometry of the surfaces, was determined from the triaxial test results presented in Figure 51 and Figure 52 based on the shearing resistance in effective stresses of the

reconstituted (ϕ' = 26° at ε_a = 2.5%) and stabilised (ϕ' = 34° ε_a = 3%) clay. Although the tests were stopped shortly after failure, the trend of the results suggests that no drop in strength would have occurred under continued strain. Moreover, the initial rapid pore-pressure build-up observed in both materials, which was reduced to a negligible rate when the tests were stopped, together with M adjusting (i.e., R^2 value) close to 1, validate the presented results (see Figure 51 (b) (c) and Figure 52 (b), (c)). The M parameter was characterised by a straight line with a slope of 1.1 ($R^2 \approx 0.99$) and 1.34 ($R^2 \approx 0.98$) for the reconstituted and stabilised clay, respectively.

For the reconstituted clay, the parameter p_{c0} was also defined based on the triaxial tests, considering the correspondent OCR, according to Equation. 30.

$$p_{c0} = \frac{p'_{max}}{2} \text{ and } OCR = \frac{p'_{max}}{p'_{final}} \qquad \text{Equation. 30}$$

Where:

p'_{max} was the maximum pressure applied during the consolidation phase.

p'_{final} was the final pressure applied during the consolidation phase that was equal to p'_0 at the beginning of the shear phase.

The p'_{max} applied was 700 kPa for OCR 4.7 (150) and OCR 2 (350) specimens, which agrees with the values of the parameter p_{c0} introduced in the model (Table 24).

For the stabilised clay, the parameter p_{c0} was not directly determined from the triaxial tests. The development of artificial cementation within the clay matrix led to the enlargement of the structure surface, which implies that both the size of the surfaces (represented by p_{c0}) and parameter r_0 that describes the relative sizes of the structure and references surfaces increased until unknown values. The values of these two parameters were then manually fitted using a trial-and-error procedure (best-fitting between the experimental and the calibrated curves). The parameter p_{c0} was varied from 84 kPa - 362 kPa (reconstituted clay) to 475 kPa - 610 kPa (stabilised clay), while the parameter r_0 from 1.2 (reconstituted clay) to 2 - 5 (stabilised clay) (Table

24 and Table 25). The parameter r_0 was fixed close to 1 for the clay as it is a reconstituted soil, meaning that the structure and reference surfaces have the same shapes. The increase of r_0 led to a higher and sharper peak in the stress-strain relationship predicted by the model. On the reconstituted clay specimens, the increase of p'_0 led to an increase of p_{c0}. However, no trend was observed on the stabilised clay. These parameter values are in line with the observed experimental behaviour, where the peak and post peak strengths increased with the increase of p'_0 for the clay (Figure 51 (a)), unlike the stabilised clay specimens (Figure 52 (a)).

Based on SEM images presented in Figure 49, both reconstituted and stabilised clays were idealized as isotropic materials, i.e., $\eta_0 = 0$.

The destructuration is controlled by 2 parameters, A and k. Parameter A controls the relative contribution of distortional and volumetric plastic strains during destructuration, ranging between $0 < A < 1$. For the reconstituted clay, A was fixed to 1, so the destructuration process was entirely caused by the distortional component of the damaged strain, which predominantly happens in undrained conditions (Table 24). For the stabilized clay, the best fit between the experimental and the calibrated curves was achieved for A values close to 0 (Table 25). The parameter k expresses the rate of damage to the structure with plastic strains, and it was manually calibrated for both materials for the p'_0 applied during the shear phase. The reduction of k increases the peak strength and stiffness because the destructuration takes place slower.

The remaining three parameters introduced by the bubble surface, i.e., the ratio of sizes of the bubble and the reference surface R, the stiffness interpolation parameter B, and the stiffness interpolation exponent Ψ, were fitted using a trial-and-error procedure until a good match between the experimental and calibrated curves was achieved. The increase of B led to a higher peak in the stress-strain plot and an increase of the plastic hardening modulus. A higher value of Ψ led to a softer behaviour from small to large strain levels or, in other words, to lower values of the overall deviatoric strength response. Lower values of R led to a stiffer response in the small strain region, with higher values of peak and residual strengths.

Figure 54 (a), (b), and (c) and Figure 55 (a) and (b) present the experimental stress-strain curves and the predicted ones using the kinematic hardening model. The full lines represent the experimental behaviour determined through triaxial tests, while the dotted lines represent the model predictions using the fitted set of parameters presented in Table 24 and Table 25.

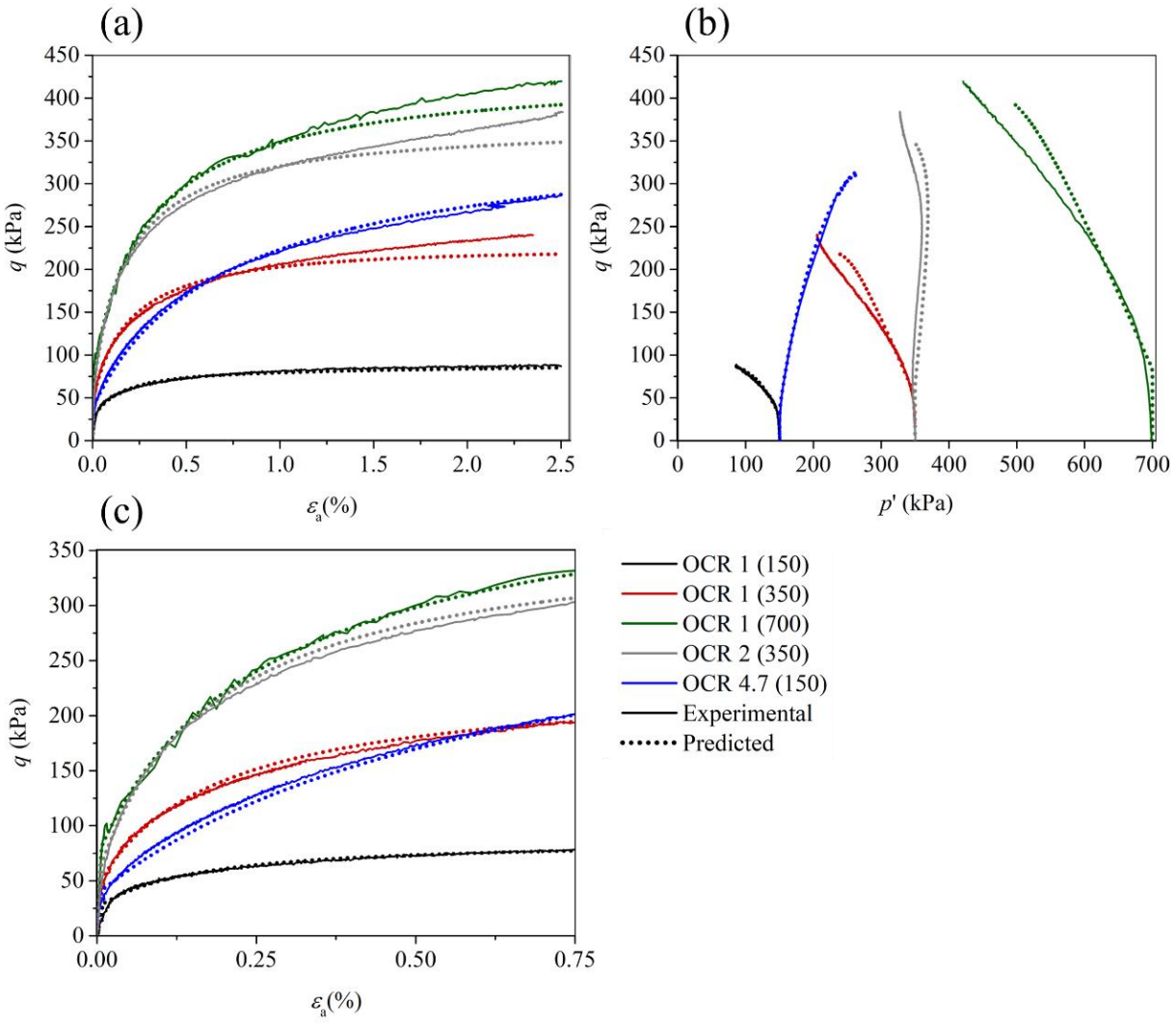

Figure 54. Experimental and predicted curves from triaxial tests for the reconstituted clay: (a) q (kPa) - ε_a (%), (b) local zoom of q (kPa) - ε_a (%) graph between 0 and 0.75%, (c) q (kPa) – p' (kPa)

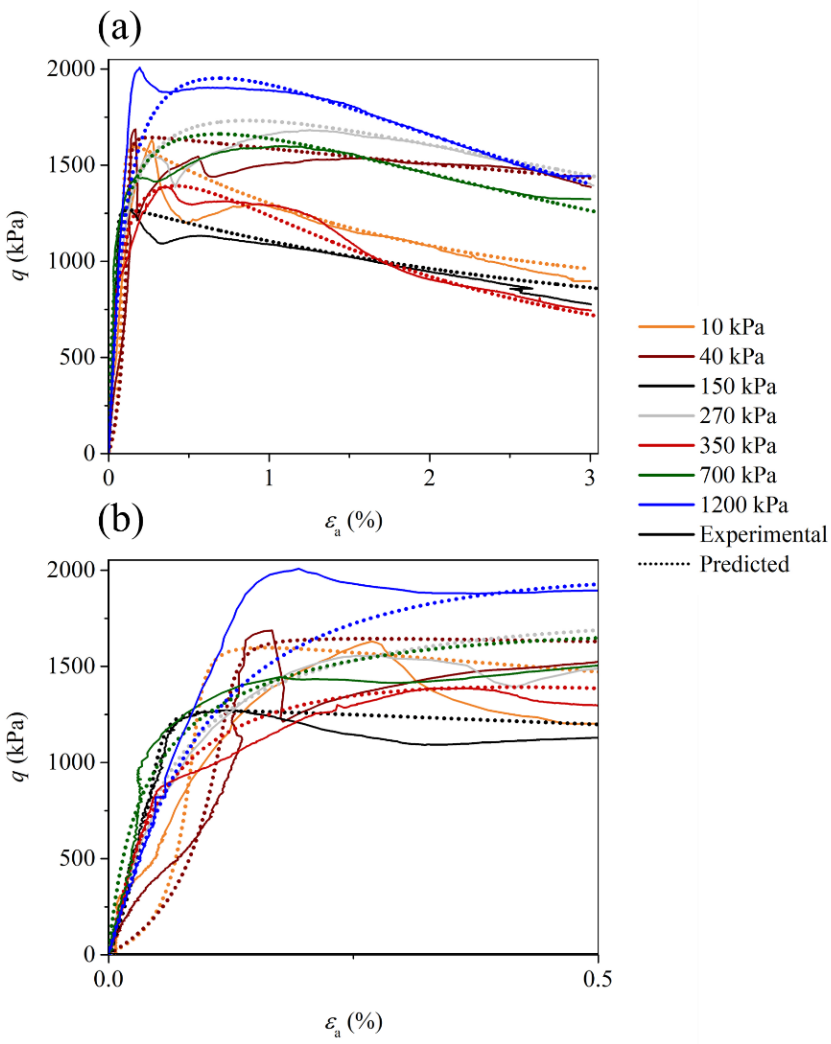

Figure 55. Experimental and predicted curves from triaxial tests for the stabilised clay: (a) q (kPa) - ε_a (%), (b) local zoom of q (kPa) - ε_a (%) graph between 0 and 0.5%

The good fit between the experimental stress-strain curves and the predicted ones using the kinematic hardening model revealed the model potential to be applied in different materials for which it was initially formulated. The model accurately predicted the trend of the strain-hardening behaviour observed for the reconstituted clay before the peak strength (Figure 54 (a)). The experimental strain-softening behaviour for almost all stabilised clay specimens was also well predicted by the model for the wide range of applied p'_0 values (Figure 55 (a)). The peak and post peak shear strengths predicted by the model are also in general coincident with those observed in the tests. The smooth response suggests that plastic deformations and

hardening occurred as the bubble starts to move inside the structure surface. The dependence of the shear modulus on the mean effective stress, together with the variation in plastic stiffness as the bubble approaches the structure surface, allow to model more accurately the non-linearity of these curves. All the predicted effective stress paths for the reconstituted clay (Figure 54 (b)) are very similar to the experimental data and converge towards the critical state line.

5.6 Conclusions

The mechanical behaviour of a reconstituted and stabilised clay at high water content was investigated after 28 curing days by means of consolidated undrained triaxial tests. The clay was stabilised using an alkali-activated binder composed of 10%GGBS-NaOH. The stress-strain curves for both materials were predicted using a kinematic hardening constitutive model formulated for natural clays. It was the first attempt of using this constitutive model in artificially cemented clays. SEM-EDS, XRD analyses and leachate tests were carried out after 28 and 90 days to complement the experimental campaign. The main conclusions from this research are summarized below:

- The main gel phase formed was N, C-A-S-H with a low CaO/SiO_2 ratio. No risk of soil contamination was detected after adding 10%GGBS-NaOH to the clay in both curing periods.
- The mechanical behaviour of the clay drastically changed after adding the binder, with increased peak/post peak shear strengths and yield stress which reveals the potential of the alkali-activated binder even when applied to soils with high water content. It is believed that for $p'_0 < p'_y$, the consolidation phase did not have a significant impact on the rearrangement of the clay particles and, therefore, the increase of p'_0 did not lead to an increase of peak/post peak shear strength and the stress-path was located on the dry side of the critical state. For $p'_0 > p'_y$, the authors believe that both the fabric and cemented structure contribute to the strength. The stress-path is located on the wet side of the critical state. Concerning the shear strength parameters, the binder added cohesion to the clay matrix and also turned the particles coarser increasing the friction angle.
- The stress-strain curves for both reconstituted and stabilised clay were accurately predicted using the kinematic hardening model for the wide range of applied p'_0, demonstrating thus the model potential to be applied in artificially cemented clays besides natural and reconstituted clays.

6. APPLICATION OF ALKALI-ACTIVATED INDUSTRIAL WASTES FOR THE STABILISATION OF A FULL-SCALE (SUB)BASE LAYER

An increasing interest in the development of alternative solutions based on the use of wastes and residues in the context of soft soils improvement has been observed in the last few years. Most of such research is related to the laboratory characterization of the soil-binder or soil-reinforcement mixtures. However, the viability and impact of the construction process associated with these alternative solutions, as well as the effect of the in situ curing conditions on the mechanical and durability properties of the improved soil cannot be properly assessed in the laboratory. The present paper describes and examines what is, to the best of the authors knowledge, the first full-scale attempt to apply alkali-activated fly ash to the stabilisation of a (sub)base layer. Different types of alkaline activated cement were tested, and soil-cement and soil-lime mixtures were also used, for comparison purposes. An 80 m long (2.5 m wide) full-scale trial was built, divided into 5 sections with different soil-binder combinations, three of which were based on alkaline activated cement. The mechanical properties of all segments were evaluated, on-site and in the laboratory, together with an environmental assessment and a preliminary financial analysis. The results show that the alkaline cement-based materials have mechanical performances similar to traditional binders, with still some margin of optimization due to, their almost embryonic stage of development.

Keywords: full-scale model; industrial wastes; alkaline binders; *in situ* tests; soil improvement

---

This Chapter is based in the article:

Miranda, T., Leitão, D., Oliveira, J., Corrêa-Silva, M., Araújo, N., Coelho, J., Fernández-Jiménez, A., Cristelo, N., 2020. Application of alkali-activated industrial wastes for the stabilisation of a full-scale (sub)base layer. J. Clean. Prod. 242, 118427. https://doi.org/10.1016/j.jclepro.2019.118427

6. APPLICATION OF ALKALI-ACTIVATED INDUSTRIAL WASTES FOR THE STABILISATION OF A FULL-SCALE (SUB)BASE LAYER

6.1 Introduction

Low geomechanical properties, together with the ambitious design requirements, frequently lead to the improvement of local soils, which is usually carried out by the addition of cement or lime. However, the production of ordinary Portland cement (OPC) imposes a very significant toll on the environment (Provis and Van Deventer, 2014), since it is one of the world´s most energy-intensive industrial processes, contributing with 5 % to 7 % of the world´s total CO_2 emissions (Pourakbar and Huat, 2017). Therefore, there is an increasing interest on the development of more sustainable binders, capable to produce similar levels of mechanical performance. The development of alkaline activated cements (AAC), resulting from the combination of low-calcium (Ca) industrial by-products with highly alkaline solutions, emerges as a very strong alternative to the most currently used material in the whole construction industry (i.e., Portland cement). The alkaline activation reactions can be summarised in the following steps (Fernández-Jiménez et al., 2006; Van Riessen et al., 2013):

- Dissolution of the aluminosilicate chains present in the precursor (fly ash (FA), in this case), into monomers, due to the high pH environment produced by the sodium-based activator solution.
- The subsequent release of the Si and Al ionic species into the solution produces an excess of negative charges, from the aluminium, which is compensated by the sodium species.
- The resulting products accumulate and precipitate, forming a three-dimensional amorphous structure, usually referred to as N-A-S-H gel, which will possibly crystalize.

Several advantages are associated with the use of such binders, especially from the environmental point of view, mainly due to the reduction of CO_2 emissions and conservation of the natural resources necessary to the production of Portland cement. The incorporation of industrial wastes in the binder compositions also allows their reintroduction in the economy, reducing the required landfill areas. However, while the precursor (i.e. FA) is an industrial by-product, with a worldwide production of more than 1,000 million tonnes per year, with less than 50 % recycled (Vargas and Halog, 2015), the activator solutions are usually prepared with commercial reagents (i.e., sodium hydroxide (NaOH) and/or sodium silicate (Na_2SiO_3)) with considerable environmental costs due to the CO_2 emissions associated with their production process (Cristelo et al., 2015).

Therefore, the development of low-cost activators, based partially or solely on wastes and residues, has recently been initiated, with encouraging results (Fernández-Jiménez et al., 2017).

Regarding the use of alkaline activation for geotechnical applications, several laboratory studies emphasize the potential of this technique. Mohammadinia et al. (2017) evaluated the strength and durability development of construction and demolition (C&D) aggregates, namely reclaimed asphalt pavement, recycled concrete aggregate, and crushed brick, activated with different ratios of activator solutions and FA for fill and pavement applications to replace the conventional pavement aggregates. The results indicate that alkali-activated FA is a viable binder for the improvement of C&D aggregates in pavement base/subbase application according to the recommendation by Texas department of transportation. Cristelo et al. (2018) also characterized the microstructure and mechanical behavior of C&D aggregates mixed with FA and chemical activators (NaOH and Na_2SiO_3). Results showed that the presence of FA improves compression strength and elasticity modulus, exceed the required values of unconfined compressive strength (UCS) for road and railway foundations or infrastructure embankments after 28 days of curing. Chemical analyses indicated the formation of the gels N–A–S–H and C–A–S–H, which were attributed to the initial high content of amorphous Si, Al and Ca of these mixtures. Mohammadinia et al. (2018) concluded that the alkali-activation of 15 % of cement kiln and 15 % of FA blended with C&D aggregates provided the optimum blend for the usage of these wastes as construction materials. In the studies carried out by Alam et al. (2019), the authors concluded that the alkaline activation of blast furnace slag (GGBS), an industrial by-product from iron production, applied in the stabilization of red mud, an industrial by-product from aluminum production, significantly increases the matrix durability under alternate wet-dry cycle condition. Sargent et al. (2016, 2013) investigated the incorporation of different industrial by-products into the composition of alkaline binders. The results showed that the soils improved with GGBS resulted in the greatest strength and durability improvements. In another study, good results were also obtained with the use of GGBS and FA as binder to control soil expansibility (Sharma and Sivapullaiah, 2016). In the study carried out by Corrêa-Silva et al. 2017, the performance of soils improved with alkaline binders was assessed and compared with traditional binders, like cement and lime. The results of these studies showed that these alternative binders can be, under some circumstances, competitive with the traditional ones in terms of geotechnical properties and in terms of environmental and economical aspects. Other characteristics, like the rheology/fluidity of alkali-

activated FA mixtures and its relation with the UCS of soils improved with these binders was investigated by Cristelo et al. (2013) for jet grouting applications. The shear strength and stiffness degradation of a silty sand improved with alkali-activated FA from small to large strains was investigated by Rios et al. (2016) and the authors concluded that the stress-strain behaviour of the material obtained in the triaxial tests is typical of cemented soils. Abdeldjouad et al. (2019) analyzed the effect of clay content on soil stabilization with and without palm oil fuel ash (POFA) mixed with a potassium-based alkaline activator. Results showed that clay minerals play an important role in soil stabilization with alkaline activation, influencing the behavior of the binder with hosted soil. Finally, Emmanuel et al. (2019) verified that the reactivity of kaolin greatly enhanced after the combined use of NaOH and Na_2SiO_3 as activator solution compared with the use of Na_2SiO_3 only. However, until now, and to the best of the authors knowledge, no studies were published regarding a full-scale application of these alternative binders in superficial soil stabilisation works. This kind of testing is essential to assess, in a broader context, the viability of the technique, especially considering the implications of the construction process and the effect of the environment in the mechanical and durability properties of the stabilised layers.

The present paper describes and examines the construction of a total of 80 meters of a stabilised layer, 2.5 meters wide, using 5 different binders, three of which are based on AAC, and the remaining two are based on OPC and lime. A combination of FA and commercial reagents (NaOH and Na_2SiO_3) was used in two of the three AAC-based segments, while the third was prepared with FA and a recycled alkaline solution, originally used to clean aluminium extrusion dies (referred to as ‘cleaning solution’, or CS). The performance was assessed by quality control tests at short (36 days) and long term (90 days), which included the Falling Weight Deflectometer (FWD) and the Plate Load (PL) field tests, and the Unconfined Compression Strength (UCS), performed on specimens collected from the field. Additionally, financial and environmental (equivalent CO_2 emissions) analyses were also performed.

6.2 Preparation and construction

A brief description of the used materials and binder compositions are referred in Chapter 6.2.1, while the construction method and the experimental campaign are detailed in Chapters 6.2.2 and 6.2.3, respectively.

6.2.1 Material characterisation and binder composition

The local soil was classified as a "CL - sandy lean clay", according to the Unified Soil Classification System (ASTM D 2487, 2011), and as a A-4-(3), according to the AASHTO's soil classification for highway construction (AASHTO M 145, 1991). Its treatment is justified, since it is a poor-quality soil for pavement subgrade, with silts and clays as the predominant fractions. Table 26 summarizes the geotechnical properties of the soil, while Figure 56 shows its particle size distribution.

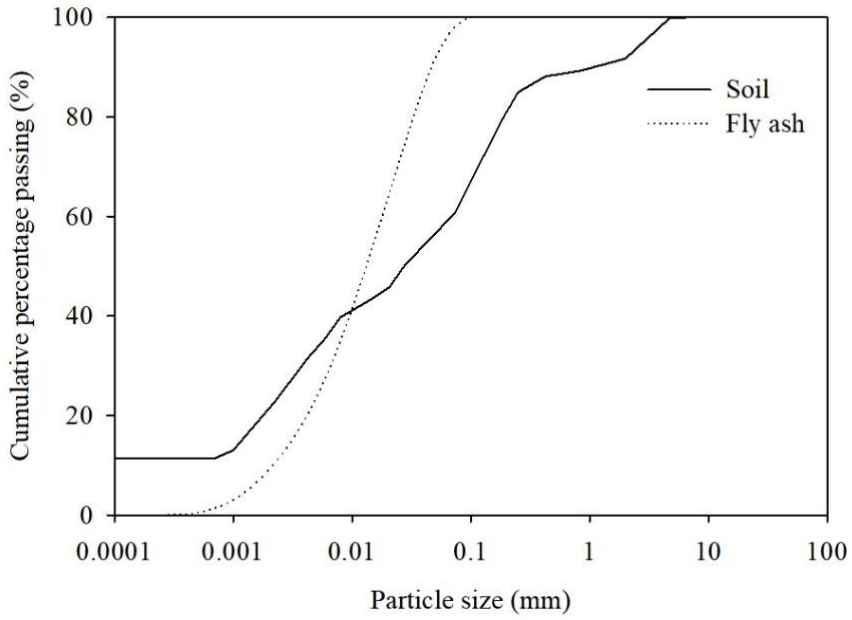

Figure 56. Particle size distribution of the soil and fly ash

6. APPLICATION OF ALKALI-ACTIVATED INDUSTRIAL WASTES FOR THE STABILISATION OF A FULL-SCALE (SUB)BASE LAYER

The industrial by-product chosen as source of silica (SiO_2) and alumina (Al_2O_3) (Table 27) was a class F FA (ASTM C 618, 2012), obtained from the thermo-electric power plant of Pego (Portugal). X-ray powder diffraction (XRD) data showed that its predominant mineralogical phases are quartz, mullite and hematite.

Table 26. Geotechnical properties of the soil

Property	Value		
Atterberg limits (a)	Liquid limit	28	%
	Plasticity limit	19	%
Methylene blue test (b)	MB	11.2	g/kg
Modified compaction test (c)	ω_{opt}	14.4	%
	$\rho_{d,max}$	1.81	Mg/m^3
CBR (d)	Unsoaked	48	%
	Soaked (f)	14	%
UCS (e)	$\sigma_{max}(\varepsilon_a = 1.2\%)$	363	kPa
	$E_{sec}(\varepsilon_a = 0.5\%)$	32	MPa

(a) (NP, 1969); (b) (NP, 2002); (c) (LNEC, 1966); (d) (LNEC, 1967); (e) (ASTM D 2166 / D 2166M, 2013); (f) around 1.2% expansion after soaking for 96 hours

Table 27. Chemical composition of the FA, as determined by X-ray fluorescence (XRF)

Compound	Na_2O	SiO_2	Al_2O_3	MgO	K_2O	CaO	TiO_2	Fe_2O_3	ZnO	ZrO_2	BaO	Others	LOI
wt. %	1.18	54.8	21.57	1.87	2.56	1.68	1.01	7.33	0.03	0.05	0.12	1.37	6.47

Two commercial reagents were chosen to produce two of the five stabilisers used in the field, namely NaOH, originally in pellets, and Na_2SiO_3, in solution form, produced through the hydrothermal process, with a SiO_2/Na_2O molar ratio of 2.063, a unit weight of 1.464 g/cm^3 and a Na_2O concentration of 13 %. The NaOH was mixed with the natural soil and water, up to a concentration of 10 molal. The Na_2SiO_3 solution was previously mixed with the 10 molal NaOH solution, in a Na_2SiO_3 / NaOH weight ratio of 0.5, and the final combined solution was mixed with the soil. An additional activator was tested, a recycled solution originally used to clean aluminium extrusion dies (CS), with a concentration of approximately 4.54 molal and a pH of 14 (Fernández-Jiménez et al., 2017). The chemical composition of the CS is presented in Table 28.

Table 28. Chemical composition of the CS, as determined by X-ray fluorescence (XRF)

Compound	Al	K	Na	S	Si
Fraction (%)	1.86	0.28	94.60	3.21	0.05

More traditional binders were also used, to establish a reference, namely Portland cement CEM II/B-L 32.5 N and quicklime CL90. Table 29 summarizes the mixtures that were implemented *in situ*, as well as their compaction properties, based on the Proctor test results.

Table 29. Binders and respective compaction conditions

Mixture	ID	Water content (%)	Dry unit weight (Mg/m^3)	NaOH / FA (wt. ratio)
4 % of lime	L4	14.2	1.80	-
5 % of cement	C5	14.5	1.84	-
20 % of alkaline activated FA with NaOH and Na_2SiO_3	FA20a	13.0	1.80	0.18
20 % of alkaline activated FA with NaOH	FA20b	13.0	1.80	0.26
20 % of alkaline activated FA with CS	FA20CS	13.4	2.10	0.03

These formulations were previously studied by Corrêa-Silva et al. (2018) and Fernández-Jiménez et al. (2017), and the promising results obtained motivated their choice for *in situ* implementation in the present work. Additional factors also contributed to the selection of these mixtures, such as the fact that commercial NaOH and Na_2SiO_3 are the most frequently used activators found in the literature, which increases the interest in studying the viability of its application *in situ*; the possibility to test, in full-scale conditions, a sustainable alternative to the commercial reagents mentioned, which have significant financial and environmental costs; cement and lime are well-known traditional binders, frequently used in the context of soil improvement, and should thus be able to establish relevant references.

6.2.2 Construction of the stabilised layer

The full-scale trial was built in the North of Portugal, near the city of Porto (Figure 57), with 2.5 m width, 0.20 m thick and a total length of 80 m, divided in 5 different segments, with the following sequence: FA20CS (10 m), FA20a (20 m), FA20b (20 m), C5 (15 m) and L4 (15 m). The adopted spatial distribution was based

on the similarity between the *in situ* water content of each section and the water content required for the compaction of the mixtures (Table 30). Also relevant is the fact that the FA-based segments are adjacent, which represents a logistic advantage during construction.

Figure 57. General view of the site before the start of the stabilisation work

Worksite preparation started 48h before the construction of the layers and included the removal of a thin layer of topsoil; FWD tests along the longitudinal axis, with 2 m between sequential points; assessment of the water content in each section, at two different places, using a nuclear density gauge. Due to the significant differences between the water content *in situ* (ω_{situ}) and the required water content (ω_n) for optimum compaction, in segments 1 (L4), 3 (FA20b) and 5 (FA20CS), it was decided to reduce the water content in these sections by mixing the soil with 3 % of quicklime, through scarification of the soil surface on a depth of 20 cm. Such low calcium content induces only metastable changes in the soil properties, as it is not enough to develop pozzolanic reactions that would produce inter-particle cementing bonds (Cristelo et al., 2009). This procedure was carried out with the ripper of a motor grader, 24h before starting the construction and, 8h later, the layer was closed and roller compacted, to limit the night humidity in the layer. On the day of the prototype construction, the *in situ* water content was again determined in these 3 segments, at two different points. All the relevant water content values are presented in Table 30, including those in the liquid activators (ω_a),

which were taken into consideration to reach the final water content, indicated by the Proctor tests (ω_{Protor}). The addition of quicklime significantly reduced the water content in the selected segments. However, this reduction was heterogeneous and insufficient, resulting in the compaction of the stabilised layers on the wet side of their respective Proctor optimum value. The most significant differences were observed in sections L4 and FA20a with water content approximately, 4.6 % and 2.95 % higher than ω_n.

Table 30. Water content *in situ* at the start (ω_0), after lime treatment (ω_{lime}) and required for stabilisation (ω_{stab})

Segment	Pre-determined			Field			
	$\omega_{Proctor}$ (%)	ω_{act} (%)	$\omega_{required}$ (b) (%)	ω_0 (c) (%)	$\omega_0 - \omega_{required}$ (%)	ω_{lime} (d) (%)	$\omega_{lime} - \omega_{required}$ (%)
L4 (a)	14.2	-	14.2	23.2	9.0	18.8	4.6
C5	14.5	-	14.5	15.3	0.8	-	-
FA20b (a)	13.0	-	13.0	19.5	6.5	14.7	1.7
FA20a	13.0	3.9	9.1	10.5	1.4	-	-
FA20CS (a)	13.4	7.0	6.4	10.2	3.8	8.0	1.6

(a) Segments submitted to a preliminary lime treatment
(b) Water content required *in situ* considering the values obtained in the Proctor tests and water to be included in the activators
(c) (d) Water content *in situ* before and after the lime treatment

All segments were constructed using conventional equipment, commonly used to stabilise soil with cement or lime. Sections L4 and C5 were constructed with the following sequence:

- Spreading of the dry binder, namely 5 % cement and 1 % quicklime (Figure 58). Only 1 % lime was added at this stage, since 3 % were already applied in the last 24h (to reduce the original water content of the soil).
- Mixture of the soil and dry binder, up to a depth of 20 cm, using the soil mixer.
- Since the water content was either similar (for the C5) or higher (4.6 %, for the L4) than required, no water was added prior to compaction.
- The compaction started with a one-way passage of a metal drum road compactor (with vibration) (Figure 59 (a)), followed by a pneumatic tyre roller (Figure 59 (b)). A motor grader was then used for surface profile correction (Figure 60). Finally, several passages of the roller compactor (this time,

without vibration) were carried out, until the compaction degree (measured with a nuclear density gauge, in different points of the segment surface) remained constant after 2 consecutive passages.

Figure 58. Spreading of the cement (a) and lime (b)

Figure 59. Compaction with a road smooth roller drum compactor (a) followed by a pneumatic tyre roller (b)

6. APPLICATION OF ALKALI-ACTIVATED INDUSTRIAL WASTES FOR THE STABILISATION OF A FULL-SCALE (SUB)BASE LAYER

Figure 60. Surface profile correction

Prior the construction of segments FA20a, FA20b and FA20CS, it was necessary to calibrate the FA flow per square meter. The segments stabilised with alkali-activated cements were constructed with the following sequence:

- Distribution of approximately 1/3 of the pre-determined FA weight (Figure 61 (a)), followed by a first passage of the soil mixer (a thickness of 20 cm was targeted) (Figure 61 (b)).
- Repetition of step i.
- Manual spreading of approximately 1/2 of the pre-determined alkaline activators (Figure 62 (a)), followed by a passage of the soil mixer (a thickness of 20 cm was again targeted) (Figure 62 (b)).
- Repetition of step i.
- Repetition of step iii.
- Compaction of the soil-stabiliser mixture, following the procedure already described for the L4 and C5 segments.

Figure 61. Spreading (a) and homogenisation (b) of the fly ash

Figure 62. Manual spreading of alkaline activators (a) followed by a passage of the soil mixer (b)

Before compaction, some samples were collected to evaluate, through laboratory tests, the effect of the subsequent compaction and *in situ* curing conditions in the mechanical behaviour of the material. Table 31 summarizes the average water content and dry unit weight of each segment, measured with a nuclear density gauge. The results show that high levels of compaction were achieved, with exception of section L4, probably due to its higher water content.

Table 31. Final properties of each segment

Segment	$\omega_{Proctor}$ (%)	ω_{final} (%)	ρ_d (Mg/m³)	Degree of compaction
L4	14.2	18.3	1.58	88
C5	14.5	13.6	1.80	97.7
FA20b	13.0	14.5	1.75	97.2
FA20a	13.0	10.6	1.95	100
FA20CS	13.4	1.3	1.87	100

The curing occurred without any protective coating layer, and the circulation of vehicles/machines was not allowed within the first 36 days, when the first *in situ* testing campaign took place. The option for not applying a protective coating was related with the fact that alkali activation reactions do require loss of water, unlike cement-based binders, which require hydration. The average meteorological conditions registered during this first month, obtained from the Portuguese Institute of the Sea and the Atmosphere (IPMA), are presented in Table 32. Harsher environmental conditions than those usually simulated in the laboratory were found, with low air temperatures and considerable precipitation.

Table 32. Meteorological conditions according to the IPM

Parameter			Value
Temperature (°C)	min.	absolute	2.7
		average	8.1
	max.	absolute	20.6
		average	16.7
Relative humidity (%)	min.		60
	max.		84
Total precipitation (mm)			59

6.2.3 *In situ* testing

The experimental campaign included quality control tests (FWD, plate load and UCS), after curing periods of 36 and 90 days. Due to the different levels of soil deformation induced by each of these tests, the deformability modulus (*E*) obtained were not directly comparable.

The FWD tests were carried out according to ASTM D 4694, 2009, also in the original soil, before stabilisation. The circular plate for load transmission had a diameter of 30 cm, and a distance between tested points of 2 m was adopted, to obtain a representative number of results in each segment. Deflections were measured at the centre of the load plate, and at distances from the centre of 300, 450, 600, 900, 1,200, 1,500, 1,800 and 2,100 mm. The deformability modulus was obtained from the deflection results. For each section, a set of deflection results close to the characteristic values (corresponding to the 85th percentile), was selected. Next, the E values were iteratively changed until the calculated deflections best matched the measured values. The model used for this inverse analysis is composed by an improved layer, with a thickness of 20 cm, over the subgrade soil and a more rigid substrate at a variable depth, with an initial reference of 2 m (which was also adjusted when necessary to obtain a better fit between the calculated and the measured deflections). Poisson coefficients of 0.4 and 0.3 were adopted for the subgrade soil and for the remaining layers, respectively.

The plate load tests were carried out in all segments according to NF (2000), in two different places, using a plate with a diameter of 30 cm.

The UCS laboratory tests were performed according to (ASTM D 1633, 2000), using samples extracted *in situ* as well as samples prepared in the laboratory, using the soil-stabilised mixture fabricated during the construction of the stabilised layer. These samples were built using static compaction and kept in a humid chamber at a constant temperature and humidity of 20°C ± 1°C and 95 %, respectively. The field specimens had a height of 200 mm (approximately) and a diameter of 100 mm, while the laboratory compacted specimens had a height of 140 mm and diameter of 70 mm (rate height/diameter of 2). The general view of some of the samples extracted from segments FA20a and FA20CS is presented in Figure 63. The FA20CS samples did not have the required height to comply with the height:diameter ratio of 2:1 due to the large size of some of the aggregates,

not present in the initial sampling and particle size distribution tests, but later found in the soil of this particular segment.

For reproducibility reasons, for each mixture and curing time, the UCS result is the average of three tested specimens. The tests were carried out under monotonic displacement control, at a rate of 6 μm/s and 3 μm/s, on the laboratory compacted and extracted specimens, respectively. Due to the variations of diameter sizes, different loading rates were used in order to apply similar strain rates to both sets of specimens.

Figure 63. Samples collected from segments FA20a (a) and FA20CS (b)

6.3 Results and discussion

The results of the mechanical tests (Chapter 6.3.1), financial analyses (Chapter 6.3.2) and environmental impact through equivalent CO_2 emissions (Chapter 6.3.3) are presented and discussed below.

6.3.1 Mechanical properties

The dynamic deformability modulus (E_d) values, as derived from the inverse analysis of the raw FWD data, are shown in Figure 64. The original soil presented very similar E_d values, around 73MPa, for all sections. Segments L4 and FA20CS revealed a very limited evolution of the E_d with curing time. This fact can be related to the high-water content (4.6 % above the optimum) on the L4 segment; and with the presence of very large aggregate

particles, observed during the construction of segment FA20CS, which might have hindered a proper homogenisation between the soil and the stabiliser.

After 36 days, the best performing segments were the FA20a and FA20b, with E_d values 3x and 2x higher than the $E_{d,C5}$, respectively. A direct comparison of the FA20a and FA20b results highlights the positive effect, in terms of stiffness, of the addition of Na_2SiO_3, which produced a 25 % increase in the E_d.

Between 36 and 90 days, an unexpected stiffness reduction was observed in segments FA20a and FA20CS. This may be due to the fact that the full-scale trial was built in an area where heavy-vehicle circulate regularly. That area was closed to traffic during the first 36 days but, for operational reasons, had to be reopened after that period, which might have influenced the evolution of the reactions. The segments C5 and FA20b presented a stiffness increase in the same period.

After 36 and 90 days, the FA-based segments FA20a and FA20b presented a significantly higher stiffness ($E_{d,FA20a}$ = 1,320 MPa and $E_{d,FA20b}$ = 1,400 MPa) than that showed by the cement-based segment ($E_{d,C5}$ = 1,000 MPa), which is relevant, considering that cement is currently the main option, worldwide, in terms of binders for soil stabilisation.

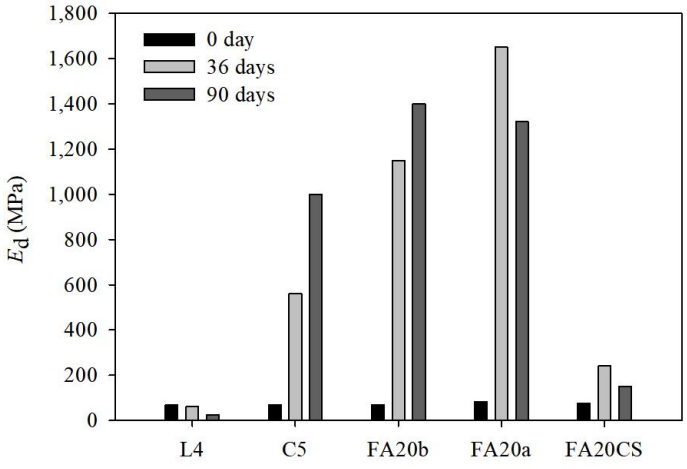

Figure 64. Dynamic deformability modulus (E_d) obtained from the FWD tests

The average results of the static deformability modulus, obtained in the second load cycle (E_{v2}) of the plate load tests are shown in Figure 65, with the respective standard deviation values. In trend with the FWD results, the lowest E_{v2} values were observed in segments L4 and FA20CS. For the remaining segments, the most relevant observation is the fact that, contrary to what was registered during the FWD tests, the C5 showed the highest EV2 (approximately 2.3 and 2.9 times higher than the average 36-day values observed for sections FA20a and FA20b, respectively), after both 36 and 90 days. However, it is relevant to point out the high variability associated with the $E_{v2,C5}$. Similarly to what was observed in the FWD tests, the E_{v2} values obtained for segment FA20a were higher than those obtained for the FA20b, again suggesting that the addition of Na_2SiO_3 has a significant impact in stiffness at short term.

In general, there was a stiffness increase with curing time, most certainly due to the development of the cementitious gels. However, the FA20CS segment showed an E_{v2} decrease of approximately 14 %, between 36 and 90 days, which is in accordance with the FWD results.

Between the 36th and the 90th day, the highest stiffness increase was observed in segment FA20b (≈160 %), followed by segments FA20a (≈28 %) and C5 (≈12 %). At 90 days, the highest E_{v2} was still obtained in segment C5, even though the stiffness increase in this period was modest, reflecting the typical behaviour of cement pastes (i.e. rapid strength/stiffness increase, stabilising after 28 days). This segment presented an average stiffness approximately 26 % higher than segment FA20b, where the activator solution was composed only by NaOH. After 90 days, and contrary to what was obtained with the FWD tests, the FA20b segment showed a higher stiffness than FA20a. It is important to emphasize that the loads imposed by the vehicles/machines had probably a lower impact on the plate load results, since they were carried out on selected surfaces (less damaged), while the FWD tests were performed at regular distances throughout the segments longitudinal axis. Although these results are not directly comparable with those from the FWD tests, due to the significantly different strain levels imposed, both pointed to the conclusion that the soil layer improvement process was more effective in segments C5, FA20b and FA20a.

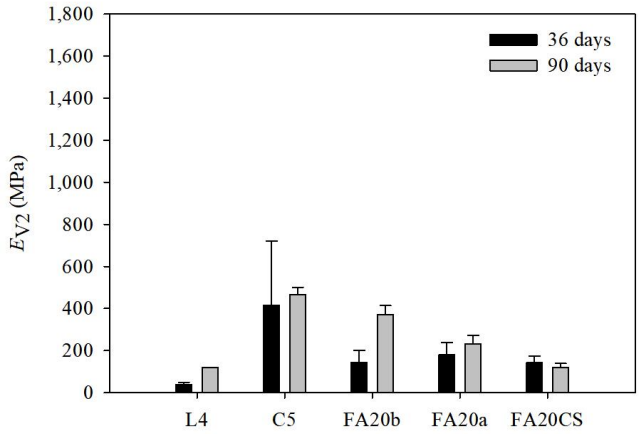

Figure 65- Static deformability modulus (E_{v2}) obtained from the plate load test

Figure 66 shows the uniaxial compressive strength results and corresponding secant deformability modulus (E_{sec}), at ε_a = 0.5 %, obtained for the specimens recovered from the field and for the specimens fabricated in the laboratory, after 36 days curing. The low standard deviation values highlight the consistency of the results obtained for all mixtures, clearly showing that the *in situ* compaction and curing conditions had, as expected, a significant influence on the overall behaviour of the composites tested. The in situ / laboratory strength ratio was found to be between 24 % and 44 %, while the stiffness ratio was even more detrimental for the *in situ* specimens (between 16 % and 44 %). The lowest ratios were observed for the mixture FA20a, suggesting a higher susceptibility to factors such as temperature, humidity, precipitation, compaction and heavy vehicle traffic.

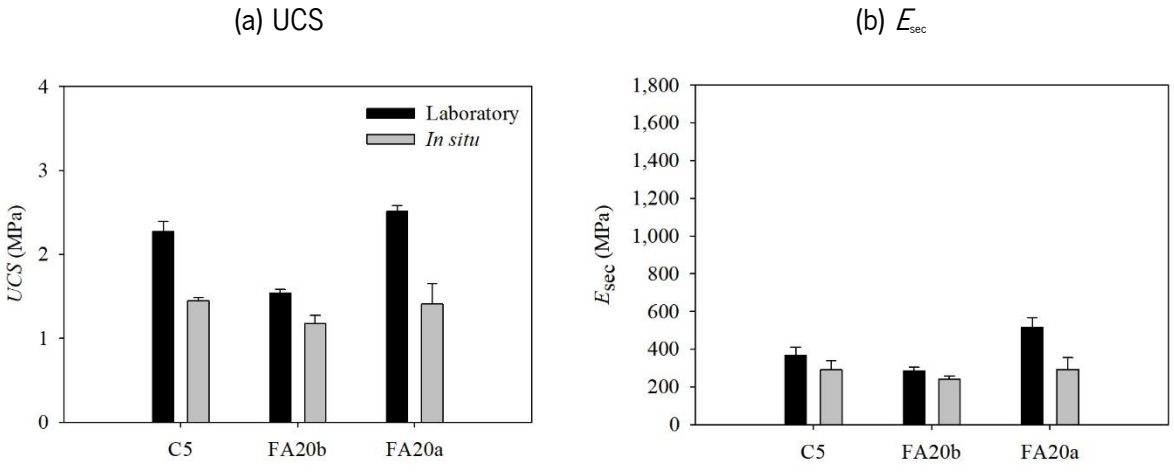

Figure 66. Laboratory and field results after 36 days: UCS (a) and E_{sec} (εa = 0.5 %) (b)

Regarding the field results, after 36 days, the mechanical properties of mixtures C5 and FA20a are similar, and higher than mixture FA20b. In agreement with the results obtained in the FWD and plate load tests, the addition of Na_2SiO_3 (FA20a) produced an increase in strength and stiffness, when compared with FA20b. Segment FA20a showed a greater difference between the laboratory and *in situ* results, which may suggest that this mixture is more dependent of the variability of the *in situ* curing conditions.

Although it was not possible to extract field specimens from segments L4 and FA20CS due to the high water content observed *in situ* and the large size of aggregates, respectively, the laboratory-prepared specimens showed UCS and stiffness results of 0.69 MPa / 2.37 MPa and 52 MPa / 322 MPa, respectively. The laboratory results obtained with mixture FA20CS are very close to those obtained with mixture C5 (the best performing mixture after 36 days), which emphasises the potential of the CS (an industrial waste) as an alkaline activator.

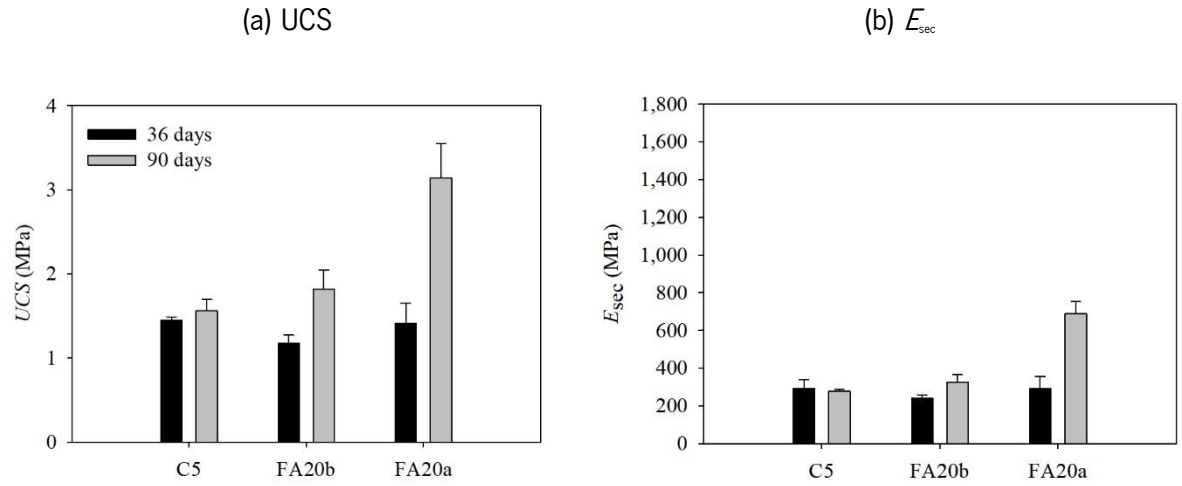

Figure 67. Field results after 36 and days: UCS (a) and E_{sec} (ε_a = 0.5%) (b)

Between the 36th and the 90th day (Figure 67), the highest increments in mechanical properties were observed for mixtures FA20b (54 % for UCS and 36 % for E_{sec}) and FA20a (123 % for UCS and 135 % for E_{sec}). The improvement of the mechanical properties shown by mixture FA20a underlines the impact of using also Na_2SiO_3 as an activator. After 90 days, both UCS and E_{sec} were almost double the corresponding values obtained for the remaining mixtures. On the other hand, C5 properties remained practically constant during the same period,

which is certainly related to the fact that cement hydration reactions mostly occur during the first 28 days. After 90 days, mixture FA20a exhibited a stiffness 2.5x and 1.7x higher than mixture C5 and FA20b, respectively.

6.3.2 Financial analysis

The financial cost of both the raw materials (prices currently charged in Portugal) and construction work, estimated for each segment, are presented in Table 33 and Figure 68, respectively. Both the average cost at the retailer and the corresponding transportation were considered in the financial analyses. Since the FA and CS are wastes, their retailer cost was considered null. Concerning transportation, some simplifications were adopted, namely:

- A rigid type vehicle was considered, with a mass greater than 17 Mg, and with an allowable transportation mass of 7.5 Mg per trip.
- Each material was transported separately, with the exception of the NaOH and the Na_2SiO_3, used for the construction of segment FA20a, since both are supplied by the same company.
- Due to the difficulty in establishing precise distances for the transport of each material (mainly due to the possibility of using different suppliers), a single value was adopted for this parameter, i.e. it was considered that all materials were transported from the same distance. i.e., 200 km. Taking this into account, a cost of 13 €/Mg was assumed for material transportation.

Labour and equipment costs were assumed equal for every segment, since it was observed that construction productivity was very similar, regardless of the stabiliser. Therefore, these costs were not included in the analysis.

Results show that the two segments built with traditional binders (L4 and C5) are the most economical options. The construction costs of segments FA20b and FA20a were significantly higher than C5 (7x and 9x, respectively). Such differences are mainly related to (i) the higher commercial cost of the NaOH and Na_2SiO_3, in comparison to cement or lime; (ii) the higher activator volumes, which influenced the transportation costs. The AAC formulations should thus become more competitive, in terms of financial cost, either by reducing the volumes

used or by replacing them with cheaper or costless alternatives, like the CS, which significantly reduced the construction costs for segment FA20CS, in line with those of the segments built with the traditional binders.

Table 33. Unit price of the raw materials

Material	Average retailer price (€/kg) (without shipping costs)
Quicklime (powder)	0.06
Cement (powder)	0.09
NaOH (pellets)	0.64
Na_2SiO_3 (solution)	0.39
CS	Free
Fly ash	Free

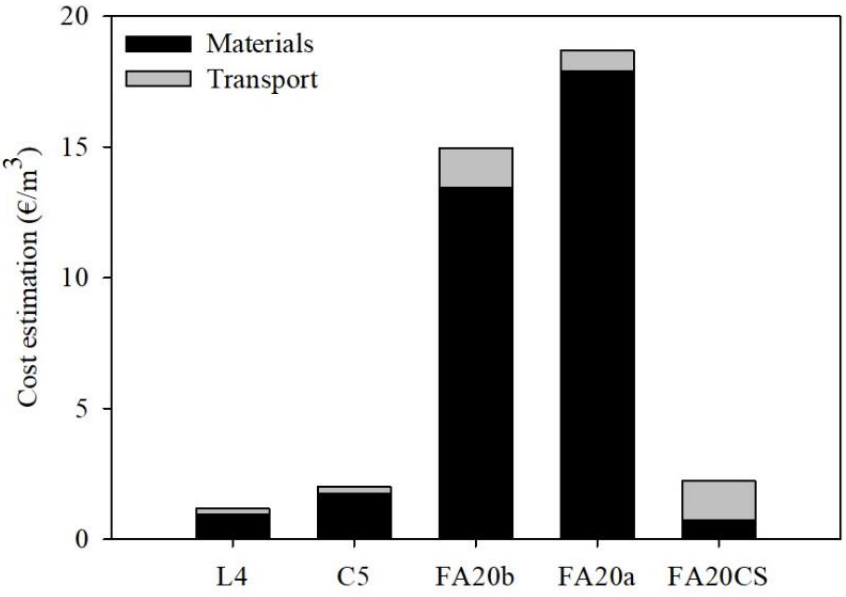

Figure 68. Construction cost estimate (€/m³)

6.3.3 Environmental analyses through equivalent CO_2 emissions

The equivalent CO_2 emissions (CO_2e) resulting from the manufacture of the raw materials and their transportation to the site was estimated using the EFFC DFI Carbon Calculator Tool (v2.0) (Lemaignan and Wilmotte, 2013),

developed by the European Federation of Foundation Contractors (EFFC) and Deep Foundations Institute (DFI). This very useful tool is organised in three main groups: deep foundations, retaining structures and soil improvement (Cristelo et al., 2015). It combines the activity production quantities A_i (tons of steel, tons.km of freight, kWh of natural gas, etc) and the corresponding emission factor EF_i (gCO_2eq/tons of steel, gCO_2eq/tons.km of freight, gCO_2eq/kWh of natural gas, gCO_2eq/etc). The latter is obtained from a combination of several national and international databases available in Europe, which rendered a very effective method to assess environmental performance of geotechnical works.

Table 34 presents the CO_2 emission factors considered for each emission source. Two sources, associated with equipment (e.g., fuel consumption) and labour (e.g., transport of workers) are presented but were not considered in the calculations, since their emission values would be identical among the different alternatives being studied. The remaining two factors considered for the estimation of the CO_2e emissions were the type and volume of material. The CO_2e emissions associated with the use of CS and FA were assumed null, since the carbon footprint associated with its production must be attributed to their original applications. Regarding the CO_2e emissions resulting from the transportation, the same assumptions adopted in the financial analysis were considered. Since the selected vehicle allows a maximum mass of 7.5 Mg, each type of material was transported to the site in one single trip, meaning that the CO2e emissions related with transportation were fundamentally influenced by the number of different materials applied in each segment. The exception occurred for the materials used in section FA20a, where the transportation of NaOH and $Na_2SiO_3$was considered in the same trip, as previously mentioned. An estimate of the CO2e emissions for each section is shown in Figure 69.

Table 34. Emission factor for each source

Source	EF_i (kgCO2/t)
NaOH	999
Na_2SiO_3	1,096
Cement	930
Lime	903
FA	4

Results show that sections L4 and C5 have the lowest total emission values. The transport related CO_2e emissions assume a considerable percentage of the total, almost similar to the raw materials. The construction of segments FA20a and FA20b presented a total of CO_2e 100 % and 27 % higher than that of segment C5, respectively. Two factors had a considerable influence on the relatively high emissions associated with the AAC-based segments, namely: (i) the fact that the production of NaOH and Na_2SiO_3 possesses a significant *global warming potential* (GWP); (ii) the need to transport more than one component per segment (e.g. the cement-based segment required only the transportation of the cement powder). Although there are no CO_2e emissions associated with the production of FA, the environmental impact resulting from the production of the reagents, as well as their subsequent transport (although less influent) penalizes the use of these alternative binders, in terms of CO_2e emissions.

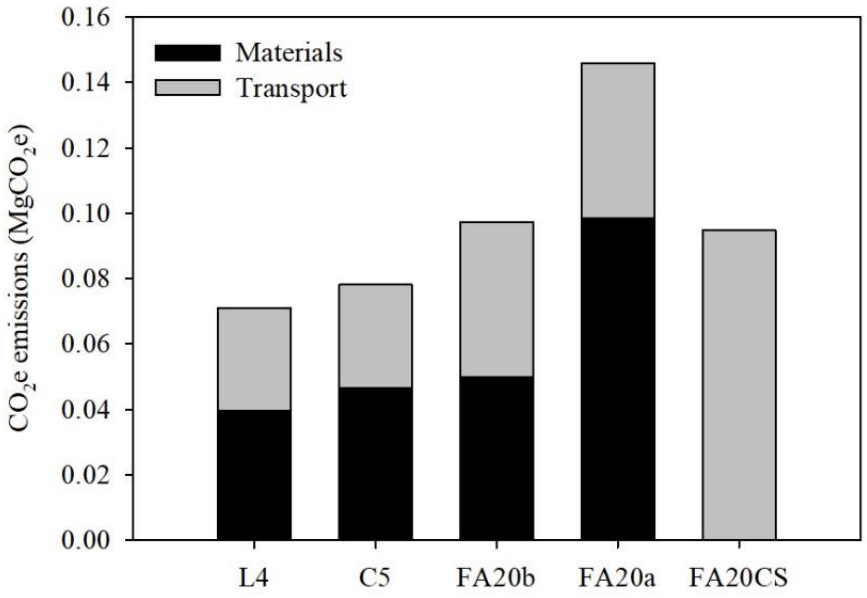

Figure 69. Estimative of CO_2e emissions

The use of a recycled material for segment FA20CS enabled a CO_2e emission which was only 18 % higher than that of segment C5, and only due to the higher volume required.

Therefore, and similarly to what was concluded in the financial analyses, the use of materials supplied by different companies, even if they are industrial by-products, without a direct CO_2 emission, strongly affects the total CO_2e emissions.

Another important aspect is the distance between the raw materials suppliers and the construction local that in this case was considered constant (200 km). The use of wastes might be feasible if the supplying company is close to the site, in order to reduce the transport-related emissions to competitive levels.

6.4 Conclusions

The viability of using different alkaline activated cements to stabilise a (sub)base layer was tested in a full-scale trial. A total area of 80 m long and 2.5 m wide was divided in five segments, three of them improved with FA and different activators and the remaining two with cement or lime (for comparison purposes). Quality control tests after 36 and 90 days upon construction, environmental impact and financial analyses were carried out.

- The use of AAC is feasible through the use of conventional equipment and procedures, similar to those used with traditional binders (e.g., cement, lime).
- The use of a higher number of components, and individual volumes of each, to fabricate the AAC, increased the overall logistic complexity.
- The use of liquid activators has a significant impact on the control of water content, therefore applying solid activators would be of great benefit for the optimization of the application procedure.
- The quality control tests showed that mixtures FA20a and FA20b exhibited strength and stiffness values similar, or even higher, than mixture C5.
- The water content and the large size of the aggregates, respectively in sections L4 and FA20CS, compromised the *in situ* mechanical performance of these mixtures. However, UCS results obtained in laboratory compacted specimens of mixture FA20CS showed that this approach can lead to interesting results if further optimised.

- After 36 days, the effect of the addition of Na_2SiO_3 in the mechanical properties of section FA20a was clear. At 90 days, this was not so clear, making the positive long-term effect of the addition of Na_2SiO_3 arguable.
- Concerning the cost and environmental impact analyses, results showed that an optimization of the alkaline binder formulations is required. This optimization should focus in the reduction of the used quantity of NaOH and/or Na_2SiO_3, or even by replacing them for a cheaper material or by other waste with no commercial cost, preferably in a solid form. The production of NaOH and/or Na_2SiO_3 jointly with the transportation generate significant CO_2e emissions that should be strongly reduced.
- Although it was not possible to evaluate the *in situ* performance of mixture FA20CS, when compared with the alternative approaches tested in this study, it is the most viable financial and environmental solution.

7. CONCLUSIONS, CONTRIBUTIONS AND FUTURE WORK

This Chapter summarises the main conclusions and contributions of the research and the recommendations for future work.

7.1 Conclusions and main contributions

The main aims of this PhD thesis were to understand the short- and long-term experimental shear behaviour of soils stabilised with AABs, more precisely the stress-strain response, stiffness degradation with strain, pore pressure and volumetric strain variations and stress-path, and the prediction of the stress-strain response for these materials using constitutive models. To accomplish the aims, consolidated undrained and drained triaxial tests were performed in two reconstituted clayey soils before and after adding the AAB at 28 and 90 days for a wide range of OCRs and p'_0. The used AAB binder was constituted by two parts of blast furnace slags and one part of NaOH. The same binder composition was added to both soils but with a distinct dosage. The binder dosage was modified based on the initial water content of the soils. One-dimensional consolidation and isotropic compression tests were performed to complement the triaxial test results. To get a global perception of the effect of adding AAB to the soils in terms of microstructure and environmental impact, SEM-EDS, XRD and leachate analyses were performed at both curing ages before and after stabilisation. The results were then used to calibrate a complex existent kinematic hardening model to predict the experimental stress-strain behaviour of both reconstituted and stabilised clayey soils at 28 and 90 curing days. A summary of the key findings and conclusions is given below.

- The **SEM-EDS** and **XRD analyses** suggested the formation of N, C-A-S-H type gel in both stabilised clayey soils at 28 and 90 curing days, with Ca/Si ratio significantly lower than what is usually found in C-S-H systems. This difference is explained by the incorporation of extra Al, as a consequence of the addition of secondary materials (in this case, blast furnace slag). It was also a consequence of the high silicon content resulting from the amorphous phase of the precursor.
- The **oedometer** and **isotropic compression tests** showed, after adding AAB, a significant reduction of both virgin compression and recompression indexes or the slopes of normal compression and swelling lines in both soils, and this reduction increased with the curing age. The addition of the AAB in both soils also led to a significant increase in the yield stress or pre-consolidation stress that increased with the curing time. According to Horpibulsuk et al., 2010, the swelling index in clays stabilised with Portland cement generally reduces compared to its natural structured or reconstituted states, but the virgin compression index often increases due to the rapid

breakdown of cementitious bonds after failure at higher stresses. The increase of the yield stress or pre-consolidation stress is common in clays stabilised with Portland Cement. The use of higher axial stresses could result in a more well-defined linear virgin compression zone.

- The **drained triaxial tests** carried out on the stabilised sandy lean clay specimens with the AAB showed a behaviour reminiscent of cement-clay mixtures, with peak/residual strength and dilatation, increased normalised strength/stiffness and normalised tendency for dilatation. The total peak/residual shear strength remained practically constant at 28 and 90 curing days. For the applied stress level, there was a clear increase of the peak and residual strength with the increase of p'_0.
- The **undrained triaxial tests** performed on the stabilised clay specimens with the AAB at high water content revealed some distinct features from the first tested soil. The shear behaviour of the clay drastically changed after adding the binder, with increased peak/residual shear strengths, stiffness and yield stress which reveals the potential of the alkali-activated binder even when applied to soils with high water content. For $p'_0 < p'_y$ (i.e., preyield state), the artificial cementation played a dominant role in the strength characteristics, with the stress paths located on the dry side of the critical state. The stress-strain curves are practically overlapped, with similar peak and residual shear strengths even for increasing p'_0. It is believed that artificial cementation is the main factor that controls the mechanical behaviour of stabilised clays when the state of stress is inside the state boundary surface. The change of the fabric, i.e., the reorientation of the stabilised clay particles during the consolidation was almost insignificant, and thus, the increase of p'_0 did not affect the shear strength. For $p'_0 > p'_y$ (i.e., postyield state), it is believed that both the fabric and cemented structure contributed to the strength, and the stress-path is located on the wet side of the critical state. In this case, there was a more evident rise of the peak deviatoric strength, which denotes that at this condition, both the progressive breakdown of the cementation and the change in the fabric contributes to the enhancement of the peak strength. The pore pressure variation trend showed that p'_0 had a significant impact on pore pressure generation at preyield and postyield states, with an increase of the peak of pore pressure with the increase of p'_0. Concerning the shear strength parameters, the binder not only increased the cohesion but also made the clay particles coarser increasing the friction angle.

The undrained triaxial tests performed on the reconstituted sandy lean clay specimens and clay specimens at high water content revealed a typical behaviour normally observed in these types of soils.

- The **leachate results** revealed that both stabilised soils are considered an 'inert material' and, therefore, there is virtually no risk of soil contamination when adding the AAB.
- The overall features of the stress-strain behaviour of both stabilised clayey soils with AAB were well captured by the **kinematic hardening model** for the range of p'_0 and OCR considered (i.e., the increased peak/residual strength and stiffness and the drastic reduction of the deviatoric stress after peak during softening recorded in some tests), which demonstrates the potential of the model to be applied to different materials than the natural clays for which it was initially formulated for. The behaviour of both soils on the reconstituted state was also well predicted by the model.

The opportunity to be integrated within a research project related to the application of alkali-activated industrial wastes *in situ* allowed me to be deeply involved in constructing a full-scale prototype of a (sub)base layer stabilised with alkali-activated binders and conventional binders. Big challenges arose, including the definition of a construction methodology, equipment selection, on-site handling of distinct materials, quality control techniques, among others. The *in situ* performance of the stabilised geomaterials was assessed through falling weight deflectometer tests, plate load field tests and unconfined compressive strength tests after 36 and 90 days. For each layer, it was estimated the financial cost of the construction and the equivalent CO_2 emissions. The following conclusions can be drawn from this research project:

- The ***in situ* application of AABs is feasible** through the use of conventional equipment and procedures, similar to those used with traditional binders (e.g., Portland cement, lime). However, the use of a higher number and volume of components to produce the AABs together with liquid activators increased the overall logistic complexity.
- The **quality control tests** showed that the AABs constituted by FA activated with NaOH and/or Na_2SiO_3 exhibited strength and stiffness values similar, or even higher, than the layer stabilised with Portland cement. Also, the AAB entirely constituted by wastes revealed interesting results if further optimised.
- The **cost** and **environmental impact analyses** showed that an optimization of the AAB formulations is required. This optimization should focus on the reduction of commercial activators used (both in

number and volume), on the replacement of the activators by cheaper materials or even by solid wastes with no commercial cost.

In sum, some of the most innovative contributions of this thesis are:

- Characterisation of the short- and long-term shear behaviour of two clayey soils stabilised with the AAB under undrained and drained conditions using BE and local instrumentation for a wide range of OCRs and p'_0. The published studies in this field are scarce, and the overall triaxial test results point to a similar behaviour to the clays stabilised with Portland cement. This finding suggests that, for instance, constitutive models, initially developed for stabilised clays with Portland cement, could be applied in clayey soils stabilised with AABs.
- The use of an advanced constitutive model to predict the stress-strain behaviour of soils stabilised with this type of binder. The model selected was the complex kinematic hardening model proposed by Rouainia and Muir Wood, 2000 for natural clays, which had not been used in artificially cemented soils. The good predictions of this model underlined its capacity to be applied in both naturally structured and artificially cemented structured clayey soils.
- The stabilisation of a full scale (sub)base layer using alkali-activated industrial wastes allowed to validate the viability of using the AABs in real scale and the performance *in situ* of these mixtures. An optimization of the AAB formulations is necessary in order to become more attractive, from the environmental impact and financial cost point of views, to use these AABs for practical purposes. The use of fewer materials in the AAB formulations and solid waste activators are some ways to optimize the AABs.

7.2 Further research

The step forward given in this PhD thesis was the characterisation of the shear behaviour of clayey soils stabilised with an AAB and the use of experimental results to predict the stress-strain response of these improved geomaterials using a kinematic hardening constitutive model. In the field of the AABs, the shear behaviour of geomaterials stabilised with AABs is little known and, studies where constitutive models are

employed to predict the shear behaviour, practically inexistent. The subjects that need further development are referred to next.

- **Regarding the characterisation of the shear behaviour of soft soils stabilised with AABs and numerical modelling:**

  An important improvement to the experimental work carried out in this thesis should be the application of higher stress levels on the stabilised specimens during oedometer and isotropic compression tests in order to obtain a more well-defined linear virgin compression zone. A well-defined virgin compression zone allows to define, with more precision, the yield stress point or pre-consolidation stress and characterise the preyield and postyield states on the triaxial tests. In this PhD thesis, it was not possible to apply higher stress levels due to equipment limitations.

  Another important improvement is regarding the use of BE to characterise the stiffness degradation from small to large strains levels. Considering the potential of the kinematic hardening model used in this PhD thesis, these experimental results would be useful to model the degradation of the stiffness of clayey soils stabilised with AABs from small to large strain levels using the same model.

  The replacement of the hall effect transducers by other more efficient methods to measure local strains and easier to install on the surface of the specimens. The use of three LVDT local strain gauges, two for the measurement of axial strains and one for radial strains, could be a replacement option. This equipment is currently available at the laboratory of the University of Minho, Portugal.

  Another interesting complement to this research could be the stabilisation of a clayey soil using increasing amounts of GGBS-NaOH and the characterisation of the mechanical behaviour of this material through triaxial tests and oedometer or isotropic compression tests. The impact of increased binder contents on the stiffness degradation curves from small to large strain levels, stress-strain behaviour, pore pressure curves and stress paths, together with the yield stress evolution, are interesting features that could be investigated. Also, these results could be used to calibrate the kinematic hardening model proposed by Rouainia and Muir Wood, 2000.

- **Regarding to the AAB development:**

Some developments could be undertaken in this field. Although the use of a high number and volume of precursor and activators materials in soil stabilisation is relatively easy at the laboratory scale, the application of these materials *in situ* is more complicated, mainly when compared with Portland Cement. The use of commercial activators (e.g., NaOH and/or Na_2SiO_3) in liquid phase is also difficult *in situ* and become the financial cost of these AABs less attractive. In this context, it is increasingly important the development of AAB binders at laboratory scale thinking on its application *in situ*, apart from the mechanical performance. The development of AAB formulations using 100% waste materials is another relevant contribution in this field.

References

AASHTO M 145, 1991. Standard Specification for Classification of Soils and Soil-Aggregate Mixtures for Highway Construction Purposes, American Association of State Highway Transportation Official. 1-10. https://doi.org/10.1520/D3282-09

AASHTO M 145-91, 2017. Standard Specification for Classification of Soils and Soil-Aggregate Mixtures for Highway Construction Purposes. Stand. by Am. Assoc. State Highw. Transp. Off.

Abdeldjouad, L., Asadi, A., Ball, R.J., Nahazanan, H., Huat, B.B.K., 2019. Application of alkali-activated palm oil fuel ash reinforced with glass fibers in soil stabilization. Soils Found. 59, 1552–1561. https://doi.org/10.1016/j.sandf.2019.07.008

Abdeldjouad, L., Asadi, A., Nahazanan, H., Huat, B., Dheyab, W., Elkhebu, A., 2019. Effect of Clay Content on Soil Stabilization with Alkaline Activation. Int. J. Geosynth. Gr. Eng. 5, 4. https://doi.org/10.1007/s40891-019-0157-y

Abdullah, H.H., Shahin, M.A., Walske, M.L., 2020. Review of Fly-Ash-Based Geopolymers for Soil Stabilisation with Special Reference to Clay. Geosciences 10, 249. https://doi.org/10.3390/geosciences10070249

Abdullah, H.H., Shahin, M.A., Walske, M.L., 2019. Geo-mechanical behavior of clay soils stabilized at ambient temperature with fly-ash geopolymer-incorporated granulated slag. Soils Found. 59, 1906–1920. https://doi.org/10.1016/j.sandf.2019.08.005

Adesina, A., 2020. Recent advances in the concrete industry to reduce its carbon dioxide emissions. Environ. Challenges 1, 100004. https://doi.org/10.1016/j.envc.2020.100004

AFNOR (Association Française de Normalisation), 2000. NF P 94-117-1 Soils: investigation and testing - Formation level bearing capacity - Part 1: Plate test static deformation module (EV2) (in French).

Ahnberg, H., 2007. On yield stresses and the influence of curing stresses on stress paths and strength measured in triaxial testing of stabilized soils. Can. Geotech. J. 44, 54–66. https://doi.org/10.1139/t06-096

Al-Rkaby, A.H.J., 2019. Evaluating shear strength of sand-GGBFS based geopolymer composite material. Acta Polytech. 59, 305–311. https://doi.org/10.14311/AP.2019.59.0305

Al-Tabbaa, A., Wood, D.M., 1989. An experimentally based `bubble' model for clay, in: Pietruszczak, S., Pande, G.N. (Eds.), International Symposium on Numerical Models in Geomechanics. Elsevier Applied Science Publishers, Canada, pp. 91–99.

Alam, S., Das, S.K., Rao, B.H., 2019. Strength and durability characteristic of alkali activated GGBS stabilized red mud as geo-material. Constr. Build. Mater. 211, 932-942. https://doi.org/10.1016/j.conbuildmat.2019.03.261

Altschaeffl, A.G., Thevanayagam, S., 1991. Characterization of clay fabric. In Microstructure of Fine-grained Sediments. Springer, New York, NY. https://doi.org/10.1007/978-1-4612-4428-8_31

Amer, I., Kohail, M., El-Feky, M.S., Rashad, A., Khalaf, M.A., 2021. A review on alkali-activated slag concrete. Ain Shams Eng. J. https://doi.org/10.1016/j.asej.2020.12.003

Andrew, R.M., 2018. Global CO2 emissions from cement production. Earth Syst. Sci. Data 10, 195. https://doi.org/10.5194/essd-10-195-2018

Araújo, N., Corrêa-Silva, M., Miranda, T., Gomes, A.T., Castro, F., Teixeira, T., Cristelo, N., 2020. Unsaturated Response of Clayey Soils Stabilised with Alkaline Cements. Molecules 25, 2533. https://doi.org/10.3390/molecules25112533

Asghari, E., Toll, D.G., Haeri, M., 2003. Triaxial behaviour of a cemented gravely sand, Tehran alluvium. Geotech. Geol. Eng. 21, 1–28.

ASTM C 618, 2012. Standard specification for coal fly ash and raw or calcined natural pozzolan for use in concrete, West Conshohocken, PA. 1-5. https://doi.org/10.1520/C0618-12A

ASTM D 1632, 2007. Standard Practice for Making and curing soil-cement compression and flexure test specimens in the laboratory. West Conshohocken.

ASTM D 1633, 2000. Standard Test Methods for Compressive Strength of Molded Soil-Cement Cylinders 1, West Conshohocken, PA. 1-4. https://doi.org/10.1520/D1633-00

ASTM D 2166 / D 2166M, 2013. Standard Test Method for Unconfined Compressive Strength of Cohesive

Soil, West Conshohocken, PA. 1-7. https://doi.org/10.1520/D2166_D2166M-13

ASTM D 2487, 2011. Standard Practice for Classification of Soils for Engineering Purposes (Unified Soil Classification System), West Conshohocken, PA. 1-12. https://doi.org/10.1520/D2487-11.

ASTM D 4694, 2009. Standard Test Method for Deflections with a Falling-Weight-Type Impulse Load Device, West Conshohocken, PA. 1-3. https://doi.org/10.1520/D4694-09

Atkinson, J.., Sallfors, G., 1991. Experimental determination of soil properties, in: Proceedings of the 10th ECSMFE. Florence, pp. 915–956.

Atkinson, J.H., Richardson, D., Stallebrass, S.E., 1990. Effect of recent stress history on the stiffness of overconsolidated soil. Géotechnique 40, 531–540. https://doi.org/10.1680/geot.1990.40.4.531

Balasubramaniam, A.S., 1975. Stress-Strain Behaviour of a Saturated Clay for States Below the State Boundary Surface. Soils Found. 15, 13–25.

Balasubramaniam, A.S., 1973. Stress history effects on stress-strain behaviour of a saturated clay. Geotech. Eng. 4, 91–111.

Bensaifi, E., Bouteldja, F., Nouaouria, M.S., Breul, P., 2019. Influence of crushed granulated blast furnace slag and calcined eggshell waste on mechanical properties of a compacted marl. Transp. Geotech. 100244.

Bernal, S.A., Rodríguez, E.D., Gutiérrez, R.M. de, Gordillo, M., Provis, J.L., 2011. Mechanical and thermal characterisation of geopolymers based on silicate-activated metakaolin/slag blends. J. Mater. Sci. 46, 5477–5486. https://doi.org/10.1007/s10853-011-5490-z

Bhatt, A., Priyadarshini, S., Mohanakrishnan, A.A., Abri, A., Sattler, M., Techapaphawit, S., 2019. Physical, chemical, and geotechnical properties of coal fly ash: A global review. Case Stud. Constr. Mater. 11, e00263. https://doi.org/10.1016/j.cscm.2019.e00263

Bian, X., Cao, Y.-P., Wang, Z.-F., Ding, G.-Q., Lei, G.-H., 2017. Effect of Super-Absorbent Polymer on the Undrained Shear Behavior of Cemented Dredged Clay with High Water Content. J. Mater. Civ. Eng. 29, 4017023. https://doi.org/10.1061/(ASCE)MT.1943-5533.0001849

Borja, R., 1991. Cam–Clay plasticity, Part II: Implicit integration of constitutive equation based on a nonlinear

elastic stress predictor. Comp Methods Appl Mech Eng 88, 225–240.

British Petroleum, 2018. BP Energy Outlook: 2018 Edition [WWW Document]. URL https://www.bp.com/content/dam/bp/en/corporate/pdf/energy-economics/energy-outlook/bp-energy-outlook-2018.pdf (accessed 3.30.21).

Brykov, A.S., Korneev, V.I., 2008. Production and usage of powdered alkali metal silicate hydrates. Metallurgist 52, 648–652. https://doi.org/10.1007/s11015-009-9108-5

BS 1377 2, 1990. Methods of test for soils for civil engineering purposes-Part 2: Classification tests. British Standard Institution. London, UK.

BS 1377 4, 1990. Method of Test for Soils for Civil Engineering Purposes – Part 4: Compaction-related tests, British Standard Institution. London, UK.

BS 1377 5, 1990. Method of Test for Soils for Civil Engineering Purposes – Part 5: Compressibility, permeability and durability tests, British Standard Institution. London, UK.

BS 1377 8, 1990. Methods of test for soils for civil engineering purposes– Part 8: Shear strength tests (effective stress), British Standard Institution. London, UK.

BSI, 2015. Code of practice for ground investigations. British standard BS, 5930, pp.2015-British.

Canakci, H., Güllü, H., Alhashemy, A., 2019. Performances of using geopolymers made with various stabilizers for deep mixing. Materials. 12, 2542. https://doi.org/10.3390/ma12162542

Casagrande, A., 1932. The structure of clay and its importance in foundation engineering. Bost. Soc. Civ. Eng. J.

Cement and Concrete Institute, 2011. Sustainable concrete [WWW Document]. URL http://www.cnci.org.za (accessed 3.30.21).

Charlton, T.S., Rouainia, M., 2021. Cyclic performance of a monopile in spatially variable clay using an advanced constitutive model. Soil Dyn. Earthq. Eng. 140, 106437. https://doi.org/10.1016/j.soildyn.2020.106437

Chibowski, E., 2011. Flocculation and Dispersion Phenomena in Soils, in: Gliński, J., Horabik, J., Lipiec, J.

(Eds.), Encyclopedia of Agrophysics. Springer, Dordrecht, pp. 301–304. https://doi.org/10.1007/978-90-481-3585-1_59

Chowdary, V.B., Ramanamurty, V., Pillai, R.J., 2021. Experimental evaluation of strength and durability characteristics of geopolymer stabilised soft soil for deep mixing applications. Innov. Infrastruct. Solut. 6, 1–10. https://doi.org/10.1007/s41062-020-00407-7

Civan, F., 2007. Reservoir formation damage: fundamentals, modeling, assessment, and mitigation, 2nd ed. Gulf Professional.

Consoli, N.C., Festugato, M. da S.C.L., Leon, H.B., Tomasi, L.F., Heineck, K.S., 2020. Ground Waste Glass–Carbide Lime as a Sustainable Binder Stabilising Three Different Silica Sands. Géotechnique 1–41. https://doi.org/10.1680/jgeot.18.P.099

Corrêa-Silva, M., Araújo, N., Cristelo, N., Miranda, T., Gomes, A.T., Coelho, J., 2019. Improvement of a clayey soil with alkali activated low-calcium fly ash for transport infrastructures applications. Road Mater. Pavement Des. 20, 1912–1926. https://doi.org/10.1080/14680629.2018.1473286

Corrêa-Silva, M., Miranda, T., Araújo, N., Coelho, J., Cristelo, N., Gomes, A.T., 2018. Improvement of a clayey soil with alkali activated low-calcium fly ash for transport infrastructures applications. Road Mater. Pavement Des. https://doi.org/10.1080/14680629.2018.1473286

Corrêa-Silva, M., Miranda, T., Araújo, N., Coelho, J., Cristelo, N., Topa Gomes, A., 2017. Improvement of a clayey soil with alkaline activation of wastes, In WASTES–Solutions, Treatments and Opportunities II. 1st Edition. CRC Press. London. 323-329. https://doi.org/10.1201/9781315206172-52

Corrêa-Silva, M., Miranda, T., Rouainia, M., Araújo, N., Glendinning, S., Cristelo, N., 2020. Geomechanical behaviour of a soft soil stabilised with alkali-activated blast-furnace slags. J. Clean. Prod. 122017. https://doi.org/10.1016/j.jclepro.2020.122017

Correia, A.G., 2004. Soil stiffness interesting the serviceability of stuctures. Geotech. J. Port. Geotech. Soc. 100, 103–122 (in Portuguese).

Cristelo, N., Fernández-Jiménez, A., Castro, F., Fernandes, L., Tavares, P., 2019. Sustainable alkaline activation of fly ash, aluminium anodising sludge and glass powder blends with a recycled alkaline

cleaning solution. Constr. Build. Mater. 204, 609–620. https://doi.org/10.1016/j.conbuildmat.2019.01.226

Cristelo, N., Fernández-Jiménez, A., Vieira, C., Miranda, T., Palomo, Á., 2018. Stabilisation of construction and demolition waste with a high fines content using alkali activated fly ash. Constr. Build. Mater. 170, 26–39. https://doi.org/10.1016/j.conbuildmat.2018.03.057

Cristelo, N., Glendinning, S., Fernandes, L., Amândio Teixeira Pinto, 2012. Effect of calcium content on soil stabilisation with alkaline activation. Constr. Build. Mater. 29, 167–174. https://doi.org/10.1016/j.conbuildmat.2011.10.049

Cristelo, N., Glendinning, S., Jalali, S., 2009. Sub-bases layers of residual granite soil stabilised with lime. Soils and Rocks. 32(2), 83-88.

Cristelo, N., Glendinning, S., Teixeira Pinto, A., 2011. Deep soft soil improvement by alkaline activation. Proc. Inst. Civ. Eng. - Gr. Improv. 164, 73–82. https://doi.org/10.1680/grim.900032

Cristelo, N., Miranda, T., Oliveira, D. V., Rosa, I., Soares, E., Coelho, P., Fernandes, L., 2015. Assessing the production of jet mix columns using alkali activated waste based on mechanical and financial performance and CO2 (eq) emissions. J. Clean. Prod. 102, 447–460. https://doi.org/10.1016/j.jclepro.2015.04.102

Cristelo, N., Soares, E., Rosa, I., Miranda, T., Oliveira, D. V., Silva, R.A., Chaves, A., 2013. Rheological properties of alkaline activated fly ash used in jet grouting applications. Constr. Build. Mater. 48, 925-933. https://doi.org/10.1016/j.conbuildmat.2013.07.063

Dafalias, Y.., Herrmann, L.., 1982. Bounding surface formulation of soil plasticity, in: G.N. Pande, O.C. Zienkiewicz (Eds.), Soil Mechanics – Transient and Cyclic Loads, Wiley & Sons. New York, pp. 253–311.

Dafalias, Y.F., 1986. Bounding Surface Plasticity. I: Mathematical Foundation and Hypoplasticity. J. Eng. Mech. 112. https://doi.org/10.1061/(ASCE)0733-9399(1986)112:9(966)

Davidovits, J., 2013. Geopolymer Cement a review. Geopolymer Sci. Tech. Tech. Pap. 21, 1–11.

Davidovits, J., 2008. Geopolymer chemistry and applications. Institute Geopolymer. Saint Quentin, France.

De Sheeran, D., RJ, R., 1971. Preparation of homogeneous soil samples by slurry consolidation. J Mater 6(2), 356–373.

Efthymiou, S., Kavvadas, M., 2019. The Behavioural Framework of a Lightly Cemented High Plasticity Clay Under Low Effective Stresses. Geotech. Geol. Eng. 37, 4269–4283. https://doi.org/10.1007/s10706-019-00906-0

Elia, G., Rouainia, M., 2016. Investigating the cyclic behaviour of clays using a kinematic hardening soil model. Soil Dyn. Earthq. Eng. 88, 399–411. https://doi.org/10.1016/j.soildyn.2016.06.014

Elia, G., Rouainia, M., Panayides, S., 2016. Finite element modelling of a deep excavation in Boston Blue Clay. Procedia Eng. 158, 242–247. https://doi.org/10.1016/j.proeng.2016.08.436

Emmanuel, E., Paris, M., Deneele, D., 2019. Insights on the clay reactivity in alkaline media: Beyond filler role for kaolin. Appl. Clay Sci. 181, 105210. https://doi.org/10.1016/j.clay.2019.105210

EN 12457-4, 2002. Characterisation of waste-Leaching-Compliance test for leaching of granular waste materials and sludges—Part, 4: one stage batch test at a liquid to solid ratio of 10 l/kg for materials with particle size bellow 10 mm (withot or with size reduction).

EuroSoilStab, 2002. Development of design and construction methods to stabilise soft organic soils: Design guide soft soil stabilisation.

Fasihnikoutalab, M.H., Pourakbar, S., Ball, R.J., Unluer, C., Cristelo, N., 2020. Sustainable soil stabilisation with ground granulated blast-furnace slag activated by olivine and sodium hydroxide. Acta Geotech. 15, 1981–1991. https://doi.org/10.1007/s11440-019-00884-w

Fernández-Jiménez, A., Cristelo, N., Miranda, T., Palomo, Á., 2017. Sustainable alkali activated materials: Precursor and activator derived from industrial wastes. J. Clean. Prod. 162, 1200–1209. https://doi.org/10.1016/j.jclepro.2017.06.151

Fernández-Jiménez, A., de la Torre, A.G., Palomo, A., López-Olmo, G., Alonso, M.M., Aranda, M.A.., 2006. Quantitative determination of phases in the alkaline activation of fly ash. Part II: Degree of reaction. Fuel. 85, 1960-1969. https://doi.org/10.1016/j.fuel.2006.04.006

Gao, X., Yu, Q., Li, X.S., Yuan, Y., 2020. Assessing the modification efficiency of waste glass powder in

hydraulic construction materials. Constr. Build. Mater. 263, 120111. https://doi.org/10.1016/j.conbuildmat.2020.120111

Garcia-Lodeiro, I., Palomo, A., Fernández-Jiménez, A., Macphee, D.E., 2011. Compatibility studies between N-A-S-H and C-A-S-H gels. Study in the ternary diagram Na2O–CaO–Al2O3–SiO2–H2O. Cem. Concr. Res. 41, 923–931. https://doi.org/10.1016/j.cemconres.2011.05.006

Gartner, E., 2004. Industrially interesting approaches to "low-CO2" cements. Cem. Concr. Res. 34, 1489–1498. https://doi.org/10.1016/j.cemconres.2004.01.021

Geraldo, R.H., Ouellet-Plamondon, C.M., Muianga, E.A.D., Camarini, G., 2017. Alkali-activated binder containing wastes: a study with rice husk ash and red ceramic. Cerâmica 63, 44–51. https://doi.org/10.1590/0366-69132017633652057

Ghadakpour, M., Choobbasti, A.J., Kutanaei, S.S., 2020. Experimental study of impact of cement treatment on the shear behavior of loess and clay. Arab. J. Geosci. 13, 184. https://doi.org/10.1007/s12517-020-5181-7

Gharzouni, A., Ouamara, L., Sobrados, I., Rossignol, S., 2018. Alkali-activated materials from different aluminosilicate sources: Effect of aluminum and calcium availability. J. Non. Cryst. Solids 484, 14–25. https://doi.org/10.1016/j.jnoncrysol.2018.01.014

Ghassemi, M., Andersen, P.K., Ghassemi, A., Chianelli, R.R., 2004. Hazardous Waste from Fossil Fuels. Encycl. Energy 119–131. https://doi.org/10.1016/B0-12-176480-X/00395-8

González, N.A., Gens Solé, A., Arroyo Alvarez de Toledo, M., Rouainia, M., 2011. A structured constitutive model for simulating the behaviour of an overconsolidated bonded clay, in: COMPLAS XI: Proceedings of the XI International Conference on Computational Plasticity: Fundamentals and Applications. CIMNE. pp. 1177–1188.

González, N.A., Rouainia, M., Arroyo, M., Gens, A., 2012. Analysis of tunnel excavation in London Clay incorporating soil structure. Géotechnique 62, 1095–1109. https://doi.org/10.1680/geot.11.P.030

González, N., Gens, A., Arroyo, M., Rouainia, M., 2011. Modelling the behaviour of structured London Clay, in: International Symposium on Deformation Characteristics of Geomaterials.

Grim, R.E., 1942. Modern concepts of clay materials. J. Geol. 50, 225–275.

Gu, C., Wang, J., Cai, Y., Sun, L., Wang, P., Dong, Q., 2016. Deformation characteristics of overconsolidated clay sheared under constant and variable confining pressure. Soils Found. 56, 427–439. https://doi.org/10.1016/j.sandf.2016.04.009

Hashiguchi, K., 1980. Constitutive equations of elastoplastic materials with elastic-plastic transition. J Appl Mech 47, 266–272.

Hattab, M., 2011. Critical state notion and microstructural considerations in clays. Comptes Rendus Mec. 339, 719–226. https://doi.org/10.1016/j.crme.2011.07.007

Hattab, M., Hicher, P.-Y., 2004. Dilating Behaviour of Overconsolidated Clay. Soils Found. 44, 27–40. https://doi.org/10.3208/sandf.44.4_27

Higgins, D., 2006. Sustainable concrete: How can additions contribute, in: Proceedings of the Institute of Concrete Technology Annual Technical Symposium. Institute of Concrete Technology Camberley, UK.

Ho, T.-O., Chen, W.-B., Yin, J.-H., Wu, P.-C., Tsang, D.C.., 2021. Stress-Strain behaviour of Cement-Stabilized Hong Kong marine deposits. Constr. Build. Mater. 274, 122103. https://doi.org/10.1016/j.conbuildmat.2020.122103

Hong, J., Chen, W., Wang, Y., Xu, C., Xu, X., 2014. Life cycle assessment of caustic soda production: a case study in China. J. Clean. Prod. 66, 113–120. https://doi.org/10.1016/j.jclepro.2013.10.009

Horpibulsuk, S., Liu, M.D., Liyanapathirana, D.S., Suebsuk, J., 2010. Behaviour of cemented clay simulated via the theoretical framework of the Structured Cam Clay model. Comput. Geotech. 37, 1–9. https://doi.org/10.1016/j.compgeo.2009.06.007

Horpibulsuk, S., Miura, N., Bergado, D.T., 2004. Undrained Shear Behavior of Cement Admixed Clay at High Water Content. J. Geotech. Geoenvironmental Eng. 130, 1096–1105. https://doi.org/10.1061/(ASCE)1090-0241(2004)130:10(1096)

IPCC, 2018. Global warming of 1.5 C. IPCC – SR15. IPCC Report.

Ismail, I., Bernal, S.A., Provis, J.L., Nicolas, R.S., Hamdan, S., Deventer, J.S.J. van, 2014. Modification of phase evolution in alkali-activated blast furnace slag by the incorporation of fly ash. Cem. Concr.

Compos. 45, 125–135. https://doi.org/10.1016/j.cemconcomp.2013.09.006

James, J., Pandian, P.K., 2015. Soil stabilization as an avenue for reuse of solid wastes: a review. Acta Tech. Napocensis Civ. Eng. Archit. 58, 50–76.

Jardine, R.J., 1992. Some Observations on the Kinematic Nature of Soil Stiffness. Soils Found. 32, 111–124. https://doi.org/10.3208/sandf1972.32.2_111

Jardine, R.J., 1991. Some practical applications of a non-linear ground model, in: Proc. XECSMFE. Florence, pp. 223–228.

Jardine, R.J., 1985. Investigations of pile-soil behaviour, with special reference to the foundations of offshore structures. Uniersity of London.

Kamruzzaman, A.H., Chew, S.H., Lee, F.H., 2009. Structuration and Destructuration Behavior of Cement-Treated Singapore Marine Clay. J. Geotech. Geoenvironmental Eng. 135, 573–589. https://doi.org/10.1061/(ASCE)1090-0241(2009)135:4(573)

Kasama, K., Ochiai, H., Yasufuku, N., 2000. On the stress-strain behaviour of lightly cemented clay based on an extended critical state concept. Soils Found. 40, 37–47. https://doi.org/10.3208/sandf.40.5_37

Kasama, K., Zen, K., Iwataki, K., 2006. Undrained Shear Strength of Cement-Treated Soils. Soils Found. 46, 221–232. https://doi.org/10.3208/sandf.46.221

Kaze, C.R., Lemougna, P.N., Alomayri, T., Assaedi, H., Adesina, A., Das, S.K., Lecomte-Nana, G.-L., Kamseu, E., Melo, U.C., Leonelli, C., 2021. Characterization and performance evaluation of laterite based geopolymer binder cured at different temperatures. Constr. Build. Mater. 270, 121443. https://doi.org/10.1016/j.conbuildmat.2020.121443

Kuhl, H., 1908. Slag cement and process of making the same.

Lambe, T., 1958. The structure of compacted clay. J. Soil Mech. Found. Div. 84, 34.

Lang, L., Chen, B., Chen, B., 2021. Strength evolutions of varying water content-dredged sludge stabilized with alkali-activated ground granulated blast-furnace slag. Constr. Build. Mater. 275, 122111. https://doi.org/10.1016/j.conbuildmat.2020.122111

Lang, L., Chen, B., Li, N., 2020. Utilization of lime/carbide slag-activated ground granulated blast-furnace slag for dredged sludge stabilization. Mar. Georesources Geotechnol. https://doi.org/10.1080/1064119X.2020.1741050

Law Decree n. 183, 2009a. Legal regime for the deposition of landfill waste. Republic Diary n. 153/2009, Series I of 2009-08-10. Ministry of Environment, Territorial Planning and Regional Development (in Portuguese)., Diário da República 1ª Série.

Law Decree n. 183, 2009b. Legal regime for the deposition of landfill waste. Republic Diary n. 153/2009, Series I of 2009-08-10. Ministry of Environment, Territorial Planning and Regional Development (in Portuguese). Diário da República 1ªSérie.

Lee, K., Chan, D., Lam, K., 2004. Constitutive Model for Cement Treated Clay in a Critical State FrameWork. Soils Found. 44, 69–77. https://doi.org/10.3208/sandf.44.3_69

Lei, Y., Zhang, Q., Nielsen, C., He, K., 2011. An inventory of primary air pollutants and CO2 emissions from cement production in China, 1990–2020. Atmos. Environ. 45, 147–154. https://doi.org/10.1016/j.atmosenv.2010.09.034

Lemaignan, B., Wilmotte, J.., 2013. EFFC DFI carbon calculator methodological & user guide v2. 1 (2013), pp. 1-74.

Li, C., Wu, M., Chen, Q., Jiang, Z., 2018. Chemical and mineralogical alterations of concrete subjected to chemical attacks in complex underground tunnel environments during 20-36 years. Cem. Concr. Compos. 86, 139–159. https://doi.org/10.1016/j.cemconcomp.2017.11.007

Li, J., Geng, G., Myers, R., Yu, Y.-S., Shapiro, D., Carraro, C., Maboudian, R., Monteiro, P.J.M., 2019a. The chemistry and structure of calcium (alumino) silicate hydrate: A study by XANES, ptychographic imaging, and wide- and small-angle scattering. Cem. Concr. Res. 115, 367–378. https://doi.org/10.1016/j.cemconres.2018.09.008

Li, J., Zhang, W., Li, C., Monteiro, P.J.M., 2019b. Green concrete containing diatomaceous earth and limestone: Workability, mechanical properties, and life-cycle assessment. J. Clean. Prod. 223, 662–679. https://doi.org/10.1016/j.jclepro.2019.03.077

Lima, P.R., Mirapalheta, A., Andrade, M.H. dos S., Vilar, E.O., Zanta, C.L. de P. e S., Tonholo, J., 2010. Energy loss in electrochemical diaphragm process of chlorine and alkali industry – A collateral effect of the undesirable generation of chlorate. Energy 35, 2174–2178. https://doi.org/10.1016/j.energy.2010.01.039

Liu, M., Carter, J., 2002. A structured Cam Clay model. Can. Geotech. J. 39, 1313–1332. https://doi.org/10.1139/T02-069

Liu, W., Tang, X., Yang, Q., 2017. A slurry consolidation method for reconstitution of triaxial specimens. KSCE J. Civ. Eng. 21, 150–159. https://doi.org/10.1007/s12205-016-0199-9

Lloyd, R.R., Provis, J.L., van Deventer, J.S., 2009. Microscopy and microanalysis of inorganic polymer cements. 1: remnant fly ash particles. J. Mater. Sci. 44, 608–619.

LNEC, 1967. Determination of CBR. Specification of the National Laboratory of Civil Engineering, ref. E 198, Lisbon (in Portuguese). 1-10.

LNEC, 1966. Compaction test. Specification of the National Laboratory of Civil Engineering, ref. E 197, Lisbon (in Portuguese). 1-9.

Maddalena, R., Roberts, J.J., Hamilton, A., 2018. Can Portland cement be replaced by low-carbon alternative materials? A study on the thermal properties and carbon emissions of innovative cements. J. Clean. Prod. 186, 933–942. https://doi.org/10.1016/j.jclepro.2018.02.138

Miranda, T., Leitão, D., Oliveira, J., Corrêa-Silva, M., Araújo, N., Coelho, J., Fernández-Jiménez, A., Cristelo, N., 2020. Application of alkali-activated industrial wastes for the stabilisation of a full-scale (sub)base layer. J. Clean. Prod. 242, 118427. https://doi.org/10.1016/j.jclepro.2019.118427

Mitchell, J.K., 1993. Fundamentals of Soil Behavior. Wiley.

Mohammadinia, A., Arulrajah, A., D'Amico, A., Horpibulsuk, S., 2018. Alkali-activation of fly ash and cement kiln dust mixtures for stabilization of demolition aggregates. Constr. Build. Mater. 186, 71-78. https://doi.org/10.1016/j.conbuildmat.2018.07.103

Mohammadinia, A., Arulrajah, A., Disfani, M.M., Bo, M.W., Darmawan, S., 2017. Alkali-activated stabilized demolition wastes for geotechnical applications, in: 9th International Conference on Soil Mechanics

and Geotechnical Engineering (ICSMGE 2017), Seoul, Korea, 17-21 September, 3171-3174.

Mujtaba, H., Aziz, T., Farooq, K., Sivakugan, N., Das, B.M., 2018. Improvement in Engineering Properties of Expansive Soils using Ground Granulated Blast Furnace Slag. J. Geol. Soc. India 92, 357–362. https://doi.org/10.1007/s12594-018-1019-2

Mukherjee, A.B., Zevenhoven, R., Bhattacharya, P., Sajwan, K.S., Kikuchi, R., 2008. Mercury flow via coal and coal utilization by-products: A global perspective. Resour. Conserv. Recycl. 52, 571–591. https://doi.org/10.1016/j.resconrec.2007.09.002

Myers, R.J., Bernal, S.A., Gehman, J.D., Deventer, J.S.J. van, Provis, J.L., 2015a. The Role of Al in Cross-Linking of Alkali-Activated Slag Cements. J. Am. Ceram. Soc. 98, 996–1004. https://doi.org/10.1111/jace.13360

Myers, R.J., Bernal, S.A., Nicolas, R.S., Provis, J.L., 2013. Generalized Structural Description of Calcium–Sodium Aluminosilicate Hydrate Gels: The Cross-Linked Substituted Tobermorite Model. Langmuir 29, 5294–5306. https://doi.org/10.1021/la4000473

Myers, R.J., L'Hôpital, E., Provis, J.L., Lothenbach, B., 2015b. Composition–solubility–structure relationships in calcium (alkali) aluminosilicate hydrate (C-(N, K-) ASH). Dalt. Trans. 44, 13530–13544. https://doi.org/10.1039/c5dt01124h

Nagaraj, T.S., Miura, N., Yamadera, A., 1997. Re-examination of classification of soft clay deposits—Needs and methodology, in: Indian Geotechnical Conf. pp. 431–434.

Nguyen, L., Fatahi, B., Khabbaz, H., 2017. Development of a Constitutive Model to Predict the Behavior of Cement-Treated Clay during Cementation Degradation: C3 Model. Int. J. Geomech. 17, 4017010. https://doi.org/10.1061/(ASCE)GM.1943-5622.0000863

Nguyen, L., Fatahi, B., Khabbaz, H., 2014. A constitutive model for cemented clays capturing cementation degradation. Int. J. Plast. 56, 1–18. https://doi.org/10.1016/j.ijplas.2014.01.007

NP, 2002. Methylene Blue Test, ref 933-9, Portuguese Standard, Lisbon (in Portuguese). 1-18.

NP, 1969. Determination of Consistency Limits, ref. 143, Portuguese Standard, Lisbon (in Portuguese). 1-6.

NP 83, 1965. Determination of the Volume Weight of Solid Particles. Portuguese Standard.

Obuzor, G.N., Kinuthia, J.M., Robinson, R.B., 2012. Soil stabilisation with lime-activated-GGBS—A mitigation to flooding effects on road structural layers/embankments constructed on floodplains. Eng. Geol. 151, 112–119. https://doi.org/10.1016/j.enggeo.2012.09.010

Onyelowe, K.C., 2019. Review on the role of solid waste materials in soft soils reengineering. Mater. Sci. Energy Technol. 2, 46–51.

Palomo, Á., Kavalerova, E., Fernández-Jiménez, A. Krivenko, P., García-Lodeiro, I. Maltseva, O., 2015. A review on alkaline activation: new analytical perspectives, Materiales de Construcción. https://doi.org/10.3989/mc.2014.00314

Panayides, S., Rouainia, M., 2011. Analysis of pressuremeter performance using a kinematic hardening constitutive model with structure, in: 13th International Conference of the Association for Computer Methods and Advances in Geomechanics. Newcastle University. (IACMAG13).

Panayides, S., Rouainia, M., Muir Wood, D., 2012. Influence of degradation of structure on the behaviour of a full-scale embankment. Can. Geotech. J. 49, 344–356. https://doi.org/10.1139/t11-104

Parry, R.H.G., 1960. Triaxial compression and extension tests on remoulded saturated clay. Geotechnique 10, 166–180. https://doi.org/10.1680/geot.1960.10.4.166

Phummiphan, I., Horpibulsuk, S., Rachan, R., Arulrajah, A., Shen, S.L., Chindaprasirt, P., 2018. High calcium fly ash geopolymer stabilized lateritic soil and granulated blast furnace slag blends as a pavement base material. J. Hazard. Mater. 341, 257–267. https://doi.org/10.1016/j.jhazmat.2017.07.067

Porbaha, A., Shibuya, S., Kishida, T., 2000. State of the art in deep mixing technology. Part III:geomaterial characterization, in: Ground Improvement. pp. 91–110. https://doi.org/10.1680/grim.2000.4.3.91

Pourakbar, S., Asadi, A., Huat, B.B., Fasihnikoutalab, M.H., 2015. Stabilization of clayey soil using ultrafine palm oil fuel ash (POFA) and cement. Transp. Geotech. 3, 24–35. https://doi.org/10.1016/j.trgeo.2015.01.002

Pourakbar, S., Huat, B.K., 2017. A review of alternatives traditional cementitious binders for engineering improvement of soils. Int. J. Geotech. Eng. 11, 206-216.

https://doi.org/10.1080/19386362.2016.1207042

Provis, J., Van Deventer, J., 2014. Alkali activated materials, State-of-the-Art Report, RILEM TC 224-AAM. 1st Edition. Springer, Netherlands. https://doi.org/10.1007/978-94-007-7672-2

Provis, J.L., 2018. Alkali-activated material. Cem. Concr. Res. 114, 40–48. https://doi.org/10.1016/j.cemconres.2017.02.009

Provis, J.L., 2014. Geopolymers and other alkali activated materials: why, how, and what? Mater. Struct. 47, 11–25. https://doi.org/10.1617/s11527-013-0211-5

Pu, S.-Y., Zhu, Z.-D., Song, W.-L., Wang, H.-R., Wei, R.-J., 2019. Deformation properties of silt solidified with a new SEU-2 binder. Constr. Build. Mater. 220, 267–277. https://doi.org/10.1016/j.conbuildmat.2019.06.016

Quiroga, A., Thompson, Z., Muraleetharan, K., Miller, G., Cerato, A., 2017. Stress–strain behavior of cement-improved clays: testing and modeling. Acta Geotech. 12, 1003–1020. https://doi.org/10.1007/s11440-017-0529-1

Ramme, B.W., Tharaniyil, M.P., 2004. Coal Combustion Products Utilization Handbook.

Richardson, I.G., 1999. The nature of CSH in hardened cements. Cem. Concr. Res. 29, 1131–1147.

Richardson, I.G., Brough, A.R., Groves, G.W., Dobson, C.M., 1994. The characterization of hardened alkali-activated blast-furnace slag pastes and the nature of the calcium silicate hydrate (C-S-H) phase. Cem. Concr. Res. 24, 813–829. https://doi.org/10.1016/0008-8846(94)90002-7

Rios, S., Cristelo, N., Miranda, T., Araújo, N., Oliveira, J., Lucas, E., 2018. Increasing the reaction kinetics of alkali-activated fly ash binders for stabilisation of a silty sand pavement sub-base. Road Mater. Pavement Des. 19, 201–222. https://doi.org/10.1080/14680629.2016.1251959

Rios, S., Cristelo, N., Viana da Fonseca, A., Ferreira, C., 2017. Stiffness Behavior of Soil Stabilized with Alkali-Activated Fly Ash from Small to Large Strains. Int. J. Geomech. 17, 4016087. https://doi.org/10.1061/(ASCE)GM.1943-5622.0000783

Rios, S., Cristelo, N., Viana da Fonseca, A., Ferreira, C., 2016a. Structural Performance of Alkali-Activated Soil Ash versus Soil Cement. J. Mater. Civ. Eng. 28, 4015125.

https://doi.org/10.1061/(asce)mt.1943-5533.0001398

Rios, S., da Fonseca, A.V., Bangaru, S.S., 2016b. Silty sand stabilized with different binders. Procedia Eng. 143, 187–195. https://doi.org/10.1016/j.proeng.2016.06.024

Rios, S., Ramos, C., Viana da Fonseca, A., Cruz, N., Rodrigues, C., 2019. Mechanical and durability properties of a soil stabilised with an alkali-activated cement. Eur. J. Environ. Civ. Eng. 23, 245–267. https://doi.org/10.1080/19648189.2016.1275987

Rivera, J.F., Cristelo, N., Fernández-Jiménez, A., Gutiérrez, R.M. de, 2019. Synthesis of alkaline cements based on fly ash and metallurgic slag: Optimisation of the SiO2/Al2O3 and Na2O/SiO2 molar ratios using the response surface methodology. Constr. Build. Mater. 213, 424–433. https://doi.org/10.1016/j.conbuildmat.2019.04.097

Rodgers, L., 2018. Climate change: The massive CO2 emitter you may not know about [WWW Document]. BBC News. https://doi.org/https://www.bbc.com/news/science-environment-46455844

Roscoe, K.., Schofield, A.., 1963. Mechanical behavior of an idealised “wet” clay, in: Proc. 2nd Eur. Conf. SMFE, Wiesbaden. pp. 47–54.

Roscoe, K., Burland, J.B., 1968. On the generalized stress-strain behaviour of wet clay, in: Engineering Plasticity. Cambridge, Cambridge University, pp. 535–609.

Roscoe, K.H., Schofield, A., Thurairajah, A., 1963. Yielding of clays in states wetter than critical. Geotechnique 13, 211–240.

Roscoe, K.H., Schofield, A., Wroth, A.P., 1958. On the yielding of soils. Geotechnique 8, 22–53.

Rouainia, M., Muir Wood, D., 2000. A kinematic hardening constitutive model for natural clays with loss of structure. Géotechnique. Géotechnique 50, 153–164. https://doi.org/10.1680/geot.2000.50.2.153

Rouainia, M., Panayides, S., Arroyo, M., Gens, A., 2020. A pressuremeter-based evaluation of structure in London Clay using a kinematic hardening constitutive model. Acta Geotech. 15, 2089–2101. https://doi.org/10.1007/s11440-020-00940-w

Samad, S., Shah, A., 2017. Role of binary cement including Supplementary Cementitious Material (SCM), in production of environmentally sustainable concrete: A critical review. Int. J. Sustain. Built Environ. 6,

663–674. https://doi.org/10.1016/j.ijsbe.2017.07.003

Samarakoon, M.H., Ranjith, P.G., Rathnaweera, T.D., Perera, M.S.A., 2019. Recent advances in alkaline cement binders: A review. J. Clean. Prod. 227, 70–87. https://doi.org/10.1016/j.jclepro.2019.04.103

Sargent, P., Hughes, P.N., Rouainia, M., 2016. A new low carbon cementitious binder for stabilising weak ground conditions through deep soil mixing. Soils Found. 56, 1021–1034. https://doi.org/10.1016/j.sandf.2016.11.007

Sargent, P., Hughes, P.N., Rouainia, M., White, M.L., 2013. The use of alkali activated waste binders in enhancing the mechanical properties and durability of soft alluvial soils. Eng. Geol. 152, 96–108.

Sargent, P., Jaber, N.H., Rouainia, M., 2020a. Mineralogy and microstructure effects on the stiffness of activated slag treated alluvium. Géotechnique Lett. 10, 327–335. https://doi.org/10.1680/jgele.19.00055

Sargent, P., Rouainia, M., Diambra, A., Nash, D., Hughes, P.N., 2020b. Small to large strain mechanical behaviour of an alluvium stabilised with low carbon secondary minerals. Constr. Build. Mater. 232, 1–16. https://doi.org/10.1016/j.conbuildmat.2019.117174

Schoenberger, H., 2001. Final draft: best available techniques reference document on the production of iron and steel. Publ. EC Eur. Comm. Jt. Res. Centre, IPTS, Eur. IPPC Bur.

Schofield, A.., Wroth, C.., 1968. Critical State Soil Mechanics. McGraw-Hill, New York.

Sharma, A.K., Sivapullaiah, P. V., 2016. Ground granulated blast furnace slag amended fly ash as an expansive soil stabilizer. Soils Found. 56, 205-212. https://doi.org/10.1016/j.sandf.2016.02.004

Shi, C., Roy, D., Krivenko, P., 2003. Alkali-Activated Cements and Concretes, 1st Editio. ed. London. https://doi.org/10.1201/9781482266900

Shubbar, A.A., Jafer, H., Dulaimi, A., Hashim, K., Atherton, W., Sadique, M., 2018. The development of a low carbon binder produced from the ternary blending of cement, ground granulated blast furnace slag and high calcium fly ash: An experimental and statistical approach. Constr. Build. Mater. 187, 1051–1060. https://doi.org/10.1016/j.conbuildmat.2018.08.021

Siddique, R., 2008. Ground Granulated Blast Furnace Slag., in: Waste Materials and By-Products in Concrete. Springer, Berlin, Heidelberg, pp. 1–39. https://doi.org/10.1007/978-3-540-74294-4_1

Siddique, R., Cachim, P., 2018. Waste and Supplementary Cementitious Materials in Concrete: Characterisation, Properties and Applications, in: Siddique, R., Cachim, P. (Eds.), Woodhead Publishing Series in Civil and Structural Engineering. https://doi.org/10.1016/C2016-0-04037-8

Siddique, R., Khan, M.I., 2011. Ground Granulated Blast Furnace Slag, in: Engineering Materials. Springer, Berlin, Heidelberg. https://doi.org/10.1007/978-3-642-17866-5_3

Singhi, B., Laskar, A.I., Ahmed, M.A., 2016. Investigation on Soil–Geopolymer with Slag, Fly Ash and Their Blending. Arab. J. Sci. Eng. https://doi.org/10.1007/s13369-015-1677-y

Suebsuk, J., Horpibulsuk, S., Liu, M.D., 2011. A critical state model for overconsolidated structured clays. Comput. Geotech. 38, 648–658. https://doi.org/10.1016/j.compgeo.2011.03.010

Suebsuk, J., Horpibulsuk, S., Liu, M.D., 2010. Modified Structured Cam Clay: A generalised critical state model for destructured, naturally structured and artificially structured clays. Comput. Geotech. 37, 956–968. https://doi.org/10.1016/j.compgeo.2010.08.002

Sukprasert, S., Hoy, M., Horpibulsuk, S., Arulrajah, A., Rashid, A.S.A., Nazir, R., 2021. Fly ash based geopolymer stabilisation of silty clay/blast furnace slag for subgrade applications. Road Mater. Pavement Des. 22, 357–371. https://doi.org/10.1080/14680629.2019.1621190

Tchakouté, H.K., Rüscher, C.H., Kong, S., Kamseu, E., Leonelli, C., 2016a. Comparison of metakaolin-based geopolymer cements from commercial sodium waterglass and sodium waterglass from rice husk ash. J. Sol-Gel Sci. Technol. 78, 492–506. https://doi.org/10.1007/s10971-016-3983-6

Tchakouté, H.K., Rüscher, C.H., Kong, S., Kamseu, E., Leonelli, C., 2016b. Geopolymer binders from metakaolin using sodium waterglass from waste glass and rice husk ash as alternative activators: A comparative study. Constr. Build. Mater. 114, 276–289. https://doi.org/10.1016/j.conbuildmat.2016.03.184

Teing, T.T., Huat, B.B., Shukla, S.K., Anggraini, V., Nahazanan, H., 2019. Effects of Alkali-Activated Waste Binder in Soil Stabilization. Int. J. 17, 82–89. https://doi.org/10.21660/2019.59.8161

Tho-In, T., Sata, V., Boonserm, K., Chindaprasirt, P., 2018. Compressive strength and microstructure analysis of geopolymer paste using waste glass powder and fly ash. J. Clean. Prod. 172, 2892–2898. https://doi.org/10.1016/j.jclepro.2017.11.125

Thomas, A., Tripathi, R.K., Yadu, L.K., 2018. A laboratory investigation of soil stabilization using enzyme and alkali-activated ground granulated blast-furnace slag. Arabian Journal for Science and Engineering. J. Sci. Eng. 43, 5193–5202.

Torres-Carrasco, M., Puertas, F., 2015. Waste glass in the geopolymer preparation. Mechanical and microstructural characterisation. J. Clean. Prod. 90, 397–408. https://doi.org/10.1016/j.jclepro.2014.11.074

United Kingdom Quality Ash Association, 2010. Embodied CO2 of UK cement, additions and cementitious material' Technical data sheet 8.3, MPA; UK quality Ash association [WWW Document].

Van Riessen, A., Jamieson, E., Kealley, C.S., Hart, R.D., Williams, R.P., 2013. Bayer-geopolymers: An exploration of synergy between the alumina and geopolymer industries. Cem. Concr. Compos. 41, 29-33. https://doi.org/10.1016/j.cemconcomp.2013.04.010

Vargas, J., Halog, A., 2015. Effective carbon emission reductions from using upgraded fly ash in the cement industry. J. Clean. Prod. 103, 948-959. https://doi.org/10.1016/j.jclepro.2015.04.136

Vatsala, A., Nova, R., Murthy, B.S., 2001. Elastoplastic Model for Cemented Soils. J. Geotech. Geoenvironmental Eng. 127, 679–687. https://doi.org/10.1061/(ASCE)1090-0241(2001)127:8(679)

Vitale, E., Russo, G., Dell'Agli, G., Ferone, C., Bartolomeo, C., 2017. Mechanical behaviour of soil improved by alkali activated binders. Environments 4, 80. https://doi.org/10.3390/environments4040080

Wang, D., Gao, X., Wang, R., Larsson, S., Mahfoud, Benzerzour, 2020. Elevated curing temperature-associated strength and mechanisms of reactive MgO-activated industrial by-products solidified soils. Mar. georesources Geotechnol. 38, 659–671. https://doi.org/10.1080/1064119X.2019.1610817

Wattez, T., Patapy, C., Frouin, L., Waligora, J., Cyr, M., 2021. Interactions between alkali-activated ground granulated blastfurnace slag and organic matter in soil stabilization/solidification. Transp. Geotech. 26,

100412. https://doi.org/10.1016/j.trgeo.2020.100412

Wood, D.M., 1990. Soil behaviour and critical state soil mechanics. Cambridge university press, England.

Xi, F., Davis, S.J., Ciais, P., Crawford-Brown, D., Guan, D., Pade, C., Shi, T., Syddall, M., Lv, J., Ji, L., Bing, L., Wang, J., Wei, W., Yang, K.-H., Lagerblad, B., Galan, I., Andrade, C., Zhang, Y., Liu, Z., 2016. Substantial global carbon uptake by cement carbonation. Nat. Geosci. 9, 880–883. https://doi.org/10.1038/ngeo2840

Xiao, H., Lee, F.H., Chin, K.G., 2014. Yielding of cement-treated marine clay. Soils Found. 54, 488–501. https://doi.org/10.1016/j.sandf.2014.04.021

Xiao, R., Ma, Y., Jiang, X., Zhang, M., Zhang, Y., Wang, Y., Huang, B., He, Q., 2020. Strength, microstructure, efflorescence behavior and environmental impacts of waste glass geopolymers cured at ambient temperature. J. Clean. Prod. 252, 119610. https://doi.org/10.1016/j.jclepro.2019.119610

Xu, B., Yi, Y., 2019. Soft clay stabilization using ladle slag-ground granulated blastfurnace slag blend. Appl. Clay Sci. 178, 105136. https://doi.org/10.1016/j.clay.2019.105136

Yang, X., Ni, W., Zhang, X., Wang, Y., 2008. Effect of alkali-activation on aluminosilicate-based cementitious materials. J. Univ. Sci. Technol. Beijing, Miner. Metall. Mater. 15, 796–801. https://doi.org/10.1016/S1005-8850(08)60290-X

Yao, K., Chen, Q., Ho, J., Xiao, H., 2018. Strain-Dependent Shear Stiffness of Cement-Treated Marine Clay. J. Mater. Civ. Eng. 30, 4018255. https://doi.org/10.1061/(ASCE)MT.1943-5533.0002460

Yao, K., Chen, Q., Xiao, H., Liu, Y., 2020. Small-Strain Shear Modulus of Cement-Treated Marine Clay. J. Mater. Civ. Eng. 32, 4020114. https://doi.org/10.1061/(ASCE)MT.1943-5533.0003153

Yao, Z.T., Ji, X.S., Sarker, P., Tang, J.H., Ge, L.Q., Xia, M.S., Xi, Y.Q., 2015. A comprehensive review on the applications of coal fly ash. Earth-Science Rev. 141, 105–121. https://doi.org/10.1016/j.earscirev.2014.11.016

Yapage, N., Liyanapathirana, D., 2019. A review of constitutive models for cement-treated clay. Int. J. Geotech. Eng. 13, 525–537. https://doi.org/10.1080/19386362.2017.1370878

Yi, Y., Li, C., Liu, S., 2015. Alkali-activated ground-granulated blast furnace slag for stabilization of marine

soft clay. J. Mater. Civ. Eng. 27, 4014146. https://doi.org/10.1061/(ASCE)MT.1943-5533.0001100

Yin, Z., Xu, Q., Hicher, P.Y., 2013. A simple critical state based double-yield-surface model for clay behavior under complex loading. Acta Geotech. 8, 509–523. https://doi.org/10.1007/s11440-013-0206-y

Yu, J., Chen, Y., Chen, G., Wang, L., 2020. Experimental study of the feasibility of using anhydrous sodium metasilicate as a geopolymer activator for soil stabilization. Eng. Geol. 264, 105316. https://doi.org/10.1016/j.enggeo.2019.105316

Zhang, J., Scherer, G.W., 2011. Comparison of methods for arresting hydration of cement. Cem. Concr. Res. 41, 1024–1036.

Zhang, M., Guo, H., El-Korchi, T., Zhang, G., Tao, M., 2013. Experimental feasibility study of geopolymer as the next-generation soil stabilizer. Constr Build Mater 47, 1468–1478. https://doi.org/10.1016/j.conbuildmat.2013.06.017

Zhang, M., Zhao, M., Zhang, G., Nowak, P., Coen, A., Tao, M., 2015. Calcium-free geopolymer as a stabilizer for sulfate-rich soils. Appl. Clay Sci. 108, 199–207. https://doi.org/10.1016/j.clay.2015.02.029

Zhang, S., Keulen, A., Arbi, K., Ye, G., 2017. Waste glass as partial mineral precursor in alkali-activated slag/fly ash system. Cem. Concr. Res. 102, 29–40. https://doi.org/10.1016/j.cemconres.2017.08.012

Publications

Araújo, N., Corrêa-Silva, M., Miranda, T., Gomes, A. T., Castro, F., Teixeira, T., & Cristelo, N. (2020). Unsaturated Response of Clayey Soils Stabilised with Alkaline Cements. Molecules, 25(11), 2533. https://doi.org/10.3390/molecules25112533

Corrêa-Silva, M., Araújo, N., Cristelo, N., Miranda, T., Gomes, A. T., & Coelho, J. (2019). Improvement of a clayey soil with alkali activated low-calcium fly ash for transport infrastructures applications. Road Materials and Pavement Design, 20(8). https://doi.org/10.1080/14680629.2018.1473286

Corrêa-Silva, M., Miranda, T., Araújo, N., Coelho, J., Cristelo, N., & Topa Gomes, A. (2017). Improvement of a clayey soil with alkaline activation of wastes. In In WASTES–Solutions, Treatments and Opportunities II. 1st Edition. CRC Press. London. 323-329. https://doi.org/10.1201/9781315206172-52

Corrêa-Silva, M., Miranda, T., Rouainia, M., Araújo, N., Glendinning, S., & Cristelo, N. (2020). Geomechanical behaviour of a soft soil stabilised with alkali-activated blast-furnace slags. Journal of Cleaner Production, 122017. https://doi.org/10.1016/j.jclepro.2020.122017

Corrêa-Silva, M., Rouainia, M., Miranda, T., & Cristelo, N. (2021). Modelling the Stress-Strain Behaviour of a Soft Soil Improved with an Environmentally Friendly Binder. International Conference of the International Association for Computer Methods and Advances in Geomechanics, 382–389. https://doi.org/10.1007/978-3-030-64514-4_35

Corrêa-Silva, M., Rouainia, M., Miranda, T., Cristelo, N., 2021. Predicting the mechanical behaviour of a sandy clay stabilised with an alkali-activated binder. Eng. Geol. 292, 106260. https://doi.org/10.1016/j.enggeo.2021.106260

Miranda, T., Leitão, D., Oliveira, J., Corrêa-Silva, M., Araújo, N., Coelho, J., ... Cristelo, N. (2020). Application of alkali-activated industrial wastes for the stabilisation of a full-scale (sub)base layer. Journal of Cleaner Production, 242. https://doi.org/10.1016/j.jclepro.2019.118427